PACIFIC CLIMATE IMPACTS CONSORTIUM

Hydrologic Impacts of Climate Change in the Peace, Campbell and Columbia Watersheds, British Columbia, Canada

—

Hydrologic Modelling Project

Final Report (Part II)

1 April 2011

Markus A. Schnorbus
Katrina E. Bennett
Arelia T. Werner
Anne J. Berland

University of Victoria

(BLANK)

Citation

Schnorbus, M.A., K.E. Bennett, A.T. Werner and A.J. Berland, 2011: *Hydrologic Impacts of Climate Change in the Peace, Campbell and Columbia Watersheds, British Columbia, Canada*. Pacific Climate Impacts Consortium, University of Victoria, Victoria, BC, 157 pp.

About PCIC

The mission of the Pacific Climate Impacts Consortium is to quantify the impacts of climate variability and change on the physical environment in the Pacific and Yukon region. The Pacific Climate Impacts Consortium is financially supported by the BC Ministry of Environment, BC Hydro, the BC Ministry of Forests and Range, as well as several regional and community stakeholders. For more information see http://www.pacificclimate.org/.

Disclaimer

This information has been obtained from a variety of sources and is provided as a public service by the Consortium. While reasonable efforts have been undertaken to assure its accuracy, it is provided by the Consortium without any warranty or representation, express or implied, as to its accuracy or completeness. Any reliance you place upon the information contained within this document is your sole responsibility and strictly at your own risk. In no event will the Consortium be liable for any loss or damage whatsoever, including without limitation, indirect or consequential loss or damage, arising from reliance upon the information within this document.

(BLANK)

Acknowledgements

We gratefully acknowledge the financial support of BC Hydro and the financial and in-kind support of the British Columbia Ministry of Environment. We wish to thank the members of BC Hydro's Technical Advisory Committee (TAC), made up variously of Stephanie Smith (BC Hydro), Doug McCollor (BC Hydro), Frank Weber (BC Hydro), Sean Fleming (BC Hydro), Alex Cannon (Environment Canada), Allan Chapman (BC Ministry of Environment), Brian Menounos (University of Northern British Columbia) and Dan Moore (University of British Columbia), for their invaluable advice, guidance and suggestions. We also acknowledge the kind support and assistance of the Climate Impacts Group, University of Washington, with special thanks to Alan Hamlet, Marketa McGuire Elsner, Eric Salathé Jr., Ted Bohn and Natalie Voisin. We also thank Andy Wood, of the Colorado Basin River Forecast Center, for his advice and guidance regarding the VIC model calibration. Ideas regarding possible future work incorporating dynamic glacier modelling benefitted greatly from discussion with Shawn Marshall (University of Calgary). We also thank Hans Schreier (University of British Columbia) and John Pomeroy (University of Saskatchewan) for their critical and valuable comments and suggestions on an earlier draft of this report. Lastly, thanks go to Hailey Eckstrand, for GIS support and assistance with figure preparation, Greg Maruszeczka and Cassbreea Dewis for document review, and Paul Nienaber and David Bronaugh for their technical and computational support.

(BLANK)

Preface

The Pacific Climate Impacts Consortium (PCIC) has completed a *Hydrologic Modelling* project with the aim of quantifying the hydrologic impacts of projected climate change in select British Columbia watersheds. The main objective of the Hydrologic Modelling project is to provide future projections of the impacts of climate change on monthly and annual streamflow in three BC watersheds: the Peace, Campbell and Columbia, for the 2050s, with particular emphasis on sites corresponding to BC Hydro power generation assets.

Due to the scope of work required for this project, reporting is accomplished using two complementary but independent reports. The current report acts as the main reporting vehicle for the Hydrologic Modelling project, focusing predominantly on the methods employed and results obtained from the hydrologic modelling exercise itself. This report provides a thorough, yet concise, summary of the methodology, results and analysis of the hydrologic modelling and resultant hydrologic projections. Nevertheless, the scope and technical nature of this subject resists a simplified interpretation in a concise document. Consequently, the current report represents, as best as we could achieve, a compromise between a detailed technical treatment of results and an easily comprehended summary of findings. A companion report (Werner 2011)[1] describes in greater detail the regional climate response throughout British Columbia based on the same climate projections that form the basis of the Hydrologic Modelling project.

Our intended audience includes technical staff and managers at BC Hydro who are planning and allocating water resources. However, due to the physiographic and climatic variability of the three study areas, we also feel that our results are valid with respect to gaining a general understanding of the hydrological consequences of projected climate change within British Columbia. This should make our results accessible to the wider scientific and operational audience. The term "impacts", as used in this report, refers to the consequences of climate change and variability on regional hydro-climatology and streamflow, which has implications for subsequent impacts studies on water resource systems and the environment. The report does not directly address implications for water resources system operations (e.g., capability to meet future hydro-power demand).

Analysis using updated data and peer-reviewed methodology forms the basis for this work. Whenever possible, our intention was also to extend and improve upon existing results. In this context general improvements include the use of a larger suite of latest-generation global climate models (the results from which form the basis of the Intergovernmental Panel on Climate Change's Fourth Assessment Report). The selection of climate change simulations used in this report covers multiple emissions scenarios and models, and includes projections for the 2050s that range from a future with relatively less warming and moistening ("cool/dry") to relatively more warming and moistening ("warm/wet"). The hydrologic impact of the various projections was assessed with a high-resolution, spatially-distributed and physically-based hydrology model.

An additional significant accomplishment of this project has been the generation of a substantial and comprehensive dataset of historical and projected hydrologic fluxes and state variables. This data is available for a large suite of climate projections, and captures model output at a daily resolution. Flux model output is available at a spatial resolution of 1/16° for spatial domains covering the three study areas, and streamflow data is available for several dozen sites within the study areas. High-resolution downscaled climate data has also been generated, which provides time series of various meteorological variables at high spatial resolution for a domain incorporating all of British Columbia plus a small portion of the United States. A detailed description and inventory of forcing and hydrologic model output data is provided in Appendix A to this report.

[1] Werner, A.T., 2011: *BCSD Downscaled Transient Climate Projections for Eight Select GCMs Over British Columbia, Canada*. Pacific Climate Impacts Consortium, University of Victoria, Victoria, BC, 63 pp.

The Hydrologic Modelling project is part of a larger *Hydrologic Impacts* research program that has been underway at PCIC to address the consequences of climate change on water resources in British Columbia (Rodenhuis et al. 2007)[2]. The research plan is composed of four distinct projects: *Climate Overview*, *Hydrologic Modelling* (the subject of the current report), *Regional Climate Modelling Diagnostics*, and the *Synthesis*. The objectives of the Climate Overview are to identify the scope and intensity of the threat of potential impacts to water resources by climate variability and change in British Columbia (Rodenhuis et al. 2009)[3]. The objectives of the Regional Climate Modelling Diagnostics project are to validate the water balance of the Canadian Regional Climate Model (CRCM) in select BC watersheds, and to use the CRCM to simulate future climate and hydrologic conditions as a parallel effort to the Hydrologic Modelling project (Rodenhuis et al. 2011)[4]. Lastly, the purpose of the Synthesis project (Shrestha et al. 2011)[5] is to compare and synthesize hydrologic projections from both the Hydrologic Modelling and the Regional Climate Modelling Diagnostics projects.

Markus A. Schnorbus, Lead Hydrologist, PCIC
Katrina B. Bennett[6], Hydrologist, PCIC
Arelia T. Werner, Hydrologist, PCIC
Anne J. Berland, Analyst - Hydrology, PCIC

23 December 2010

[2] Rodenhuis, D., A.T. Werner, K.E. Bennett, and T.Q. Murdock, 2007: *Research Plan for Hydrologic Impacts*. Pacific Climate Impacts Consortium, University of Victoria, Victoria, BC, 34 pp.
[3] Rodenhuis, D., K.E. Bennett, A.T. Werner, T.Q. Murdock and D. Bronaugh, 2009: *Climate Overview 2007: Hydro-climatology and Future Climate Impacts in British Columbia*. Pacific Climate Impacts Consortium, University of Victoria, Victoria, BC, 132 pp.
[4] Rodenhuis, D., B. Music, M. Braun and D. Caya, 2011: *Climate Diagnostics of Future Water Resources in BC Watersheds*. Pacific Climate Impacts Consortium, University of Victoria, 74 pp.
[5] Shrestha, R.R., A.J. Berland, M.A. Schnorbus, A.T. Werner, 2011: *Climate Change Impacts on Hydro-Climatic Regimes in the Peace and Columbia Watersheds, British Columbia, Canada*. Pacific Climate Impacts Consortium, University of Victoria, Victoria, BC, 37 pp.
[6] Now with the University of Alaska Fairbanks, International Arctic Research Center

Hydrologic Impacts of Climate Change in the Peace, Campbell and Columbia Watersheds, British Columbia, Canada

Executive Summary

According to the Intergovernmental Panel on Climate Change (IPCC) Fourth Assessment Report, it is now "very likely" that observed widespread warming of the atmosphere and oceans are due to historical anthropogenic greenhouse gas emissions, predominantly from fossil fuel use. Further, climate change trends will persist with continued emissions of greenhouse gases, such that we can expect further changes in global, regional and local temperature and precipitation patterns. Continued warming and changing precipitation patterns will have a large effect on the hydrology of western North America, with the possibility for subsequent impacts to various water-related resources and activities, including hydroelectric generation, municipal water supply, flood management, in-stream flow needs and fish habitat, irrigated agriculture, recreation and navigation. Although these water-related issues are germane to British Columbia, sustainable and self-sufficient generation of electricity in British Columbia is a significant concern and a major policy objective. Hydroelectricity is BC's largest source of electric power generation and much of this hydroelectric power is generated by BC Hydro, the third largest electrical utility in Canada. Approximately 85% of BC Hydro's generation is produced by hydroelectric means from large heritage assets in the Peace and Columbia River systems which may be susceptible to the hydrologic impacts of climate change.

A high-resolution, physically-based macro-scale hydrologic model has been applied to quantify the hydrologic impacts of projected climate change within the Peace, Campbell and Upper Columbia watersheds in British Columbia. The three study watersheds contain numerous important BC Hydro heritage assets for hydroelectric generation and represent a range of hydro-climatic regimes and scales. Streamflow projections were made for several project sites within the study areas, corresponding to current BC Hydro heritage asset sites, potential sites of future hydroelectric development (i.e., Site C), as well as several natural drainages. This study utilized a suite of eight global climate models (GCMs) driven by three emissions scenarios, intended to capture a range of high, medium and low projected greenhouse gas emissions and to project a wide range of potential climate responses for the 2050s time period (2041-2070). Climate projections were statistically downscaled and used to drive the hydrology model at high spatial resolution. This methodology of selecting multiple GCMs coupled to three emissions scenarios covers a large range of potential future climates for BC and explicitly addresses both emissions and GCM uncertainty in the final hydrologic projections.

The general conclusions of this work can be summarized as follows:

Climate response:

- All projections indicate higher temperatures in all seasons and all study areas by the 2050s, with strong agreement between GCMs and scenarios. The highest temperature increase is projected for the winter season in all three study areas for all three emissions scenarios.
- Precipitation projections are less robust for the 2050s (i.e., the range of individual GCM projections includes both positive and negative changes), but suggest increased precipitation in the winter, spring and fall for all study areas and all emissions scenarios. Increased annual precipitation is projected for the interior study areas (Peace and Upper Columbia) but negligible changes are projected for the coastal Campbell River study area. Regional differences are also apparent for summer precipitation trends, with decreased precipitation projected for the Campbell and Upper Columbia study areas (southern BC) versus negligible changes in summer precipitation projected for the Peace study area (northern BC).

Annual discharge:

- Annual discharge is projected to increase in the Peace River study area, a response that is generally consistent between project sites, although local inflow to the Peace River above Pine River shows a weaker response. Annual discharge in the Upper Columbia study area is projected to increase at the

majority of project sites for all emissions scenarios. Annual discharge changes for the Campbell River study area are projected to be negligible.

- At all three study areas, increases in annual discharge are attributed to projected changes in annual precipitation for the 2050s. The variation in annual discharge response between study areas is due primarily to regional variation in projected precipitation trends, where increased annual precipitation is projected for the interior study areas (Peace and Upper Columbia) but negligible changes are projected for the coastal Campbell River study area.

Monthly discharge:

- Monthly streamflow projections for the Peace River project sites show a consistent response of higher future discharge during fall and winter, an earlier onset of spring freshet, higher peak monthly discharge, and reduced discharge during late summer and early fall. Changes in the timing and duration of the spring freshet result in the largest absolute changes in monthly discharge. Differences in the monthly discharge response between the three emissions scenarios are negligible. Monthly streamflow projections for the Upper Columbia are similar, although between sites, projections are less consistent regarding changes in the month of peak discharge as well as changes in the magnitude of peak monthly discharge.
- Monthly streamflow projections for the Campbell River study area show a strong shift in seasonality due to a transition from a hybrid nival-pluvial regime to an almost exclusively pluvial regime. This transition results in large increases in fall and winter discharge, and decreases in spring, summer, and early fall discharge, resulting in a longer and more severe low flow period, although remnant freshet runoff is still projected to occur in the 2050s.
- Changes in monthly streamflow timing, seasonality and magnitude are largely attributed to projected changes in the dynamics of natural snow storage. These changes include 1) changes in the proportion of winter precipitation received as rainfall versus snowfall, 2) changes in seasonal snow accumulation, and 3) changes in the timing and magnitude of snowmelt. The most prominent regional variation is apparent in the degree to which snow storage dynamics in the three study areas respond to projected climate response.
- The coastal Campbell River site is projected to undergo the most dramatic change, shifting from what is already a transitional hybrid regime to a predominantly pluvial regime. Although the Peace River in northeastern BC shows signs of shifting to a more hybrid regime in the 2050s, it will still retain sufficient snow that the monthly hydrograph will maintain the characteristic signal of a nival regime, albeit with a freshet that will be advanced in time. The Upper Columbia arguably shows the least sensitivity to climate change, although it is still responsive to changes in temperature and precipitation. This is largely attributed to a hypsometry that places much of the study area at high enough elevation to avoid significant changes in snow storage dynamics, despite rising temperatures. In fact, in contrast to the Peace and Campbell, snow storage throughout much of the Upper Columbia reflects winter precipitation trends more so than temperature trends.

Glacier mass balance:

- Glacier mass balance in the Upper Columbia study area is projected to vary with elevation, being predominantly negative at elevations below 2400 m and increasingly more positive at elevation greater than 2400 m. Total cumulative mass balance between 1995 and 2070 for the entire study area, based on the ensemble medians for the A1B, A2, and B1 scenarios, is negative for the A1B and A2 scenarios, but slightly positive for the B1 scenario. Differences in overall cumulative mass balance are mainly attributed to differences in projected temperature changes, which become progressively less pronounced for the A1B, A2 and B1 scenarios, respectively. Glacier area is projected to shrink by roughly 50% for all three emissions scenarios. Nevertheless, the projected trends in mass balance and glacier area may be under- and over-estimated, respectively, due to the absence of glacier dynamics in the hydrology model.

Global climate model and emissions sensitivity:

- For annual and monthly discharge at the Peace and Upper Columbia project sites, differences between GCM runs combined with inter-annual variability for any given GCM-driven run are larger than streamflow differences between emissions scenarios, suggesting that projections for the 2050s are largely insensitive to the chosen emissions trajectories.
- Only projections for Campbell River at Strathcona Dam indicate some potential sensitivity to differences between the three emissions scenarios for the 2050s period. For this small coastal watershed, the hydro-climatic response to the mid-21st century emissions projected by the A1B scenario may be sufficiently stronger than that from either A2 or B1 scenarios that annual and monthly discharge displays a detectably different response. Only the A1B ensemble indicates statistically significant increases in annual discharge (although only a 4% difference in median historic and future discharge is projected in this case). The monthly streamflow projections from the A1B-prescribed emissions also tend to exhibit larger changes than those derived from either A2 or B1. Nevertheless, as the climate response for this small study area is likely derived from a very limited number of GCM model grid cells, such differences should be interpreted cautiously.

Several next steps are recommended for future work, including:

- Incorporating a coupled dynamic glacier response within the hydrologic modelling process. This would incorporate a hydrologic response due to more realistic changes in glacier mass, volume, area and hypsometry as a response to transient climate warming. Coupled modelling would also incorporate important feedbacks based on differential mass balance response by elevation and changes in surface albedo.
- Updating the current hydrologic projections by incorporating new climate projections. Climate projections from the IPCC's upcoming Fifth Assessment Report, based on the latest GCM technology and new emission projections scenarios, will be available in the very near future.
- Extension of the current work into the investigation of sub-monthly hydrologic and streamflow phenomenon, such as changes in the magnitude and frequency of extreme, or threshold design events. This will require refinement of current downscaling approaches to explicitly capture the daily transient climate response.
- Investigation of climate and hydrologic impacts projected to the end of the 21st century. Although the A1B emissions scenario displays the largest impacts for the mid-21st century, differences between emissions scenarios are small. Scenario differences are anticipated to become substantial by the end of the 21st century, when the A2 scenario will result in the largest impacts. Hydrologic impacts projected for the 2050s based on the chosen emissions scenarios are expected to become even more pronounced by the end of the 21st century.

(BLANK)

Acronyms and Abbreviations

Acronym/Abbreviation	Description
AHCCD	Adjusted Historical Canadian Climate Data (http://www.cccma.ec.gc.ca/hccd/)
ASP	automated snow pillow
AVHRR	Advanced Very High Resolution Radiometer
BCSD	Bias Corrected Spatial Disaggregation
BTM	Baseline Thematic Mapping
CCCma	Canadian Centre for Climate Modelling and Analysis (Victoria, Canada) (http://www.cccma.ec.gc.ca/)
CCSM3.0	Community Climate System Model, version 3.0 (NCAR, US)
CCSR	Center for Climate System Research (University of Tokyo, Tokyo, Japan)
CGCM3.1	Coupled Global Climate Model, version 3.1 (CCCma, Canada)
CGIAR-CSI	Consultative Group on International Agricultural Research – Consortium for Spatial Information (http://csi.cgiar.org/meeting/index.asp)
CIG	Climate Impacts Group (University of Washington, Seattle, USA)
ClimateWNA	Climate Western North America (http://www.genetics.forestry.ubc.ca/cfcg/ClimateWNA/ClimateWNA.html)
CMIP3	Coupled Model Intercomparison Project, phase 3 (http://cmip-pcmdi.llnl.gov/cmip3_overview.html)
CMIP5	Coupled Model Intercomparison Project, phase 5 (http://cmip-pcmdi.llnl.gov/cmip5/index.html)
CSIRO	Commonwealth Scientific and Research Organization (Australia) (http://www.csiro.au/)
DEM	Digital Elevation Model
DSMW	Digital Soil Map of the World
EC	Environment Canada
ECHAM5	European Centre Hamburg Model, version 5 (MPI, Germany)
EOSD	Earth Observation for Sustainable Development
ENSO	El Niño/Southern Oscillation
FAO	Food and Agricultural Organization (http://www.fao.org/)
GCM	global climate model
GFDL	Geophysical Fluid Dynamics Laboratory (http://www.gfdl.noaa.gov/)
GHG	greenhouse gas
HADCM3	Hadley Centre Coupled Model, version 3 (Hadley Centre, UK)
HADGEM1	Hadley Centre Global Environmental Model, version 1 (Hadley Centre, UK)

IPCC	Intergovernmental Panel on Climate Change (http://www.ipcc.ch/)
IQR	inter-quartile range
IRF	instantaneous response function
ISRIC	International Soil Reference and Information Centre (http://www.isric.org/)
LOESS	locally weighted regression
MCPI	Model Climate Performance Index
MIROC	Model for Interdisciplinary Research on Climate (CCSR, Japan)
MOCOM	Multi-Objective Complex Evolution Method
MPI	Max Planck Institute (http://www.mpg.de/english/portal/index.html)
MVI	Model Variability Index
NARCCAP	North American Regional Climate Change Assessment Program (http://www.narccap.ucar.edu/)
NARR	North American Regional Reanalysis
NCAR	National Center for Atmospheric Research (http://ncar.ucar.edu/)
NCEP	National Centers for Environmental Prediction (http://www.ncep.noaa.gov/)
PCMDI	Program for Climate Model Diagnosis and Intercomparison (http://www-pcmdi.llnl.gov/)
POI	point of interest
PDO	Pacific Decadal Oscillation
PRISM	Parameter-elevation Regressions on Independent Slopes Model
RCM	regional climate model
RCP	Representative Concentration Pathways
SOM	self-organizing maps
SLP	sea level pressure
SPOT-4	Satellite Pour l'Observation de la Terre, satellite 4
SRES	Special Report on Emissions Scenarios
SRTM	Shuttle Radar Topography Mission
SVATS	soil-vegetation-atmosphere transfer scheme
SWE	snow water equivalent
UKMO	United Kingdom Meteorological Office (http://www.metoffice.gov.uk/)
UNESCO	United Nations Educational, Scientific and Cultural Organization (http://www.unesco.org/new/en/unesco/)
USHCN	United States Historical Climatology Network (http://cdiac.ornl.gov/epubs/ndp/ushcn/ushcn.html)
VIC	Variable Infiltration Capacity model (http://www.hydro.washington.edu/Lettenmaier/Models/VIC/)

WCRP	World Climate Research Program (http://www.wcrp-climate.org/)
WSC	Water Survey of Canada (http://www.ec.gc.ca/rhc-wsc/)

(BLANK)

1. Introduction and Background

According to the Intergovernmental Panel on Climate Change (IPCC) Fourth Assessment Report, it is now "very likely" that observed widespread warming of the atmosphere and oceans is due to historical anthropogenic greenhouse gas emissions, predominantly from fossil fuel use (IPCC 2007). Further, climate change trends will persist with continued emissions of greenhouse gases, such that we can expect changes in global, regional and local temperature and precipitation patterns. Continued warming and changing precipitation patterns will have a large effect on the hydrology of western North America, with significant implications for water resources, the economy, infrastructure, and ecosystems (e.g., Milly et al. 2008; Schindler and Donahue 2006).

The hydro-climatology of British Columbia is complex, in part due to its close proximity to the Pacific Ocean, mountainous terrain and large latitudinal expanse. Historical changes to climate and hydrology have been documented in British Columbia (BC) and western North America (Rodenhuis et al. 2009). While they are attributable to climate variability, such as teleconnection patterns coming from El Niño/Southern Oscillation (ENSO) or the Pacific Decadal Oscillation (PDO), recent hydro-climatic trends in western North America have also been attributed to anthropogenic climate change, predominantly in the form of increased regional warming (Barnett et al. 2008; Bonfils et al. 2008; Pierce et al. 2008). Moreover, the dominance of snowpack and glaciers in BC and the sensitive response of these cryosphere components to climate change increases regional susceptibility to hydrologic impacts (Fleming and Clarke 2003; Barnett et al. 2005; Stahl et al. 2008; Adam et al. 2009; Moore et al. 2009). Changes can potentially affect all aspects of the hydrologic cycle with implications for the hydrologic extremes of flood and drought severity and occurrence (Hamlet and Lettenmaier 2007; Sheffield and Wood 2008).

Throughout most of British Columbia, seasonal runoff is either snow-dominated (nival regimes), or snow influenced (hybrid nival-pluvial or nival-glacial regimes). Within such regimes, documented trends in hydrology over recent decades generally include less snowpack, earlier onset of spring melt, decrease in summer flow, and delay in the onset of autumn flows, resulting in an extension in the warm hydrologic season (Whitfield and Cannon 2000; Regonda et al. 2005; Déry et al. 2009). The detailed effects can be confounded by regional variability in future changes in temperature and precipitation. For instance, resulting changes in snow storage dynamics are strongly affected by elevation, generating large spatial variation in regions of complex topography (Kim 2001; Knowles and Cayan 2004; Mote et al. 2005). Also, rainfall-dominated (i.e., pluvial) and hybrid nival-pluvial systems will tend to be more sensitive to regional precipitation and rainfall trends (Whitfield et al. 2002). Recent trends of declining glacier mass have been associated with negative trends in August discharge detected in glacier-fed catchments throughout BC, with the exception of northwest BC, where some positive trends were detected (Stahl and Moore 2006). In northwest BC (and southwest Yukon), Fleming and Clarke (2003) also detected positive trends in annual streamflow in glacierized catchments, consistent with a region-wide warming trend. However, they detected a negative streamflow trend for non-glacierized catchments. Observed hydro-climatic trends are generally projected to continue into the future, with the possibility of subsequent impacts to various water-related resources and water-dependent activities, including hydroelectric generation, municipal water supply, flood management, in-stream flow needs and fish habitat, irrigated agriculture, recreation and navigation (Cohen et al. 2000; Mote et al. 2003; Hayhoe et al. 2004; Payne et al. 2004; Merritt et al. 2006; Hamlet et al. 2010; Mantua et al. 2010; Vano et al. 2010a; Vano et al. 2010b). Ultimately it is recognized that the hydro-climatic system can no longer be considered stationary, and from a management perspective the past may become progressively less informative of future conditions (Milly et al. 2008).

Although each of the aforementioned water-related issues are germane to BC, sustainable and self-sufficient generation of electricity in British Columbia has been identified as a significant concern and a major policy objective for the BC government (*BC Energy Plan*, Ministry of Energy 2010a). Hydroelectricity is BC's largest source of electric power generation (approximately 90%), the majority of

which is generated from regulated storage (i.e., reservoirs) (Ministry of Energy 2010b). Much of this hydroelectric power is generated by BC Hydro, the third largest electrical utility in Canada. Approximately 85% of BC Hydro's generation, between 43,000 and 54,000 gigawatt hours (GWh) of electricity annually depending upon annual variability in runoff, is produced by hydroelectric means from large heritage assets in the Peace and Columbia River systems (BC Hydro 2010). The degree to which hydroelectric power generation in BC may be susceptible to the impacts of climate change is of considerable concern.

The foundation for understanding the consequences of a changing climate (temperature and precipitation) on water resources at regional scales requires knowledge of projected changes in the hydrological regime (rain, snow, ice), hydrological storage (snowpack, glaciers, reservoirs, lakes, wetlands, groundwater and soil moisture), and hydrological fluxes (evaporation, transpiration, runoff and streamflow). Therefore, possible future hydrologic changes are often explored using hydrologic models driven by climate change scenarios (Blöschl and Montanari 2010). To this end, a high-resolution, physically-based macro-scale hydrologic model has been applied to quantify the hydrologic impacts of projected climate change within three study areas, the Peace, Campbell and Columbia River watersheds of British Columbia. The three study watersheds contain numerous important BC Hydro assets for hydroelectric generation. Streamflow projections were made for several sites within the study areas, corresponding to current BC Hydro generation sites, potential sites of future hydro-electric development (i.e., Site C), as well as several natural drainages. The hydrologic modelling is driven by climate projections statistically downscaled from a suite of eight latest-generation global climate models (GCMs). The GCMs are driven by three emissions scenarios and include projections for the 2050s that range from a future with relatively less warming and moistening ("cool/dry") to relatively more warming and moistening ("warm/wet"). This ensemble approach explicitly addresses both emissions and GCM uncertainty in the final hydrologic projections.

Our choice of methodology and use of the most recent climate projections expands upon older studies conducted for the Peace, Campbell and Columbia basins (Loukas et al. 2002a, 2002b; Toth et al. 2006). This work also complements and expands upon a large body of work conducted for the Canadian portion of the Columbia by United States-based research groups (Hamlet and Lettenmaier 1999; Payne et al. 2004; Wood et al. 2004). In addition, as the three study areas selected represent a range of hydro-climatic and physiographic regimes, these results are appropriate to gaining a general understanding of the hydrological consequences of projected climate change within British Columbia as a whole.

The report is organized into four main sections that provide, respectively: 1) methods, including the means of generating hydrologic projections and a description of the three study areas, 2) a description of the VIC hydrologic model, the main tool used to generate hydrologic projections, 3) results and discussion, and 4) conclusions. Figures are included with the text and captions are numbered by section. All references plus figure and table listings are located at the end of the report.

2. Methods

2.1 Hydrologic Projections

Obtaining projections of changes in the hydrologic cycle due to a change in global climate is an involved process requiring several steps. This process, represented graphically by the steps in Figure 2-1, involves: a) specification of emissions trajectories, b) conversion of projected emissions to radiative forcing, c) conversation of radiative forcing to a global climate response, d) statistically downscaling the global climate response to obtain a regional climate response, e) translating the regional climate response to the regional and local hydrologic response, and lastly, step g) involves comparing historic and future hydrology to quantify potential changes in water resources. Although discussion of steps a) through c) will provide essential background and context to the work described in this report, in order to satisfy the requirements of the Hydrologic Modelling project, PCIC was only directly involved in activities supporting steps d), e) and g).

An alternative approach to projecting future changes in streamflow using statistical downscaling and hydrologic modelling (steps d and e, Figure 2-1) is to use a Regional Climate Model (RCM). Via an RCM, GCM output can be dynamically downscaled and changes to the hydrologic cycle can be explored directly at the native resolution of the RCM within a fully coupled land-ocean-atmosphere environment (step f, Figure 2-1). Such an approach has also been pursued at PCIC as a parallel project (Rodenhuis et al. 2007). Discussion of those results is beyond the scope of this report and the reader is referred to Rodenhuis et al. (2010) for further details.

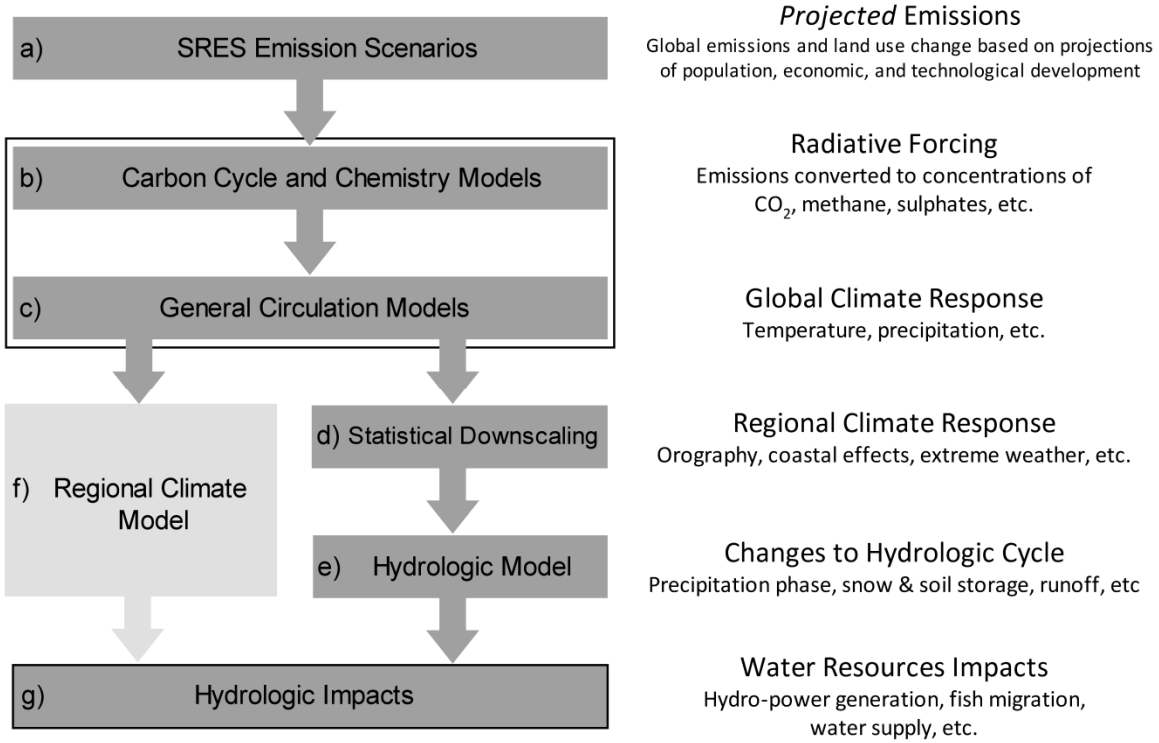

Figure 2-1. Method for quantifying hydrologic impacts under projected future climates

Future emissions trajectories are provided by the Intergovernmental Panel on Climate Change (IPCC) Special Report on Emissions Scenarios (SRES) (Nakićenović and Swart 2000). The SRES scenarios are based on four different narrative storylines that cover a wide range of demographic, social, economic, technological, and environmental developments. These storylines describe divergent future development and are intended to encompass a significant portion of the underlying uncertainties in the main factors controlling emissions (demographic change, social and economic development, and the rate and direction of technological change) (Nakićenović and Swart 2000). The final emissions scenarios are quantitative interpretations of the storylines, translated into greenhouse gas (GHG) emissions, sulfur emissions, and land-use change (e.g., loss of forest cover). The scenarios only deal with anthropogenic forcing (e.g., no large volcanic eruptions). The scenarios should be interpreted as projections, as they are neither predictions nor forecasts of the future and the storylines are speculative in nature. As such, they are all equally as likely (or unlikely) to occur and have no probabilities or likelihoods assigned. In other words, there is no 'best guess'. However, the actual emissions trajectory since 2000 is close to (or exceeding, depending upon source data) the trajectory cast by the most pessimistic SRES scenario (A1F1) (Raupach et al. 2007). In the current project, we use climate projections that are based on a subset of the full SRES scenario suite, namely the A1B, A2 and B1 scenarios.

The projected future global emissions provide the forcing for global climate models (GCMs). Carbon cycle and chemistry models are used to convert emissions and land use change into concentrations of radiatively active species, often in concert with the modelling of the ocean-climate system (steps b and c in Figure 2-1) (Meehl et al. 2007b). These concentrations are translated into a radiative forcing which drives the modelling of the global climate system. This combined process (steps b and c in Figure 2-1) is used to estimate the global climate response to prescribed emissions trajectories (Meehl et al. 2007b). Our study uses GCM model output contributed by the World Climate Research Programme (WCRP) through its Coupled Model Intercomparison Project phase 3 (CMIP3) multi-model dataset (Meehl et al. 2007a) (data was obtained from the Program for Climate Model Diagnosis and Intercomparison (PCMDI) website at http://www-pcmdi.llnl.gov/). The CMIP3 project provides results for a total of 24 GCMs from 17 modelling groups from 12 countries. The CMIP3 climate change experiments are based primarily on the A1B, A2 and B1 scenarios. These scenarios are chosen to reflect a range of high (A2: CO_2 concentration about 820 ppm by 2100), medium (A1B: CO_2 concentration about 700 ppm by 2100) and low (B1: CO_2 concentration about 550 ppm by 2100) forcings from 2000 to 2100. Note that the emissions trajectories for A2 and A1B are such that the projected climate response to A1B is generally larger than for the A2 by the mid-21st century (Figure 2-2).

In order to reduce computational time, remove outliers, screen poorly performing GCMs, and ease interpretation of results, PCIC has used output from a subset of eight (8) of the CMIP3 models. The process of GCM selection is described in detail by Werner (2011), and is briefly summarized herein. Model selection was based on using performance metrics that identify GCMs that are robust and perform best at replicating the historical climate over the globe, the Northern Hemisphere, North America and western North America. GCM output for the A1B, A2 and B1 emissions scenarios were selected, when available for a given model, to fully explore the range of possible responses to the emissions pathways and provide results that can be compared to other studies, such as those conducted by the University of Washington's Climate Impacts Group (CIG) (Climate Impacts Group 2009) or NARCCAP (see http://www.narccap.ucar.edu/). Climate projections from a final suite of eight GCMs and three emissions scenarios were used as input for the hydrologic modelling, and these are summarized in Table 2-1. Note that only a total of 23 hydrology model runs (vice 8 x 3 = 24) are used as the UKMO HadGEM1 model does not have output for the B1 scenario (Table 2-1). This methodology of selecting multiple GCMs coupled to three emissions scenarios covers a large range in potential wet/dry and warm/cool projected future climates for BC (Figure 2-2). All climate projections are based on a single GCM run. Therefore, we did not make use of the multiple projections that are available for some GCMs. For the purposes of hydrologic modelling, climate projections were obtained from the GCMs in the form of monthly

temperature and precipitation time series for the 1950 to 2100 period (with the exception of UKMO HADGEM1 which was available to December 2098 only).

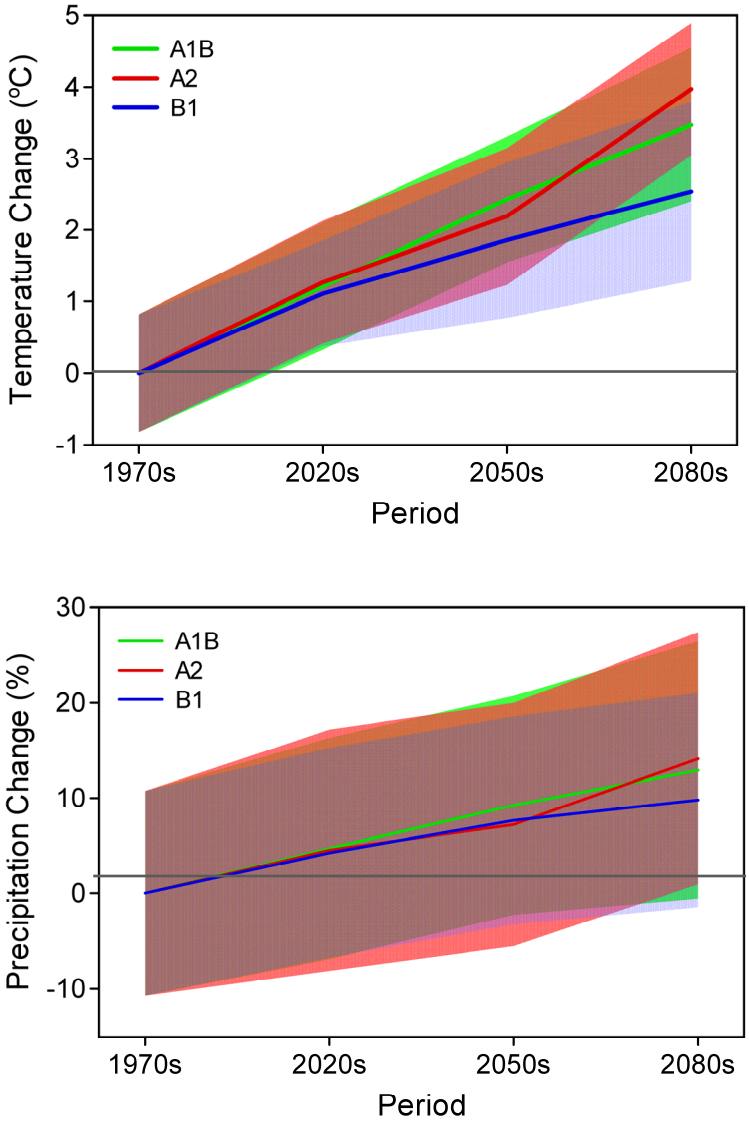

Figure 2-2. Projected changes in BC-average a) temperature and b) precipitation climatology for the thirty-year periods centred on 1961 to 1990 (1970s), 2011 to 2040 (2020s), 2041 to 2070 (2050s) and 2071 to 2100 (2080s) for the eight GCMs from Table 2-1. Changes are calculated with respect to the multi-model 1970s ensemble mean.

The global climate response to a prescribed emissions scenario generated by a GCM is currently of too coarse a spatial resolution to be used directly in obtaining a hydrologic response for the study areas. The output from a GCM does not typically contain sufficient regional detail on the change in climate, which is affected by such factors as local topography, orography, and coastal effects (Wilby and Wigley 1997). Therefore, downscaling the global climate signal into a regional climate signal is a necessary intermediate

step. Such downscaling is often based on statistical, or empirical, models (step d in Figure 2-1). In this case, GCM climate projections were downscaled statistically using the Bias Corrected Spatial Disaggregation (BCSD) approach (Wood et al. 2002; Wood et al. 2004; Salathé 2005). The reader is referred to Werner (2011) for a complete description of BCSD and its application for the current study and the method is briefly summarized herein. BCSD was utilized to generate a daily time series of temperature and precipitation for the period 1950 to 2100 for each GCM-scenario run at the resolution of the hydrologic model (1/16°) (see also Section 3).

Table 2-1. Global Climate Model and SRES Scenario Selection

Global Climate Model	SRES Emissions Scenarios		
	A1B	A2	B1
CCCMA CGCM 3.1 T47	X	X	X
CSIRO MK 3.0	X	X	X
GFDL CM 2.1	X	X	X
CCSR MIROC 3.2 (medres)	X	X	X
MPI ECHAM5	X	X	X
NCAR CCSM3.0	X	X	X
UKMO HADCM3	X	X	X
UKMO HADGEM1	X	X	not avail

The BCSD approach involves three main steps. First, monthly temperature and precipitation biases exhibited by the large-scale GCM simulations are removed non-parametrically by mapping quantiles to those of observed gridded monthly temperature and precipitation, which has been aggregated to the resolution of the GCM (Wood et al. 2002). Derivation of the observed temperature and precipitation data is described in Section 3.2. Second, the bias-corrected monthly temperature and precipitation values from the GCM simulations are spatially downscaled by interpolating monthly anomalies to the higher target resolution of the hydrologic model. Third, this monthly time series is temporally downscaled by using month-long daily patterns sampled from the historic record (1950-2006) at 1/16° resolution (Wood et al. 2002). This temporal downscaling applies a stochastic technique, wherein a historic month is chosen randomly, constrained by a check to ensure a relatively wet historic month is picked when a wet month is being downscaled. The temperatures are then chosen from the same month to match the one selected for precipitation and both are selected for the entire region of interest from that month to preserve a degree of synchronization in the weather components driving the hydrologic response (Wood et al. 2004). The daily temperature and precipitation of the analog month are then re-scaled to the bias-corrected downscaled monthly means (multiplicative for precipitation and additive for temperature) for each grid point. Daily wind speed is also required as input to the hydrologic model. However, the BCSD approach does not include wind downscaling and wind data is taken without adjustment from observed values for the selected analog month (Wood et al. 2002).

The BCSD approach has been used to explicitly downscale the monthly climate response to radiative forcing from the selected GCM simulations. Although BCSD could hypothetically use daily GCM data directly, fewer modelling centres archive CMIP3 daily data, and the daily data are arguably less skillful, particularly for precipitation and especially when it comes to downscaling large grid cell information to the local scale (Leavesly 1994; Maurer and Hidalgo 2008). Given the decision to not incorporate daily

information directly from the GCM, it is important to note that the daily characteristics of the downscaled data are an artifact of the temporal re-sampling procedure and do not reflect direct changes to statistical properties of daily weather projected by individual GCMs. Although the daily magnitude of temperature and precipitation will scale with the evolving monthly response, such statistics as the frequency of dry or wet days will remain unaltered from the base climate. Nevertheless, BCSD captures the potentially altered monthly statistics simulated by the GCM (i.e., changes in monthly mean, variance and sequencing). This method also explicitly captures the transient nature of the emissions scenarios, which is useful for projecting the trend in the regional climate and hydrologic response.

Once downscaled, the regional climate response is used to force a hydrologic model (step e, Figure 2-1), from which we explicitly examine the change in the hydrologic cycle within the study areas as a consequence of projected changes in future climate. The hydrologic model is forced using the transient downscaled daily weather for the period 1950 to 2098[7] from each GCM-scenario run. Changes in the various components of the hydrologic cycle are quantified by comparing the simulated fluxes (e.g., precipitation, evaporation, snowmelt, and runoff) and states (snow and soil moisture) from two 30-year periods within the transient simulation representing historical and future conditions, respectively. The historical baseline period covers 1961 to 1990 (the 1970s) and the future period covers 2041 to 2070 (the 2050s). The hydrologic modelling is done with the Variable Infiltration Capacity (VIC) model (Liang et al. 1994). The VIC model is spatially distributed (i.e., gridded) to explicitly capture regional variation in the hydrologic cycle due to variation in topographic, physiographic, and climate controls. The VIC model is also physically-based, allowing for more confident extrapolation of hydrologic processes into un-observed future climate regimes (Leavesley 1994; Ludwig et al. 2009). The combination of statistical downscaling with BCSD in conjunction with hydrologic modelling using the VIC model is a validated approach. It has, for instance, been recently applied in a high-profile study of the detection and attribution of observed changes in snowpack, air temperature and the hydrological cycle of the western United States (Barnett et al. 2008; Bonfils et al. 2008; Pierce et al. 2008). The VIC model and its implementation to the three study areas is discussed in further detail in Section 3. General results of the BCSD downscaling (i.e., BC-wide climate change projections) are reported in Werner (2011).

Uncertainty is an inherent component of the process of obtaining hydrologic projections. The quantification of hydrologic impacts is derived from results obtained via a cascade of up to five different modelling processes all constrained by projections of future emissions trajectories (Figure 2-1). Each model step has inherent limitations, assumptions and errors, potentially introducing bias and artifacts into the model cascade. Further, observational uncertainty affects all steps in the cascade. Our reliance on only one respective downscaling and hydrology model, with fixed parameterizations, means that our results do not incorporate uncertainties from these two sources. Depending upon the projection horizon, the choice of emissions scenario can also represent a significant source of uncertainty. However, for the 2050s period, province-wide climate projections (Figure 2-2) obtained under the different emissions trajectories (A1B, A2 and B1) are relatively indistinguishable. Recent research suggests that differences in global climate response to greenhouse forcings between different GCMs (steps b and c in Figure 2-1) is the largest source of uncertainty in the model cascade, and uncertainties attributed to downscaling, emissions scenarios and hydrologic modelling are of much lesser magnitude (Wilby 2005; Bennett et al. 2009; Prudhomme and Davies 2009; Blöschl and Montanari 2010). Regardless, our methodology of using an ensemble of multiple GCMs coupled to three emissions scenarios explicitly addresses both emissions and GCM uncertainty. Specifically, GCM uncertainty stems from errors and uncertainty in initial conditions, boundary conditions (e.g., greenhouse gas concentrations and radiative forcing), parameter uncertainty, and structural uncertainty (Tebaldi and Knutti 2007). By using a single run from each GCM, we employ an ensemble of climate projections that predominantly addresses structural uncertainty, which stems from different choices regarding model physics (e.g., which processes are included, which processes are

[7] Hydrologic simulations end at 2098 as climate projections from the HADGEM GCM only run to 2098.

excluded, and how small-scale phenomena are parameterized), and model numerics (temporal and spatial resolution, type of grid, numerical algorithms, etc.).

The statistical paradigm that informs our methodology of GCM selection and interpretation of climate projections can be formally classified as "indistinguishable-weighted" (Tebaldi 2010, pers. comm.). It has been argued that the reliability of model projections may be improved if GCM results are weighted according to some measure of skill (i.e., GCM results are not treated equally) (Annan and Hargreaves 2010; Knutti et al. 2010; Tebaldi and Knutti 2007). Along these lines, our decision to use results from eight of the original suite of models from CMIP3 (see Werner 2011) effectively applies a binary weighting (i.e., 0 or 1) to the full set of results. Furthermore, climate projections from the final ensemble of GCM runs are treated as statistically indistinguishable (Annan and Hargreaves 2010; Knutti et al. 2010). In such a case, it is taken that "the truth is drawn from the same distribution as the ensemble members, and thus no statistical test can reliably distinguish one from the other" (Annan and Hargreaves 2010). Each ensemble member is considered indistinguishable from all possible outcomes of the Earth's chaotic processes (Knutti et al. 2010). However, despite a potentially strong argument for pooling the hydrologic results generated from all 23 GCM runs into a single ensemble, due to negligible differences between climate projections for the different scenarios in the 2050s (Figure 2-2), we stratified the hydrologic projections by emissions scenario for impact analysis. This accounts for the possibility that the (often non-linear) transformation of the projected climate response into a hydrologic response may result in detectable differences between the three emissions trajectories.

Many stages of the modelling cascade identified in Figure 2-1 rely on steps or processes that are empirical in nature (i.e., bias-correction in statistical downscaling, etc.) and that assume stationary statistical relationships between past and future climates. This is not assured and adds an additional element of uncertainty to the results. Additionally, hydrologic modelling is based on parameterizations that are also assumed to remain stationary over the projection horizon (i.e., the next 100 years). For instance, the hydrologic projections do not account for such possibilities as changes in land cover (either anthropogenic or climate-related) or evolving changes in surface or sub-surface drainage efficiency under increasingly wetter or drier climates.

2.2 Study Areas

Hydrologic impacts were modelled in three main study areas located within the Peace, Campbell and Columbia River basins in British Columbia (Figure 2-3). These three study areas represent a range of climatic, topographic and physiographic conditions. Hydrologic impacts are modelled and projected for each of the study areas as a whole. In addition, streamflow projections are provided for specific project sites within each study area, typically corresponding to BC Hydro projects. Note that at the majority of project site locations, streamflow projections are based on local inflow only (i.e., exclusive of streamflow from upstream project sites; see Section 3.6 for more details). The project sites, as well as the local drainage characteristics, are listed in Table 2-2. What follows is a brief summary of each study area. The climatic summaries (precipitation, rainfall, snowfall, and air temperature) reported in this section are based on monthly normals (1961-1990) spatially-averaged over each study area, which are estimated from gridded observed meteorological data.

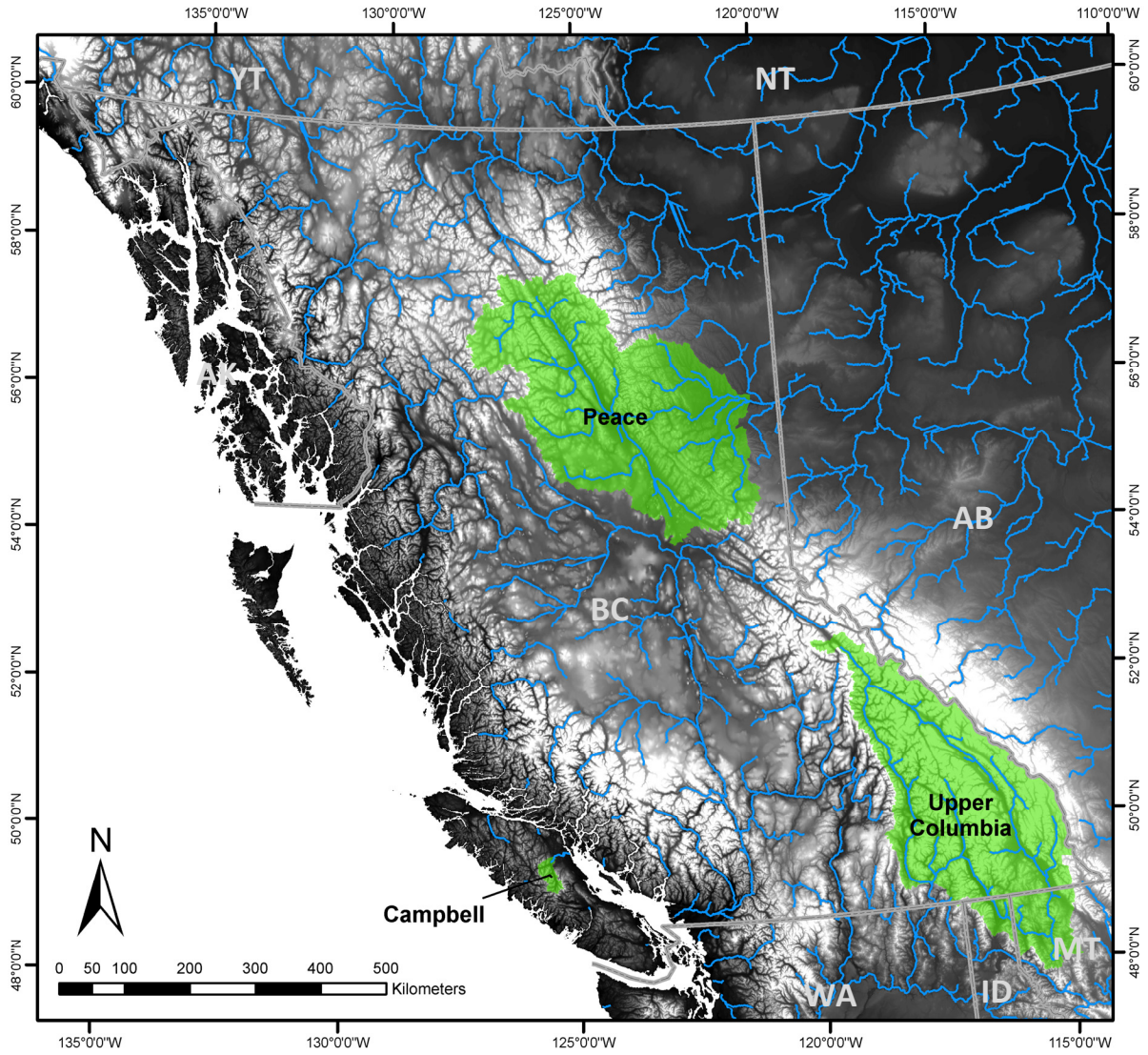

Figure 2-3. Study areas of the hydrologic modelling project.

The Peace River study area is located in interior north-eastern British Columbia and encompasses the 101,000 km^2 drainage area upstream of Taylor, BC (Figure 2-3). This area, which drains from the northern Rocky Mountains and the Alberta Plateau, forms the headwaters of the Peace River system that ultimately drains into the large inland Peace-Athabasca Delta in northern Alberta. Elevation in the Peace River study area ranges from 400 to over 2800 m (Figure 2-4). The region has a continental climate, with frequent outbreaks of Arctic air and precipitation that is derived from eastward moving frontal systems during the winter and local convective activity during the summer (Demarchi 1996). Monthly average temperatures range from -12.0 °C in January to 12.3 °C in July, averaging 0.2 °C over the year. Annual average precipitation is 810 mm, distributed with a slight seasonal pattern of summer maximum and spring minimum (Figure 2-5a). The Peace River has a nival regime, with approximately 54% of annual

precipitation (438 mm) falling as snow (mostly during October through April) and 64% of natural[8] streamflow occurring during the freshet months of May through July (Figure 2-5a). The lowest flows occur during the winter and early spring. Two BC Hydro project sites are located in the Peace study area: the W.A.C. Bennett Dam, which forms the Williston Reservoir (1,761 km^2 in surface area), and the Peace Canyon Dam, which is located 23 km downstream of the W.A.C. Bennett Dam and forms the 21 km long Dinosaur Reservoir (Figure 2-6). The proposed BC Hydro Site C Dam project is located along the Peace River mainstem, approximately 20 km upstream from Taylor, BC, just above the confluence of the Peace and Pine Rivers ("Peace above Pine" in Figure 2-6) (BC Hydro 2009). The outlet of the study area is located along the Peace River at Taylor, BC. Streamflow projections are provided for the W.A.C. Bennett Dam, the Peace River above Pine River, and the Peace River at Taylor (Table 2-2). Streamflow projections for both the Peace River above Pine River and at Taylor are based on local inflow (i.e., absent inflow from upstream sites). As the difference in absolute discharge between the W.A.C. Bennett and Peace Canyon Dams is negligible, streamflow projections for the Peace Canyon Dam are not provided.

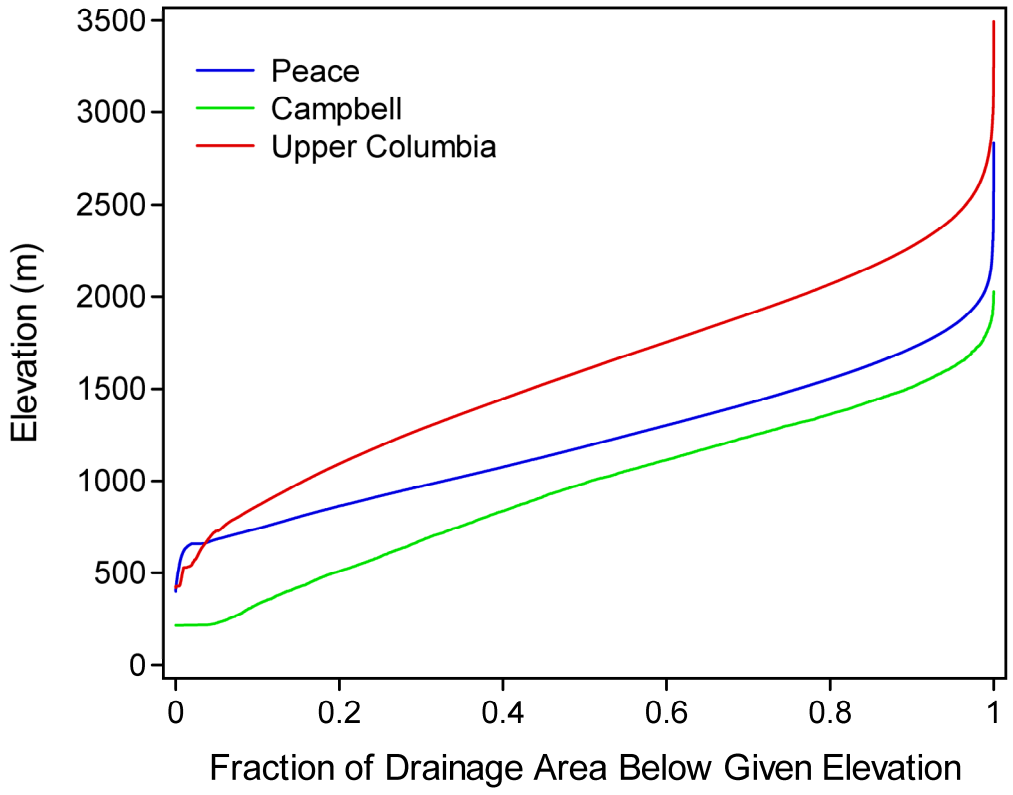

Figure 2-4. Hypsometric curves of the Campbell, Peace and Upper Columbia study areas based on 15-arc seconds (approximately 450 m) digital elevation model.

[8] Due to the effects of upstream regulation, raw observed streamflow in many locations in the study areas no longer represents a climate-driven seasonal pattern, but instead is dictated by the timing and magnitude of reservoir releases. Natural streamflow, or streamflow in the absence of regulation, must be inferred or estimated by models.

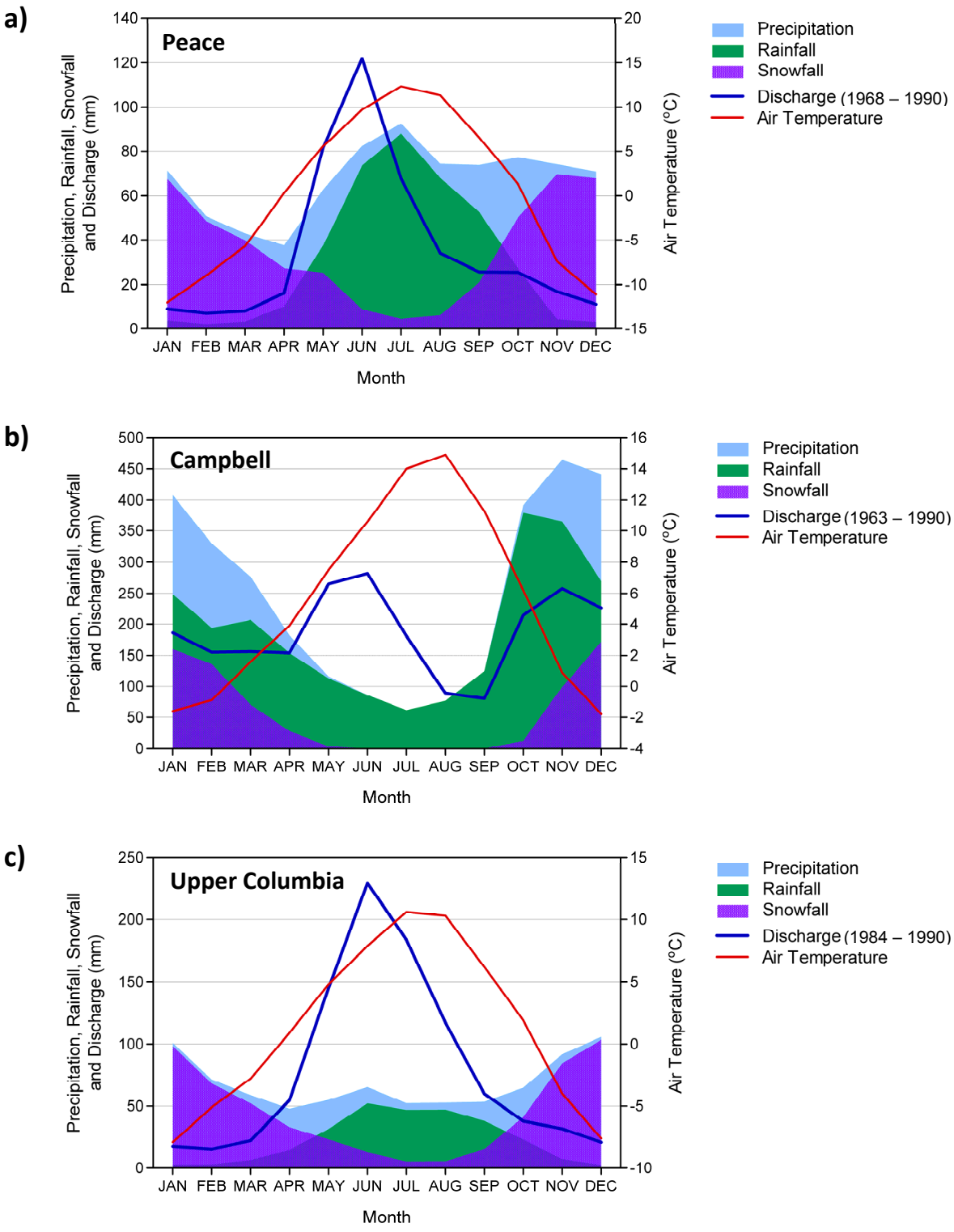

Figure 2-5. Area-average precipitation, rainfall, snowfall and temperature normals (1961-1990) for a) Peace River above Taylor , b) Campbell River above Strathcona Dam, and c) Columbia River above Columbia-Kootenay confluence. Average natural discharge (period varies) is also shown for a) Campbell River at Strathcona Dam, b) Peace River at Taylor, and c) Columbia River at outlet of Arrow Lakes.

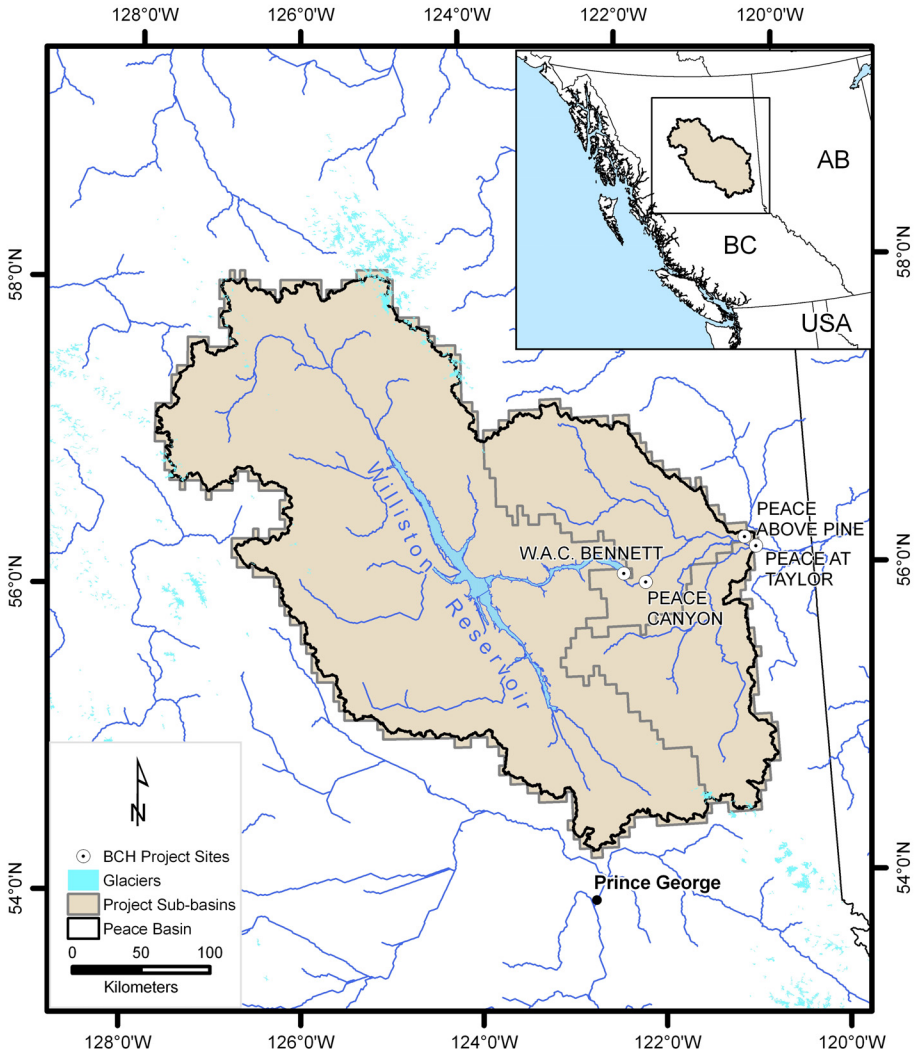

Figure 2-6. Peace River study area, showing the basin outlines and study site locations (with VIC model 1/16° sub-basin outlines).

The Campbell River is a small, coastal watershed that drains the mountains of central Vancouver Island to the Strait of Georgia near the town of Campbell River (Figure 2-3). The region exhibits a typical coastal climate, with mild, wet winters and warm dry summers (Figure 2-5b) (Demarchi 1996). Temperature averages 5.6 °C annually and monthly average values range from -1.8 °C in December to 14.0 °C in August. Annual precipitation in the study area is 2,960 mm with a pronounced seasonal distribution, with 78% of precipitation falling during the six-month period of October to March. Due to the mountainous topography, 23% of precipitation (680 mm) falls as snow at higher elevations, such that natural streamflow exhibits a hybrid nival-pluvial regime with a characteristic double peak in both the fall and spring (Figure 2-5b). Approximately 32% of annual discharge occurs during the freshet months of May, June and July, with June receiving the highest discharge during the year. Rainfall runoff during the fall months of October through November is also high, accounting for 31% of annual discharge. Low flow

occurs during the months of August and September. The Campbell River has three dams on the Campbell mainstem: John Hart (lowermost), Ladore and Strathcona (uppermost). The Campbell study area occupies the 1,200 km^2 drainage area upstream of BC Hydro's Strathcona Dam, which impounds the Upper Campbell Lake and the Buttle Lake Reservoir (Figure 2-7). The study area rises from 139 m elevation at the dam to 2,200 m elevation at the mountain peaks in the Vancouver Island Ranges (Figure 2-4). Although the Upper Campbell Reservoir sporadically received diverted flow from the upper Heber River (Fish and Wildlife Compensation Program 2000), this diversion has been permanently closed for several years and hydrologic modelling of the study basin does not include the upper Heber River basin. The study area, however, does include the Crest Creek basin, which is a tributary of the Heber River that has been permanently diverted into Upper Campbell Lake via the Elk River (Fish and Wildlife Compensation Program 2000). Streamflow projections are provided for the Campbell River at Strathcona Dam (Table 2-2).

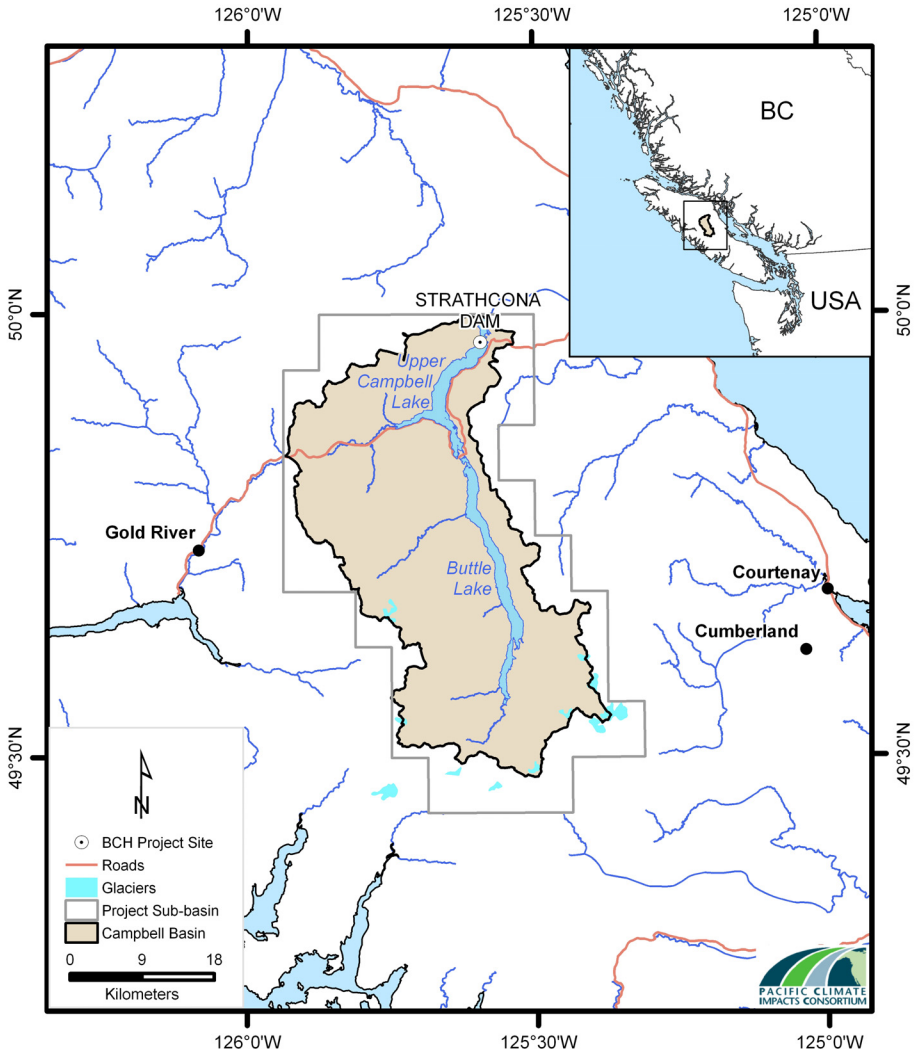

Figure 2-7. Campbell River study area, showing the basin outlines and study site location (with VIC model 1/16° sub-basin outlines).

The Columbia River study area is located in interior south-western British Columbia and occupies the drainage area upstream of the confluence of the Kootenay and Columbia Rivers, a 104,000 km^2 area that lies predominantly within Canada (referred to as the Upper Columbia), although a portion of the Kootenay River drainage lies within the United States (Figure 2-3). The study area is centred on the Columbia Mountains and is bordered to the east by the Rocky Mountains and to the west by the Shuswap-Okanagan Highlands. Elevation within the Columbia study area ranges from 420 m to numerous peaks well over 3,000 m (Figure 2-4). The climate can be classified as humid-continental (Demarchi 1996). Annual temperature averages 1.9 °C and monthly average values range from -9.4 °C in January to 13.4 °C in July. Air masses from the west deposit moisture in the winter as they pass over the Columbia and Rocky mountains, and summer rainfall occurs from a combination of both local convective activity and frontal systems. This results in precipitation that falls more or less uniformly throughout the year, with some slight seasonal variation (precipitation is highest in the winter). Approximately 65% of annual precipitation falls as snow, with snowfall possible throughout the year at the highest elevations. In addition, approximately 4% of the area is covered by glaciers, where glacial runoff can contribute as much as 10% of annual discharge and up to 15-20% of late summer (August-September) discharge. Consequently, natural streamflow in the study area exhibits a glacial-nival regime, where the hydrologic cycle is dominated by the spring freshet, with a gradual recession in flow during the late summer and fall, and lowest flow occurring during the winter (Figure 2-5c). The Upper Columbia basin is highly regulated and it contains 17 dams and/or power generation sites on its mainstem and various tributaries (BC Hydro 2007). Streamflow projections are provided for 11 locations, nine of which correspond to BC Hydro project sites (Figure 2-8; Table 2-2). Like the Peace, streamflow projections at the majority of locations within the Upper Columbia are based on local inflow only. More details are provided in Section3.6.

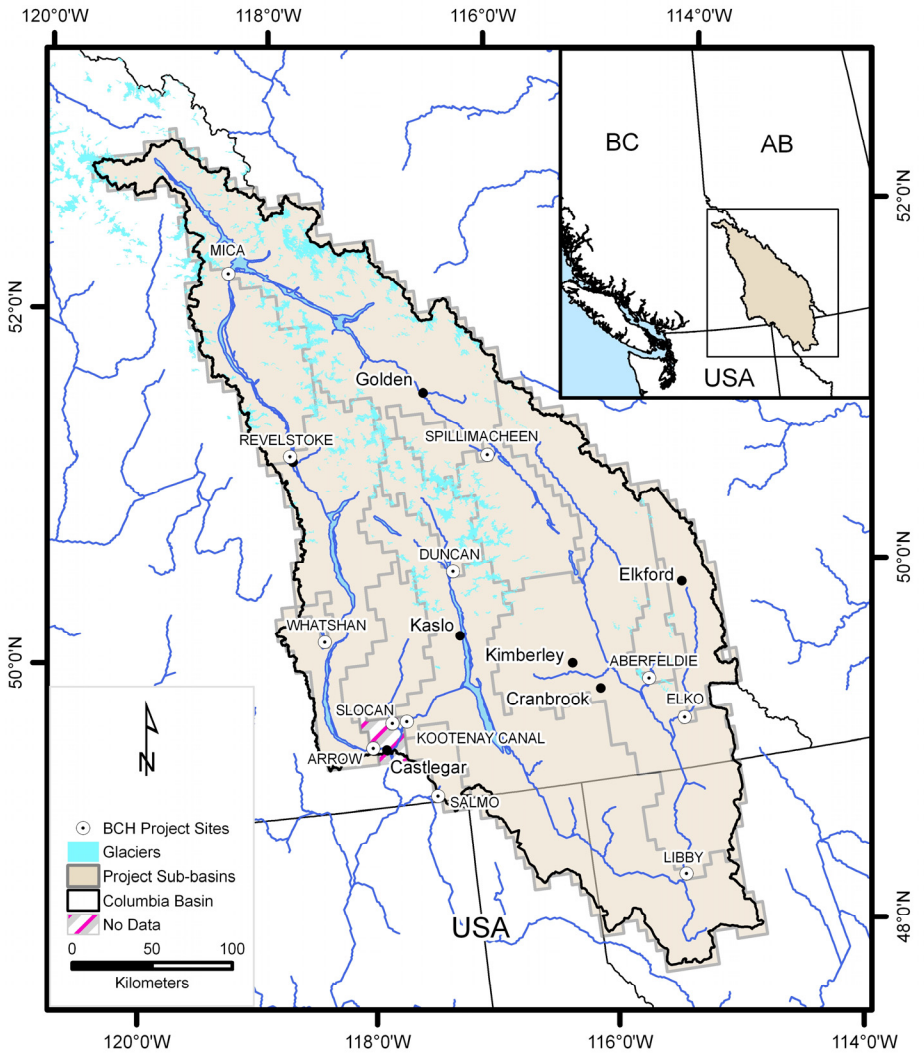

Figure 2-8. Upper Columbia River study area, showing the basin outlines and study site locations (with VIC model 1/16° sub-basin outlines).

Table 2-2. Description of Project Sites.

Study Area	Project Name	VIC ID	Storage	Project Site Location (decimal deg)[‡]	Local Drainage Area (km^2)	Local Elevation (m)			Local Glacier Cover (%)[#]
						min	med	max	
Campbell	Strathcona Dam	BCSCA	Upper Campbell Lake	50.55; -125.58	1193	139	978	2200	1.8
Peace	W.A.C. Bennett Dam	BCGMS	Williston Reservoir	56.02; -122.20	72078	515	1269	2711	0.2
Peace	Site C (Peace River above Pine)	PEAPN	n/a	56.20; -120.81	11822	418	922	2468	0.0
Peace	Peace near Taylor	PEACT	n/a	56.16; -120.66	17100	409	1097	2406	0.0
Columbia	Spillimacheen	SPINS	Run-of-river	50.90; -116.43	1430	783	1916	3171	7.6
Columbia	Mica Dam[§]	BCHMI	Kinbasket Reservoir	52.08; -118.55	21134	617	1851	3548	7.8
Columbia	Revelstoke Dam	BCHRE	Revelstoke Reservoir	51.07; -118.20	5253	536	1601	3322	4.5
Columbia	Keenlyside Dam[†]	BCHAR	Arrow Lake Reservoir	49.35; -117.78	10272	411	1504	3232	1.7
Columbia	Whatshan Dam	BCWAT	Whatshan Lake Reservoir	49.92; -118.13	393	685	1208	2282	0.0
Columbia	Aberfeldie (Bull River near Wardener)	BULNW	Run-of-river	49.48; -115.37	1530	914	1795	3136	3.3
Columbia	Elko Dam	BCHEL	Run-of-river	49.29; -115.10	3530	913	1866	3044	0.0
Columbia	Duncan Dam	BCHDN	Duncan Reservoir	50.25; -116.95	2426	548	1862	3038	5.9
Columbia	Kootenay Canal	BCHKL	Run-of-river	49.45; -117.52	20700	519	1402	3047	0.2
Columbia	Slocan River	SLONC	n/a	49.46; -117.56	3320	481	1611	2639	1.3
Columbia	Salmo River	SALNS	n/a	49.05; -117.29	1230	610	1487	2285	0.0

[‡] Coordinates given in decimal degrees; northing then easting
[§] Includes Spillimacheen (SPINS)
[#] Source: Baseline Thematic Mapping, version 1 (c. 1995)
[†] Includes the Coursier and Walter Hardman projects

3. VIC Model

3.1 Description

The Variable Infiltration Capacity (VIC) hydrologic model (Liang et al. 1994 and 1996) was used to quantify the hydrologic impacts of climate change within the Peace, Campbell and Upper Columbia basins. The VIC model is a spatially-distributed macro-scale hydrologic model that was originally developed as a soil-vegetation-atmosphere transfer scheme (SVATS) for global climate models (GCMs). The VIC model has been previously applied to evaluate climate change impacts on global river systems (Nijssen et al. 2001), in the Canadian portion of the Columbia River Basin (Hamlet and Lettenmaier 1999; Payne et al. 2004) and in the mountainous western United States (Christensen et al. 2004; Hamlet et al. 2005; VanRheenen et al. 2004; Elsner et al. 2010). The version of the VIC model applied in this study is 4.0.7. Some distinguishing features of this version of the VIC model include (Figure 3-1):

- multiple-layer characterization of the soil column (three in the Peace, Campbell and upper Columbia applications);
- subgrid variability in soil infiltration (and fast surface runoff), represented by a spatial probability distribution;
- drainage from the lower soil layer (baseflow) as a nonlinear recession;
- subgrid variability in land surface vegetation classes;
- subgrid variability in topography represented using elevation bands;
- multiple soil rooting zones and variable root distribution;
- multi-layer energy balance snow model incorporating canopy effects (e.g., attenuation of wind and solar radiation, canopy interception and sublimation) (Storck and Lettenmaier 1999);
- wet canopy evaporation, dry canopy transpiration and bare soil evaporation represented using the Penman-Monteith approach and including canopy effects to wind profile and surface radiation (Wigmosta et al. 1994).

For this study the VIC model has been applied at a resolution of 1/16° (approximately 27-31 km^2, depending upon latitude) and used to quantify streamflow impacts for sub-basins in the study areas ranging in area from 393 to 101,000 km^2. Using the specified boundary conditions and initial states, the VIC model solves the 1-dimensional water and energy balance for each grid cell.

The VIC model operates at such a spatial resolution that moisture and energy fluxes between neighboring grid cells can reasonably be considered negligible. Therefore, there is no transfer of water and energy across grid cell boundaries. However, this assumption means that the VIC model does not explicitly represent the mass and energy balance and dynamics of spatially contiguous 'regional' storage features such as large (i.e., multi-cell) lakes, glaciers or aquifers. Although the VIC model does not explicitly include glacier processes, the occurrence and change in glacier mass on a grid cell basis can nevertheless be mimicked using snow process modelling (described in Section 3.7).

The VIC model was run at a daily timestep (one-hour timestep for the snow model), generating daily baseflow and "fast" runoff fluxes from each grid cell (Figure 3-1). These fluxes were then collected and routed downstream using an offline routing model, the details of which can be found in Lohmann et al. (1996). Surface routing through the channel network is the only means by which water moves between grid cells. Note that routing does not include the effects of regulation, extraction or diversion and, as such, represents 'natural' flow conditions. Set-up and preparation of the VIC model requires construction of the driving data (Section 3.2), specification of soil properties (Section 3.3), land cover (Section 3.4), topography (Section 3.5), surface routing (Section 3.6), glacier state (Section 3.7), and model calibration and validation (Section 3.8).

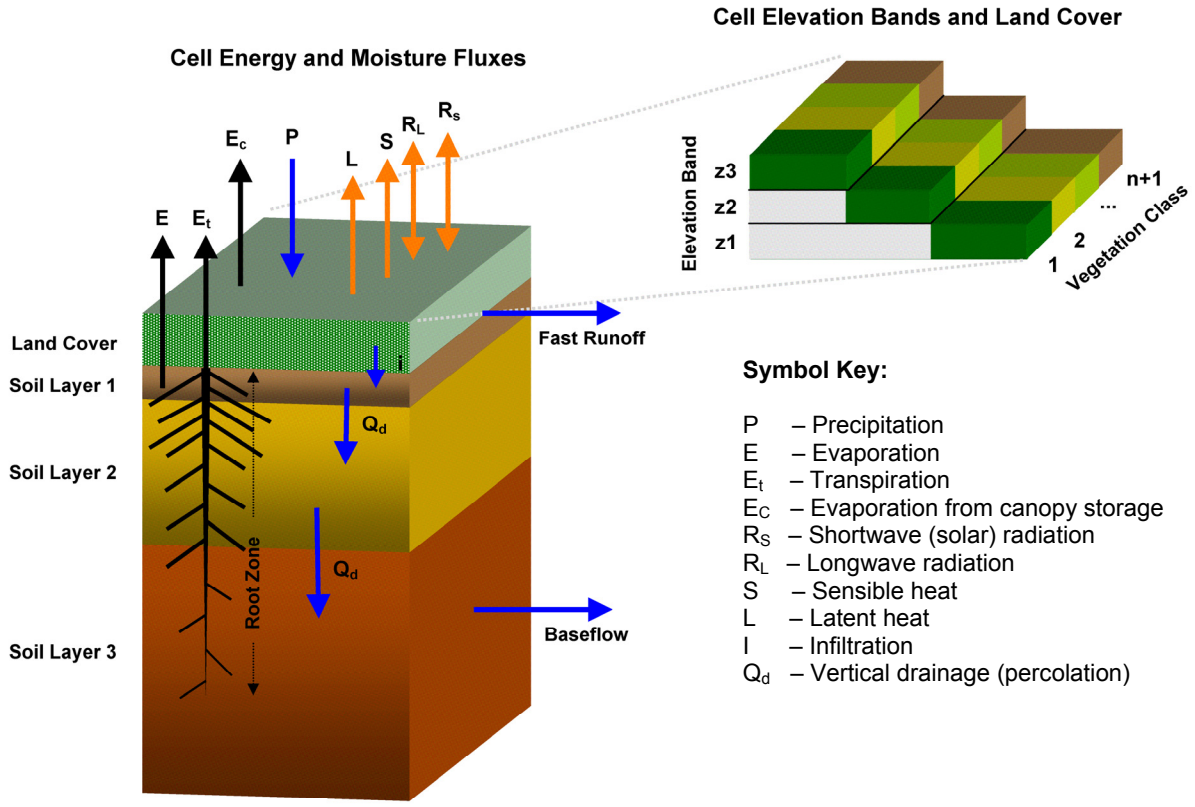

Figure 3-1. Conceptual representation of the Variable Infiltration Capacity (VIC) model, showing energy and moisture fluxes for a single computational grid element. Also shown is the apportionment of the grid cell "surface" to account for topography and land cover. In this example three land cover classes (plus the default base soil class) are divided amongst three elevation bands of increasing median elevation *z*1, *z*2 and *z*3. Note that land cover area fractions in each elevation band are identical. (Figure adapted from Department of Civil and Environmental Engineering, University of Washington; http//www.hydro.washington.edu/Lettenmaier/Models/VIC/).

3.2 Forcing Data (Observed)

Although hydrologic projections are simulated by forcing the model with downscaled GCM projections, calibration of both the hydrologic model and BCSD requires observed forcing data. This forcing data is in the form of daily gridded surfaces of maximum and minimum temperature, precipitation and daily average wind speed at the spatial resolution of 1/16°. The generation of the daily surfaces followed the technique described by Maurer et al. (2002) and Hamlet and Lettenmaier (2005). Raw temperature and precipitation surfaces were created by gridding daily station observations collected during the period 1950 through 2006 using the SYMAP algorithm (Shepard 1984). Daily temperature and precipitation observations were obtained from Environment Canada (EC), the US Co-operative Station Network, the British Columbia Ministry of Forests and Range's Fire and Weather Network, the British Columbia Ministry of Environment's Automated Snow Pillow (ASP) network, and BC Hydro's climate network. Any spurious trends or artifacts in the raw interpolated data, introduced by changes in collection techniques, station relocations or inclusions of stations with different record lengths, were corrected by making the interpolated fields temporally consistent with data from the Historical Canadian Climate Database (AHCCD; Mekis and Hogg 1999; Vincent and Gullett 1999) and the US Historical Climate

Network (USHCN, Hughes et al. 1992; Easterling et al. 1999). The interpolated data is lastly corrected for elevation effects by adjusting the climatology of the interpolated fields of temperature and precipitation to the 1961-1990 PRISM climatology of western Canada (Daly et al. 1994) interpolated to higher resolution (15-arc seconds) using Climate Western North America (ClimateWNA, http://www.genetics.forestry.ubc.ca/cfcg/ClimateWNA/ClimateWNA.html, Hamann and Wang 2005; Wang et al. 2006). This interpolation and gridding technique maintains as much of the spatial information as possible from the relatively high-density EC station observations, while still adjusting the time series characteristics of the gridded data such that they are consistent with the time series characteristics of the smaller number of highly quality controlled and homogenized AHCCD and USHCN stations. Daily wind speed surfaces were generated by re-gridding estimates of 10-m wind speed from the National Centers for Environmental Prediction-National Center for Atmospheric Research (NCEP-NCAR) reanalysis (Kalnay et al. 1996).

Additional meteorological 'drivers', which include daily solar (direct and diffuse) and longwave radiation and dewpoint temperature, are also required as input by the VIC model. If not supplied as input (as was the case for this project) these variables are calculated by the VIC model at runtime from the supplied (downscaled or observed) time series of daily temperature and precipitation using techniques described in Maurer et al. (2002). Generally, dewpoint is derived using relationships with daily minimum temperature and precipitation; downward shortwave radiation is estimated from the diurnal temperature range, dewpoint temperature and precipitation; and downward longwave radiation is estimated from daily air temperature and the dewpoint temperature (Thorton and Running 1999; Kimball et al. 1997).

3.3 Soil Cover

Soil parameters are defined explicitly for each grid cell. Although most of the soil parameters nominally represent physical properties, the resolution of the model is such that the parameters mainly provide "effective" values, intended only to give a plausible representation of the grid-cell average soil properties and large-scale spatial variability. Additionally, the values of the soil parameters that govern fast runoff and baseflow generation, which is represented conceptually in the VIC model, are estimated during model calibration (see Section 3.8). Soil classification and parameterization was based primarily on physical soil data from the Soils Program in the Global Soil Data Products CD-ROM (GSDT 2000). The soils data contained in the Soils Program are from a global pedon-database produced by the International Soil Reference and Information Centre (ISRIC) (Batjes 1995) and the FAO-UNESCO Digital Soil Map of the World (DSMW) (FAO 1995). Physical soils parameters were extracted from the soils program, interpolated from 5x5 arc-minutes (1/12°) to the 1/16° VIC grid, and then used to generate the remaining values required to run the VIC model. Parameters such as hydraulic conductivity, bulk density, porosity, wilting point, and soil textures (i.e., sand, silt, and clay content) are extracted or derived by the soils program. Some of these soil properties are contained within the soils program's pedon[9] records, while others are derived from the primary data via pedotransfer[10] functions (Scholes et al. 1995). For instance, the parameters that define several soil water properties (such as saturated hydraulic conductivity) are estimated for each horizon in the global pedon database using the neural network analysis models of Schaap et al. (1998). Soil bulk density was estimated as per Kern (1995) and soil field capacity and wilting point were estimated as per van Genuchten (1980). Once all soils parameters are extracted from the soils program and interpolated to the model scale, further parameters were calculated from the

[9] A pedon is the smallest element of landscape that can be called soil, which generally has an area from one to 10 square metres.

[10] Pedotransfer function, which is a term commonly used in soil science literature, is a predictive function of certain soil properties from other more readily available, easily, or routinely measured properties.

observed Soils Program information. Field capacity was estimated from the Cosby et al. (1984) lookup table, based on the USDS soil texture triangle. These parameters were then used to calculate other hydraulic properties of the soil, such as soil density, initial soil moisture, residual soil moisture, and bubbling pressure of the soil. Average grid-cell elevations were specified in the soil file and were derived from a post-processed version (version 3) of the Shuttle Radar Topography Mission (SRTM)-based 90-m digital elevation model (Farr et al. 2007) downloaded from the Consultative Group on International Agricultural Research – Consortium for Spatial Information (CGIAR-CSI) website (http://srtm.csi.cgiar.org/). The depth of the first and second soil layers was set uniform across all grid cells at 0.1 m and 0.3 m, respectively. The depth of the third soil layer, *d3*, varies spatially and was estimated at 1/16° resolution using a DEM-based algorithm (K. Westrick, unpublished algorithm, University of Washington) that relates soil depth to elevation and slope, constrained by arbitrary minimum and maximum depth limits as:

$$d3 = d_{min} + (d_{max} - d_{min}) \left\{ 0.5 \left[1 - \left(\frac{s_{temp}}{s_{max}} \right)^{0.25} \right] + 0.5 \left[1 - \left(\frac{z_{temp}}{z_{max}} \right)^{0.75} \right] \right\} \quad (1)$$

where

$$s_{temp} = \begin{cases} s, & s \le s_{max} \\ s_{max}, & s > s_{max} \end{cases}$$

$$z_{temp} = \begin{cases} z, & z \le z_{max} \\ z_{max}, & z > z_{max} \end{cases}$$

and s is grid cell slope (%), z is grid cell elevation (m), d_{min} is 0.1 m, d_{max} is 3.4 m, s_{max} is 30% (algorithm default value) and z_{max} is 3000 m (algorithm default value).

3.4 Land Cover

Land cover within the VIC model is described by assigning vegetation classes to each model grid cell. A cell can have more than one vegetation class and, in such cases, vegetation classes are assigned a fractional area of the grid cell. If elevation bands are present (Section 3.5), vegetation classes are assigned to a fraction of each band based on the grid cell fraction. Geographic locations or configurations of land cover types are not considered, and the VIC model combines all patches of the same cover type into one tile per elevation band (Figure 3-1). Fluxes and storages from the tiles are averaged together (weighted by area fraction) to give a grid-cell average for writing to output files. In addition to several vegetation classes, the VIC model has an internal default bare soil class which is invoked when portions of a grid cell are not covered in vegetation (Liang et al. 1994).

Land cover information from the Earth Observation for Sustainable Development of Forests (EOSD) project (see http://cfs.nrcan.gc.ca/subsite/eosd/home) was used as the basis for the VIC land cover classification. The EOSD land cover mapping was produced by the Canadian Forest Service in partnership with the Canadian Space Agency, and is based on circa-2000 imagery (Wulder et al. 2003 and 2008). We used a post-processed version of the original 25-m resolution EOSD data set, which is upscaled to 1-km resolution by taking the modal 25-m occurrence class in each target grid cell. This "majority 1km" product was obtained directly from the Pacific Forestry Centre, from the EOSD Land Cover Diversity dataset (unpublished data provided by J. White, Pacific Forestry Centre, Natural Resources Canada, 2009). Voids or no data values in the original EOSD classification were filled using the University of Maryland's Advanced Very High Resolution Radiometer (AVHRR)-based Global Land Cover Classification data (http://glcf.umiacs.umd.edu/data/landcover/data.shtml). Vegetation classes

include bryoids, herb, shrub (low and tall), wetland (treed, shrub and herb), coniferous forest, deciduous forest, mixed forest and bare soil. Forest (i.e., treed) vegetation classes are further classified by vegetation density and categorized as dense, open or sparse.

A vegetation library defines common parameters for each vegetation class. An overstory is assigned to all treed vegetation classes; all remaining classes do not contain overstory vegetation. The presence of an overstory triggers canopy attenuation of wind and radiation. Leaf area index (*LAI*), which effectively describes the density and vigor of the vegetation cover (Ryan et al. 1997), is an important vegetation parameter. *LAI* affects precipitation interception (and subsequent evaporation), transpiration (via canopy resistance), and the below-canopy energy balance (via radiation attenuation). *LAI* values were calculated for each vegetation class and month from a Canada-wide, 1-km resolution time series of 10-day *LAI* composites produced by Natural Resources Canada, which were derived from SPOT-4 VEGETATION satellite-based observations collected from April through October, 1998 to 2004 (Fernandes et al. 2003). VIC *LAI* parameter values were estimated from year 2000 data, as this is the same capture year of the EOSD land cover. Although large areas of forest in the BC interior have experienced defoliation due to the effects of mountain pine beetle over the *LAI* capture period (Westfall and Ebata 2007), the extent of the mountain pine beetle infestation during the 2000 capture year was sufficiently limited in area (BC Ministry of Forests and Range 2009) that *LAI* values are not expected to exhibit noticeable bias. Values for *LAI* range from 1.4 m^2/m^2 to 4.1 m^2/m^2 for treed vegetation classes and 0.6 m^2/m^2 to 2.8 m^2/m^2 for non-treed vegetation, with values increasing alongside increasing vegetation density and maximum values occurring in summer and minimum values in the winter. The VIC model estimates the fraction of shortwave radiation transmitted by the overstory as a function of *LAI* using the Beer-Lambert model (Liang et al. 1994), where the parameter controlling the rate of radiation attenuation is taken from Schnorbus et al. (2010). Roughness and displacement height of vegetation were set as functions of vegetation height (Campbell and Norman 1998), where values range from 0.4 m to 1.5 m and 0.2 m to 11.2 m, for roughness and displacement, respectively. Vegetation architectural and resistance parameters, which control transpiration, were taken from Ducoudré et al. (1993) and Shuttleworth (1993). Minimum canopy resistance values are fairly conservative, ranging from 100 s/m to 150 s/m across all vegetation classes, where resistance is higher for treed vegetation, and increases alongside increasing vegetation density. Land cover albedo values were obtained from Bras (1990), Campbell and Norman (1998) and Roberts (2000), where values are lowest for coniferous vegetation (0.12) and highest for non-treed vegetation and bare ground (0.18 to 0.2). Values for the *RGL* parameter, which is the approximate point at which stomatal resistance is equal to twice the minimum stomatal resistance, were taken from Dickenson et al. (1991) and Roberts (2000). Values for *RGL* range from 100 W/m^2 for bryoids and herbs to 30 W/m^2 for coniferous vegetation. Rooting depths and root distributions were also specified for each vegetation class, such that short vegetation draws moisture mainly from the upper soil layer while trees draw moisture from deeper soil layers (Jackson et al. 1996).

Forests, the dominant land cover in the study areas, are dynamic ecosystems wherein the physical components change over time scales of decades and centuries in response to physical, biotic and anthropogenic processes (Kimmins 2005), such that land cover is a transient state. Additionally, climatic change is anticipated to also have an influence on future forest dynamics, affecting the evolving state of land cover and its influence on the hydrologic cycle. Some examples include species shifts or migration (Malcolm et al. 2002; Walther et al. 2002; Gonzalez et al. 2010) or altered disturbance regimes (e.g. wildfire frequency and pests) in response to climate change (Carroll et al. 2006; Dale et at. 2001; Flannigan and Van Wagner 1991; Gavin et al. 2007; Logan and Powell 2001; Marlon et al. 2009), or by possible changes in tree physiology or water-use efficiency due to changes in atmospheric CO_2 concentration (Gedalof and Berg 2010; Huang et al. 2007). Nevertheless, due to the non-trivial and somewhat speculative nature of back-casting historical and projecting future transient forest properties, it is well outside the scope of the current project to incorporate dynamic land cover. Consequently, forest cover is assumed static at circa-2000 conditions and both vegetation parameters and the spatial distribution of vegetation classes are stationary throughout the projection timeframe (1950-2098).

3.5 Topography

In areas of high relief, variation in sub-grid topography is simulated via the application of elevation bands within each VIC model grid cell. The elevation bands are used to improve model performance in areas of complex topography, where the effect of elevation dominates variations in local climate in general, and snow pack accumulation and ablation in particular (Barry 1992). Geographic locations or configurations of elevation bands are not considered explicitly, and the VIC model combines all areas of common elevation range into one band. Fluxes and storages from the bands are averaged together (weighted by area fraction) to provide grid-cell average values. However, the band-specific values of some variables can be written separately to output.

Grid cell elevations and elevation band information was derived from the CGIAR-CSI SRTM 90-m DEM, re-sampled to 15-arc seconds resolution (approximately 500 m) using bi-linear interpolation. Elevation bands were created by sampling the 225 high-resolution DEM cells within each 1/16° VIC model cell. The VIC model grid cells were divided into a maximum of five elevation bands, with the number of bands ranging from one in cells with low relief to five in cells with high relief. The number of bands per cell was constrained such that the difference in mean elevation between adjacent bands always exceeds 500 m.

During model runtime, input values of temperature and precipitation for each grid cell (as described in Section 3.2) are interpolated to each elevation band. Precipitation is adjusted for elevation by using a precipitation gradient, which is estimated by identifying the grid cell precipitation fractions in each elevation band based on the PRISM annual average precipitation climatology for 1961-1990 (interpolated to 15-arc seconds resolution using ClimateWNA). Within each elevation band, grid cell input temperature is lapsed to each individual band at a rate of 6.5 °C/km, applied over the difference between the mean band elevation and the mean grid cell elevation (which is specified in the soil parameter file).

3.6 Surface Routing

The routing model transports grid cell surface runoff and baseflow produced by the VIC model within each grid cell to the outlet of that grid cell (grid-cell routing) then into the river system (channel routing). A full description of the routing model methodology can be found in Lohmann et al. (1996, 1998a and 1998b). The in-grid dynamics of surface routing are described with a grid cell instantaneous response function (or *IRF* i.e., unit hydrograph), and is intended to capture the flow of water through the sub-grid surface runoff network to the grid cell 'outlet'. Channel routing (i.e., surface routing between grid cells) is done using the linearized Saint-Venant equations based on the model river networks shown in Figure 3-2 through Figure 3-4. The surface routing network is conceptually defined by specifying a flow direction and distance for each 1/16° model grid cell. A dominant flow direction is specified for each cell, in the sense that although the area represented by a grid cell may in reality have several rivers flowing in different directions, only one flow direction can be specified. Channels can flow in one of eight directions: north, north-east, east, south-east, south, south-west, west or north-west. For a grid cell of actual dimensions Δx by Δy, channel length is the horizontal (Δx; east or west flow directions), vertical (Δy; north or south flow directions) or diagonal ($\sqrt{\Delta x^2 + \Delta y^2}$; north-east, south-east, south-west and north-west flow directions) flow distance in each grid cell. Note that the actual horizontal and diagonal flow distance is not constant between grid cells, but varies with latitude. The Saint-Venant equations are parameterized by specifying values of flow velocity (i.e., wave celerity) and flow diffusion for each grid cell. Routing parameters were assigned by classifying routing segments as either river channels or natural lakes (e.g., Duncan Lake, Kootenay Lake and Arrow Lakes), with separate parameter sets for each. Values of flow velocity and diffusion were adopted from Schnorbus et al. (2010). Surface routing

assumes natural (i.e., unregulated) flow; consequently man-made reservoirs (i.e., Revelstoke Reservoir and Lake Koocanusa) are treated as river channels.

For the purpose of estimating streamflow at some point of interest, the study domain was divided into sub-basins, where a sub-basin represents the area upstream of a given point and identifies which VIC cells' fluxes must be integrated to generate streamflow. For instance, the sub-basin outlines for the various project sites are identified in Figure 3-2, Figure 3-3 and Figure 3-4 for the Peace, Campbell and Upper Columbia study areas, respectively. Due to the effects of storage regulation, which from a management perspective effectively divides natural drainages into separate independent sub-basins, streamflow projections at the project sites are based on discharge generated from the local drainage area only (i.e., absent inflow from upstream project sites). For instance, streamflow for the Peace River above Pine (PEAPN) is based on runoff and baseflow generated from grid cells upstream of PEAPN but downstream of BCGMS (Figure 3-2). An exception includes the run-of-river project sites (SPINS, BULNW and BCHEL), which are included as part of the local drainage of the immediate downstream project site. A schematic of the network topology of all project sites for the Peace and Upper Columbia study areas are shown in Figure 3-2 and Figure 3-4, respectively (the Campbell has only the single project site). Although projections for the Kootenai[11] River at Libby Dam (BCHLB) are not included in this report, projections for the BCHKL project site are based on local inflow generated downstream of this site.

As raw model streamflow at a point is based on runoff and baseflow integrated from all upstream model cells, local streamflow for any given project site had to be isolated using

$$Q_{loc}(t) = Q_{out}(t) - \sum_{i=1}^{n} \left(\int_0^t Q_{in,i}(t-s) h(x_i, s) ds \right), \quad (2)$$

where $Q_{out}(t)$ and $Q_{in,i}(t)$ are, respectively, total streamflow at a given project site and streamflow from upstream project sites $i = 1, 2, \ldots, n$ at time t, x is the routing distance, and $h(x, t)$ is the impulse response function of the channel routing model (Lohmann et al. 1996). For locations with short routing distances and where routing times are substantially shorter than one day (e.g., PEAPN to PEACT or BCHMI to BCHRE), (2) was simplified to

$$Q_{loc}(t) = Q_{out}(t) - \sum_{i=1}^{n} Q_{in,i}(t). \quad (3)$$

[11] This refers to a site in the US portion of the Kootenay River basin, hence the US spelling of the river is employed.

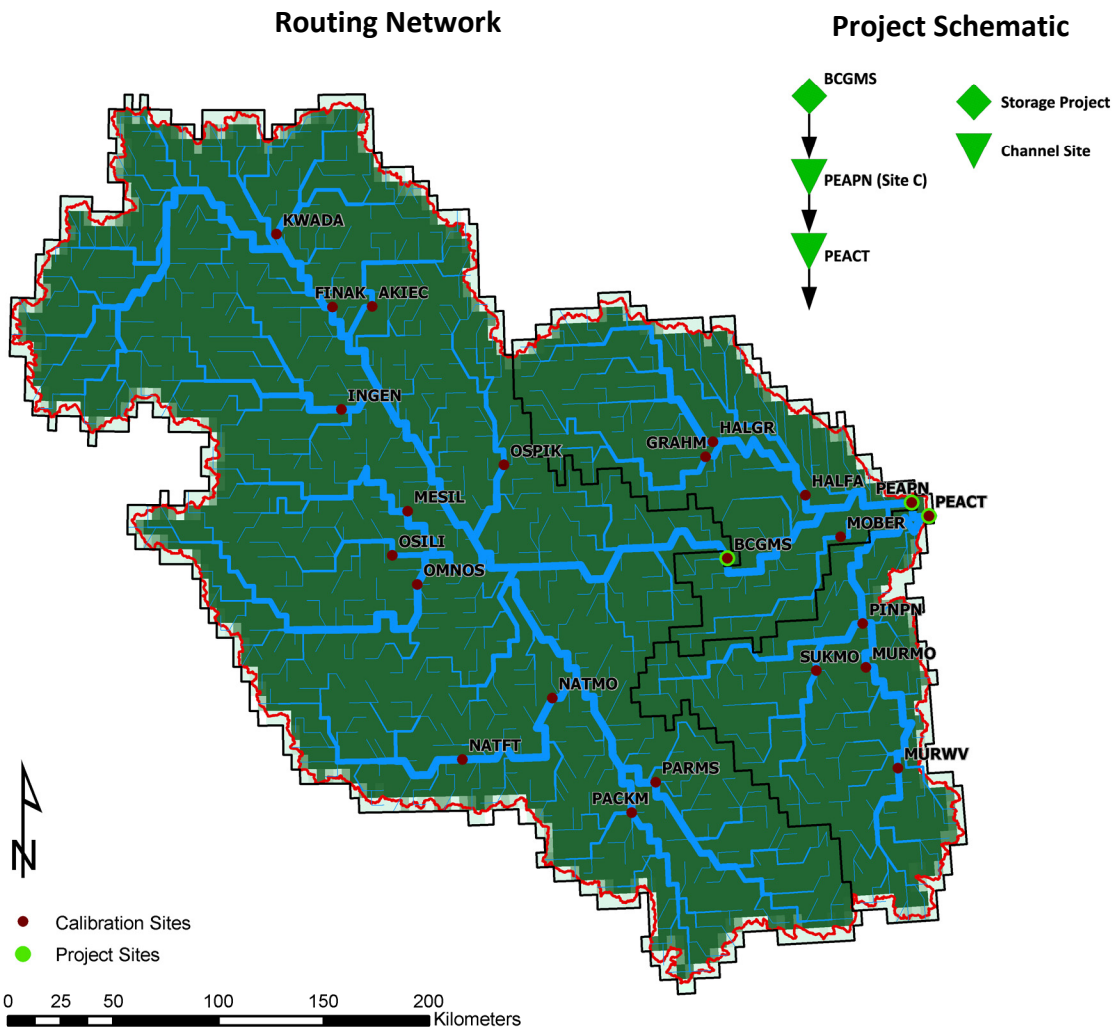

Figure 3-2. VIC model 1/16° surface routing network and project site schematic for the Peace River study area. The width of the routing network, shown in blue, is proportional to the upstream drainage area. Also shown is the 1:20K study area outline (red line), the model basin outlines for the Bennet Dam, Peace at Pine and Peace at Taylor project sites (black line), the location of the project sites and calibration sites. Background color denotes the drainage flow fractions (proportion of flow from each grid cell that is routed through the channel network), which range from 1.0 (dark green) to 0.004 (light green). Note that, in order to clarify the presentation, the routing network has been simplified be removing zero-order segments. The project site schematic (inset figure) shows the routing topology between project sites.

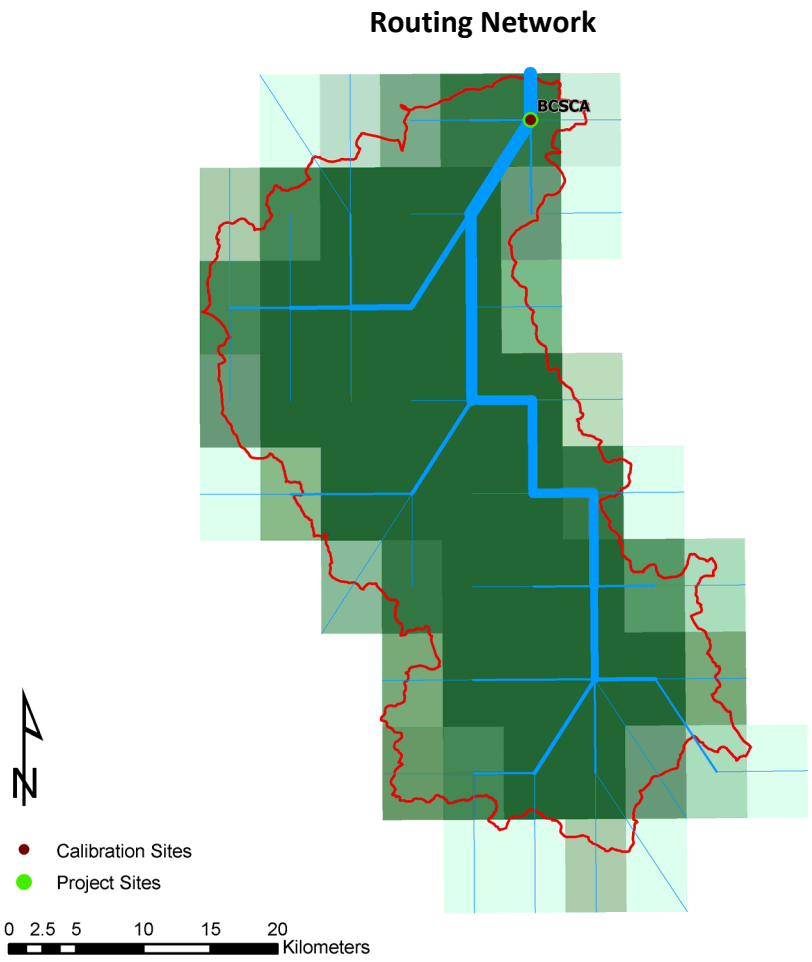

Figure 3-3. VIC model 1/16° routing network for the Campbell River study area, where the width of the routing network, shown in blue, is proportional to the upstream drainage area. Also shown is the 1:20K study area outline (red line), the model basin outline (black) and location for the Strathcona Dam project site. Background color denotes the drainage flow fractions (proportion of flow from each grid cell that is routed through the channel network), which range from 1.0 (dark green) to 0.004 (light green).

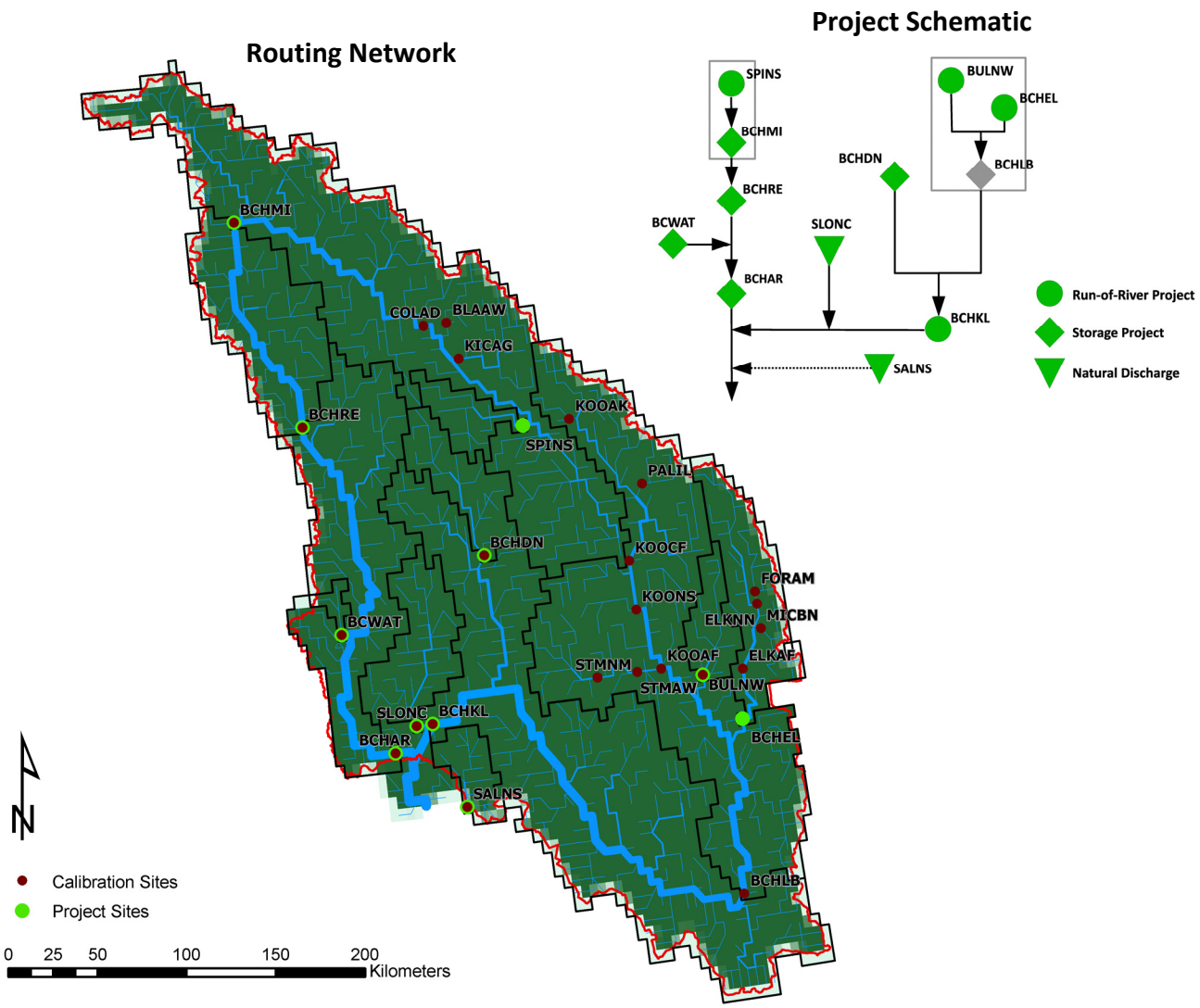

Figure 3-4. VIC model 1/16° routing network and project site schematic for the Upper Columbia study area. The width of the routing network, shown in blue, is proportional to the upstream drainage area. Also shown is the 1:20K study area outline (red line), and the model basin outlines (black line) and locations of the project sites, and locations of the calibration sites. The background color denotes the drainage flow fractions (proportion of flow from each grid cell that is routed through the channel network), which range from 1.0 (dark green) to 0.004 (light green). Note that, in order to clarify the presentation, the routing network has been simplified be removing zero-order segements. The project site schematic (inset figure) shows the routing topology between project sites.

3.7 Glaciers

A conceptual representation of glacier mass balance has been introduced into the VIC model, specifically for projecting the hydrologic response in the Upper Columbia system. Glaciers are modelled very simplistically using excess snow water to mimic glacier ice, where the snow water in certain cells is augmented, or increased, using the VIC model's state file structure. Specific VIC model cells in the Upper Columbia study area have been identified as glacier cells, forming a glacier mask. The glacier mask assumes that any VIC model grid cell with more than 33% of its area composed of glaciated terrain, based on the 1:250,000 Baseline Thematic Mapping (BTM) version 1 land cover dataset (BCILMB 1995), is a "glacier" cell. This process provides a glacier mask for circa-1995 (the approximate capture date of the BTM data) composed of 135 grid cells (Figure 3-5). The glacier mask captures the larger, more spatially contiguous areas of ice cover, but filters out the smaller and more spatially distributed glaciers in the southern portion of the study area. A threshold of 33% of grid cell area was chosen such that the actual glacier surface area and the area of the VIC glacier mask for the Upper Columbia domain were roughly equivalent (3,770 km^2 versus 3,600 km^2, respectively). The additional water equivalent required to "add" glaciers to these grid cells was estimated from volume-area scaling (Bahr et al. 1997*;* Stahl et al. 2008) based on the glacier surface areas in the original BTM dataset. The estimated glacier volume was converted to an equivalent depth (assuming an average glacier ice density of 700 kg/m^3) (Schiefer et al. 2007), which was then normalized by grid cell area (Figure 3-5) and scaled for elevation and area fraction for individual snow bands in each grid cell (Figure 3-6). The subsequent glacier ice water equivalent for each snow band in each glacier cell is introduced back into the VIC model using the VIC model's initial state file. This 1995 "glacier state" was used for calibration of the Upper Columbia sub-basins (Section 3.7). Glacier dynamics (i.e., adjustments of glacier size/area in response to mass balance changes) are not explicitly represented. However, the potential loss or accumulation (in the form of perennial snow) of glacier ice from individual grid cell elevation bands would implicitly represent (albeit simplistically) changes in glacier area in response to mass balance changes over the Upper Columbia domain as a whole. As snow is used to mimic glaciers, model output does not explicitly distinguish glacier runoff from snowmelt runoff.

Hydrologic projections for the Upper Columbia study area require specification of a glacier state for the 1950 start year. Two options were considered. Option one is to extrapolate a 1950 glacier state, which could be accomplished by adding 20 m water equivalent to the 1995 glacier state. The figure of 20 m water equivalent is based on the regional cumulative mass balance between 1960 and 1995 estimated using observations from northwest US and south-west Canada (Dyurgerov and Meier 2005; Kaser et al. 2006). Unfortunately, as we have no simple means of estimating glacier area for 1950, the added mass would need to be added to the 1995 footprint. Nevertheless, in such a case, the transient runs would start at 1950 with a 1950 glacier state and "free-run" uninterrupted to 2098. However, due to uncertainty in specifying both the 1995 and 1950 glacier states (mass as well as area), and the simple method by which glaciers are represented in the VIC model, there appears to be little advantage to the added "realism" of trying to back-cast an initial state for 1950. As well, due to a lack of glacier dynamics in this simplified representation, there is concern that the glacier cells may experience some mass drift if allowed to free run during the entire simulation period. Therefore, the second option considered was to: a) conduct historic runs from 1950 to 1995, starting with 1995 glacier state on October 1, 1950, and b) conduct future runs from 1995 to 2098, re-initializing glacier cells with the observed 1995 glacier state on October 1, 1995. Option two was the adopted method for Upper Columbia hydrologic projections. Therefore, unlike the transient runs for the Peace and Campbell study areas, which run uninterrupted from 1950 to 2098, the Upper Columbia projections are a combination of both a pre- and a post-1995 transient simulation.

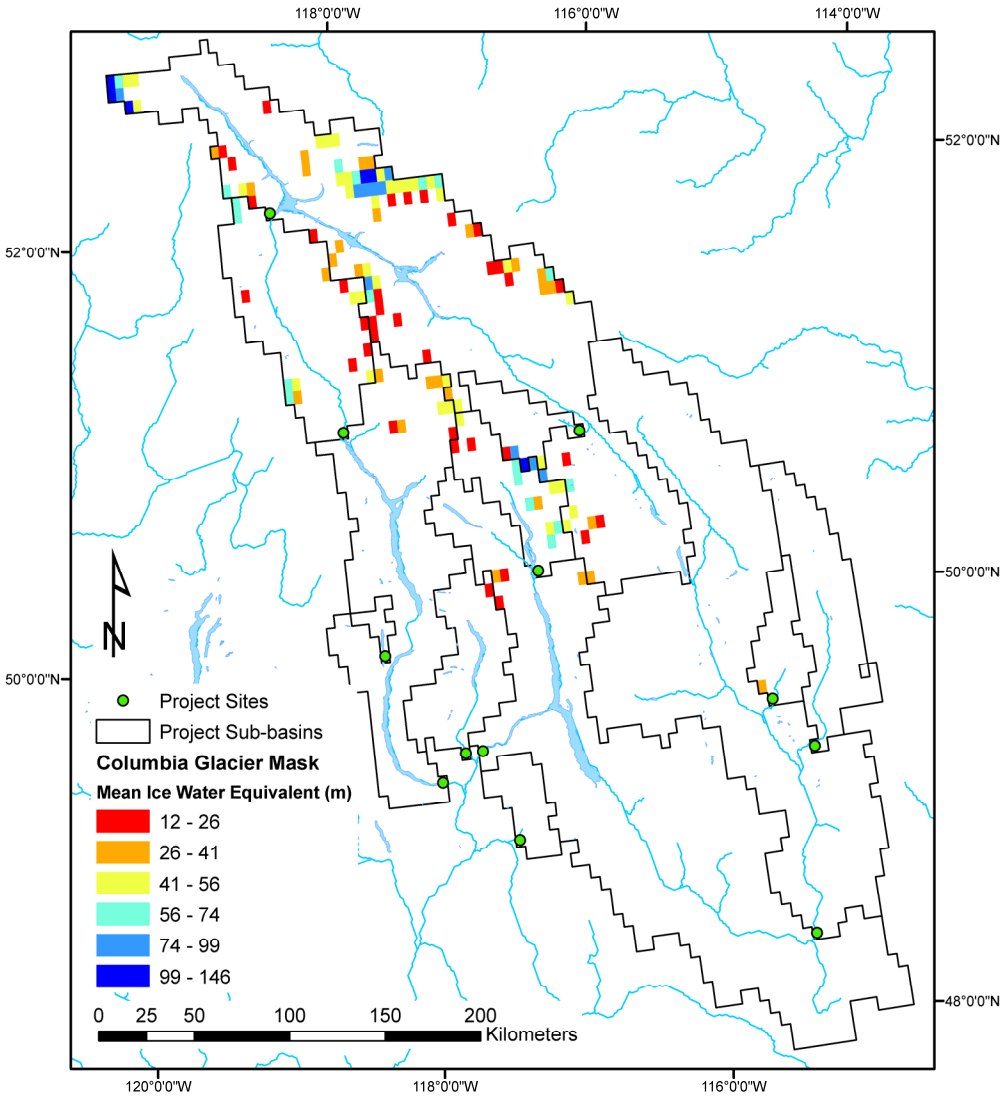

Figure 3-5. Glacier mask (circa-1995) showing VIC model cells identified as glaciers and estimated mean ice water equivalent in each cell.

The updating of the glacier state in 1995 is practically accomplished by taking the VIC model state captured on 30 September, 1995 and adjusting the band-specific snow water equivalent (SWE) values in glacier cells to conform to the 1995 "observed" glacier state. However, adjusting only the SWE, while simple and straightforward, effectively introduces an imbalance in the water and energy budget of the simulated snowpack (i.e., other model state values such as cold content, snow depth, etc. are not adjusted). In most cases, the effect is transient and the VIC model rapidly (within one month) re-balances the water and energy budget in the affected grid cells. Nevertheless, on rare occasions the adjustment causes numerical instability and the post-1995 transient simulation cannot be completed for that particular grid cell. This was the case for several grid cells in the BCHAR local drainage for all three (A1B, A2 and B1) of the CSIRO runs (see Section 4.3 for further details).

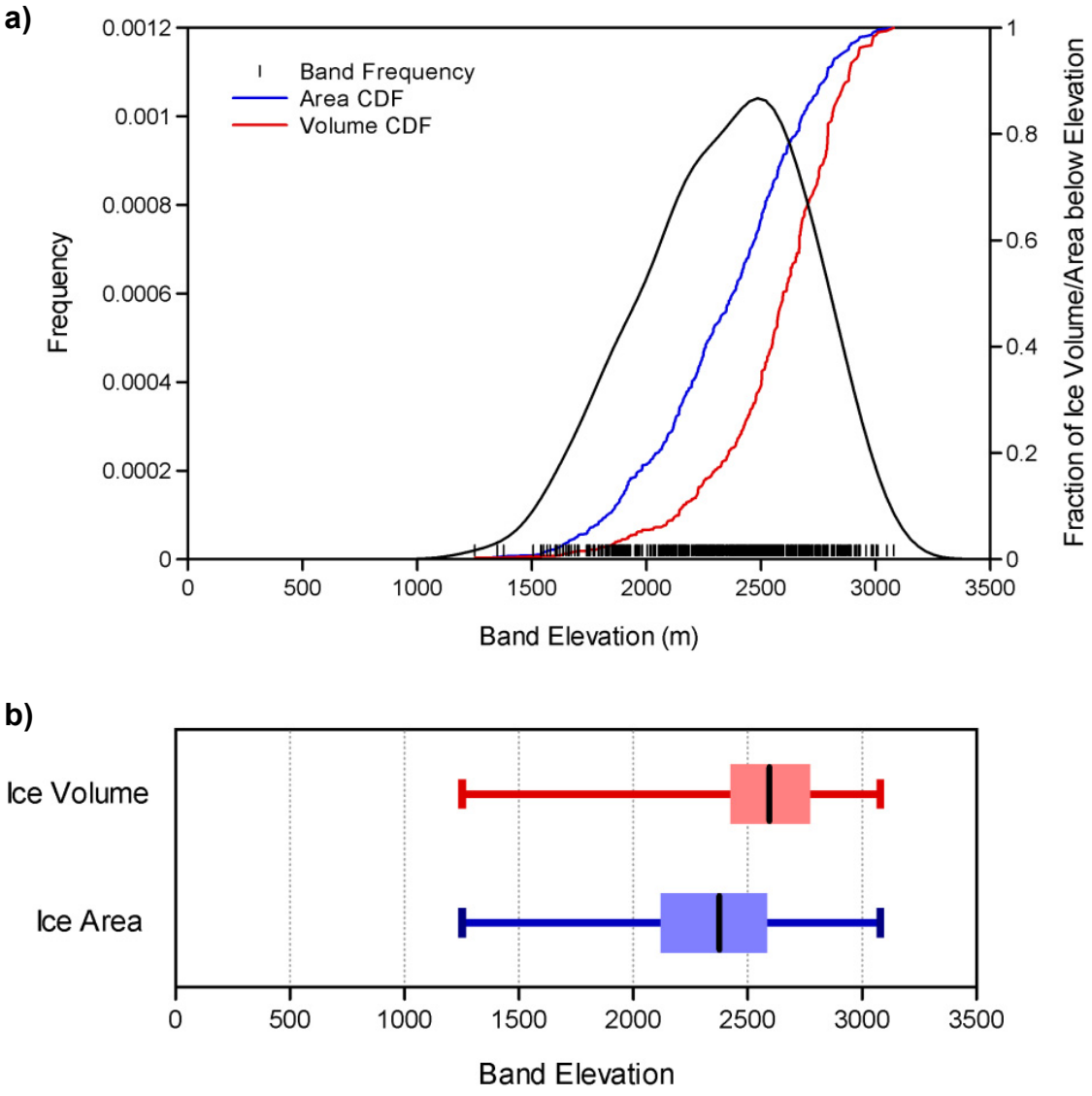

Figure 3-6. Elevation distribution of glacier area and volume for the estimated 1995 VIC glacier state shown as: a) glacier hypsometry (with frequency of VIC snow bands by elevation), and b) box-plots (median, inter-quartile range and maximum/minimum).

3.8 Calibration and Validation

3.8.1 Routing Model

Due to the effects of regulation, direct calibration of routing parameters in most of the study domain was not possible. Consequently the routing model was not calibrated for the Peace and Campbell applications and routing parameters were taken from Schnorbus et al. (2010) based on application of the same routing model to the Fraser River in central BC. Routing parameters for the majority of the Upper Columbia model domain were also taken directly from Schnorbus et al. (2010). The default channel routing parameters (specifically flow velocity and diffusion) for the unregulated stretch of the Columbia River main stem above Donald were found to be unsuitable, generally due to the meandering nature of the channel and the presence of many small lakes and wetlands. Parameters for this channel section were re-calibrated using an offline and simplified version of the routing model with observed discharge forming the upstream (inflow) and downstream (outflow) boundaries.

3.8.2 VIC Model

Model calibration involves the adjustment (by either manual or automated means) of various model parameters such that a desired simulated model output is in close agreement to observed output. Parameters within the VIC model can generally be classified as vegetation, soil or global. Vegetation parameters are specified in a vegetation library and are unique to each vegetation class (a given class can appear in more than one grid cell). Soil parameters are local in that they are specified by individual grid cell and can potentially be set to unique values for every grid cell (e.g., soil depth); although in practice many soil parameters are set as spatially uniform values corresponding to different soil classes. The VIC model also utilizes several global parameters that affect the entire model domain.

In practice, during calibration most parameters (vegetation, soil and global) are taken as 'measured' (e.g., soil depth, soil porosity, leaf area index, etc.) and are held fixed. Nevertheless, Schnorbus et al. (2010), who applied the VIC model in the Fraser River watershed, determined that they had to manually adjust several global model parameters affecting snow albedo decay and precipitation phase from their default values in order to improve simulation of snow accumulation and melt in the Fraser River region of BC. The albedo decay values of Schnorbus et al. (2010) have been adopted for our work in the Peace, Campbell and Columbia study areas. The temperature threshold parameters controlling precipitation phase (rain, snow or mixed rain-snow) were checked and, if necessary, adjusted manually based on initial calibration runs. The VIC model requires two threshold temperatures, T_s (the temperature below which all precipitation is snow) and T_r (the temperature above which all precipitation is rain). For temperatures between T_s and T_r, the proportion of precipitation as rain and snow is a linear function of temperature (i.e. rain and snow fractions are 50% each of precipitation for $T = (T_s + T_r)/2$). Rain and snow threshold temperatures are mainly a function of the thickness and temperature of the atmospheric layers (Gray and Prowse 1993), although cloud type, air mass movement and humidity have also been identified as important factors (Barry 1992; Kienzle 2008). Syntheses of surface weather observations in Canada (Bartlett et al. 2006) and the United States (Auer 1974) suggest that the temperature range for mixed rain/snow generally occurs between 0 °C and 6 °C on an annual basis, and those values appear appropriate for the interior basins of the Peace and Upper Columbia (the same values were used by Schnorbus et al. 2010 for application to the Fraser River basin). However, temperature thresholds are known to vary regionally (Barry 1992; Kienzle 2008) and preliminary calibration of the Campbell River application indicated that the temperature threshold in this coastal environment had to be changed to -0.5 °C to 4 °C. Temperature thresholds have been observed to increase with increasing elevation, reflecting locally steeper lapse rates (Barry 1992), which potentially explains the higher threshold temperatures in the higher-elevation Peace and Columbia basins (see Figure 2-4).

The main effort of model calibration involves adjustment of a small sub-set of five VIC empirical soil parameters. This calibration set is composed of those parameters that have been shown to have the highest sensitivity on VIC model runoff and discharge (Demaria et al. 2007). These parameters, *b_infilt*, *Ds*, *Ws*, *Dsmax* and *exp*, regulate infiltration, baseflow and transpiration. The *b_infilt* parameter controls the partitioning of net precipitation or snowmelt into surface (or quick) runoff and infiltration (and ultimately baseflow or evapotranspiration) and affects the high-frequency variability of the hydrograph. The *Ds*, *Ws* and *Dsmax* parameters control the rate of baseflow discharge as a function of soil moisture in the lowest (3^{rd}) soil layer and influence the overall magnitude and timing of the hydrograph. The baseflow curve also affects the rate of soil moisture storage change over time, which indirectly affects the volume of moisture available for transpiration. The *exp* parameter controls the variation of hydraulic conductivity as a function of soil moisture, which governs the rate of vertical percolation between the three soil layers.

Achieving a calibrated model by strictly adjusting soil parameters assumes that the interpolated precipitation, *P*, in the driving data is without error or bias. However, Schnorbus et al. (2010) noted that satisfactory calibration is often unachievable due to large biases in the interpolated precipitation data, such that they introduced a global precipitation adjustment, *Padj*, as a sixth calibration parameter. The *Padj* parameter is a precipitation multiplicative factor that is applied uniformly (and without seasonal variation) to grid-cell precipitation within a sub-basin (i.e. adjusted precipitation in grid cell *i* is $P_i' = Padj \cdot P_i$). Such biases in interpolated precipitation data are not unexpected due to the fact that grid-cell precipitation values are interpolated from a sparse climate network weighted towards lower elevations (Adam et al. 2006; Stahl et al. 2006) and precipitation gauges are subject to undercatch, particularly for solid precipitation (Adam and Lettenmaier 2003), which would tend to be more pronounced at high elevation stations where more precipitation falls as snow. Consequently, the application of precipitation bias correction factors is commonly required for modelling alpine hydrology, and bias correction factors are a common feature of hydrology models applied to the mountainous topography of BC (e.g., Quick 1995; Stahl et al. 2008).

Calibration of the six selected parameters was performed using the automated Multi-Objective Complex Evolution (MOCOM) method (Yapo et al. 1998). MOCOM is a technique that treats hydrologic model calibration as a multiple objective global optimization problem. As multi-objective problems tend not to have unique solutions, MOCOM converges to and provides the so-called Pareto set, which is the set of all parameter vectors that produce non-dominated values of the objective function vector. Application of MOCOM was based on three objective functions calculated using daily discharge, which were chosen to constrain different aspects of the streamflow regime. The first is the Nash-Sutcliffe Efficiency (*NS*; Nash and Sutcliffe 1970)

$$NS = 1 - \frac{\sum_{t=1}^{T}(Q_o^t - Q_m^t)^2}{\sum_{t=1}^{T}\left(Q_o^t - \overline{Q}_o\right)^2}, \tag{4}$$

where Q_o^t and Q_m^t are observed and modelled discharge, respectively, at time *t* and $\overline{Q}_o$ is average observed discharge over time $t = 1$ to T. Nash-Sutcliffe efficiencies can range from $-\infty$ to 1. An efficiency of $NS=1$ corresponds to a perfect match of modelled discharge to the observed data, an efficiency of $NS=0$ indicates that model predictive skill is as accurate as the mean of the observed data, whereas an efficiency less than zero ($-\infty<NS<0$) occurs when the observed mean is a better predictor than the model. The second objective function is the *NS* of the log-transformed discharge, *LNS*. This is equivalent to (4) except that the discharge values are substituted with the natural log-transformed values. The third objective function is the percent volume bias error which is

$$\%VB = 100 \cdot \frac{(\overline{Q}_m - \overline{Q}_o)}{\overline{Q}_o}, \quad (5)$$

where $\overline{Q}_m$ is the average modelled discharge. Model optimization was practically implemented by minimizing 1-*NS*, 1-*LNS* and |%*VB*|. These three objective functions tend to produce parameter sets that result in different simulated hydrographs. The *NS* function predominantly responds to the magnitude of phase and timing errors in daily discharge, but is also affected to a lesser degree by the presence of bias. The *NS* function tends to emphasize on high/peak flow periods and therefore produces parameters that optimize hydrograph performance during the freshet. The *LNS* objective tends to place more uniform emphasis through the entire flow range and therefore tends to generate parameter sets that have better hydrograph performance during the recession and low flow periods. The *%VB* objective strictly emphasizes volume conservation over the calibration period and is not sensitive to errors in streamflow timing or seasonality. The final optimized parameter vector for each sub-basin was chosen from the respective Pareto set in order to maximize, yet balance, both *NS* and *LNS* performance while still, where possible, keeping *%VB* within 10%.

Automatic calibration was based on the comparison of observed to simulated discharge at various locations. Although soil parameters are local, calibration to observed discharge (which is the integrated runoff from a given upstream area) required that the five calibration parameters were set uniformly across the calibrated sub-basin. As such, the emphasis during calibration was to fully exploit the distributed nature of the VIC model by dividing the study domain into as many sub-basins as practical in order to calibrate the model parameters in as spatially explicit a manner as possible. Nevertheless, division of the study areas was subject to the location and spatial density of Water Survey of Canada (WSC) and BC Hydro measurement sites with discharge records that satisfied the calibration requirements (drainage area > 400 km^2 and data available for 1985 through 1995; see below). In this fashion 23, 1, and 24 such sub-basins were identified for the Peace, Campbell and Upper Columbia study areas, respectively (Table 3-1, Figure 3-2, Figure 3-3 and Figure 3-4). Where possible, the VIC model was calibrated directly to discharge at each of the project sites listed in Table 2-2. However, due to lack of data, the model could not be calibrated directly to the Spillimacheen (SPINS) or Elko (BCHEL) project sites in the Upper Columbia. Although no data was available for the Aberfeldie project site, due to its proximity the WSC gauge site at the Bull River near Wardner (BULNW) was used as a proxy discharge record.

Due to the VIC model's structural paradigm, the planar morphology of each sub-basin is described based on the spatial arrangement of individual square (in latitude-longitude coordinates) computational grids. For relatively small basins, the geometry of the square grid can result in unrealistic basin morphology, which manifests as large errors in drainage area and the location of the drainage divide. Experience suggests that at a threshold drainage area of 400 km^2 (ten times the area of a single computational grid at the southern extreme of the model domain, rounded up to the nearest 100-square kilometres), these errors become negligible. Therefore, only gauging records for drainage areas >400 km^2 were used for model calibration.

Calibration and model validation is based on streamflow records collected from January 1, 1985 through December 31, 1995, which is the period of highest streamflow data density in all three study areas (i.e., largest number of hydrometric stations with complete and overlapping records). The VIC model was calibrated to data observed during January 1990 through December 1995 for the Campbell and Peace sites, where it is presumed that this latter period will have the most similar land cover to the circa-2000 data used for vegetation classification (see Section 3.4). Sites in the Upper Columbia were calibrated to data collected from 1990 through 1994, as some sites were missing data for 1995. The BCHLB site only had naturalized flow data for the 2003 to 2006 period, which was used for model calibration (due to lack of data this site was not explicitly validated). Other than the exceptions already noted, all VIC model

parameterizations were validated to the 1985 through 1989 discharge data. Although the Spillimacheen project site could not be calibrated, data was available for validation.

The six-year calibration period is assumed to contain sufficient intra-annual and seasonal variability that parameter estimates will be robust to high frequency variability. However, low frequency, inter-annual and decadal climate variability, such as ENSO or PDO, is also known to strongly influence hydro-climatology in BC (Moore and McKendry 1996; Romolo et al. 2006; Stahl et al. 2006; Fleming et al. 2007), although the effects are spatially variable (Fleming and Whitfield 2010). The calibration period does not represent the full ENSO range, being dominated by the warm phase in both 1991/92 and 1994/95 and neutral conditions in the remainder of the period (although it does end during the start of a cold phase period in 1995), based on the Oceanic Niño Index (CPC 2010). The validation period contains both cold (1984/85, 1988/89) and warm (1986/87) ENSO phases. Both the calibration and validation periods were dominated by the warm phase of the PDO (JISAO 2010).

As the majority of calibration sites correspond to locations with records unaffected by regulation, we used the observed records of the corresponding WSC gauge directly in the calibration process (HYDAT Database; http://www.ec.gc.ca/rhc-wsc/default.asp). However, for those calibration sites affected by storage regulation (see Table 3-1), the calibration process required naturalized flow, which was obtained from BC Hydro (BC Hydro, unpublished data). For the Upper Columbia project sites and for the BCGMS site unregulated local flows were calculated using the principle of conservation of mass. Local inflow is estimated as the residual of power and non-power releases plus change in reservoir storage over a given time interval minus any regulated discharge from upstream projects. Unregulated local inflows are used as a proxy for natural local inflow, where discrepancies arise from unaccounted for losses due to lake/reservoir evaporation and seepage through dams and groundwater, measurement error (i.e., non-representative reservoir elevation measurements), and uncertainty in turbine and stage-storage rating curves. Estimation of natural inflow data for BCSCA followed the same procedure, which included the removal of regulated flow from the Heber River diversion (but includes flow from Crest Creek). Naturalized streamflow data for PEAPN and PEACT were generated by BC Hydro using the WATFLOOD hydrologic model.

Calibration of headwater basins is straightforward, as calibration is based on observed (or naturalized) discharge at the basin outlet. However, in order to eliminate the possible cascade of errors or calibration artifacts, sub-basins located downstream of neighboring sub-basins (i.e., non-headwater sub-basins) were calibrated strictly to local inflow. This was accomplished in one of two ways: 1) for unregulated basins (or regulated basins with naturalized flow data available like the Peace River at Taylor), discharge from any upstream sub-basin(s) is supplied as a boundary condition in the form of observed (or naturalized) streamflow, and 2) for regulated basins where only naturalized local inflow is provided (i.e., Columbia River at Revelstoke), no upstream boundary conditions are supplied and parameters are calibrated directly to local inflow.

Table 3-1. Meta-data of VIC model calibration sites for the Peace, Campbell and Upper Columbia study areas.

WSC or BCH Site ID	Station Name	VIC ID	Latitude[#]	Longitude[#]	Flow Regime	Total Drainage Area (km^2)
		Peace River Study Area				
07EA002	Kwadacha River near Ware	KWADA	57.46875	-125.65625	Natural	2410
07EA004	Ingenika River above Swannell River	INGEN	56.71875	-125.15625	Natural	4200
07EA005	Finlay River above Akie River	FINAK	57.15625	-125.21875	Natural	16000
07EA007	Akie River near the 760 m contour	AKIEC	57.15625	-124.90625	Natural	1700
07EB002	Ospika River above Aley Creek	OSPIK	56.46875	-123.90625	Natural	2220
07EC002	Omineca River above Osilinka River	OMNOS	55.96875	-124.59375	Natural	5490
07EC003	Mesilinka River above Gopherhole Creek	MESIL	56.28125	-124.65625	Natural	2980
07EC004	Osilinka River near End Lake	OSILI	56.09375	-124.78125	Natural	1960
07ED001	Nation River near Fort St. James	NATFT	55.21875	-124.28125	Natural	4350
07ED003	Nation River near the Mouth	NATMO	55.46875	-123.59375	Natural	6720
07EE007	Parsnip River above Misinchinka River	PARMS	55.09375	-122.84375	Natural	4900
07EE010	Pack River at outlet of McLeod Lake	PACKM	54.96875	-123.03125	Natural	3690
07FA003	Halfway River above Graham River	HALGR	56.53125	-122.28125	Natural	3780
07FA004	Peace River above Pine River	PEAPN	56.21875	-120.78125	Regulated	83900
07FA005	Graham River above Colt Creek	GRAHM	56.46875	-122.34375	Natural	2200
07FA006	Halfway River near Farrell Creek	HALFA	56.28125	-121.59375	Natural	9350
07FB001	Pine River at East Pine	PINPN	55.71875	-121.21875	Natural	12100
07FB006	Murray River above Wolverine River	MURWV	55.09375	-121.03125	Natural	2370
07FB002	Murray River near the Mouth	MURMO	55.53125	-121.21875	Natural	5620
07FB003	Sukunka River near the Mouth	SUKMO	55.53125	-121.59375	Natural	2510
07FB008	Moberly River near Fort St. John	MOBER	56.09375	-121.34375	Natural	1520
BCH GMS	Peace River at Bennett Dam (GMS Hudson Hope)	BCGMS	56.03125	-122.21875	Regulated	72078
07FD002	Peace River at Taylor	PEACT	56.15625	-120.65625	Regulated	101000
		Campbell River Study Area				
BCH SCA	Campbell River at Strathcona Dam	BCSCA	49.96875	-125.59375	Regulated	1193

[#] Coordinates of VIC grid cell centre in which hydrometric site is located

Table 3-1. Continued

WSC or BCH Site ID	Station Name	VIC ID	Latitude[#]	Longitude[#]	Flow Regime	Total Drainage Area (km^2)
	Upper Columbia River Study Area					
08NA006	Kicking Horse River at Golden	KICAG	51.28125	-116.90625	Natural	1850
08NB005	Columbia River at Donald	COLAD	51.46875	-117.15625	Natural	9710
08NB012	Blaeberry River above Willowbank Creek	BLAAW	51.46875	-116.96875	Natural	588
08NF001	Kootenay River at Kootenay Crossing	KOOAK	50.90625	-116.09375	Natural	420
08NF002	Kootenay River at Canal Flats	KOOCF	50.15625	-115.78125	Natural	5390
08NF006	Palliser River in Lot SL49	PALIL	50.53125	-115.59375	Natural	653
08NG002	Bull River near Wardner	BULNW	49.53125	-115.34375	Natural	1530
08NG012	St. Mary River at Wycliffe	STMAW	49.59375	-115.84375	Natural	2360
08NG046	St. Mary River near Marysville	STMNM	49.59375	-116.15625	Natural	1480
08NG053	Kootenay River near Skookumchuck	KOONS	49.90625	-115.78125	Natural	7120
08NG065	Kootenay River at Fort Steele	KOOAF	49.59375	-115.65625	Natural	11400
08NK002	Elk River at Fernie	ELKAF	49.53125	-115.03125	Natural	3110
08NK016	Elk River near Natal	ELKNN	49.84375	-114.84375	Natural	1870
08NK018	Fording River at the mouth	FORAM	49.90625	-114.84375	Natural	619
08NK020	Michel Creek below Natal	MICBN	49.71875	-114.84375	Natural	637
BCH HLK	Columbia River at Keenlyside Dam	BCHAR	49.34375	-117.78125	Regulated	36659
BCH DCN	Duncan River at Duncan Dam	BCHDN	50.28125	-116.90625	Regulated	2426
BCH MCA	Columbia River at Mica Dam	BCHMI	52.09375	-118.59375	Regulated	21134
BCH REV	Columbia River at Revelstoke Dam	BCHRE	51.03125	-118.21875	Regulated	26387
BCH WGS	Whatshan River at Whatshan Dam	BCWAT	49.96845	-118.09375	Regulated	393
BCH LIB	Kootenai River at Libby Dam	BCHLB	48.40625	-115.28125	Regulated	23271
BCH KCL	Kootenay River at Kootenay Canal	BCHKL	49.46875	-117.46875	Regulated	46398
08NJ013	Slocan River near Crescent Valley	SLONC	49.46875	-117.59375	Natural	3320
08NE074	Salmo River near Salmo	SALNS	49.03125	-117.28125	Natural	1230

[#] Coordinates of VIC grid cell centre in which hydrometric site is located

3.8.3 Calibration Results

Calibration and validation results of the combined routing and VIC model are summarized in Table 3-2, Table 3-3 and Table 3-4 for the Peace, Campbell and Upper Columbia study areas, respectively. Although parameters for individual sub-basins are calibrated to local inflow only, calibration and validation performance as reported in the tables more conservatively reflects simulation of the entire upstream drainage (including nested upstream basins) to each point.

Table 3-2. Summary of calibration and validation results for Peace River sub-basins for three performance measures. *NS* is Nash-Sutcliffe, *LNS* is Nash-Sutcliffe of log-transformed discharge, and *%VB* is percent volume bias. Project sites are indicated with bold text.

Basin	Calibration 1990-1995			Validation 1985-1989		
	NS	*LNS*	*%VB*	*NS*	*LNS*	*%VB*
AKIEC	0.64	0.77	1	0.71	0.83	-6
BCGMS[#]	**0.64**	**0.84**	**1**	**0.75**	**0.86**	**-11**
FINAK	0.66	0.88	0	0.83	0.91	-13
GRAHM	0.71	0.84	0	0.72	0.70	-4
HALFA	0.58	0.75	1	0.58	0.63	3
HALGR	0.57	0.75	0	0.53	0.64	4
INGEN	0.76	0.86	0	0.82	0.84	-13
KWADA	0.61	0.71	0	0.79	0.78	-11
MESIL	0.84	0.86	0	0.83	0.80	-16
MOBER	0.77	0.69	0	0.58	0.65	-17
MURMO	0.73	0.71	-1	0.58	0.70	-15
MURWV	0.76	0.75	0	0.67	0.77	-12
NATFT	0.91	0.89	0	0.74	0.86	-16
NATMO	0.92	0.88	0	0.73	0.85	-16
OMNOS	0.87	0.82	0	0.81	0.79	-18
OSILI	0.83	0.86	0	0.81	0.80	-20
OSPIK	0.70	0.88	0	0.74	0.84	8
PACKM	0.90	0.77	1	0.83	0.75	-6
PARMS	0.78	0.77	0	0.81	0.74	-8
PEACT[#]	**0.71**	**0.86**	**1**	**0.78**	**0.91**	**-10**
PEAPN[#]	**0.64**	**0.83**	**1**	**0.76**	**0.89**	**-9**
PINPN	0.79	0.79	-2	0.71	0.74	-15
SUKMO	0.85	0.80	-1	0.78	0.74	-17
Average	0.75	0.81	0	0.73	0.78	-10

[#] Calibrated and validated to naturalized discharge

In the Peace River study area *NS* during the calibration period ranges from 0.57 to 0.92, averaging 0.75 between the 23 calibration sites (Table 3-2). Performance as indicated by *LNS* is somewhat superior,

ranging from 0.71 to 0.91, averaging 0.81. The %*VB* indicates negligible bias during the calibration period, ranging from -2% to 1%. As expected, performance tends to degrade somewhat during the validation period. In particular, performance degrades with respect to *%VB*, ranging from -20% to 8%, and averaging -10% during the validation period. This likely indicates over-fitting of the *Padj* parameters. This may be the result of calibrating to a precipitation bias that arises specifically to precipitation patterns that dominate during warm phase ENSO conditions, which doesn't account for the switch to more frequent wet type synoptic events that likely prevailed over the region during cold phase ENSO conditions of the validation period (Romolo et al. 2006). The *NS* and *LNS* values also show poorer performance during the validation period, although the change is marginal: average performance is 0.73 and 0.78 for *NS* and *LNS*, respectively. Therefore, despite an increase in overall bias during the validation period, the *NS* and *LNS* values suggest that there has been no major degradation in the ability of the model to replicate inter- and intra-annual streamflow variability in the Peace study area.

For the Campbell River study area, performance is 0.72, 0.67 and 2% for *NS*, *LNS* and %*VB*, respectively, during the model calibration period (Table 3-3). For this particular application of the model there is no evidence of over-fitting, and model performance changes little in the validation period (0.72, 0.68 and 6% for *NS*, *LNS* and %*VB*, respectively). In fact, validation statistics calculated during an alternative period (1996 - 2006) suggest that the VIC model parameters are fairly robust, as model performance only degrades slightly to 0.68, 0.66 and 2% for *NS*, *LNS* and %*VB*, respectively.

Table 3-3. Summary of calibration and validation results for Campbell River basin for three performance measures. *NS* is Nash-Sutcliff, *LNS* is Nash Sutcliff of log-transformed discharge, *%VB* is percent volume bias.

Basin	Calibration 1990-1995			Validation 1985-1989			Validation 1996 – 2006		
	NS	*LNS*	*%VB*	*NS*	*LNS*	*%VB*	*NS*	*LNS*	*%VB*
BCSCA	0.72	0.67	2	0.72	0.68	6	0.68	0.66	2

Model performance is somewhat higher for the Upper Columbia study area (Table 3-4). *NS* values for the calibration period range from 0.65 to 0.99, with a mean of 0.83 over the 24 calibration basins. For *LNS*, performance across calibration sites is similar overall, with a domain-average of 0.80. However, *LNS* performance shows higher inter-basin variability, with values ranging from 0.27 to 0.99. The %*VB* errors during the calibration period range from -15% to 10%, with a mean of -4%. Nevertheless, the majority of absolute %*VB* values (23 of 24 sites) are ≤ 10%. Due to some over-fitting, validation statistics are slightly lower overall than during the calibration period. Nevertheless, the VIC model parameterizations seem robust; basin by basin, the *LS*, *LNS* and %*VB* performance measures do not degrade substantially during the validation period. *NS* values range from 0.67 to 0.91 (with a mean of 0.79) and *LNS* values range from 0.38 to 0.88 (with a mean of 0.73). Underestimation of total runoff volume persists during model validation, where an average %*VB* of -7% suggests a slightly larger underestimation of total discharge than calculated for the calibration period. Again, as for the Peace this may suggest a slight over tuning of the *Padj* parameters to specific precipitation patterns experienced during the calibration period. Also, the variability of %*VB* is larger, ranging from -20% to 17%. Note that although BCHKL (which is downstream of BCHLB) was calibrated to naturalized local inflow for 1990 through 1994, it could only be validated to total flow during 2003 to 2006 (i.e., when data was available for BCHLB). This validation was based on data constructed by combining BCHKL discharge to that from BCHLB and

BCHDN. However, as the discharge from upstream sites was not explicitly routed to the BCHKL site, we validated BCHKL to monthly discharge (i.e., routing effects are presumed negligible on a monthly timescale).

Table 3-4. Summary of calibration and validation results for Columbia River sub-basins for three performance measures. *NS* is Nash-Sutcliffe, *LNS* is Nash-Sutcliffe of log-transformed discharge, and *%VB* is percent volume bias. Project sites are indicated with bold text.

Basin	Calibration 1990-1994			Validation 1985-1989		
	NS	*LNS*	*%VB*	*NS*	*LNS*	*%VB*
BCHAR[#$]	**0.78**	**0.84**	**-2**	**0.80**	**0.65**	**-8**
BCHDN[#]	**0.65**	**0.54**	**-7**	**0.73**	**0.59**	**-8**
BCHKL[#†]	**0.67**	**0.60**	**-7**	**0.72**	**0.74**	**4**
BCHMI[#]	**0.89**	**0.83**	**-9**	**0.88**	**0.79**	**-7**
BCHRE[#$]	**0.97**	**0.97**	**-4**	**0.92**	**0.81**	**-10**
BCWAT[#]	**0.76**	**0.75**	**-10**	**0.74**	**0.67**	**-12**
BLAAW	0.72	0.86	10	0.75	0.87	-3
BULNW	**0.83**	**0.77**	**-4**	**0.81**	**0.72**	**-17**
COLAD	0.94	0.94	-2	0.91	0.88	-1
ELKAF	0.99	0.97	-3	0.81	0.69	-13
ELKNN	0.89	0.92	-3	0.75	0.77	-8
FORAM	0.66	0.70	-6	0.72	0.74	-1
KICAG	0.77	0.87	-8	0.77	0.86	-2
KOOAF	0.99	0.99	3	0.85	0.80	-4
KOOAK	0.78	0.77	-4	0.75	0.68	17
KOOCF	0.91	0.91	-4	0.84	0.86	-4
KOONS	0.98	0.99	0	0.85	0.83	-6
MICBN	0.75	0.80	-5	0.76	0.79	-15
PALIL	0.80	0.77	-4	0.80	0.80	-10
SALNS	**0.74**	**0.27**	**-15**	**0.73**	**0.38**	**-12**
SLONC	**0.78**	**0.66**	**-2**	**0.78**	**0.72**	**-2**
SPINS[‡]				**0.67**	**0.82**	**-1**
STMAW	0.99	0.99	-2	0.84	0.63	-16
STMNM	0.76	0.46	-10	0.82	0.47	-20
BCHLB[#&]	0.97	0.93	-1			
Average	0.83	0.80	-4	0.79	0.73	-7

[#] Calibrated and validated to naturalized discharge (see text)
[$] Validation based on monthly streamflow (see text)
[†] Validation based on monthly streamflow over 2003 to 2006 (see text)
[‡] Uncalibrated; validation based on 1980 to 1984 period
[&] Calibrated based on 2003 to 2006 period

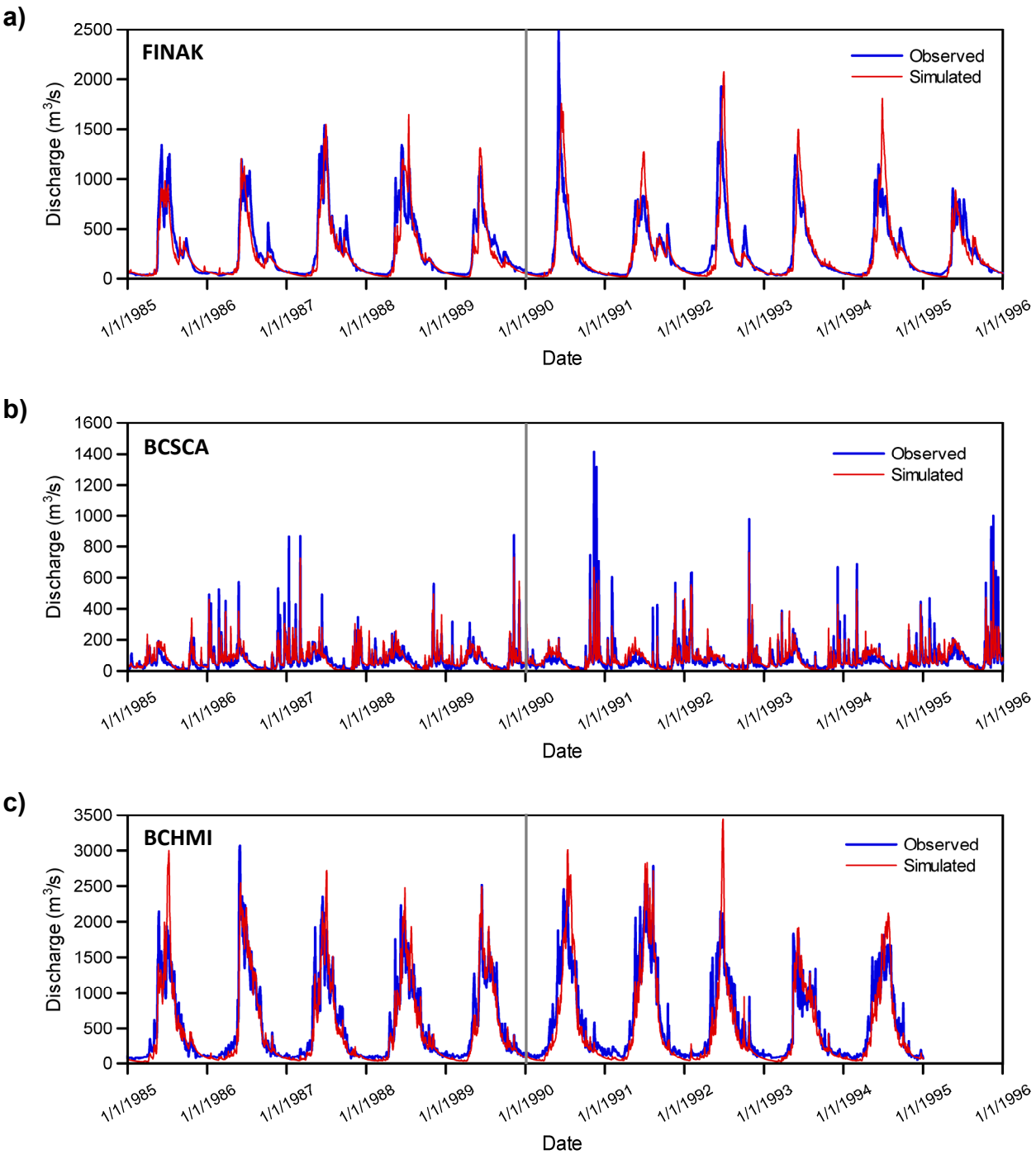

Figure 3-7. Observed and simulated daily discharge for the calibration and validation periods for a) Finlay River above Akie Creek (FINAK), b) Campbell River at Strathcona Dam (BCSCA), and c) Columbia River at Mica Dam (BCHMI). Note that observed discharge refers to naturalized discharge for BCSCA and BCHMI. The calibration (1/1/1990 through 31/12/1995) and validation (1/1/1985 through 31/12/1989) periods are demarcated by the vertical gray line.

A comparison of modelled and observed discharge during the calibration and validation periods is shown for three sub-basins in Figure 3-7. The Finlay River above Akie River (FINAK; Figure 3-7a) is the largest (16,000 km^2) natural gauged tributary flowing into the Williston Reservoir. The FINAK hydrograph represents a typical nival discharge regime. The Campbell River at Strathcona Dam (BCSCA, Figure 3-7b) represents the entire Campbell River study area. The hydrograph for BCSCA shows the typical discharge signature of a hybrid nival-pluvial regime. The Columbia River at Mica Dam (BCHMI, Figure 3-7c) is a 21,134 km^2 basin that drains the headwaters of the Columbia River. It contains 5.5% of its drainage area in glaciers and represents a glacial-nival discharge regime. In all cases the VIC simulations do a suitable job of capturing the seasonal and intra-annual discharge pattern and variability at the target stations, and inter-annual variability is also captured. As expected, daily discharge is not as well matched, particularly when it comes to matching fall rainstorm peaks in the BCSCA system.

4. Results and Discussion

Prior to presenting and discussing results, details of the analysis methodology are briefly reviewed. Results are presented in the form of runs and ensembles. A run is a single transient hydrologic simulation forced with downscaled climate data from a single GCM driven by one of three emissions scenarios for the period 1950 to 2098, with 23 runs in total. As discussed previously, to account for the possibility of a detectable difference between different emission forcings, hydrologic projections have been categorized by emissions scenario. Consequently, runs have also been grouped into ensembles, where each ensemble contains runs derived from the same emissions scenario (but different GCMs). As recent 21st century emissions have been more pessimistic than the worst-case SRES scenario (Raupach et al. 2007), the A1B emissions trajectory is presumed to currently be the most "realistic", or representative, of the chosen three emissions scenarios for the 2050s period (e.g., Figure 2-2). Therefore, much of the detailed discussion that follows focuses on results for the A1B scenario.

Potential hydrologic responses to climate change are quantified by comparing historic and future hydrologic fluxes annually, monthly and by season, where the seasons are defined as winter (December, January and February), spring (March, April and May), summer (June, July and August) and fall (September, October and November). In the discussion that follows, hydrologic impacts are quantified by comparing statistics of streamflow, or other hydrologic fluxes, of respective 30-year historic (1961-1990) and future (2041-2070) periods. The median value is most often used to both summarize results from individual runs, and also to reflect the "consensus" estimate when summarizing and comparing ensembles of runs. Percentiles are used to quantify the variability or range of an ensemble projection. Streamflow changes are quantified based on comparison between simulated historical and future streamflow, rather than direct comparison of simulated future projections with historical observations. This relative comparison removes the effect of any residual bias in the simulated streamflow projections that may remain, despite careful calibration of the statistical downscaling and hydrologic models.

When statistical significance testing of potential future changes in streamflow or other hydrologic fluxes is conducted, the Wilcoxon rank-sum test is used (Helsel and Hirsch 2002). This test is for whether values from one sample or ensemble (i.e. future) have a tendency to be larger or smaller than values from another sample or ensemble (i.e. historical). Specifically, we employ the two-sided test:

Null hypothesis (H_0): $\text{Prob}[x > y] = 0.5$,

Alternate hypothesis (H_1): $\text{Prob}[x > y] \neq 0.5$,

where x represents future values and y represents historical values. All tests are at the 5% significance level ($p < 0.05$).

4.1 Peace River Study Area

4.1.1 Climate Projections

Projected climate change for the 2050s is summarized as temperature and precipitation anomalies in Table 4-1. Anomalies are grouped by emissions scenario and presented for the entire study area as the median change as well as the 5th and 95th percentile change. The median anomaly temperature projections for the Peace River basin illustrate an increase in temperatures, with the strongest projected increases occurring for the A1B and A2 scenarios (median annual change of 2.5 °C and 2.4 °C, respectively). All scenarios project an increase in temperatures almost 1°C above other seasons for the winter. For the A1B scenario, the spring, summer and fall projections are of a similar range (2.4-2.7 °C). Precipitation is projected to increase in all seasons and annually, with the largest increases projected for the fall, winter and spring. A similar pattern is exhibited in all scenarios. Summer precipitation is projected to increase

only marginally (+3%) for the A1B and A2 scenarios, with slight higher projections for the B1 emissions scenario (+6%). Nevertheless, the range in temperature and precipitation for each of the emissions scenario ensembles show considerable overlap (e.g., comparing the range in the 5th and 95th percentiles in Table 4-1). Therefore, there is no meaningful difference in climate response between the three scenarios for the 2050s period.

Spatially, most of the basin responds uniformly in terms of temperature increases (Figure 4-1). For the winter and fall, precipitation anomalies exhibit a gradient of increasing wetness from west to east, as exemplified by the composite map of median A1B anomalies (Figure 4-2). In summer the precipitation anomalies are more spatially uniform, with most of the basin exhibiting negligible precipitation change (median A1B, Figure 4-2c), but with a small region in the north-west showing increased precipitation. Precipitation anomalies in the spring are positive and spatially uniform (Figure 4-2b). As the BCSD downscaling approach explicitly preserves the temperature and precipitation trends from the downscaled GCMs, the spatial trend patterns shown in Figure 4-1 and Figure 4-2 (i.e., locations of temperature isotherms and precipitation isohyets) are predominantly an artifact of the underlying resolution of the source GCMs (Maurer and Hidalgo 2008).

Table 4-1. Projected 2050s climate anomalies for the Peace River study area.

Emissions Scenario	Variable	Percentile	Anomaly by Season				
			Annual	Winter (DJF)	Spring (MAM)	Summer (JJA)	Fall (SON)
A1B	Temperature (°C)	5th	2.2	2.0	1.6	1.7	1.8
		Median	2.5	3.6	2.4	2.7	2.5
		95th	3.5	3.9	3.2	3.8	3.6
	Precipitation (%)	5th	1	11	4	-18	3
		Median	13	19	17	3	20
		95th	22	29	29	12	28
A2	Temperature (°C)	5th	1.8	1.2	1.4	1.5	1.6
		Median	2.4	3.1	2.1	2.6	2.1
		95th	3.3	3.6	2.9	3.6	3.3
	Precipitation (%)	5th	4	6	6	-8	4
		Median	11	14	15	3	15
		95th	20	25	26	14	30
B1	Temperature (°C)	5th	1.4	1.1	1.1	1.1	1.2
		Median	1.8	2.7	1.8	1.9	1.7
		95th	2.8	3.7	2.7	3.0	2.2
	Precipitation (%)	5th	7	9	8	-3	8
		Median	12	14	14	6	14
		95th	20	29	22	15	23

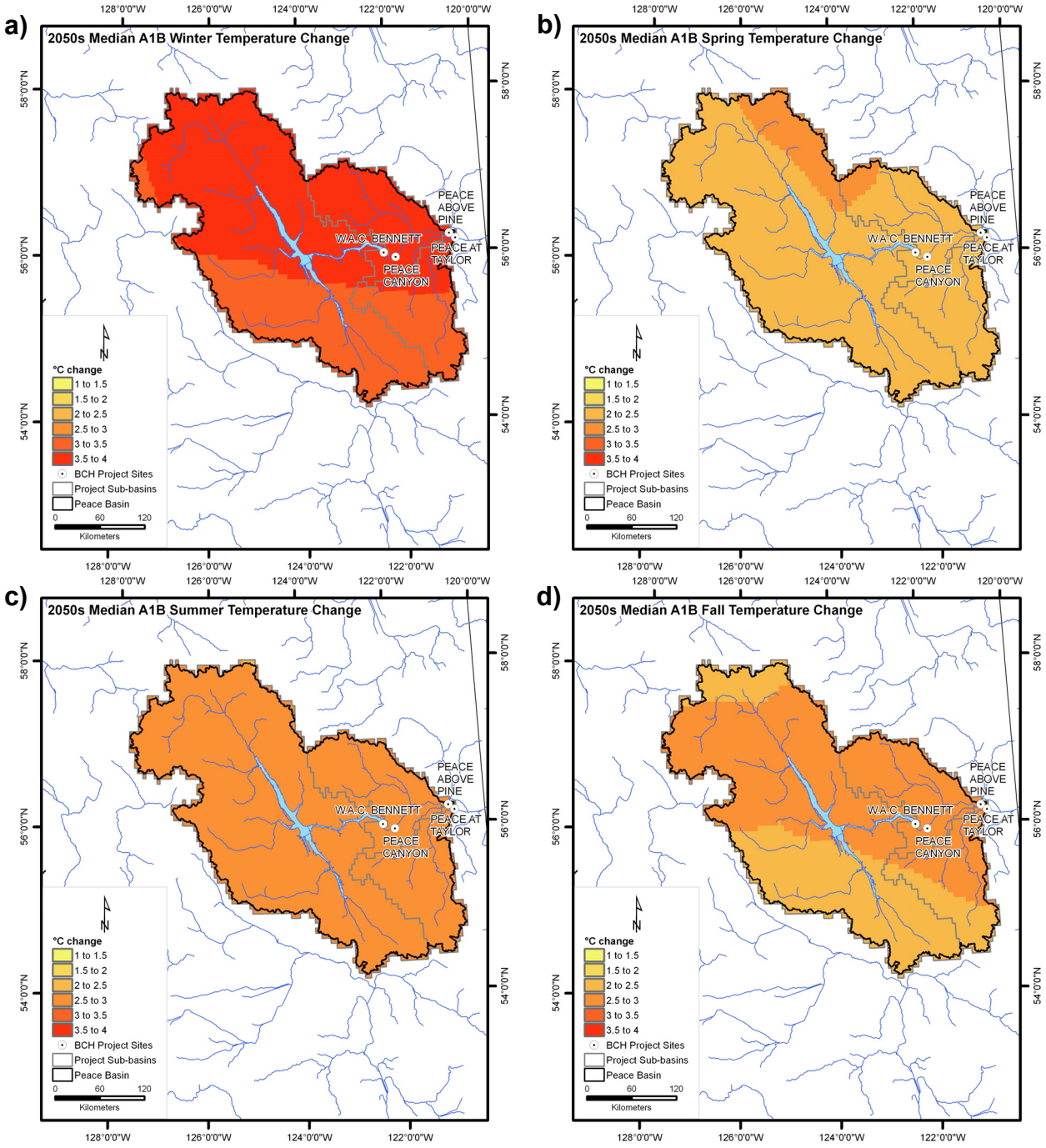

Figure 4-1. Median A1B seasonal temperature changes for the Peace River study area for a) winter (DJF), b) spring (MAM), c) summer (JJA), and d) fall (SON).

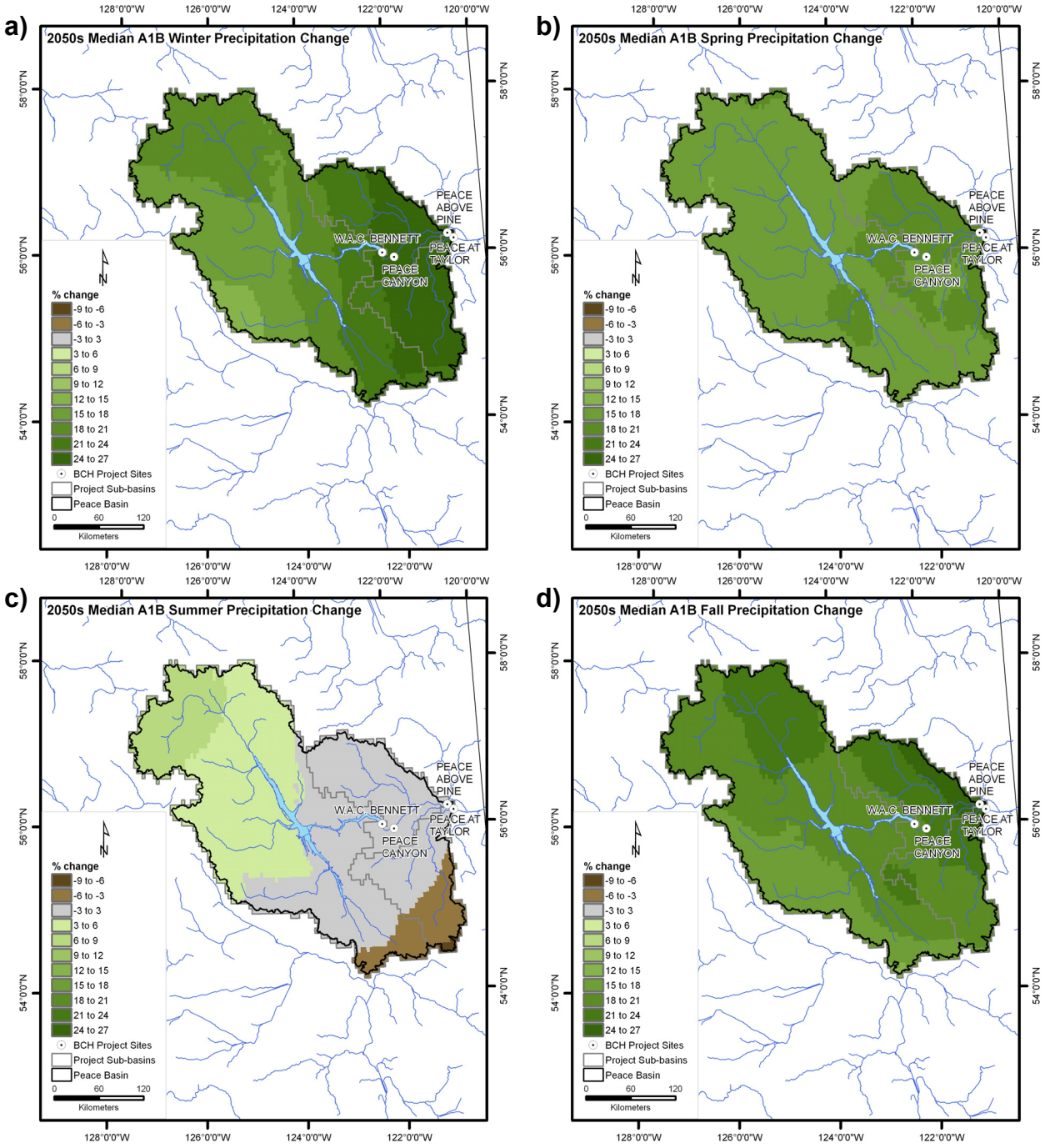

Figure 4-2. Median A1B seasonal precipitation changes for the Peace River study area for a) winter (DJF), b) spring (MAM), c) summer (JJA), and d) fall (SON).

4.1.2 Annual Streamflow

A comparison of historical to projected annual discharge for each project site in the Peace River study area is shown graphically in Figure 4-3. The box-plots compare the historical and future ensembles of annual discharge for each emissions scenario, with one box-plot per study site. The single historical ensemble samples all historical runs (23 runs x 30 years), whereas the future ensembles sample the individual scenarios (8 runs x 30 years). In each figure, the box shows the inter-quartile range (*IQR*; 25th to 75th percentiles), the thick horizontal line indicates the median, and the whiskers show the minimum and maximum values (dotted line). Values corresponding to the box-plots are tabulated in Table 4-2. Note that the range indicated by the box-plots is a function both of inter-annual and inter-GCM variability (i.e., climate model differences). A small triangle under a box-plot for the future period indicates that differences in the future and historical ensemble values are statistically significant (i.e., individual values in the future ensemble tend to be larger (or smaller) than values from the historical ensemble). Streamflow was analyzed for the BCGMS site (Figure 4-3a), the Peace River above Pine (PEAPN; Figure 4-3b), and the Peace River at Taylor (Figure 4-3c). Streamflow is projected to increase by the 2050s at both BCGMS (i.e., Williston inflow) and PEACT, with changes in median annual discharge ranging from 11% to 15%, depending on site and emissions scenario. All changes are considered statistically significant at the 5% level. Projected changes in annual discharge are not as large for PEAPN, with only the B1 scenario showing a statistically significant increase (14%). For the BCGMS and PEACT, the differences between scenarios is trivial, whereas for PEAPN, the projected change for the B1 scenario is larger than those projected for either A1B or A2.

Table 4-2. Historic and future annual discharge ensemble statistics and anomalies for the Peace River project sites.

Percentile	Annual Discharge Statistics by Period and Emissions (m^3/s)				Relative Difference		
	1961 to 1990	2040 to 2071					
		B1	A1B	A2	B1	A1B	A2
			BCGMS				
minimum	701	783	767	717	0.12	0.09	0.02
75th	957	1063	1049	1027	0.11	0.1	0.07
median	1036	1163	1171	1146	0.12	0.13	0.11
25th	1144	1280	1292	1275	0.12	0.13	0.11
maximum	1417	1600	1618	1630	0.13	0.14	0.15
			PEAPN				
minimum	51	52	46	47	0.02	-0.10	-0.08
75th	83	91	84	84	0.10	0.01	0.01
median	97	111	99	100	0.14	0.02	0.03
25th	117	134	116	124	0.15	-0.01	0.06
maximum	167	193	163	182	0.16	-0.02	0.09
			PEACT				
minimum	111	130	105	109	0.17	-0.05	-0.02
75th	165	184	182	178	0.12	0.10	0.08
median	186	213	209	206	0.15	0.12	0.11
25th	208	247	241	236	0.15	0.12	0.11
maximum	270	327	325	318	0.15	0.12	0.11

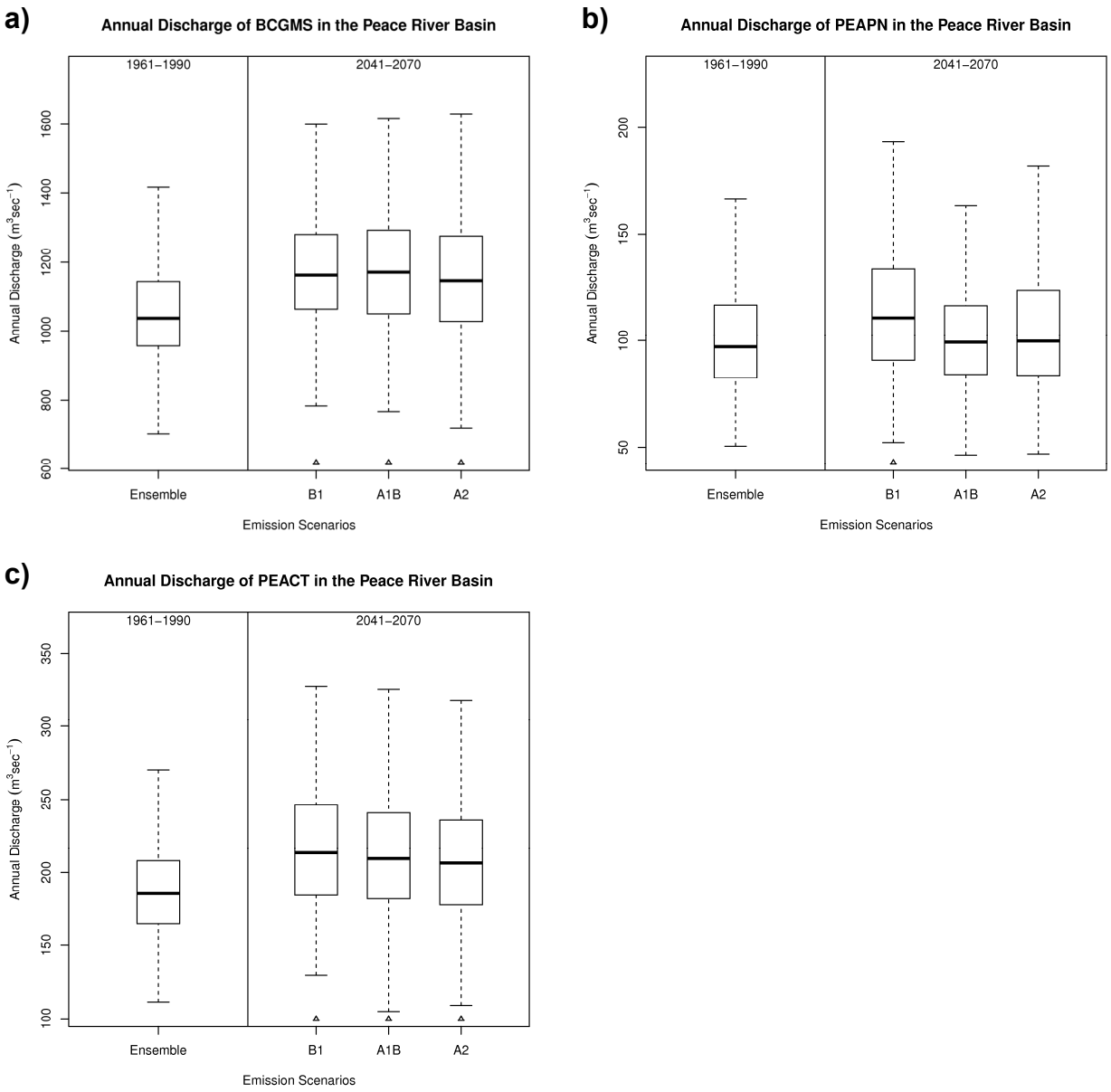

Figure 4-3. Annual discharge box-plots by scenario for the historic (1961 - 1990) and future (2041 to 2070) period for a) Peace River at Bennett Dam (BCGMS), b) Peace River above Pine River (PEAPN) and c) Peace River at Taylor (PEACT). Each box-plot summarizes the median (thick horizontal line), inter-quartile range (IQR; box showing 75th to 25th percentile) and the minimum and maximum (dotted lines). Those cases where the future ensemble is significantly different than the historical ensemble are indicated by a triangle below the plot.

4.1.3 Monthly Streamflow

Monthly streamflow projections are reported for BCGMS, PEAPN and PEACT in Figure 4-4, Figure 4-5 and Figure 4-6, respectively. The top panel in each figure shows the median monthly hydrograph for the historic and future periods. The historic hydrograph is the median of all 23 historic runs (sample size of 23 x 30 per month), whereas future streamflow is shown as a single median hydrograph for each individual GCM-scenario run (sample size 30; 23 in total per month). The bottom panel displays the

monthly streamflow anomaly as an absolute change between each future monthly hydrograph and the historic median monthly hydrograph. By the 2050s, monthly streamflow at the BCGMS dam site is projected to increase throughout most of the fall, winter and spring periods (Figure 4-4a). The median monthly projections indicate a tendency towards an earlier freshet onset and some runs suggest that the peak flow month is starting to shift from June to May. Regardless, all runs indicate that June will remain the month of peak discharge, with most runs projecting increased peak monthly discharge. Projected declines in monthly discharge begin in late June or early July, and persist until about September or even October, depending on the GCM-scenario run. Projected absolute changes in median monthly discharge are highest in May (ranging from 202 m^3/s to 1,040 m^3/s) and projected summer declines are greatest during July (ranging from -13 m^3/s to -1,424 m^3/s). Winter increases are projected by most models.

At the PEAPN site local monthly median streamflow is also projected to increase throughout most of the late fall, winter and spring periods (Figure 4-5a) during the 2050s. The median monthly projections indicate a stronger tendency towards an earlier freshet onset than that projected for BCGMS, with most runs showing a shift of the peak flow month from June to May. However, the response is mixed with respect to the projected magnitude of peak monthly discharge. Roughly 50% of runs indicate reduced peak discharge. Consequently, projected absolute changes in median monthly discharge are highest in May, but range from -12 m^3/s to 220 m^3/s. Projected changes in monthly discharge in June are mixed, ranging from -121 to 81 m^3/s (Figure 4-5b). Monthly discharge is generally projected to be reduced in July and August, but the response is mixed for the early fall (September and October). Given that there is substantial overlap between individual median runs from the three emissions scenarios, no consistent forcing response can be distinguished for the 2050s.

The PEACT projections illustrate a somewhat similar pattern to that projected for PEAPN (Figure 4-6). Monthly streamflow is projected to increase during the late fall, winter and spring, with an almost unanimous shift of peak monthly discharge from June to May. Again, this leads to the highest discharge changes projected to occur in May, ranging from -81 m^3/s to 206 m^3/s. An earlier freshet peak is projected to lead to large changes in monthly discharge during June, with the majority of runs showing reduced discharge in the future (changes range from -338 m^3/s to 84 m^3/s). Summer declines are projected to persist in a similar pattern to those exhibited at the PEAPN station, falling during late June and early July and in decline through the summer until October, when flow begins to increase. Like the PEAPN, there appears to be no distinguishable response in median monthly streamflow to the separate A1B, A2 or B1 forcing scenarios.

Projected changes in monthly streamflow can be diagnosed by directly comparing projected changes in temperature, precipitation (including the separate phases of rainfall and snowfall) and snowmelt with those of discharge. Such a comparison is made in Figure 4-7 by comparing respective historical and future monthly percentiles for BCGMS sub-basin for the A1B scenario ensemble. The historical range provides an estimate of natural variability, which can be compared to the projected range to assess the significance of future projections based on the degree of difference between the historic and future monthly distributions. As well, any historic and future monthly ensembles that exhibit statistically significant differences are indicated directly in Figure 4-7. The monthly temperature distribution shows a signal of consistently warmer temperatures in the 2050s throughout the year (Figure 4-7a). Future monthly precipitation is projected to be higher throughout the fall and winter (Figure 4-7b). This manifests as an increase of both rainfall (Figure 4-7c) and snowfall (Figure 4-7d) during winter, but due to warmer temperatures, increased rainfall at the expense of reduced snowfall during the fall. Increased rainfall in the spring is the result of both increased precipitation in general, but also from a conversion of rainfall to snowfall due to higher temperatures. In the future, the BCGMS basin is also projected to experience an increase in mid-winter snowmelt as well as an earlier onset of spring snowmelt (Figure 4-7e); both attributed to increasing temperatures. The shift in the distribution to higher monthly discharge in the future during the winter correlates with increases in the snowmelt and rainfall distributions. Figure 4-7f shows more clearly that the freshet is projected to begin earlier and over a shorter period of time in

the 2050s compared to the historical period. In this case, changes in the timing and magnitude of the freshet are attributed to increases in spring snowmelt (Figure 4-7e), augmented by an increase in early-summer rainfall (Figure 4-7c). Future and historical monthly discharge percentiles for BCGMS, PEAPN and PEACT have been summarized by emissions scenario in separate appendices for A1B, A2 and B1, respectively.

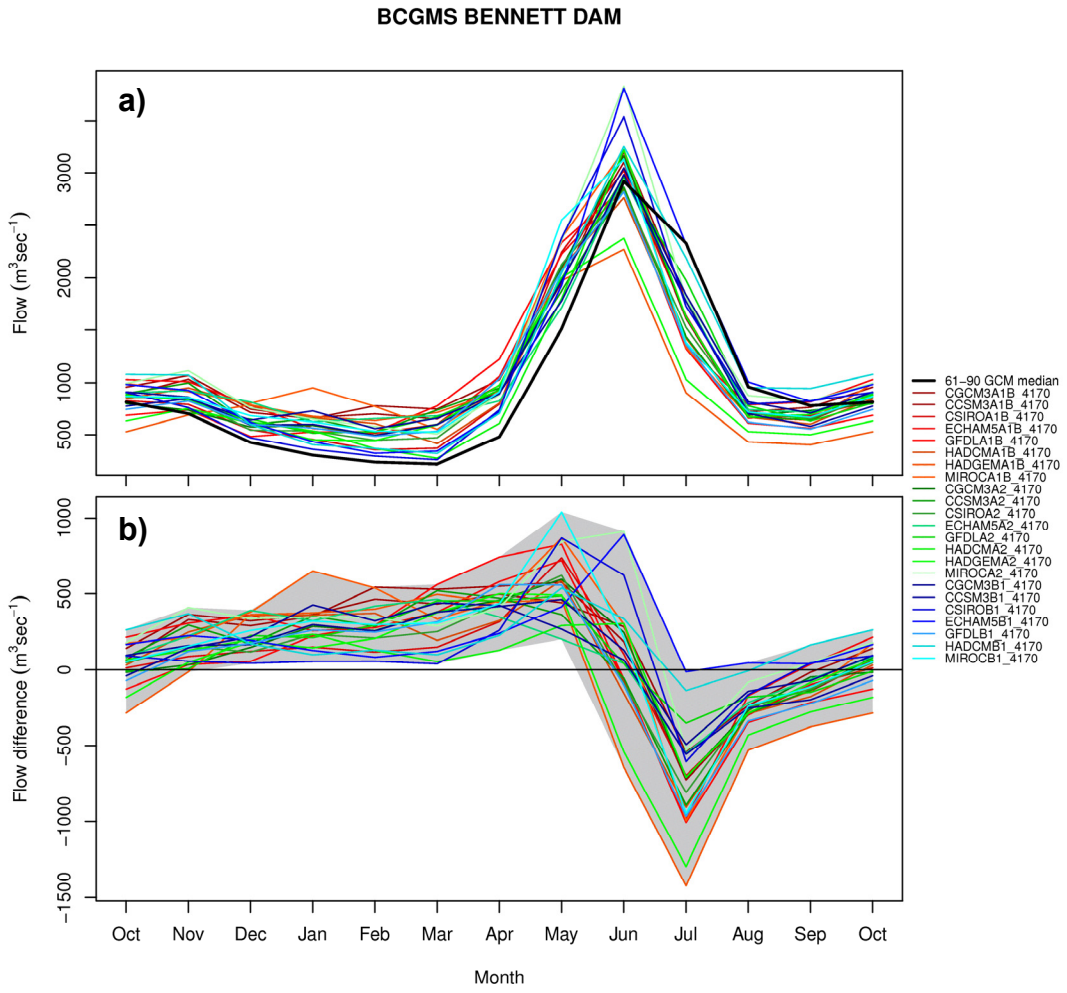

Figure 4-4. Median monthly discharge for the Peace River at Bennett Dam (BCGMS) showing: a) historic (1961 - 1990) and future (2041 - 2070) discharge, and b) the 2050s anomaly. Historic discharge (black line) is presented as the full ensemble median (23 runs x 30 years) and each future discharge value is the median of each GCM run (1 run x 30 years). Anomalies represent the future monthly median minus the historic ensemble monthly median.

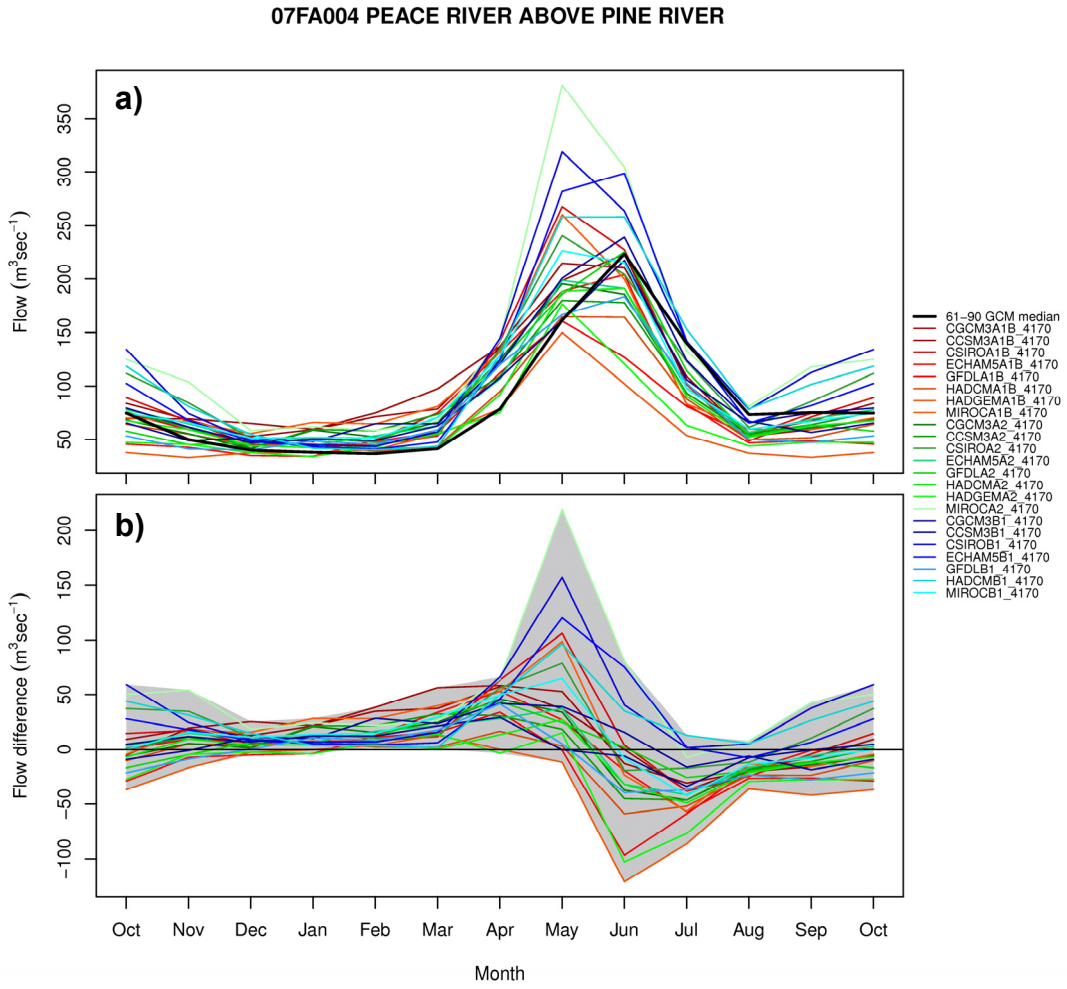

Figure 4-5. Median monthly discharge for the Peace River above Pine River (PEAPN) showing: a) historic (1961 - 1990) and future (2041 - 2070) discharge, and b) the 2050s anomaly. Historic discharge (black line) is presented as the full ensemble median (23 runs x 30 years) and each future discharge value is the median of each GCM run (1 run x 30 years). Anomalies represent the future monthly median minus the historic ensemble monthly median.

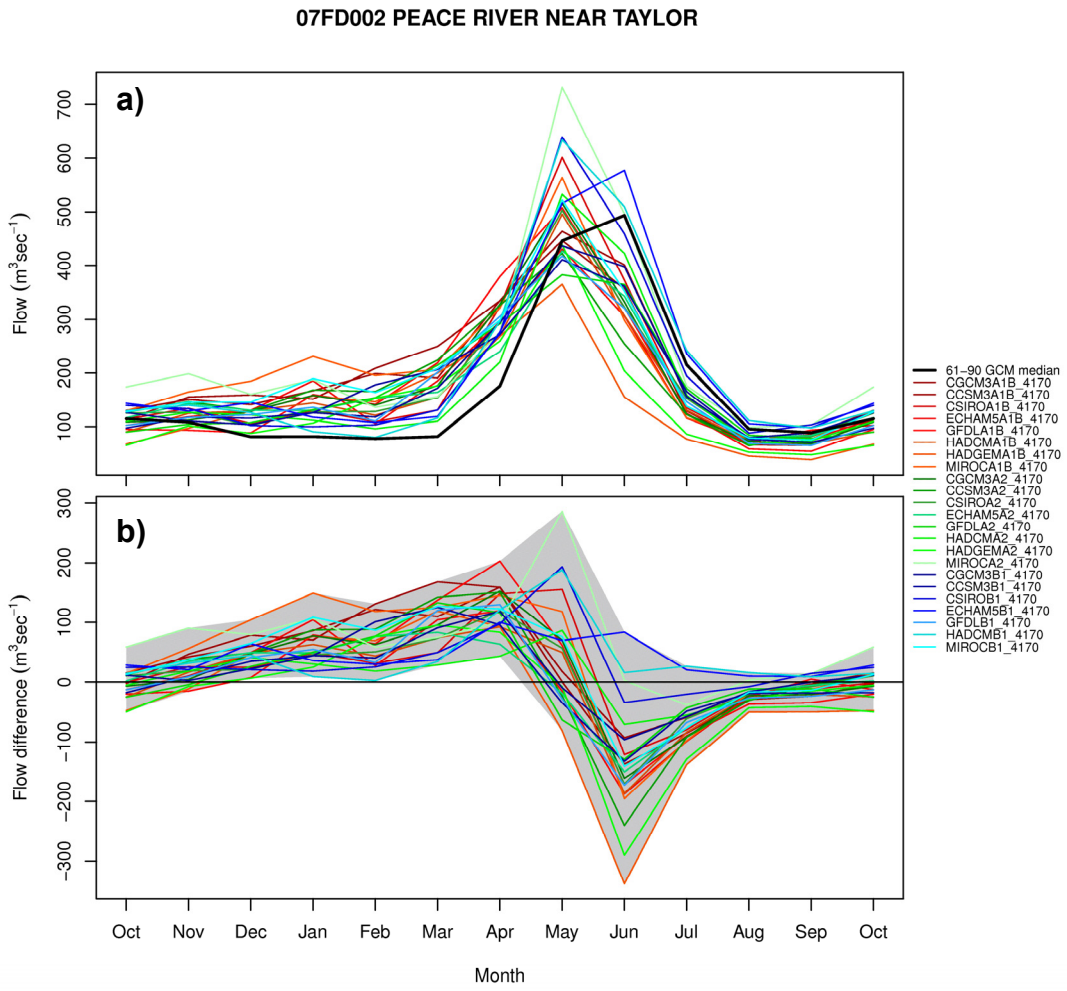

Figure 4-6. Median monthly discharge for the Peace River at Taylor (PEACT) showing: a) historic (1961 - 1990) and future (2041 - 2070) discharge, and b) the 2050s anomaly. Historic discharge (black line) is presented as the full ensemble median (23 runs x 30 years) and each future discharge value is the median of each GCM run (1 run x 30 years). Anomalies represent the future monthly median minus the historic ensemble monthly median.

A comparison of historical versus future cumulative monthly discharge over the water year (October through September) also reveals changes in the monthly streamflow regime at BCGMS (Figure 4-8). Using the median of the A1B ensemble, it can be seen that for any given month in the future, a greater volume of discharge is projected to accumulate, which is a function of both increased discharge and changes in streamflow timing (Figure 4-8a). The largest absolute difference for A1B will occur around May, when an additional 7.43 km^3 is projected to accumulate. When normalized by respective total annual volume, changes in streamflow timing are still apparent such that the half-flow month (that month when 50% of annual discharge is expected to accumulate) is projected to occur roughly one month sooner in the future (Figure 4-8b).

4.1.4 Snowpack and Runoff

Snowpack changes in the Peace River basin were considered using an index variable that compares peak (i.e., 1 April) snow water equivalent as a proportion of total winter precipitation (October through March), SWE_p/P_w, across the Peace River basin (Barnett et al. 2008). This ratio provides a quantitative means of examining changes to the relative contribution of snow storage to the annual discharge cycle. Nival regimes will have high ratios (i.e., ≥ 0.5), whereas hybrid regimes will have values in the order of 0.1 to 0.5, and rainfall regimes will have ratios less than 0.1 (Elsner et al. 2010). The A1B ensemble median of SWE_p/P_w is mapped in Figure 4-9 for both the historic and future periods (panels a and b, respectively). These figures indicate that the higher-elevation headwater regions of the Finlay, Kwadacha and Akie watersheds in the north-west of the study area are projected to remain snow dominated into the 2050s, along with a portion of the Parsnip drainage in the south (compare Figure 4-9a and b). The southwestern portions of the Upper Peace River basin, which encompass the Pine, Moberly, Halfway and Graham Creek basins, are projected to transition from snow dominated to either snow/rain or rainfall dominated (in particular, the Moberly, Pine, and Sukunka, and Murray watersheds). Drainage areas on the Alberta Plateau east of the Rocky Mountains are the most impacted, with the majority of this area projected to be largely rainfall dominated during the winter season. These results indicate that the watershed is in transition to a more hybrid rain-snow system, but that these effects are geographically variable. The consequent effect is that SWE_p is projected to decrease throughout most of the Peace River in the 2050s (Figure 4-9c), with reductions as high as 50% of historical SWE_p in many regions, however, potentially small increases may occur in a small region in the northwest of the study area.

Runoff changes for the median of the A1B ensemble for all four seasons illustrate a spatial pattern of change that reflects the impacts of changes in temperature, precipitation and snow storage (Figure 4-10). Winter runoff is projected to increase consistently throughout the basin, with some lesser runoff projected for the Graham/Halfway watersheds. The summer, on the other hand, is consistent in the pattern of decline projected across the Peace River watersheds, on the order of -10% to -30%. The spring signal is for increasing runoff (> 40%) in the upper Finlay, Kwadacha and Akie River basins, and for moderate increases throughout the rest of the basin. The fall signal is mixed, with some areas of the watershed projected to experience declines in runoff, and other regions projected to have slight increases in runoff.

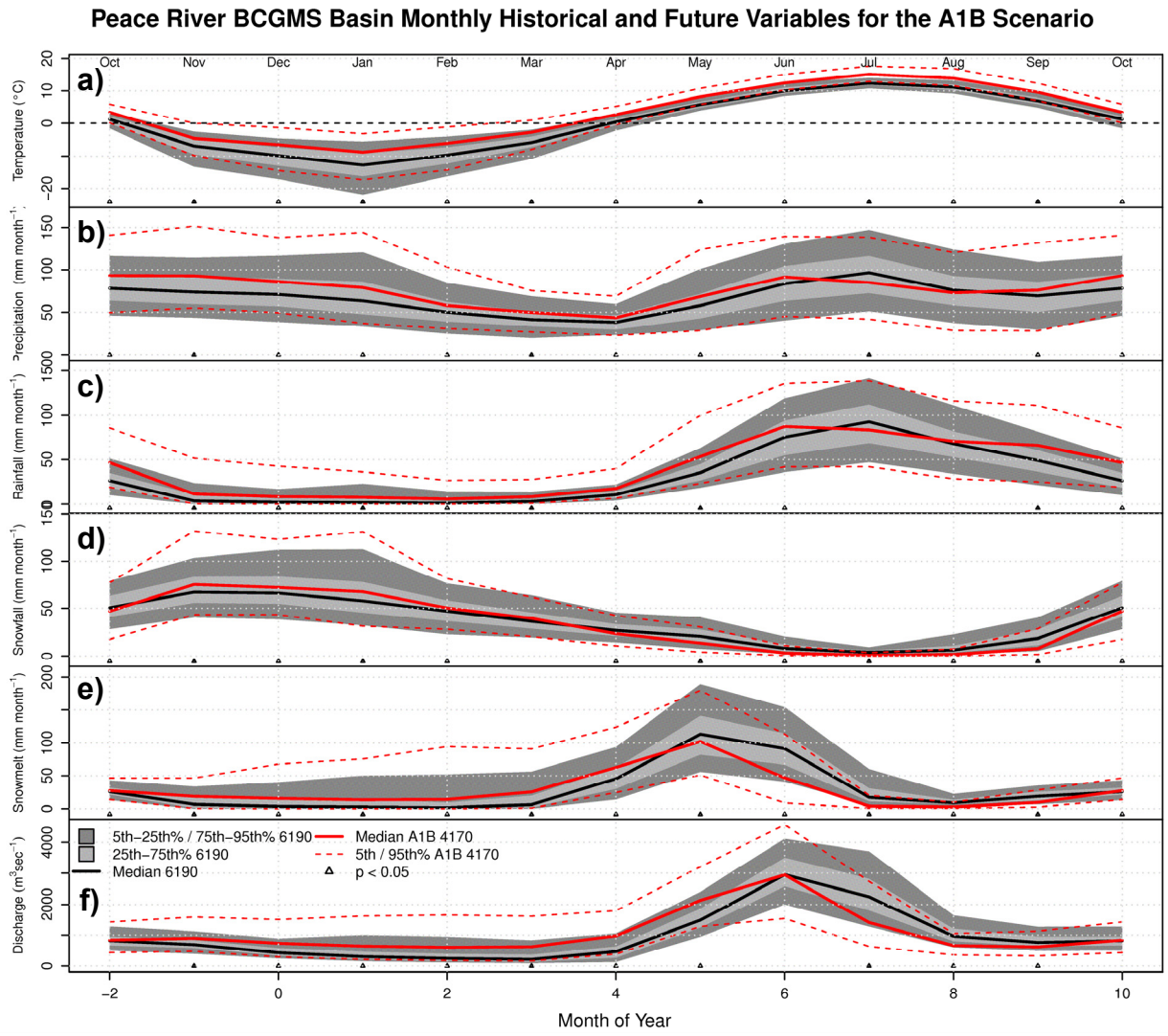

Figure 4-7. Comparison of historic (1961 - 1990) and future (2041 - 2070) monthly a) temperature, b) precipitation, c) rainfall, d) snowfall, e) snowmelt, and f) discharge statistics for the A1B ensemble for the Peace River at Bennett Dam (BCGMS). Temperature, precipitation, rainfall, snowfall and snowmelt are spatial averages for the entire basin. Historic values are represented by the median, inter-quartile range and the 5th and 95th percentiles. For clarity of presentation, future values are only represented by the median, 5th and 95th percentiles. Those months and variables where the future and historic monthly ensembles are significantly different are indicated by a triangle.

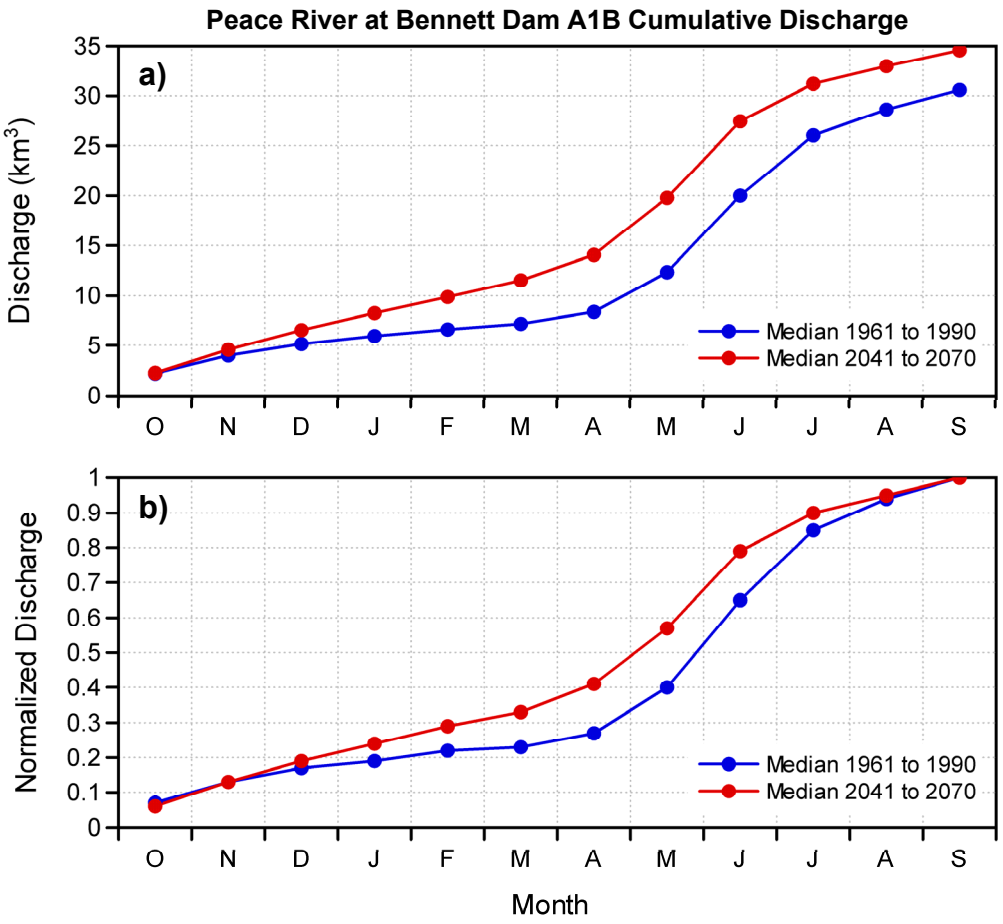

Figure 4-8. Cumulative median A1B historic and future monthly discharge over the water year (October through September) for the Peace River at Bennett Dam (BCGMS). Panels show a) absolute discharge and b) discharge normalized by the respective historic or future water year totals.

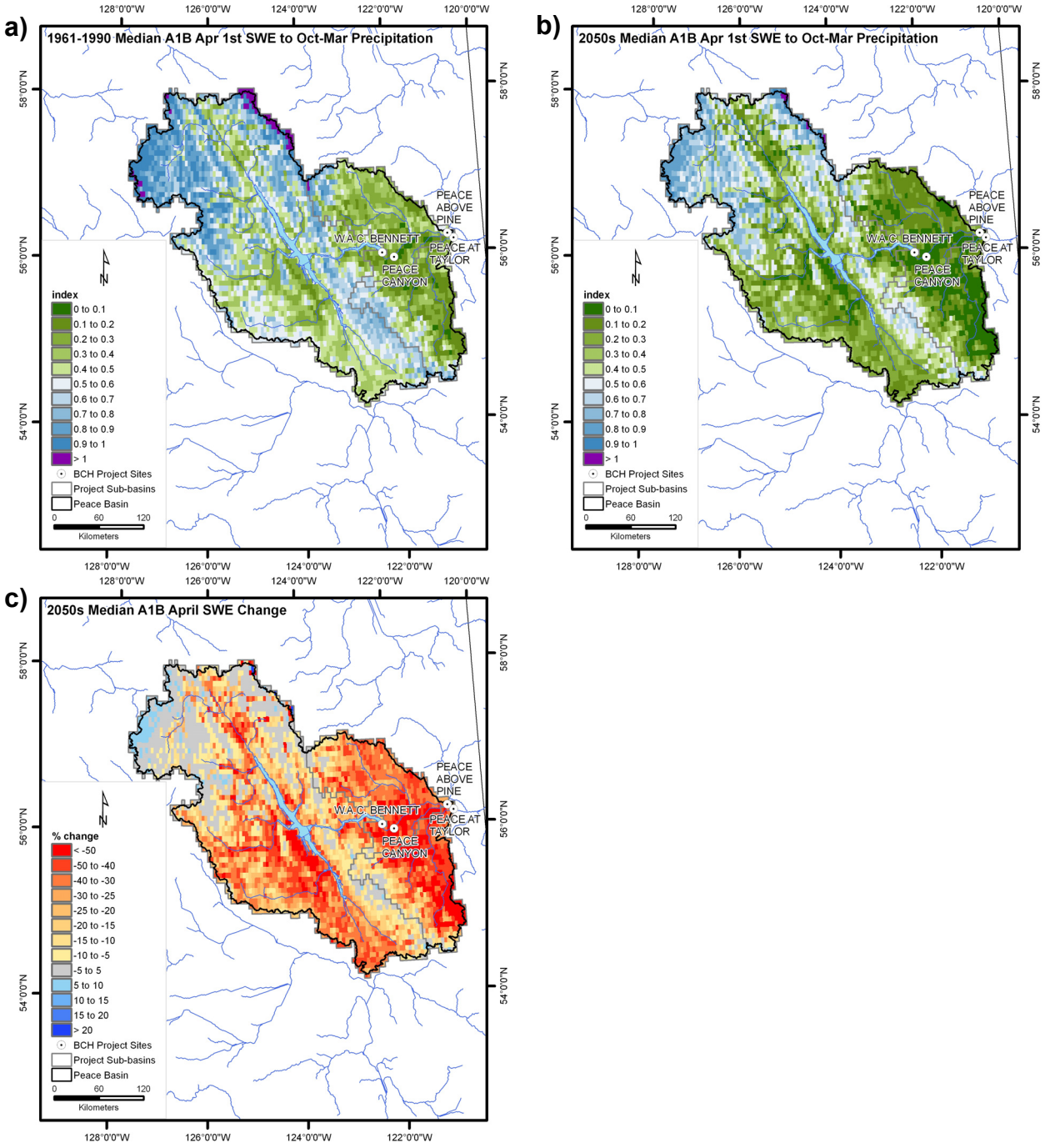

Figure 4-9. Snow storage in the Peace River study area, given as the median of the A1B ensemble of the ratio of April 1 SWE to winter precipitation (October through March) for the a) 1970s, b) the 2050s and c) the median A1B April 1 SWE relative anomaly.

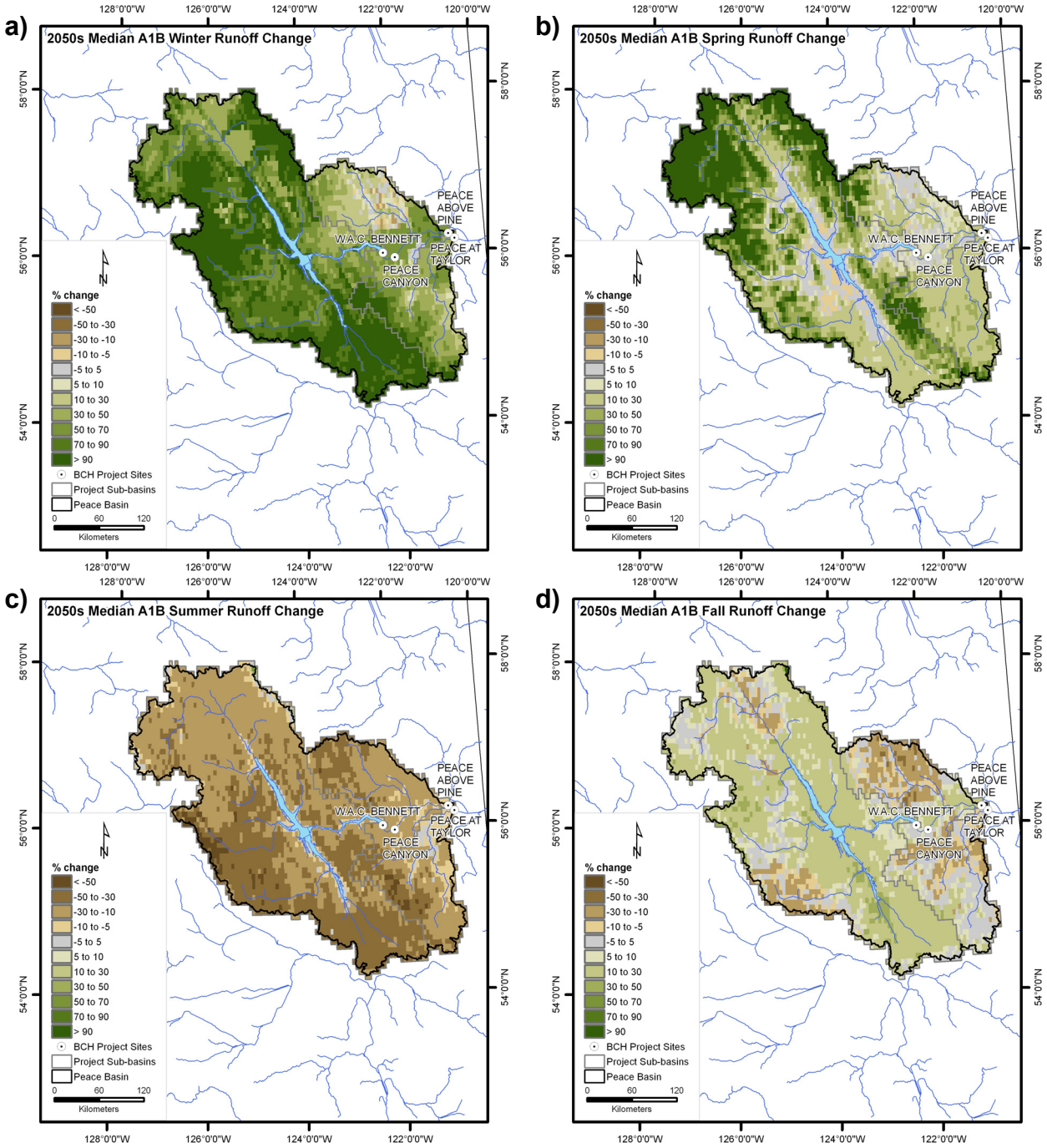

Figure 4-10. Median A1B 2050s seasonal runoff anomalies for the Peace River study area for a) winter, b) spring, c) summer, and d) fall.

4.2 Campbell River Study Area

4.2.1 Climate Projections

Projected ensemble median annual temperature increases for the Campbell region range from 1.8 °C under the B1 scenario to 2.2 °C under the A1B scenario (see Table 4-3). The projected median annual temperature change for the A2 scenarios was close to that of the B1 scenario at 1.9 °C. Temperature is projected to increase from 2.0 °C to 2.3 °C based on the median values for the three emissions scenarios in winter and from 1.8 °C to 2.5 °C in summer. Although it is acknowledged that there is considerable overlap in the projected range of temperature anomalies between all three scenarios, it would seem that the seasonal response is variable between emissions scenario ensembles, with the highest warming projected for the summer for A1B and A2 and the winter for B1. The temperature signal is robust across runs, with all 5th percentile values for all seasons and emissions ensembles showing positive anomalies (Table 4-3).

Table 4-3. Projected 2050s climate anomalies for the Campbell River study area.

Emissions Scenario	Variable	Percentile	Anomaly by Season				
			Annual	Winter (DJF)	Spring (MAM)	Summer (JJA)	Fall (SON)
A1B	Temperature (°C)	5th	1.9	1.4	1.6	1.9	1.9
		Median	2.2	2.3	2.0	2.5	2.4
		95th	3.0	2.6	3.2	3.6	3.0
	Precipitation (%)	5th	0	0	-2	-40	-1
		Median	2	4	3	-14	11
		95th	15	16	19	-3	21
A2	Temperature (°C)	5th	1.5	0.8	1.4	1.7	1.4
		Median	1.9	2.0	1.7	2.2	1.8
		95th	2.9	2.4	3.1	3.4	3.0
	Precipitation (%)	5th	-3	-4	-2	-32	-2
		Median	0	0	2	-16	5
		95th	10	10	12	-3	12
B1	Temperature (°C)	5th	1.4	1.8	1.3	1.4	1.3
		Median	1.8	2.1	1.6	1.8	1.6
		95th	2.3	2.4	2.1	2.5	2.1
	Precipitation (%)	5th	-1	-2	2	-19	2
		Median	6	5	5	-13	5
		95th	8	10	15	6	15

Projected median annual precipitation changes range from 0% under the A2 emissions scenario to +6% under the B1 emissions scenario. Winter precipitation was projected to increase under the B1 and A1B scenarios (by 5% and 4%, respectively), but no change was projected for A2 according to the median response. Similar precipitation increases were projected for the other seasons under all scenarios, except during summer when decreases of -13% to -16% were projected. These projected changes in precipitation, though not relatively large in most seasons, represent large volumes in an absolute sense in this wet climate. The precipitation signal is not as robust as that for temperature. The 95th percentile and median precipitation anomalies are generally positive throughout the winter, spring and fall, but several 5th percentile anomalies have slightly negative (or zero) percentage changes. The summer precipitation signal is consistently one of negative anomalies for the A1B and A2 scenarios, although results are not as consistent for the B1 scenario, where the 95th percentile gives a positive summer precipitation anomaly (Table 4-3). Due to the relatively small size of the Campbell study area in relation to the source resolution of the underlying GCMs, the seasonal temperature and precipitation anomalies, as represented by maps of the composite medians from the A1B ensemble, are spatially uniform (Figure 4-11 and Figure 4-12, respectively).

4.2.2 Annual Streamflow

Box-plots in Figure 4-13 are used to compare historical to projected annual discharge for the Strathcona Dam (BCSCA) study site. Values corresponding to the box-plots are summarized in Table 4-4. Historically median annual flow rates in the Upper Campbell were 83 m^3/s (with a range of approximately 54 m^3/s to 112 m^3/s) over the 1961-1990 period. On an annual basis, projected relative changes in median annual streamflow for the 2050s are negligible, being only 4%, 0% and 2% for scenarios A1B, A2 and B1, respectively. These changes correlate somewhat with the projected median annual precipitation changes (Table 4-3). For the A2 and B1 scenarios, the distribution of annual discharge projected for the 2050s is not significantly different from the historical distribution. Only the A1B scenario indicates a statistically significant difference in the historical and future annual discharge ensembles. Nevertheless, the change in median annual discharge for the A1B scenario is negligible and, arguably, operationally insignificant.

4.2.3 Monthly Streamflow

In the 2050s, the Campbell is projected to change from a hybrid to a predominantly rainfall-dominated (pluvial) regime, with increased monthly streamflow from October to April and decreased streamflow from May to September, due to a substantial reduction in the historical spring freshet (Figure 4-14). Based on all 23 runs, the largest increases in median monthly streamflow are projected to take place in January (changes range from 2 m^3/s to 91 m^3/s), and the largest decreases are projected for June (changes range from -44 m^3/s to -114 m^3/s). For the majority of the months, except include May, September and October, all scenarios and runs agree on the direction of change. Changes in streamflow for the A1B runs are generally the largest in magnitude, particularly for changes projected during the fall and winter months. The shift from a hybrid to a more pluvial regime is expected to result in large changes in monthly streamflow timing, as exemplified by the median A1B historical and future cumulative monthly discharge curves shown in Figure 4-15. Discharge volume is projected to accumulate more rapidly during the winter and early spring, which is predominantly a function of changes in streamflow timing, as projected changes in annual volume are negligible (Figure 4-15a). When normalized for total annual volume we note that the half-flow month is projected to occur roughly two months sooner in the future, in January as opposed to March (Figure 4-15b).

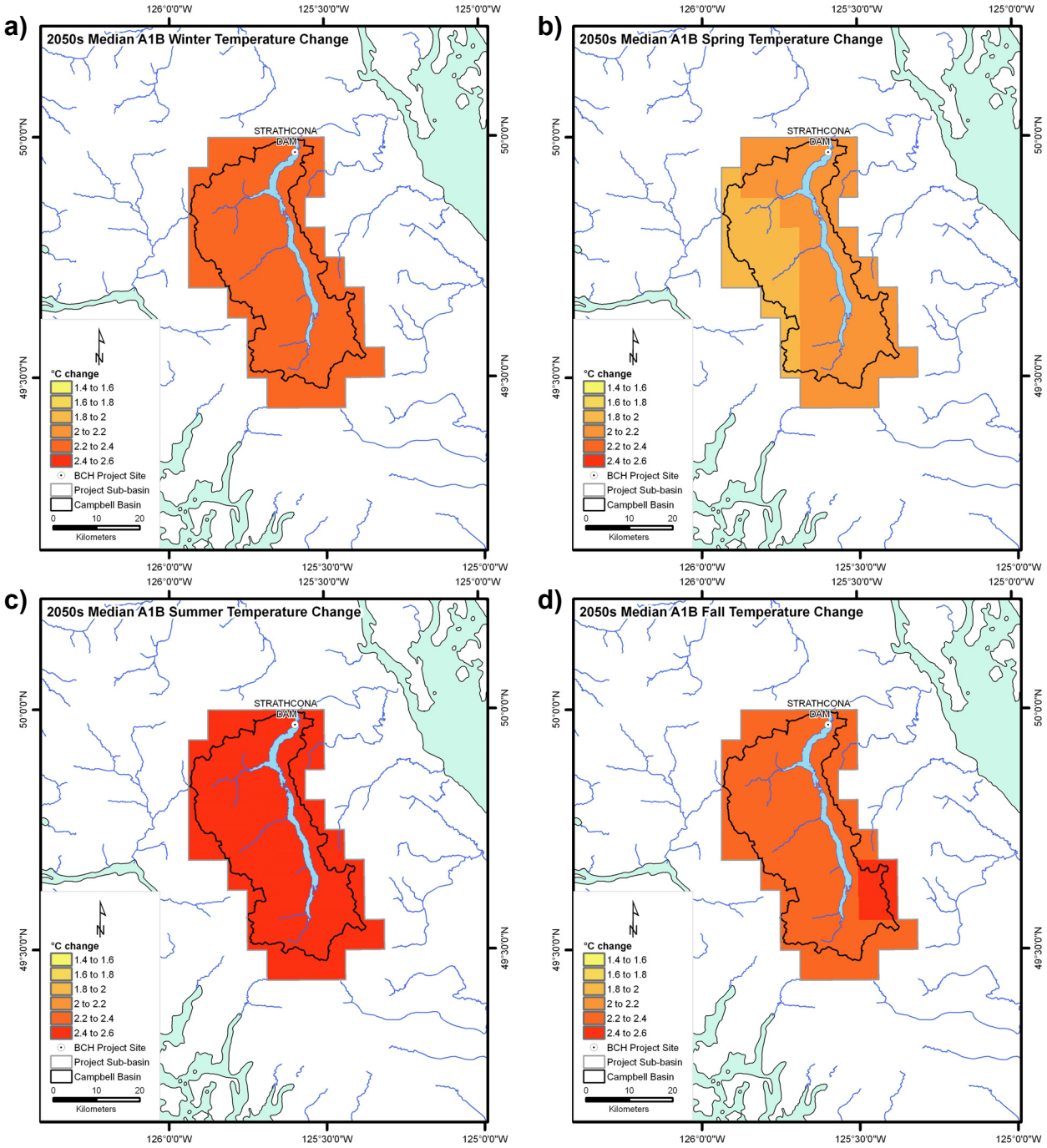

Figure 4-11. Median A1B seasonal temperature changes for the Campbell River study area for a) winter (DJF), b) spring (MAM), c) summer (JJA), and d) fall (SON.

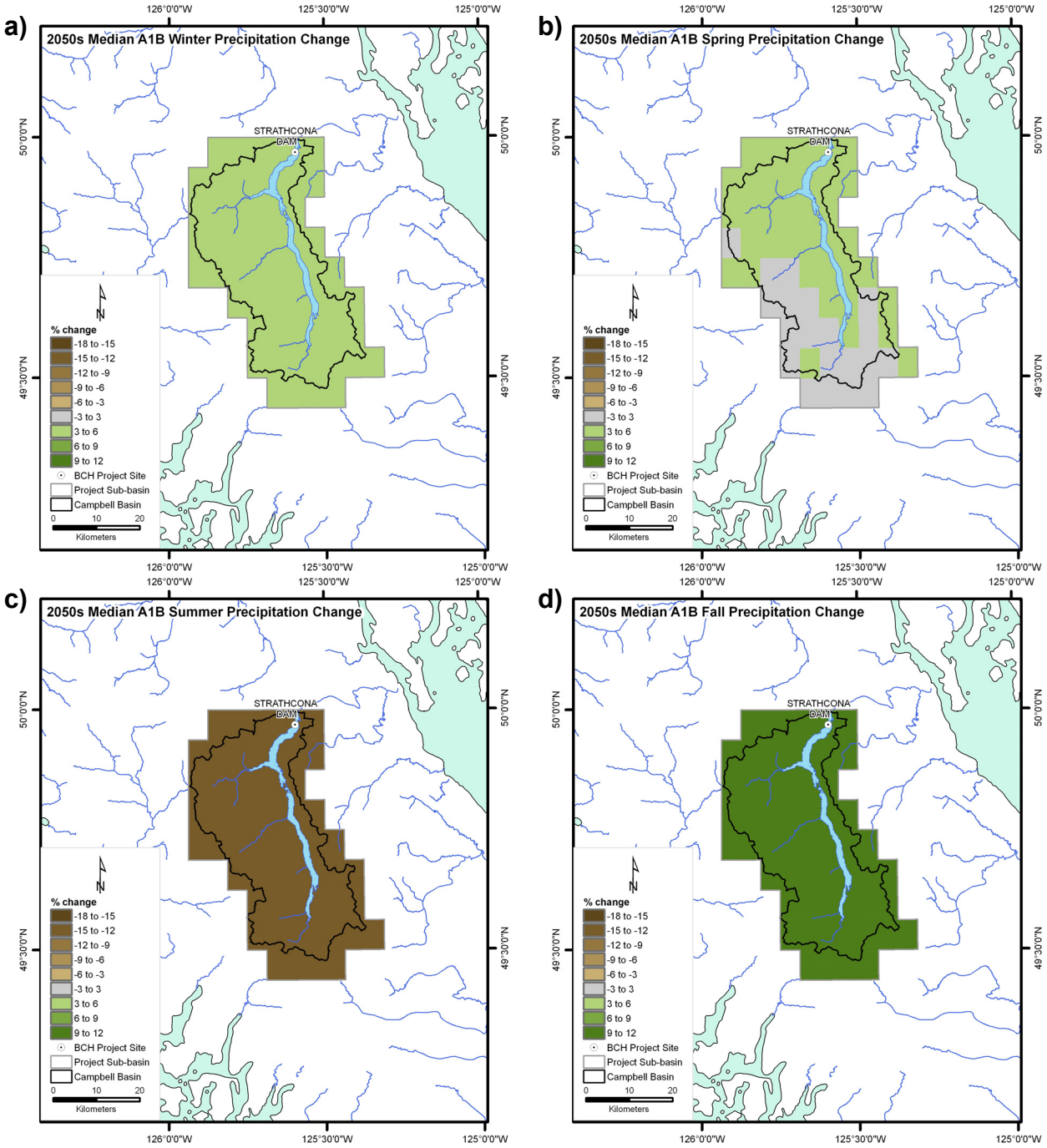

Figure 4-12. Median A1B seasonal precipitation changes for the Campbell River study area for a) winter (DJF), b) spring (MAM), c) summer (JJA), and d) fall (SON).

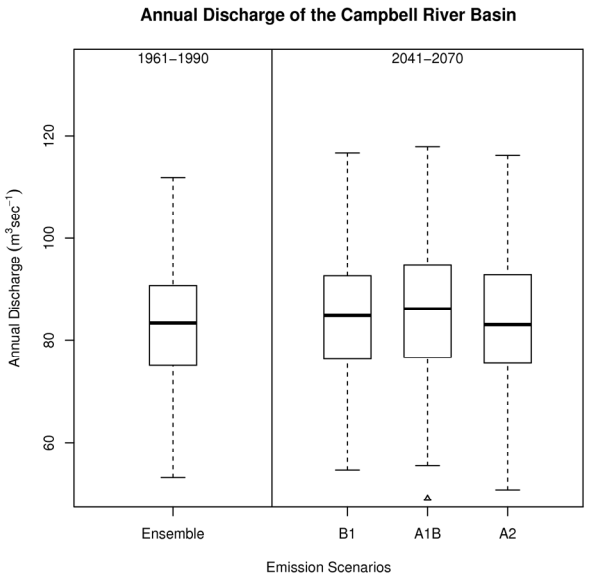

Figure 4-13. Annual discharge box-plots by emissions scenario for the historic (1961 - 1990) and future (2041 - 2070) period for the Campbell River at Strathcona Dam (BCSCA). Each box-plot summarizes the median (thick horizontal line), inter-quartile range (IQR; box showing 75th to 25th percentile) and the minimum and maximum (dotted lines). Those cases where the future ensemble is significantly different than the historical ensemble are indicated by a triangle below the box.

Table 4-4. Historic and future annual discharge ensemble statistics and anomalies for the Campbell River project site.

Percentile	Annual Discharge Statistics by Period and Emissions (m^3/s)				Relative Difference		
	1961 to 1990	2040 to 2071					
		B1	A1B	A2	B1	A1B	A2
			BCSCA				
minimum	54	55	55	51	0.02	0.02	-0.06
75th	75	76	77	75	0.01	0.03	0.00
median	83	85	86	83	0.02	0.04	0.00
25th	91	93	95	93	0.02	0.04	0.02
maximum	112	117	118	116	0.04	0.05	0.04

The historic and future A1B monthly temperature, precipitation (including rainfall and snowfall), snowmelt and discharge percentiles for the BCSCA sub-basin are compared in Figure 4-16. The monthly temperature distributions show a strong and statistically significant signal of shifting to warmer temperatures in the 2050s in all months, but particularly in the summer months of July, August and September (Figure 4-16a). A signal of precipitation change in the 2050s is only evident for the summer months of June, July and August (reduced precipitation) and the fall and winter months of October through December (increased precipitation; Figure 4-16b). Although the reduction in median summer precipitation is projected to be relatively large (-14% for A1B, Table 4-3), summer is the driest part of the

year on Vancouver Island and the absolute projected shift in the distribution of future precipitation is negligible (Figure 4-16b). When compared to historical variability, the projected changes in the distribution of monthly precipitation are not as strong as those for temperature. Projections indicate that rainfall will generally increase and snowfall will generally decrease throughout the fall, winter and spring (Figure 4-16c and Figure 4-16d, respectively), and that these respective changes are larger in magnitude (and statistically significant for a larger number of months) than those projected for precipitation. This leads to the conclusion that increased rainfall is predominantly in response to a change in precipitation phase due to higher temperatures during the winter season, which results in a proportionate reduction in snowfall. Warmer temperatures are projected to result in increased mid-winter and early-spring snowmelt, whereas reduced snowfall results in less snow available for melt during the historical freshet period of April through July (Figure 4-16e). The evidence suggests that the dominant driver of higher discharge in the fall and winter (Figure 4-16f) is a change to warmer temperatures, which results in proportionately more precipitation falling as rain. The loss of snow storage, coupled to warmer temperatures, which also raises evaporative demand (not shown) in the spring and summer results in a rather substantial shift to less discharge in the months of June, July, August and September, effectively extending the summer low flow period. Future and historical monthly discharge percentiles for BCSCA have been summarized by emissions scenario in separate appendices for A1B, A2 and B1, respectively.

4.2.4 Snowpack and Runoff

Elevation in the Campbell ranges from 139 m to 2200 m (Figure 2-4), with a median elevation of roughly 1000 m. This elevation range results in large spatial variability of precipitation phase over the study area. The A1B ensemble median values of SWE_p/P_w over 1961 - 1990 range from 0 to 0.1 in the north-east (i.e., almost entirely rainfall) to over 0.5 to 0.7 in the south-east, with intermediate (or hybrid) values in the remainder of the study area (Figure 4-17a). However, due to the high absolute precipitation amounts observed in the area, even moderate or small SWE_p/P_w values can be associated with large snow accumulations (e.g., Figure 2-5). In the 2050s, the ratio of peak snow water to total October-to-March precipitation is projected to change dramatically. Roughly 50% of the study area, particularly in the north and along the Buttle Lake valley, will be entirely rainfall dominated ($SWE_p/P_w \leq 0.1$) (Figure 4-17b). Mid-elevations will see only slightly more snow ($SWE_p/P_w \leq 0.2$), and the south-east region of the study that is historically snow-dominated will only experience SWE_p/P_w in the order of 0.2 to 0.4 (Figure 4-17b). The peak SWE on April 1 will decrease across the basin in the 2050s as compared to the 1970s (Figure 4-17c). The largest relative decrease in peak SWE (< -80%) is projected to occur in the north, with relative changes of -30% to -40% projected to occur in the historically snow-dominated region in the south-east.

The spatial A1B median seasonal runoff anomalies are presented in Figure 4-18. Runoff is projected to increase over the entire study area during the winter (anomalies range from 10% to > +50%) and fall (+5 to +10%) (Figure 4-18a and d). The winter runoff anomalies correlate with elevation, becoming increasingly positive with increasing elevation. Due to both orographic enhancement of precipitation and increasing snow accumulation with elevation, warmer future temperatures will generate proportionately more rainfall with increasing elevation. Runoff anomalies are more spatially uniform during the fall (Figure 4-18d). At this time of year projected area-wide warming will have little effect on precipitation phase as historical temperatures are already above freezing (Figure 4-16a). Therefore the increase in runoff is likely attributed to the increase in fall precipitation projected by the A1B ensemble (Table 4-3). During the spring the median A1B ensemble projects decreased runoff at low elevation and increased runoff at high elevation (Figure 4-18b), likely reflecting changes in the position of the climatological snow line between the historical and future periods (not shown). Despite negative peak SWE anomalies throughout the study area (Figure 4-17c), there will still be snow accumulating at higher elevations. Also,

where snow is still present in the future in sufficient volume (at the highest elevations), higher temperatures are expected to increase melt rates and, hence, snowmelt runoff during the spring. Conversely, where snow will no longer be present at low elevations, snowmelt runoff will be non-existent and spring runoff anomalies will be negative. Median A1B ensemble projections show decreased runoff across the study area in summer, generally in the order of -50% or more (Figure 4-18c). The negative summer runoff anomalies are attributed to the earlier loss of snow cover (and earlier draw-down of soil moisture storage) and increased evapotranspiration (not shown).

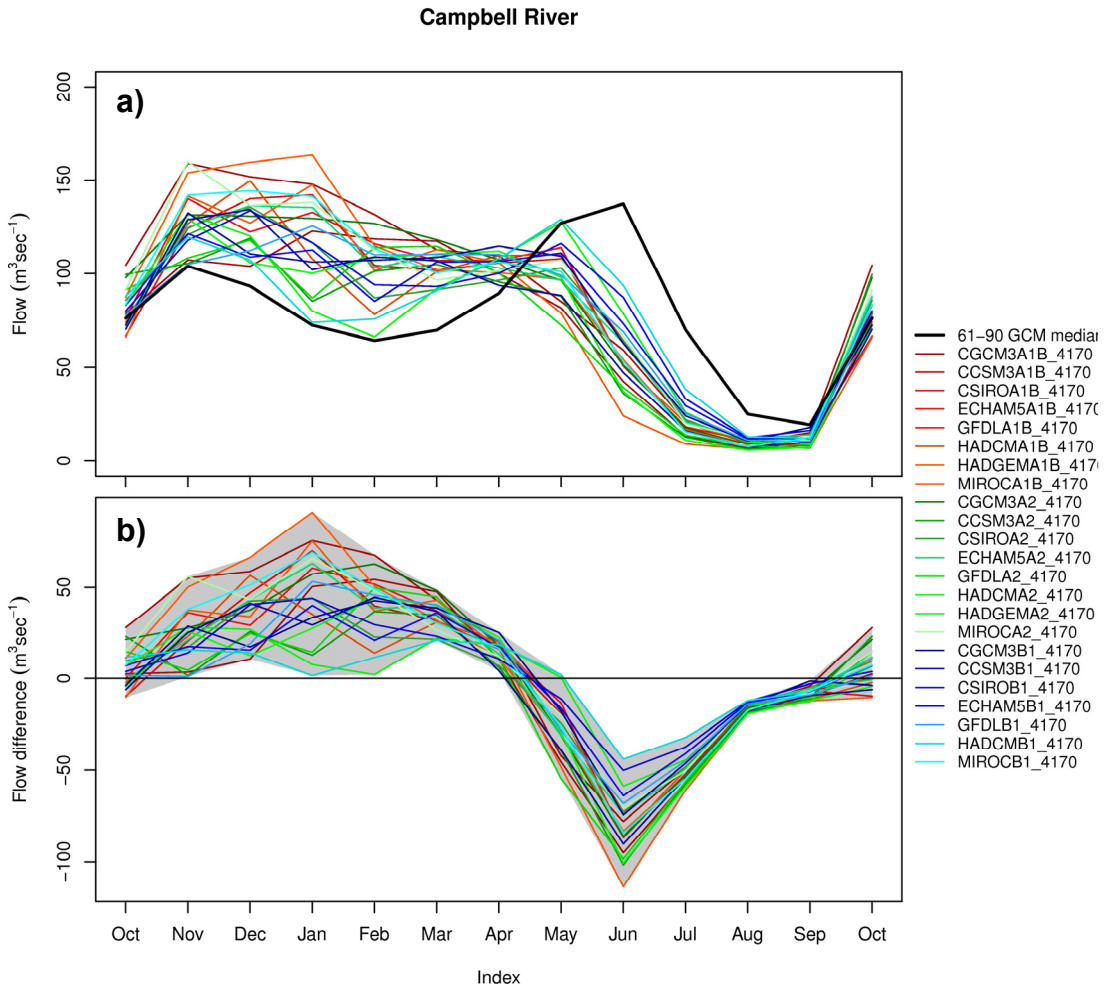

Figure 4-14. Median monthly discharge for the Campbell River at Strathcona Dam (BCSCA) showing: a) historic (1961 - 1990) and future (2041 - 2070) discharge, and b) the 2050s anomaly. Historic discharge (black line) is presented as the full ensemble median (23 runs x 30 years) and each future discharge value is the median of each GCM run (1 run x 30 years). Anomalies represent the future monthly median minus the historic ensemble monthly median.

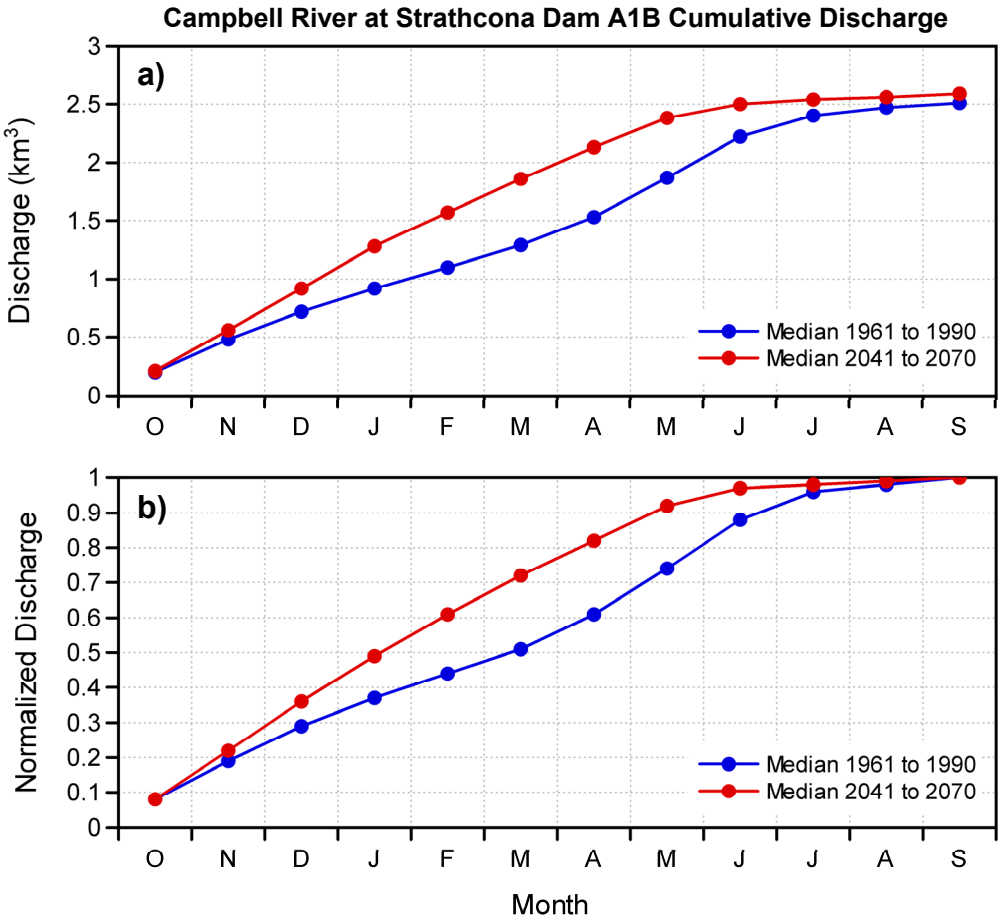

Figure 4-15. Cumulative median A1B historic and future monthly discharge over the water year (October through September) for the Campbell River at Strathcona Dam (BCSCA). Panels show a) absolute discharge and b) discharge normalized by the respective historic or future water year totals.

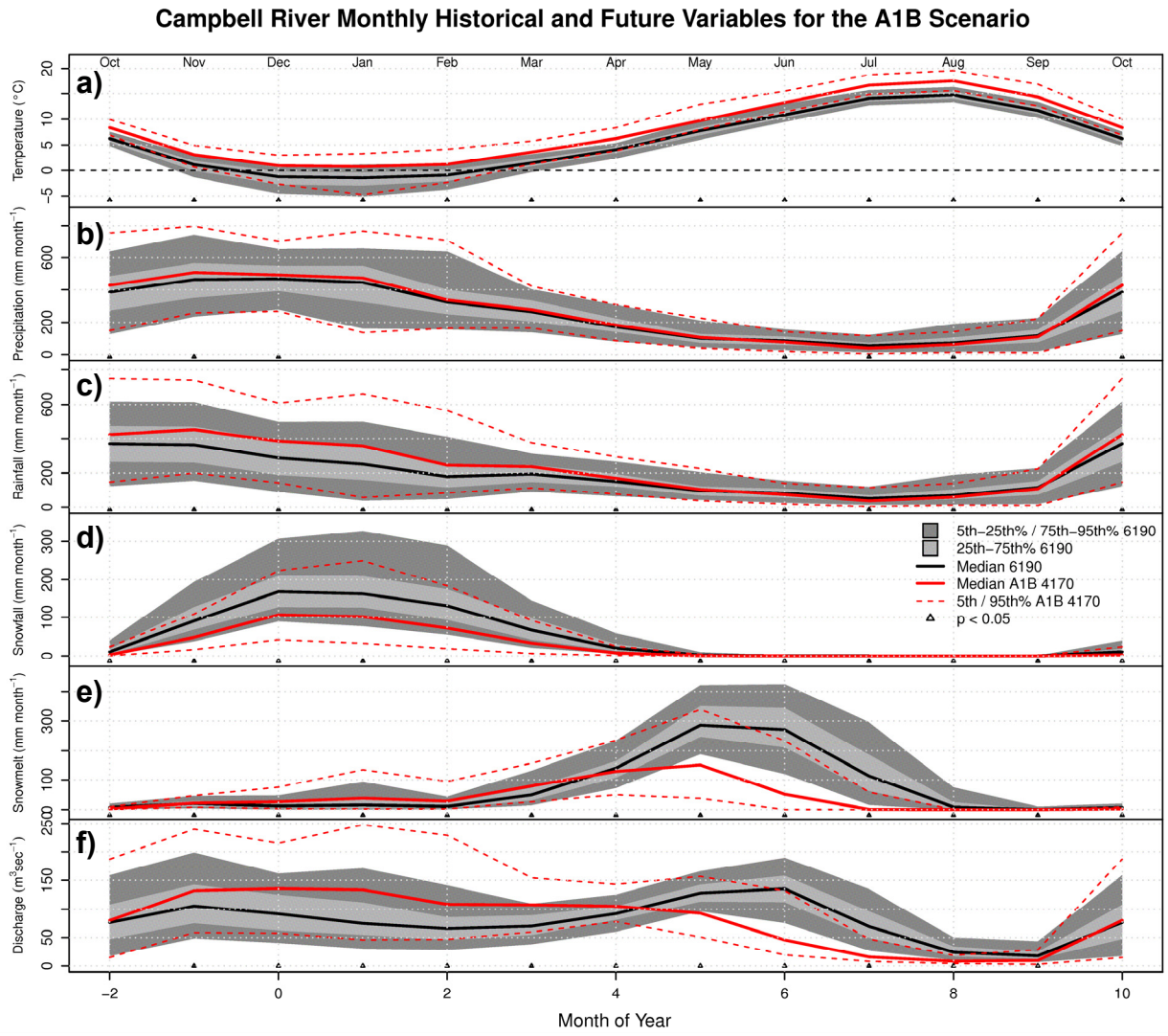

Figure 4-16. Comparison of historic (1961 - 1990) and future (2041 - 2070) monthly a) temperature, b) precipitation, c) rainfall, d) snowfall, e) snowmelt, and f) discharge statistics for the A1B ensemble for the Campbell River at Strathcona Dam (BCSCA). Temperature, precipitation, rainfall, snowfall and snowmelt are spatial averages for the entire basin. Historic values are represented by the median, inter-quartile range, and the 5th and 95th percentiles. For clarity of presentation, future values are only represented by the median, 5th and 95th percentiles. Those months and variables where the future and historic monthly ensembles are significantly different are indicated by a triangle.

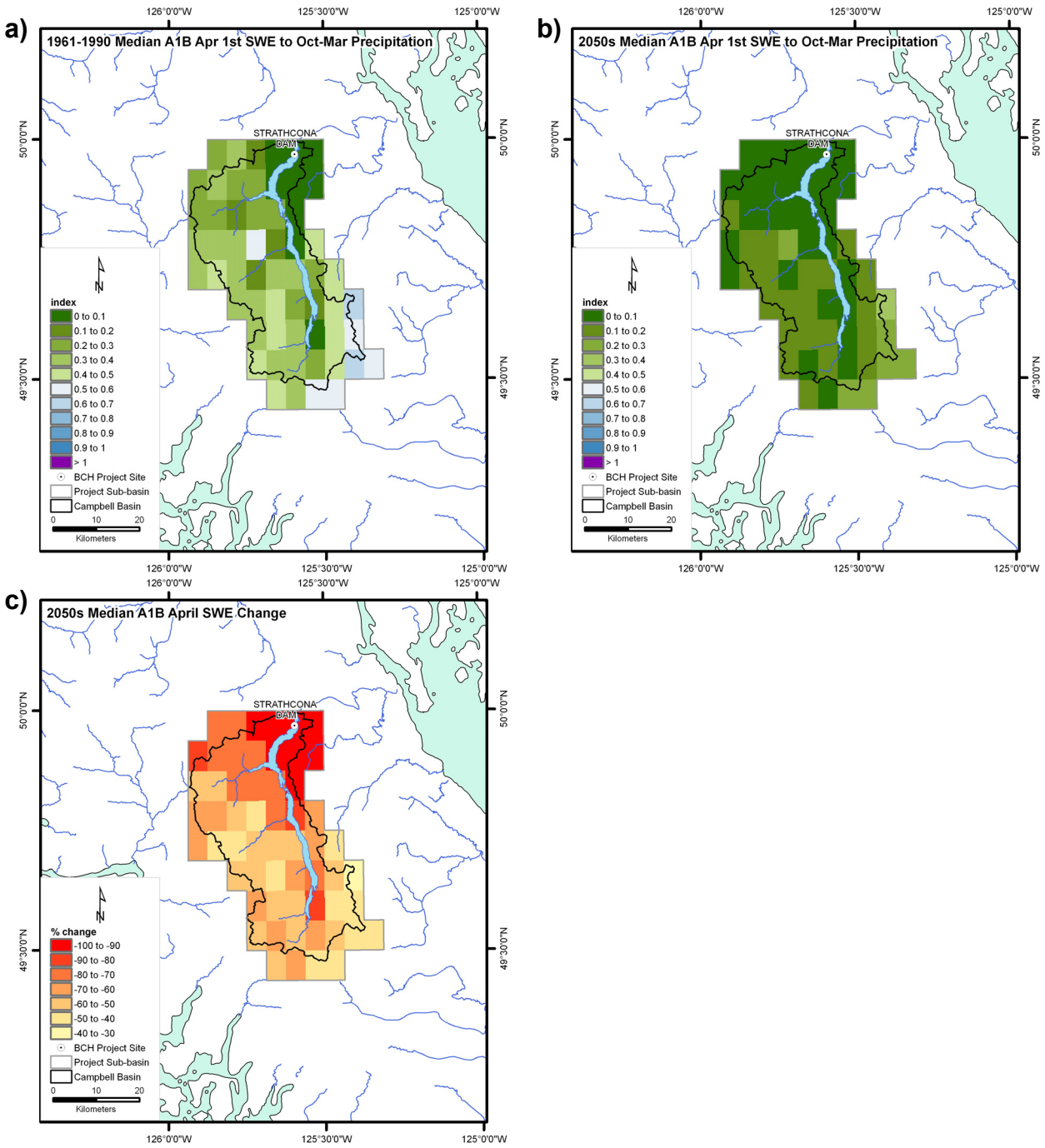

Figure 4-17. Snow storage in the Campbell River study area, given as the median of the A1B ensemble of the ratio of April 1 SWE to winter precipitation (October through March) for the a) 1970s, b) the 2050s and c) the median A1B April 1 SWE relative anomaly.

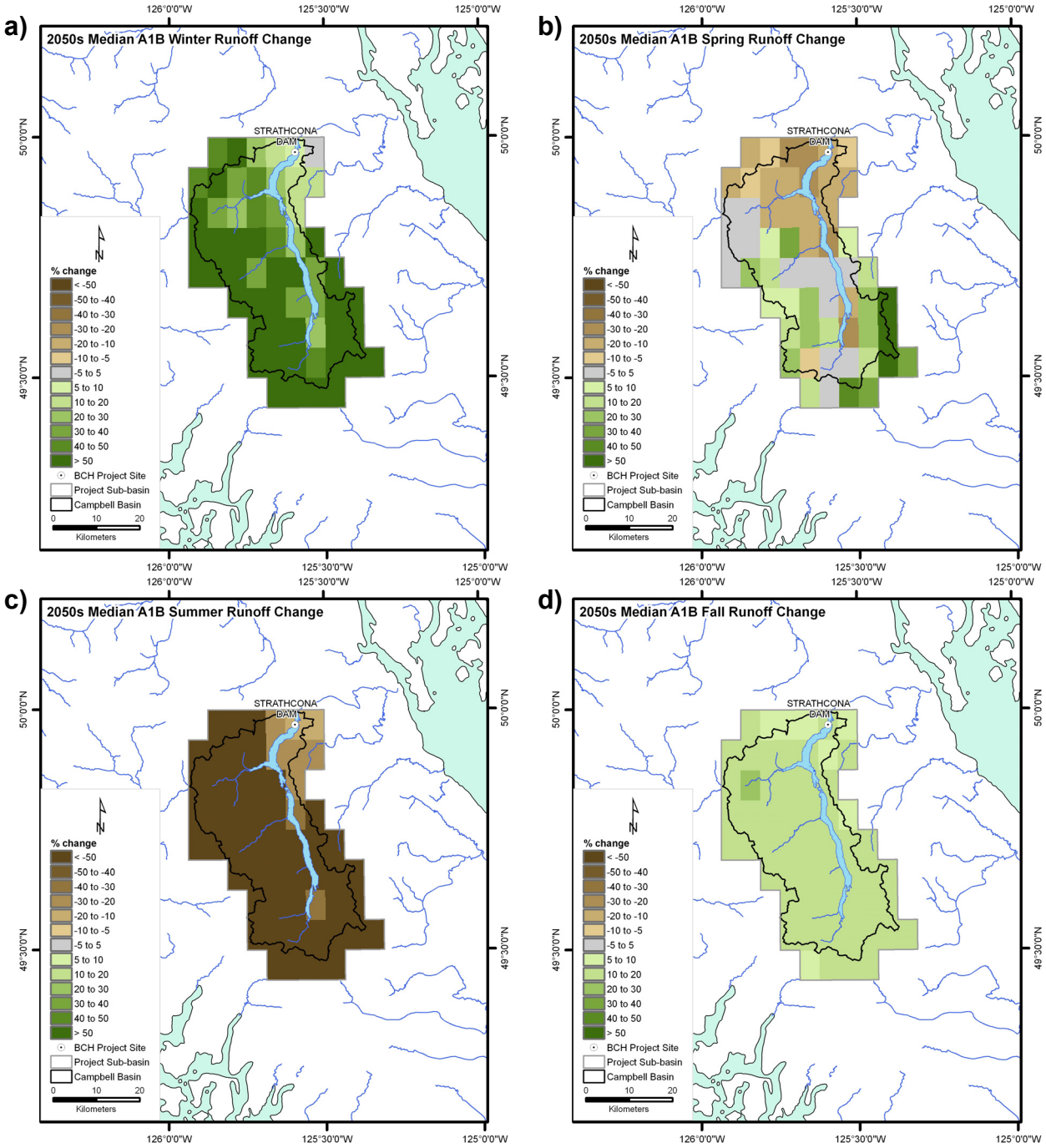

Figure 4-18. Median A1B 2050s seasonal runoff anomalies for the Campbell River study area for a) winter, b) spring, c) summer, and d) fall.

4.3 Upper Columbia Study Area

The use of the VIC state files to re-initialize SWE in glacier cells introduced some model instabilities for all three (A1B, A2 and B1) CSIRO-driven runs. This problem was localized to a few cells in the BCHAR sub-basin. This issue did not affect any of the remaining runs, nor did it affect VIC simulations in the remainder of the Upper Columbia study area for the CSIRO-generated runs. The CSIRO runs exhibit an anomalously high precipitation bias (as compared to the other GCMs) over the Upper Columbia study area for the 1950 to 1995 historical period (3% annually and 4% in winter). Therefore, despite bias-correction in the statistical downscaling, a (presumed) residual bias in the CSIRO-driven downscaled daily precipitation fields resulted in an overestimation of glacier accumulation simulated over the historical period in several high-elevation grid cells. In this case, updating the glacier state to observed conditions in 1995 required reducing SWE in the cells in question, introducing a sufficiently large imbalance in the water and energy budgets that the VIC model simulations could not be completed. Nevertheless, streamflow-based analysis for the BCHAR study site does not incorporate runs generated by the CSIRO MK3 GCM. Also, for spatial consistency, none of the map-based analysis uses VIC model output data from any of the CSIRO-based runs.

4.3.1 Climate Projections

Projected climate change for the 2050s is summarized as temperature and precipitation anomalies in Table 4-5. Anomalies are grouped by emissions scenario and presented for the entire study area as the median change as well as the 5th and 95th percentile change. Temperatures in the Upper Columbia are projected to increase, with all projections indicating a very robust (i.e., consistent) signal across emissions scenarios, seasons, and individual GCM runs (i.e., all percentiles show a positive anomaly). Warming is projected to be greatest in the summer, with median changes of 4.1 °C, 3.3 °C and 2.3 °C for the A1B, A2 and B1 emissions scenarios, respectively. Warming is of roughly similar magnitude in the remaining seasons. Annual median temperature anomalies are 2.7 °C, 2.3 °C and 1.8 °C for the A1B, A2 and B1 emissions scenarios, respectively. The spatial distribution of the seasonal temperature anomalies, mapped as the median change by grid cell for the A1B scenario ensemble, is shown in Figure 4-19. The spatial patterns of the seasonal temperature changes generally reflect the temperature trends inherent in the coarse resolution source GCMs. The median A1B temperature anomalies are spatially uniform for the winter, spring and fall seasons, although a slight east-west gradient and south-north gradient of increasingly positive temperature anomalies are evident for winter and spring, respectively. Summer temperature anomalies show the strongest spatial gradient, ranging from 3 °C in the north to almost 5 °C in the south.

The precipitation projection for the Upper Columbia is less robust than that for temperature. Although the winter, spring and fall are generally projected to get wetter, median changes are marginal and the 5th percentile changes indicate that some GCMs project little change or even slightly drier conditions (Table 4-5), particularly for the A2 emissions scenario. At the opposite extreme, many of the 95th percentile changes are in excess of 20%, particularly in winter and fall for all three emissions scenarios. Summers in the Upper Columbia are projected to become drier. As per the other seasons, the range in GCM results (as indicated by the 5th and 95th percentile changes) for summer is large, ranging from -26% (5th percentile for A1B) to 5% (95th percentile for B1). On an annual basis, precipitation is expected to change only marginally, with median precipitation anomalies of 7%, 5%, and 10%, respectively for the A1B, A2 and B1 emissions scenarios. The spatial distribution of the seasonal precipitation anomalies, mapped as the median change by grid cell for the A1B scenario ensemble, is shown in Figure 4-20. Like temperature, the spatial patterns of the precipitation changes reflect the precipitation trends of the coarse resolution source GCMs. Both winter and fall median precipitation anomalies, which are positive throughout the study area, indicate gradients of increasing wetness from east to west and south to north. Median precipitation

anomalies for spring, also positive throughout the study area, exhibit somewhat less spatial cohesion, although an east-west and south-north gradient of increasing wetness is suggested. Summer mean precipitation anomalies are negative across the study area, exhibiting a weak gradient of increasing dryness from south to north.

Table 4-5. Projected 2050s climate anomalies for the Upper Columbia River study area.

Emissions Scenario	Variable	Percentile	Anomaly by Season				
			Annual	Winter (DJF)	Spring (MAM)	Summer (JJA)	Fall (SON)
A1B	Temperature (°C)	5th	2.3	1.6	1.7	2.6	2.2
		Median	2.7	2.7	2.2	4.1	2.7
		95th	3.7	3.5	3.3	5.0	3.7
	Precipitation (%)	5th	0	6	-1	-26	4
		Median	7	14	13	-13	14
		95th	19	29	20	-3	30
A2	Temperature (°C)	5th	1.9	0.8	1.3	2.4	1.7
		Median	2.3	2.5	2.0	3.3	2.1
		95th	3.5	3.2	3.2	4.8	3.6
	Precipitation (%)	5th	-2	-2	8	-25	-4
		Median	5	15	13	-11	7
		95th	16	27	18	-3	24
B1	Temperature (°C)	5th	1.7	0.9	1.1	1.9	1.5
		Median	1.8	2.1	1.5	2.3	1.7
		95th	2.8	3.3	2.8	3.1	2.3
	Precipitation (%)	5th	4	-1	9	-11	1
		Median	10	15	14	-5	13
		95th	15	25	21	5	28

4.3.2 Annual Streamflow

A comparison of historical to projected annual discharge for each study site in the Upper Columbia study area is shown graphically via box-plots in Figure 4-21 and summarized in Table 4-6. The reader is reminded that the range of values presented in the box-plots represents the combined effect of inter-GCM variability in response to emissions forcing and inter-annual variability in simulated streamflow. In the headwaters of the Columbia River annual discharge for the Spillimacheen project site (SPINS) is projected to increase in the 2050s (Figure 4-21a), with increases in median discharge of 17%, 12% and 14% for the A1B, A2 and B1 scenarios, respectively. However, the ensemble ranges, particularly for the A1B scenario runs, are higher in the future. For the A1B scenario, the lower limit of future projections is 3% less than the historic limit, whereas the upper limit is 26% higher than the historic limit (Table 4-6). Projected changes in the ensembles of annual discharge for all three scenarios are statistically significant. For the Columbia River at Mica Dam (BCHMI), the uppermost regulated project on the Columbia River, annual discharge is projected to increase in the future (Figure 4-21b; Table 4-6). Increases in median

discharge are 16%, 17% and 22% for the B1, A2 and A1B scenarios, respectively. Increases are statistically significant for all three scenarios. As well, the 25th percentile annual discharge for the 2050s exceeds the historic 75th percentile for all emissions scenarios (i.e., 75% of future projected annual discharge values exceed the 75th percentile of the historic ensemble; Table 4-6). Although annual discharge projected for the A1B scenario exhibits the largest change, projections also exhibit more variability than either the A2 or B1 scenarios.

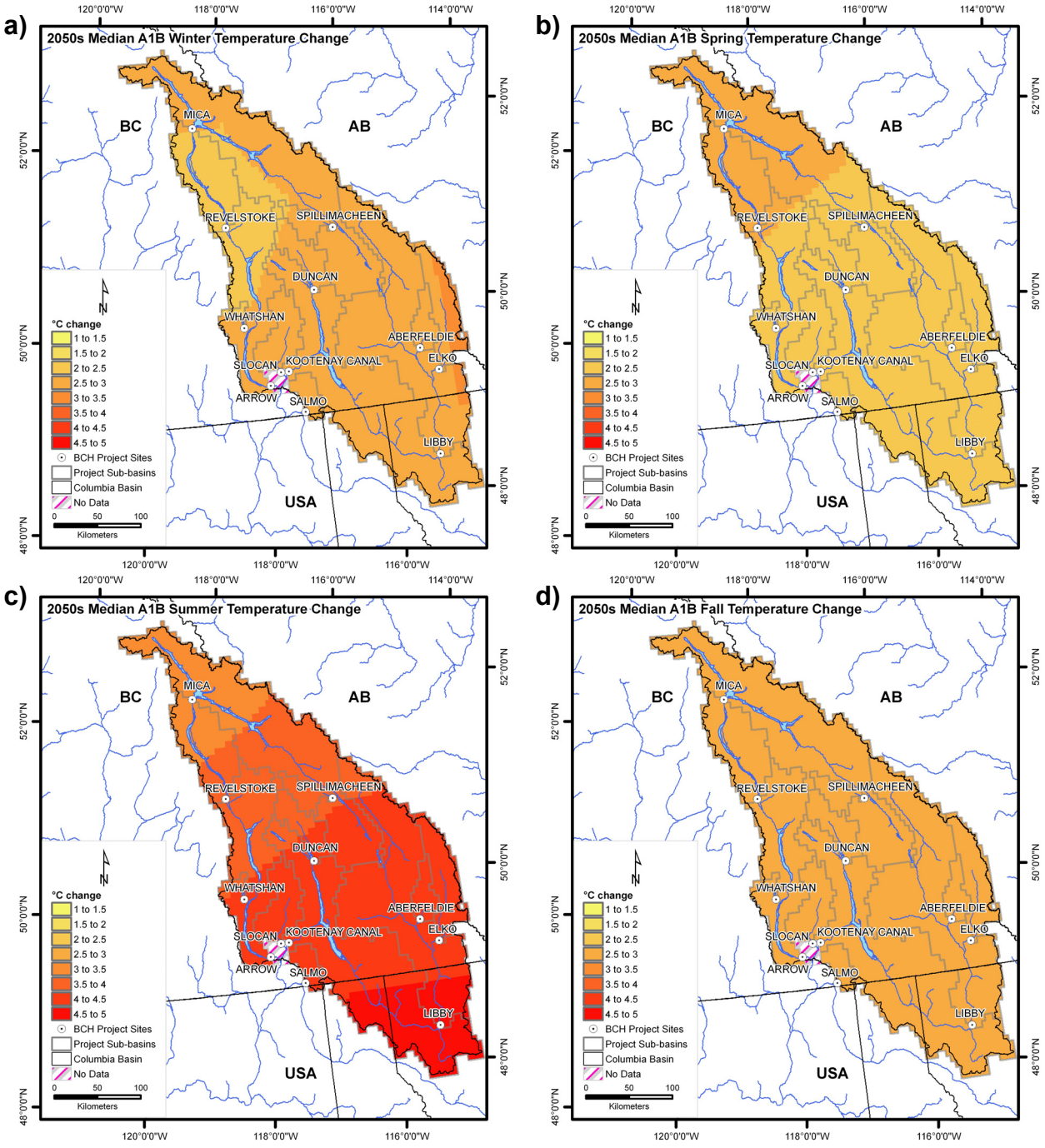

Figure 4-19. Median A1B seasonal temperature changes for the Upper Columbia study area for a) winter (DJF), b) spring (MAM), c) summer (JJA), and d) fall (SON).

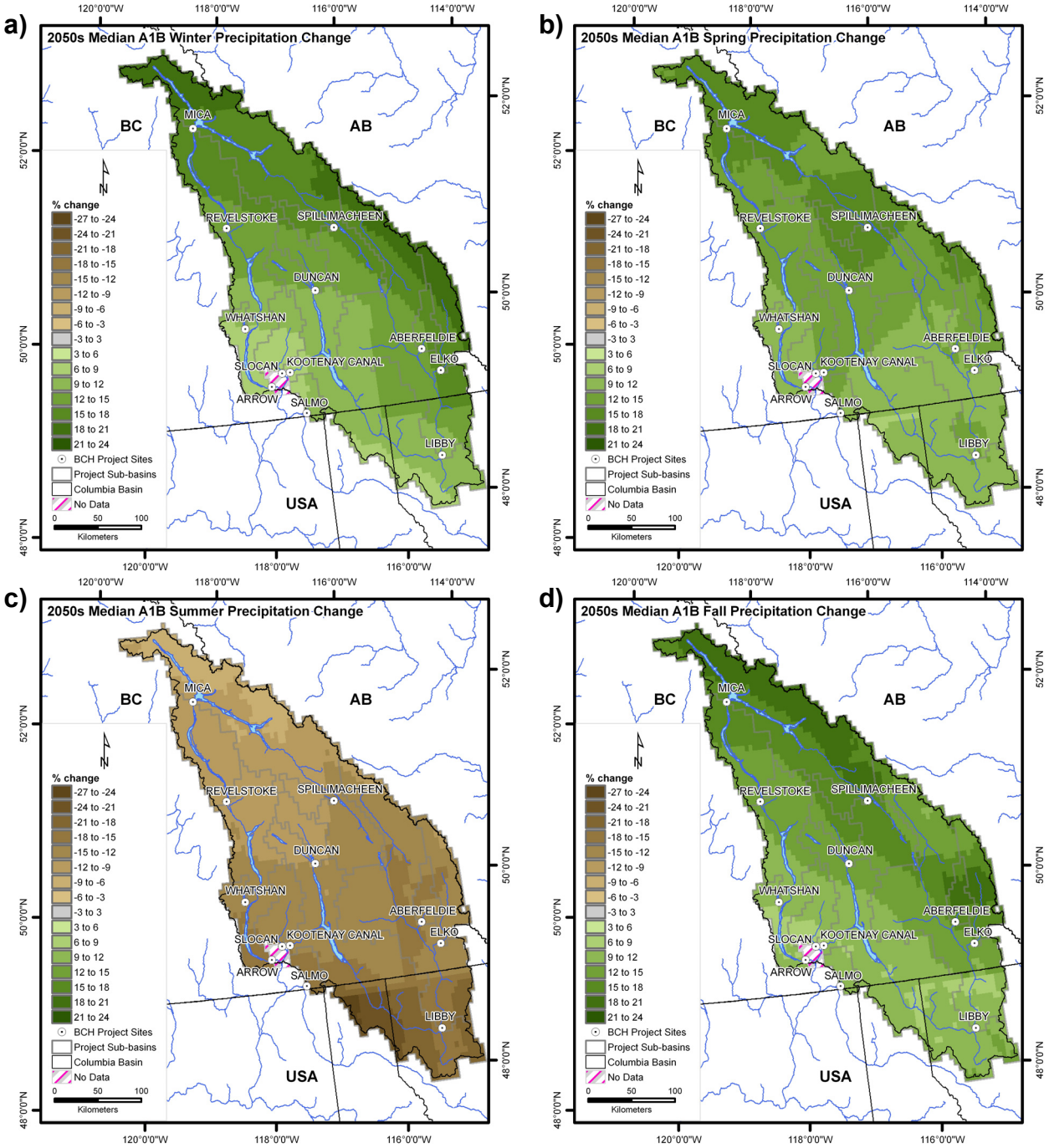

Figure 4-20. Median A1B seasonal precipitation changes for the Upper Columbia study area for a) winter (DJF), b) spring (MAM), c) summer (JJA), and d) fall (SON).

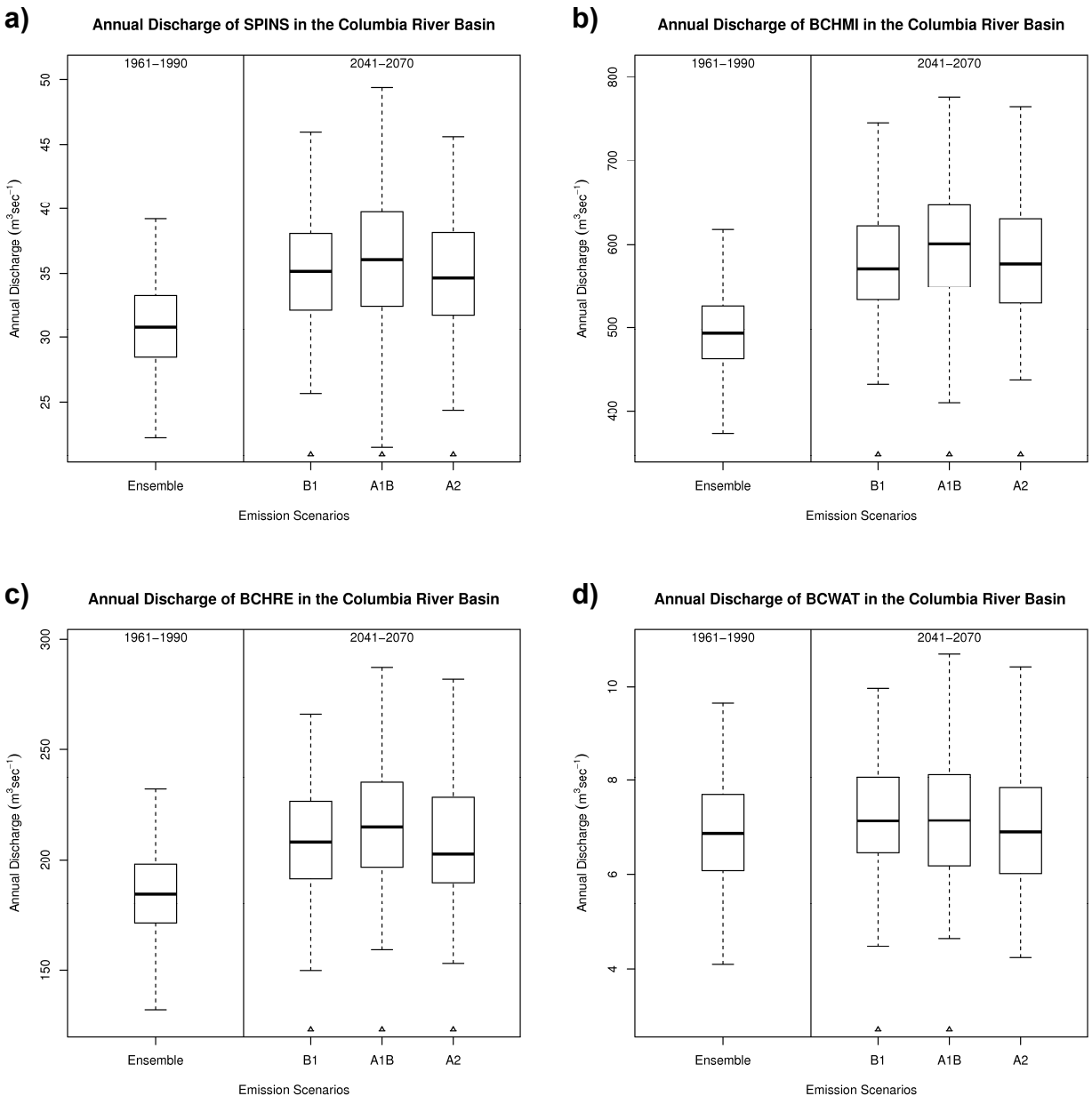

Figure 4-21. Annual discharge box-plots by scenario for the historic (1961 - 1990) and future (2041 - 2070) period for the a) Spillimacheen River near Spillimacheen (SPINS), b) Columbia River at Mica Dam (BCHMI), c) Columbia River at Revelstoke Dam (BCHRE), d) Whatshan River at Whatshan Dam (BCWAT), e) Columbia River at Keenlyside Dam (BCHAR), f) Bull River near Wardner (BULNW), g) Elk River at Elko Dam (BCHEL), h) Duncan River at Duncan Dam (BCHDN), i) Kootenay River at Kootenay Canal (BCHKL), j) Slocan River near Crescent Valley (SLONC) and k) Salmo River near Salmo (SALNS). Each box-plot summarizes the median (thick horizontal line), inter-quartile range (IQR; box showing 75th to 25th percentile) and the minimum and maximum (dotted lines). Those cases where the future ensemble is significantly different than the historical ensemble are indicated by a triangle below the plot.

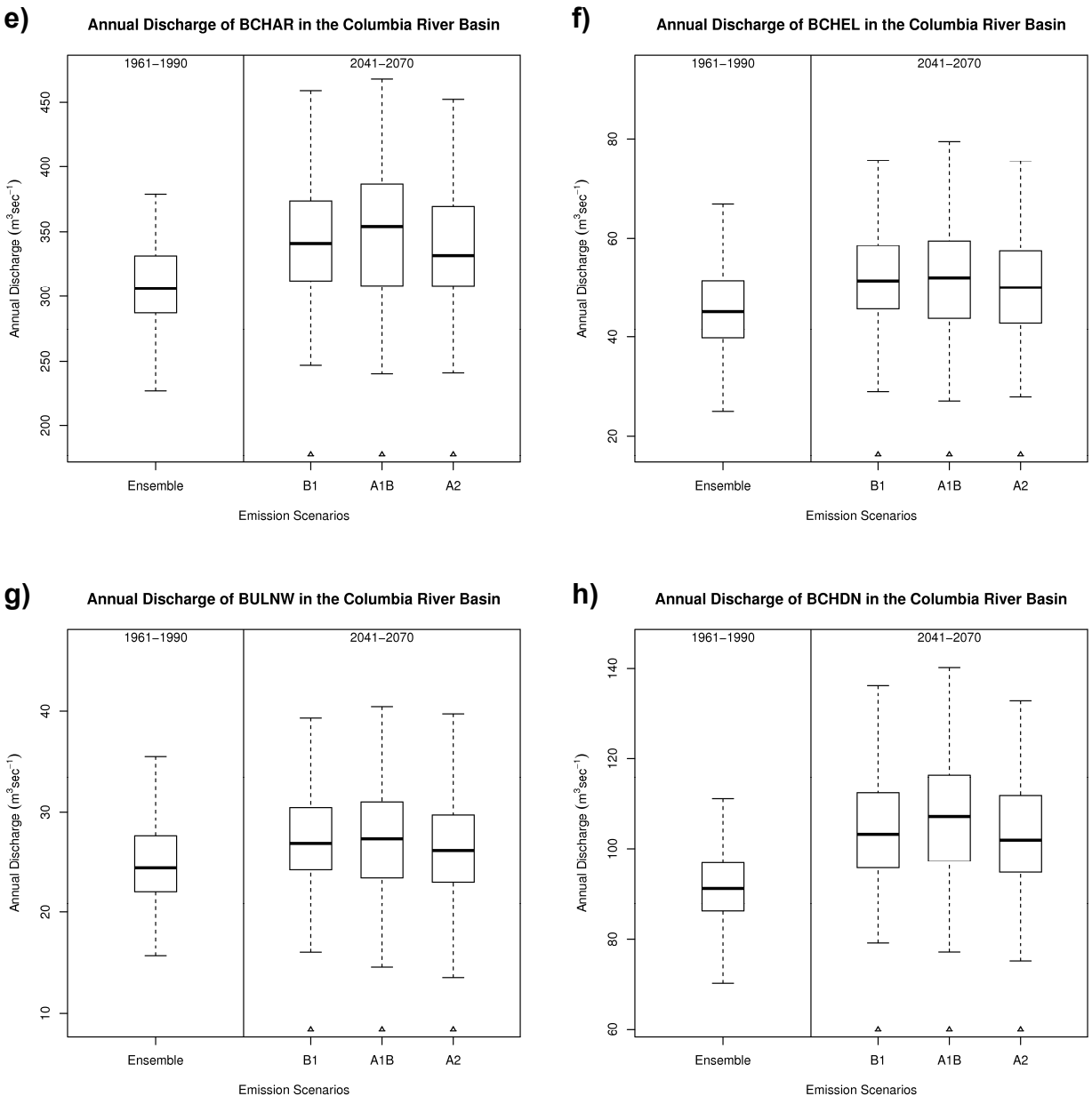

Figure 4-21. Continued.

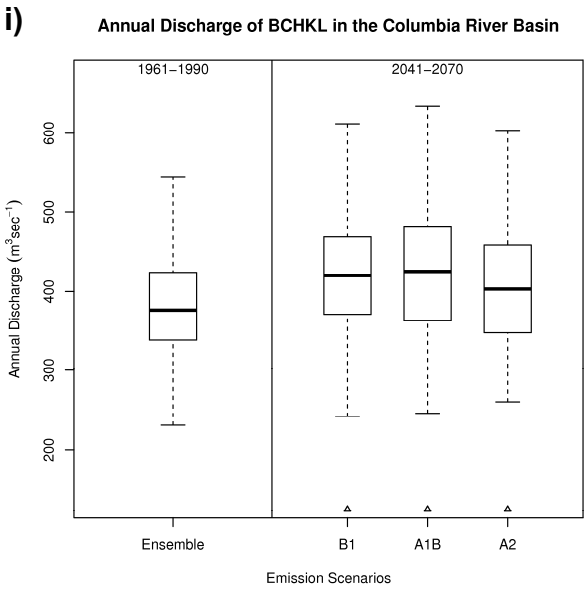

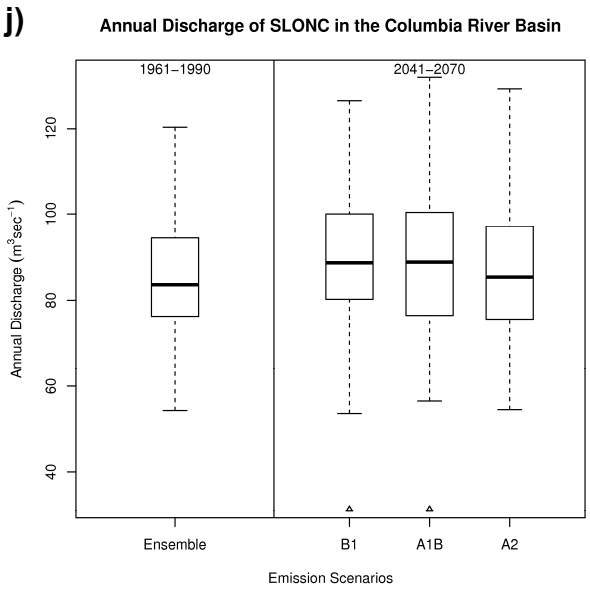

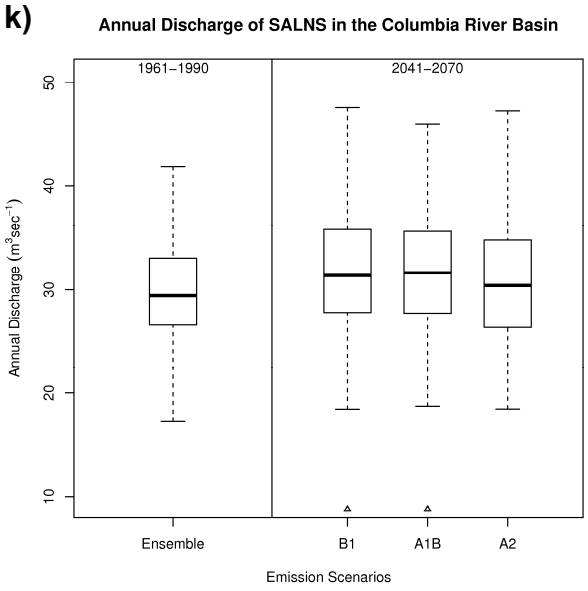

Figure 4-21. Continued.

Table 4-6. Historic and future annual discharge ensemble statistics and anomalies for the Upper Columbia project sites.

Percentile	Annual Discharge Statistics by Period and Emissions (m^3/s)				Relative Difference		
	1961 to 1990	2040 to 2071					
		B1	A1B	A2	B1	A1B	A2
			SPINS				
minimum	22	26	21	24	0.16	-0.03	0.10
75th	28	32	32	32	0.13	0.14	0.11
median	31	35	36	35	0.14	0.17	0.12
25th	33	38	40	38	0.15	0.20	0.15
maximum	39	46	49	46	0.17	0.26	0.16
			BCHMI				
minimum	373	432	410	437	0.16	0.10	0.17
75th	463	533	549	529	0.15	0.18	0.14
median	493	570	601	576	0.16	0.22	0.17
25th	526	622	646	630	0.18	0.23	0.20
maximum	618	745	776	765	0.21	0.26	0.24
			BCHRE				
lwhisker	132	150	159	153	0.13	0.21	0.16
75th	171	191	196	189	0.12	0.15	0.11
median	184	208	215	203	0.13	0.17	0.10
25th	198	227	235	228	0.15	0.19	0.15
maximum	232	266	287	282	0.15	0.24	0.22
			BCWAT				
minimum	4.1	4.5	4.7	4.2	0.09	0.13	0.03
75th	6.1	6.5	6.2	6.0	0.06	0.02	-0.01
median	6.9	7.1	7.2	6.9	0.04	0.04	0.00
25th	7.7	8.1	8.1	7.8	0.05	0.06	0.02
maximum	9.6	10.0	10.7	10.4	0.03	0.11	0.08
			BCHAR				
minimum	227	247	240	241	0.09	0.06	0.06
75th	287	312	308	308	0.09	0.07	0.07
median	306	341	354	331	0.12	0.16	0.08
25th	331	374	387	369	0.13	0.17	0.11
maximum	379	459	467	452	0.21	0.23	0.19
			BULNW				
minimum	16	16	15	14	0.02	-0.07	-0.14
75th	22	24	23	23	0.10	0.06	0.04
median	24	27	27	26	0.10	0.12	0.07
25th	28	30	31	30	0.10	0.12	0.08
maximum	35	39	40	40	0.11	0.14	0.12

Table 4-6. Continued

Percentile	Annual Discharge Statistics by Period and Emissions (m^3/s)				Relative Difference		
	1961 to 1990	2040 to 2071					
		B1	A1B	A2	B1	A1B	A2
			BCHEL				
minimum	25	29	27	28	0.16	0.08	0.11
75th	40	46	44	43	0.15	0.10	0.08
median	45	51	52	50	0.14	0.15	0.11
25th	51	58	59	57	0.14	0.16	0.12
maximum	67	76	79	75	0.13	0.19	0.13
			BCHDN				
minimum	70	79	77	75	0.13	0.10	0.07
75th	86	96	97	95	0.11	0.13	0.10
median	91	103	107	102	0.13	0.18	0.12
25th	97	112	116	112	0.16	0.20	0.15
maximum	111	136	140	133	0.23	0.26	0.20
			BCHKL				
minimum	231	242	246	260	0.05	0.07	0.13
75th	338	371	363	348	0.10	0.07	0.03
median	376	420	426	403	0.12	0.13	0.07
25th	424	468	481	458	0.10	0.13	0.08
maximum	545	612	634	604	0.12	0.14	0.11
			SLONC				
minimum	54	54	57	49	-0.01	0.04	-0.10
75th	76	80	75	75	0.05	-0.02	-0.02
median	84	89	86	84	0.06	0.03	0.01
25th	94	100	98	95	0.06	0.04	0.01
maximum	120	126	132	121	0.05	0.10	0.01
			SALNS				
minimum	17	18	17	18	0.07	-0.01	0.03
75th	27	28	26	26	0.05	-0.01	-0.03
median	29	31	31	30	0.07	0.06	0.02
25th	33	36	35	35	0.08	0.05	0.04
maximum	42	48	46	47	0.14	0.10	0.13

Along the Columbia River local annual discharge changes at Revelstoke (BCHRE) are qualitatively similar to those for BCHMI (Figure 4-21c). Discharge is projected to increase in the future, with median discharge changes of 17%, 10% and 13% for the A1B, A2 and B1 scenarios, respectively. The tendency for projected annual discharge for all three emissions scenarios to be larger than historical values is statistically significant. The projected changes in annual discharge for the Whatshan River (BCWAT) are small (Figure 4-21e); changes in median annual discharge are only 4%, 4% and 0% for the A1B, A2 and

B1 scenarios, respectively. Nevertheless, the tendency for future values to be larger for the A1B and B1 ensembles is still statistically significant. Local annual discharge changes for the Columbia River at Keenlyside Dam (BCHAR) are qualitatively similar to those for both BCHMI and BCHRE, although the magnitude of projected changes is slightly lessened at this location (Figure 4-21d). Differences in median annual discharge between the historic and future periods are 16%, 8% and 12% for scenarios A1B, A2 and B1, respectively. For BCHAR, annual discharge of three scenario ensembles is significantly different than annual discharge of the historical ensemble.

In the Kootenay River system the box-plots indicate a general shift towards higher annual discharge for the 2050s at Elko project site (BCHEL; Figure 4-21f), with differences in median discharge of 15%, 11% and 14% for the A1B, A2 and B1 scenarios, respectively. All three future ensembles tend to generate discharge that is significantly larger than the historical ensemble. For the Aberfeldie project site (BULNW) there is a general and statistically significant shift in the distribution of annual discharge to higher values in the future (Figure 4-21g), with difference in median annual discharge of 12%, 7% and 10% for the A1B, A2 and B1 scenarios, respectively. Nevertheless, the lower whiskers for both the A1B and A2 scenarios are decreased (-7% and -14%, respectively) with respect to the historic period, indicating that some projections of future annual discharge are less than the lower limit of the historic period. For the Duncan River at Duncan Dam (BCHDN), annual discharge is projected to increase (Figure 4-21h), with increases in median annual discharge of 18%, 12% and 13% for the A1B, A2 and B1 scenarios, respectively. As well, future projections display a substantially larger range than the corresponding historic ensembles, such that increases in the extreme annual discharge values (as indicated by the upper lines) are 26%, 24% and 21% for the A1B, A2 and B1 scenarios, respectively. At BC Hydro's Kootenay Canal project site (BCHKL), more modest increases in local annual discharge are projected. Although changes in median annual discharge are 13%, 7% and 12%, respectively for the A1B, A2 and B1 scenarios, there remains substantial overlap in the corresponding historic and future IQRs and the lower whiskers show little change (i.e., the lowest values of annual discharge projected for the future are slightly higher than the lowest values of the historic period; Figure 4-21i and Table 4-6). Nevertheless, the tendency for higher projected values in the future ensembles is statistically significant for all three scenarios.

Projected changes in annual discharge are modest and qualitatively similar for both the Slocan (SLONC; Figure 4-21j) and Salmo (SALNS; Figure 4-21k) watersheds. Changes in median annual discharge are 3%, 1% and 6%, respectively for the A1B, A2 and B1 scenarios for SLONC, with only the B1 ensemble being statistically significantly larger than the historical ensemble. Changes in median annual discharge are 6%, 2% and 6%, respectively for the A1B, A2 and B1 scenarios for SALNS, with both the A1B and B1 ensemble being statistically significantly larger than the historical ensemble.

In general, changes in annual streamflow at most project sites are projected to be largest for the A1B scenario and smallest for the A2 scenario. Exceptions include the SLONC and SALNS, where the largest increases in annual discharge occur for the B1 scenario. In many cases, however, the differences in hydrologic response on an annual basis between scenarios are small or negligible, and there is substantial overlap in the projected ensemble spread between all three scenarios. In other words, the differences between scenarios are generally smaller than the combined inter-annual and inter-model differences represented by the range of annual discharge values for a given scenario ensemble. Regardless, there is strong consensus between sites and between scenarios that annual discharge is projected to increase in the 2050s period.

4.3.3 Monthly Streamflow

The effect of climate change on median monthly streamflow for all 11 project sites is shown graphically in Figure 4-22 through Figure 4-32. Generally, although individual sites may differ in the details, the

effects of climate change on monthly discharge is consistent between sites. There is a consistent signal of increased discharge in the late fall and winter period, and an earlier freshet onset, resulting in substantially higher discharge during the spring and/or early summer. Although more evident at some sites than others, there is also a signal of an advance in the month of peak discharge. Somewhat less consistent, both between sites and within a site (i.e., between runs), is the effect on the magnitude of peak monthly discharge. At all sites there is general consensus that monthly discharge in the late summer and early fall period will be lower in the future than in the past. The results for the various project sites also generally indicate that differences between projections of median monthly discharge are largely attributed to differences in GCM response to climate forcing. Compared to combined inter-annual and inter-GCM variability for a given scenario, inter-scenario differences for a given GCM are small. As such, projections of median monthly discharge for the 2050s are largely insensitive to the assumptions regarding the trajectory of future emissions.

Projections for the Spillimacheen (SPINS) project site indicate higher monthly discharge in the winter and early spring (November through March) and an earlier onset of the spring freshet (April and May) (Figure 4-22). Most median projections agree that the freshet peak will shift one month earlier from July to June and that monthly peak discharge will be higher in the future. Consequently, the largest absolute changes in monthly discharge are projected to occur during the historical freshet months of June and July. The largest increases are projected for June, and range from 7 m^3/s to 50 m^3/s. The largest absolute decreases in median monthly discharge are for July, but range from -66 m^3/s to +14 m^3/s. All runs project lower median monthly discharge in the 2050s for August and September. At the Columbia River at Mica dam (BCHMI) project site, projections indicate higher monthly discharge in the fall and winter (November through March) and an earlier onset of the spring freshet (April and May) (Figure 4-23). Results indicate that the peak of the freshet will shift to an earlier occurrence, with several runs shifting the month of peak discharge from July into June. There is a consistent signal of higher projected peak monthly discharge, whether it occurs in June or July, and the highest absolute changes in monthly discharge are projected to occur during those two months. Projected changes in June range from 125 m^3/s to 871 m^3/s and projected changes in July range from -519 m^3/s to 302 m^3/s. The majority of runs project reduced future discharge during August and September.

Along the main stem of the Columbia River results for BCHRE and BCHAR are both qualitatively similar to BCHMI. At BCHRE (Figure 4-24) the largest changes in local median monthly discharge result from a shift in the onset and timing of the spring freshet and are projected for May and July. Changes in May range from 43 m^3/s to 242 m^3/s and changes in July range from -269 m^3/s to 74 m^3/s. Peak monthly median discharge, which most runs project will occur one month earlier, will also be higher in the future. At BCHAR (Figure 4-25) the largest changes in local median monthly discharge are also projected to occur in May, ranging from 30 m^3/s to 309 m^3/s, and in July, ranging from -318 m^3/s to 50 m^3/s. Most the runs for BCHAR also project a shift in the occurrence of peak monthly discharge from July into June. The remaining runs project peak monthly discharge will occur in July, as it did during the historical period. Most projections are for higher peak monthly median discharge in the future. At the BCWAT project site there is consensus of higher median monthly discharge in the future during the fall and winter, an advance in the onset of spring freshet (e.g., increased discharge in April and May), a shift in peak monthly discharge from June to May, and higher peak monthly discharge (Figure 4-26). There is also a consistent signal of lower future discharge during the months of June through August, although there is high variability between the individual runs in June. The largest absolute changes are in April (3.3 m^3/s to 10.1 m^3/s) and in June (-15.3 m^3/s to -0.9 m^3/s).

At the Bull River near Wardner (BULNW) project site there is consensus for higher median monthly discharge in the future during the winter and early spring (December through March) and an advance in the onset of spring freshet (e.g., increased discharge in April and May) (Figure 4-27). The projected change in peak monthly discharge is mixed between runs. Although discharge in May is projected to increase for all runs, for the most part, the peak discharge month continues to occur in June, as it has in

the past. The projected change in the magnitude of peak monthly discharge is inconsistent, with over half the runs projecting lower monthly peak discharge in the future. The largest absolute changes between future and historic monthly medians are projected to be for May (changes range from 2 m^3/s to 39 m^3/s) and June (changes range from -42 m^3/s to 19 m^3/s). Results are similar for the Elk River at Elko (BCHEL) project site (Figure 4-28). At this location the largest absolute changes between future and historic monthly medians are also projected to occur in May (8 m^3/s to 97 m^3/s) and in June (-94 m^3/s to 32 m^3/s).

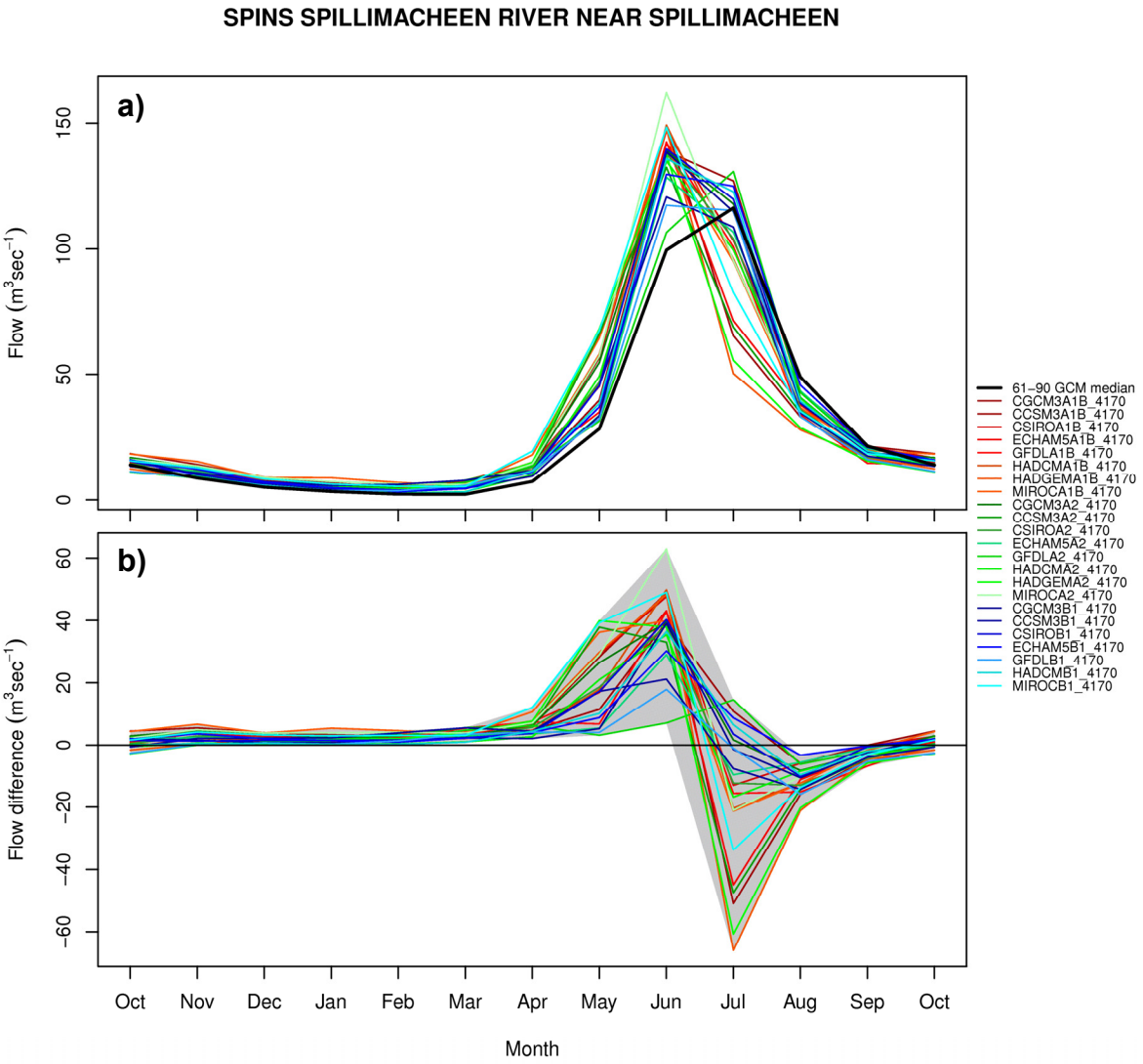

Figure 4-22. Median monthly discharge for the Spillimacheen River near Spillimacheen (SPINS) showing: a) historic (1961 - 1990) and future (2041 - 2070) discharge, and b) the 2050s anomaly. Historic discharge (black line) is presented as the full ensemble median (23 runs x 30 years) and each future discharge value is the median of each GCM run (1 run x 30 years). Anomalies represent the future monthly median minus the historic ensemble monthly median.

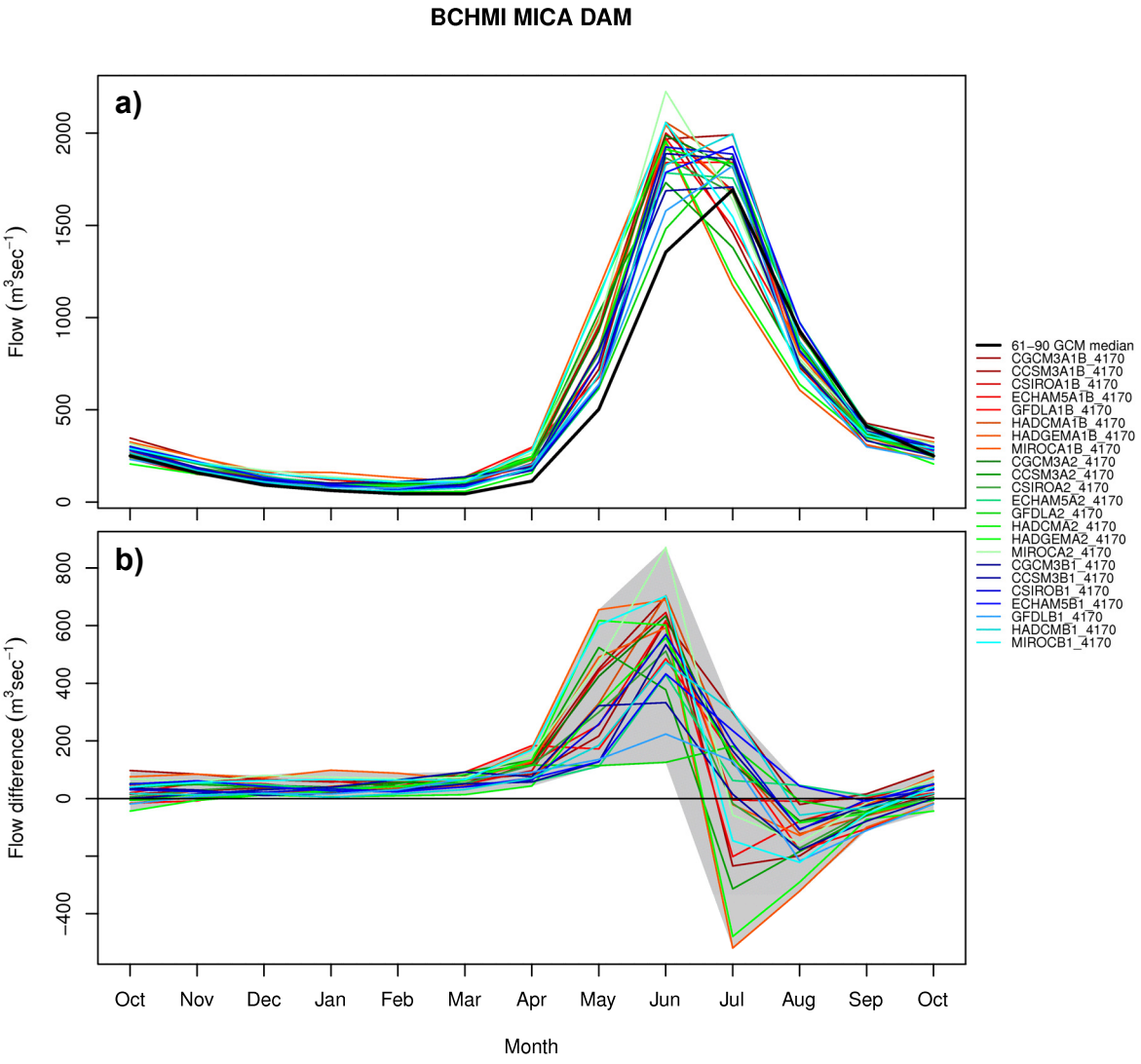

Figure 4-23. Median monthly discharge for the Columbia River at Mica Dam (BCHMI) showing: a) historic (1961 - 1990) and future (2041 - 2070) discharge, and b) the 2050s anomaly. Historic discharge (black line) is presented as the full ensemble median (23 runs x 30 years) and each future discharge value is the median of each GCM run (1 run x 30 years). Anomalies represent the future monthly median minus the historic ensemble monthly median.

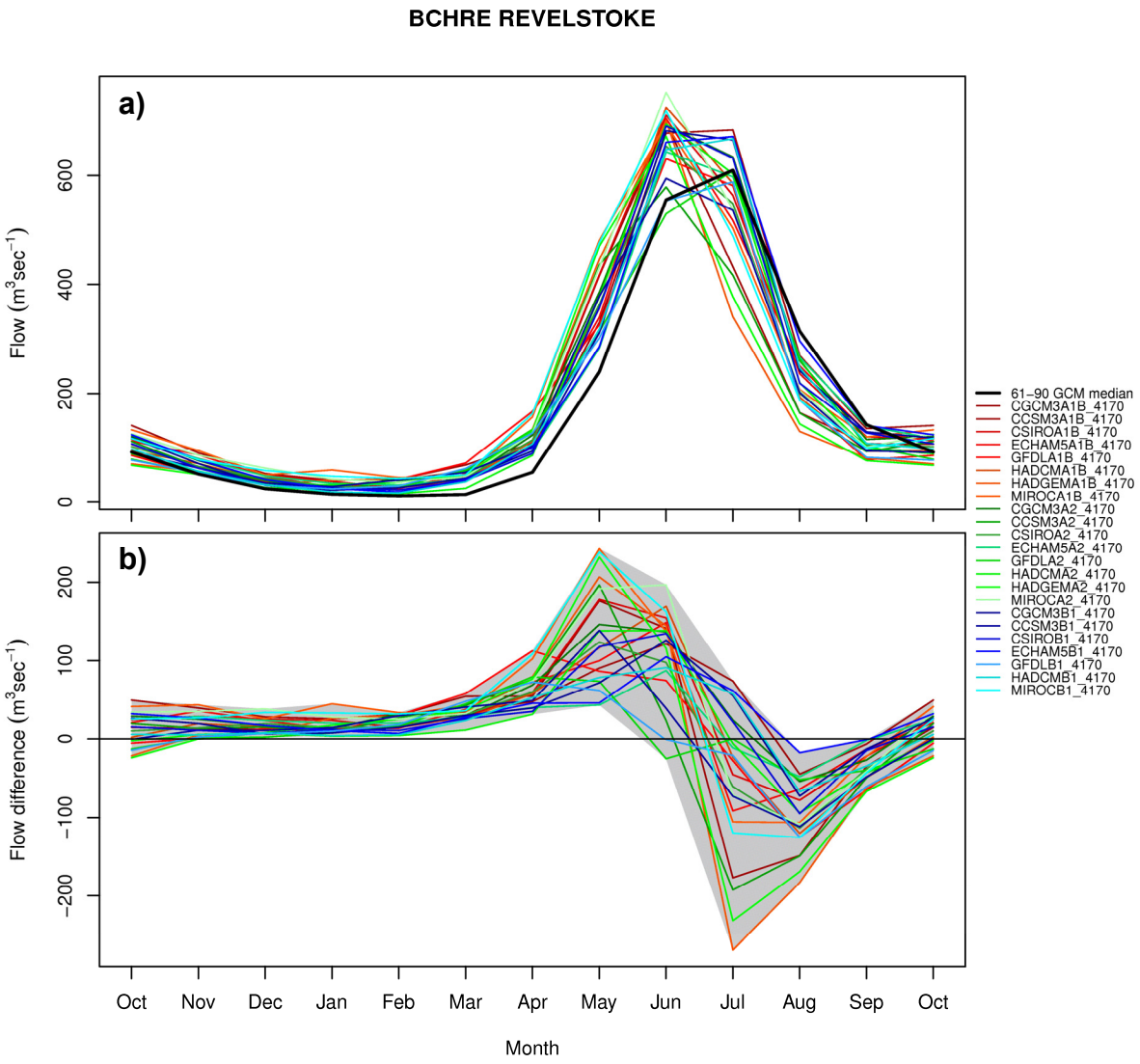

Figure 4-24. Median monthly discharge for the Columbia River at Revelstoke Dam (BCHRE) showing: a) historic (1961 - 1990) and future (2041 - 2070) discharge, and b) the 2050s anomaly. Historic discharge (black line) is presented as the full ensemble median (23 runs x 30 years) and each future discharge value is the median of each GCM run (1 run x 30 years). Anomalies represent the future monthly median minus the historic ensemble monthly median.

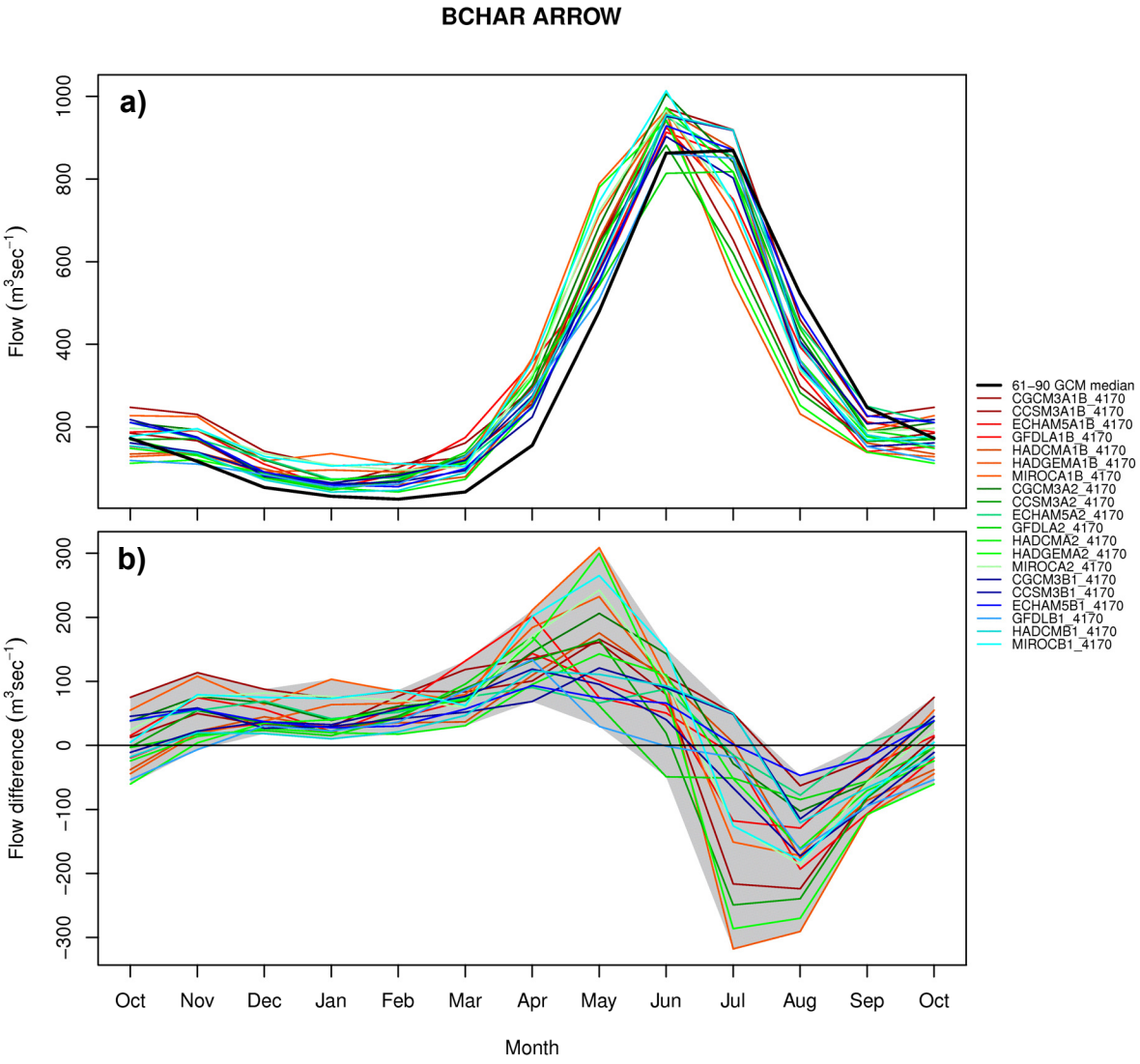

Figure 4-25. Median monthly discharge for the Columbia River at Keenlyside Dam (BCHAR) showing: a) historic (1961 - 1990) and future (2041 - 2070) discharge, and b) the 2050s anomaly. Historic discharge (black line) is presented as the full ensemble median (23 runs x 30 years) and each future discharge value is the median of each GCM run (1 run x 30 years). Anomalies represent the future monthly median minus the historic ensemble monthly median.

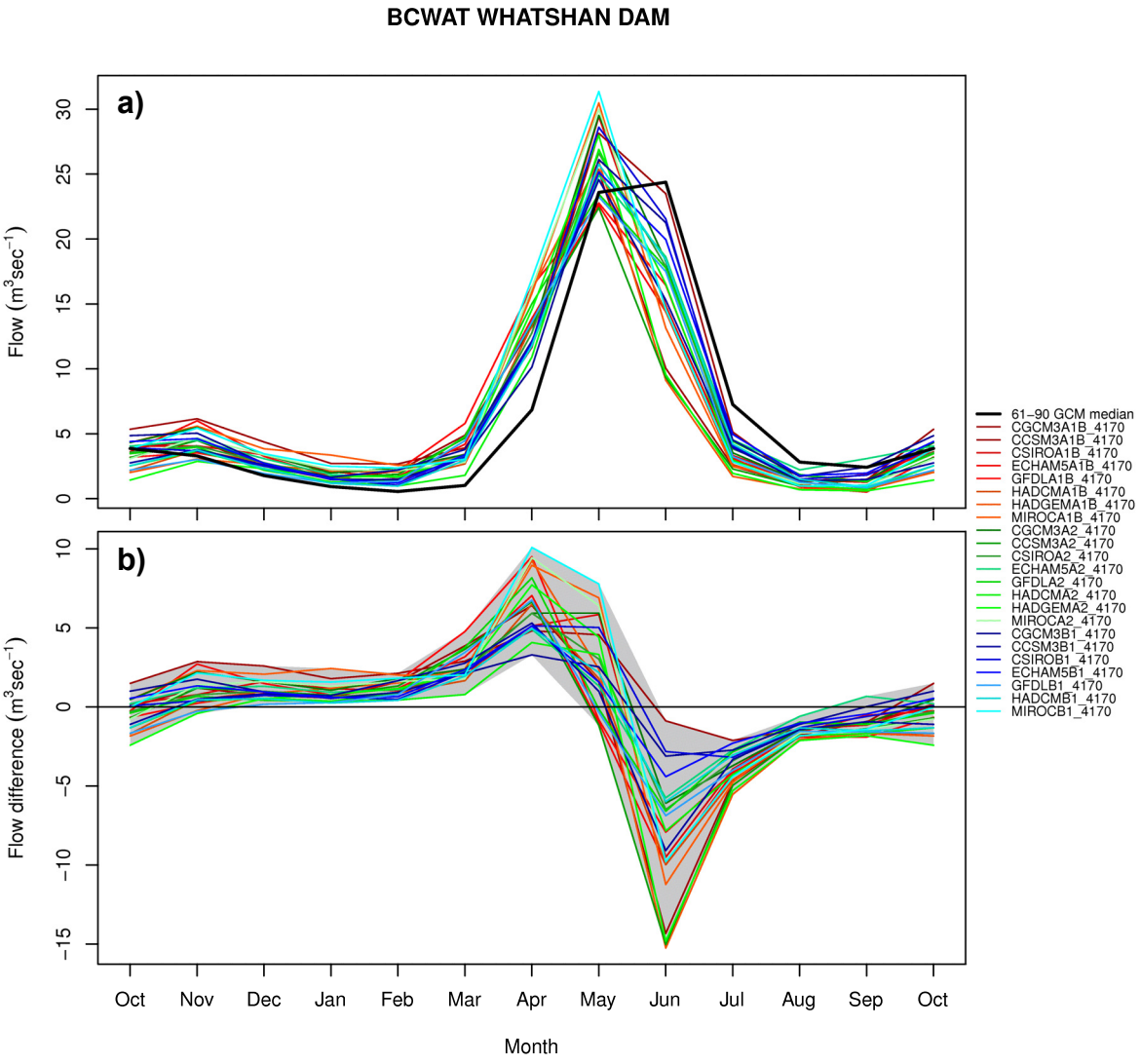

Figure 4-26. Median monthly discharge for the Whatshan River at Whatshan Dam (BCWAT) showing: a) historic (1961 - 1990) and future (2041 - 2070) discharge, and b) the 2050s anomaly. Historic discharge (black line) is presented as the full ensemble median (23 runs x 30 years) and each future discharge value is the median of each GCM run (1 run x 30 years). Anomalies represent the future monthly median minus the historic ensemble monthly median.

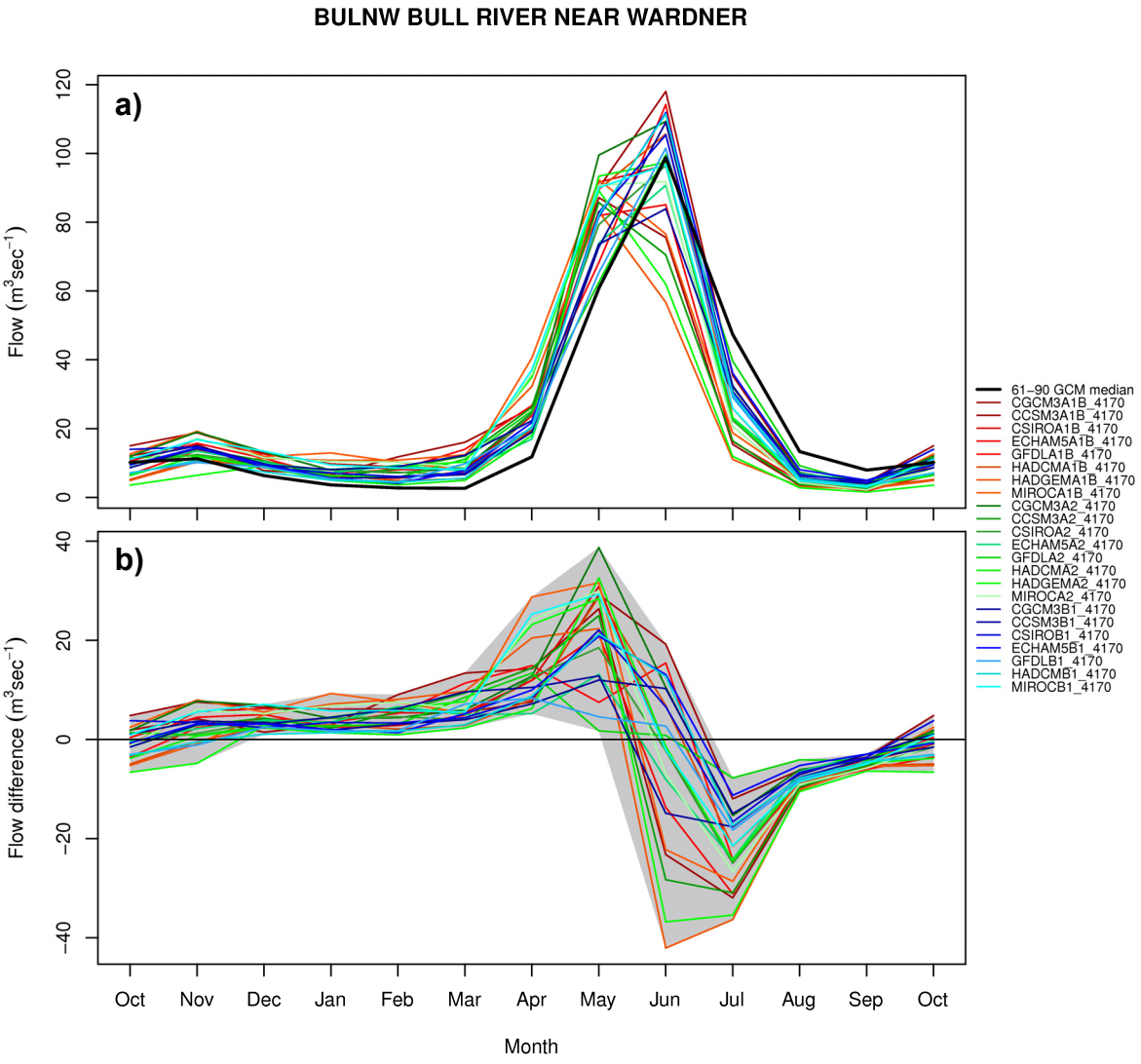

Figure 4-27. Median monthly discharge for the Bull River near Wardner (BULNW) showing: a) historic (1961 - 1990) and future (2041 - 2070) discharge, and b) the 2050s anomaly. Historic discharge (black line) is presented as the full ensemble median (23 runs x 30 years) and each future discharge value is the median of each GCM run (1 run x 30 years). Anomalies represent the future monthly median minus the historic ensemble monthly median.

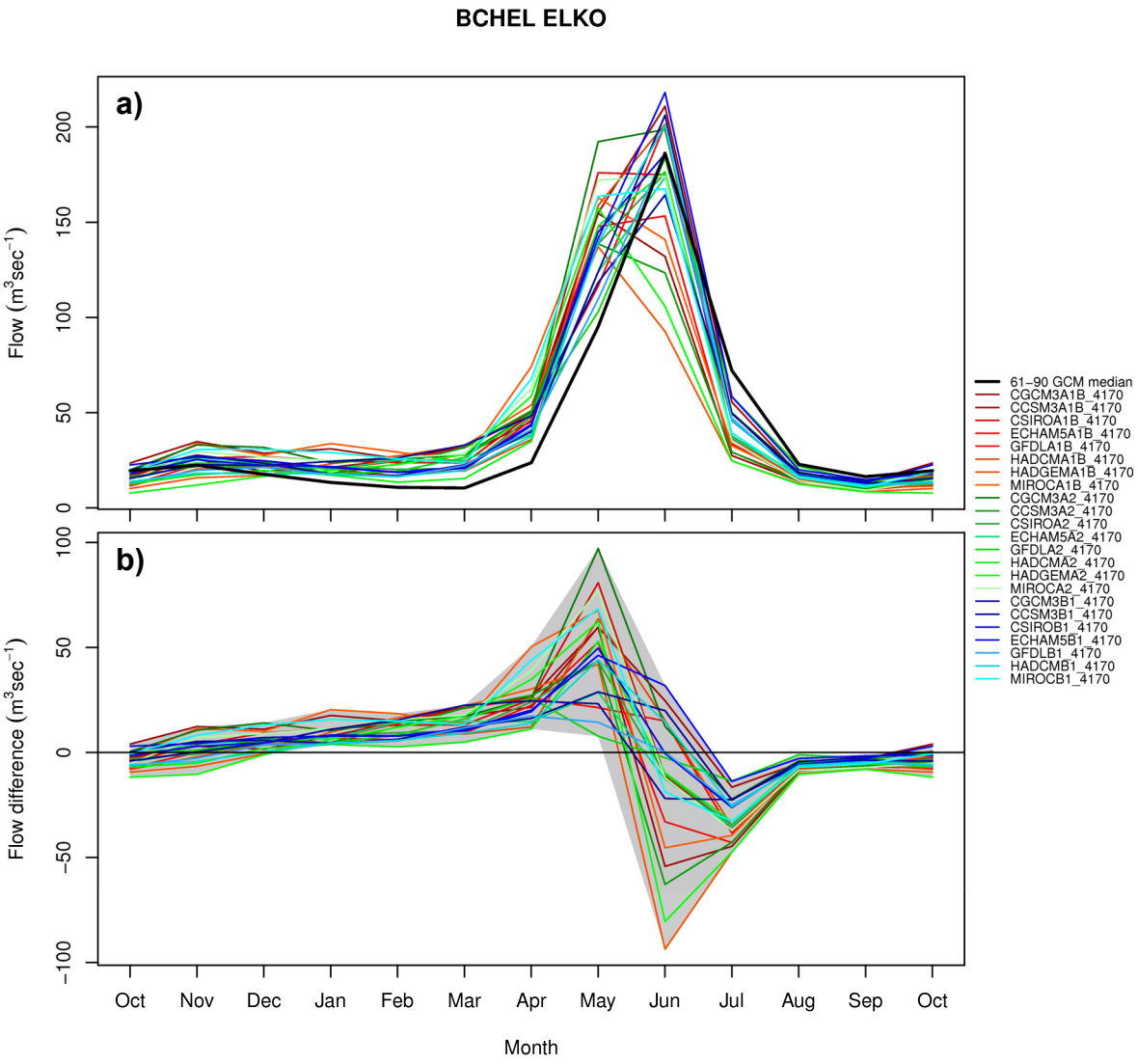

Figure 4-28. Median monthly discharge for the Elk River at Elko Dam (BCHEL) showing: a) historic (1961 - 1990) and future (2041 - 2070) discharge, and b) the 2050s anomaly. Historic discharge (black line) is presented as the full ensemble median (23 runs x 30 years) and each future discharge value is the median of each GCM run (1 run x 30 years). Anomalies represent the future monthly median minus the historic ensemble monthly median.

The Duncan River at Duncan Dam (BCHDN) presents a climate change response that is qualitatively similar to those of project sites along the Columbia River main stem (e.g., BCHMI, BCHAR) (Figure 4-29). The majority of projections for median monthly discharge show a signal of increased discharge during the winter and early spring, although the change is rather small in absolute terms (ranging from -0.3 to 11.0 m^3/s). All projections agree on an earlier rise during the freshet (higher discharge in April, May and June), and most projections show a shift in peak monthly discharge from July to June. Most projections also show an increase in the magnitude of median peak monthly discharge. The largest absolute changes between future and historic monthly medians are projected to occur in June (15 m^3/s to 164 m^3/s) and July (-153 m^3/s to 51 m^3/s).

At the Kootenay Canal project site (BCHKL), local monthly median discharge is consistently projected to be higher in the future during the winter period (Figure 4-30). Discharge is also projected to be higher during the rise to the spring freshet (April and May), with the largest absolute increases projected to occur in May (with changes ranging from -6 to 402 m^3/s). Most projections of median monthly discharge agree that the month of peak discharge (June) is not expected to change, but that the magnitude of monthly peak discharge will increase. Discharge projections show decreased discharge at the end of the freshet (July) and lower discharge during August and September. The largest absolute decreases in monthly median discharge are projected for July, but with individual changes ranging from -676 m^3/s to -105 m^3/s.

Individual runs of median monthly discharge in the Slocan River (SLONC) consistently project increased discharge during the fall and winter months (Figure 4-31a). An earlier start and end to the freshet is also consistently projected, resulting in the largest absolute discharge changes occurring in the months of May and July (Figure 4-31b). For May, changes in median monthly discharge range from 11 m^3/s to 152 m^3/s, whereas for July changes range from –183 m^3/s to –16 m^3/s. The majority of runs project increased peak monthly discharge to occur in June, as in the historical period, but with increased magnitude. Discharge is consistently projected to decrease during the late summer and early fall. The monthly discharge response of the Salmo River (SALNS) is qualitatively similar (Figure 4-32). The largest absolute changes in monthly discharge, occurring in April and June, are projected to result from a shift in freshet timing. Projected changes are consistently positive in April, ranging from 11 m^3/s to 51 m^3/s in April. Although the largest absolute decrease in monthly discharge is projected for June, results are somewhat less consistent between runs and changes range from -64 m^3/s to 2.3 m^3/s.

The A1B historical and monthly temperature, precipitation (including rainfall and snowfall), snowmelt, and discharge percentiles for the BCHMI sub-basin are shown in Figure 4-33. The monthly distributions of basin-average temperature show a shift to warmer temperatures throughout the year in the 2050s (Figure 4-33a). Nevertheless, winter monthly temperatures are, as a basin average, projected to remain below freezing during the months of November through March. Therefore, the fairly strong signal of increasing precipitation during the fall and winter (Figure 4-33b), does not translate into substantially increased rainfall (Figure 4-33c), but predominantly to increased snowfall and snow accumulation, in contrast to the Peace and Campbell study areas (Figure 4-33d). This results in only small projected changes to absolute monthly discharge during this period (Figure 4-33f) which is attributed to increases in rainfall strictly at lower elevations within the BCHMI drainage area. The projected shift to higher monthly discharge from April through June is primarily related to increased snowmelt, which is attributed to higher spring temperatures, and secondarily to increased rainfall. The increased discharge is also a lagged response to increased snow accumulation through the winter. Future and historical monthly discharge percentiles for all the Upper Columbia project sites have been summarized by emissions scenario in separate appendices for A1B, A2 and B1, respectively.

Due to both an increase in annual runoff volume and a shift towards an earlier freshet projected to occur throughout the Upper Columbia, more runoff is expected to accumulate sooner over the water year. This is exemplified by comparing historical and future monthly cumulative discharge for BCHMI (Figure 4-34; based on A1B median monthly streamflow). Comparing the median response, 52% more volume (a difference of 3.62 km^3) is projected to accumulate from October through June (the peak of the future freshet) in the 2050s as compared to 1961 - 1990 (Figure 4-34a). By the end of the water year (September), the relative difference will be closer to 20%. When normalized by respective total annual runoff, the half flow date will be approximately half a month sooner during the 2050s than during the historic period (Figure 4-34b).

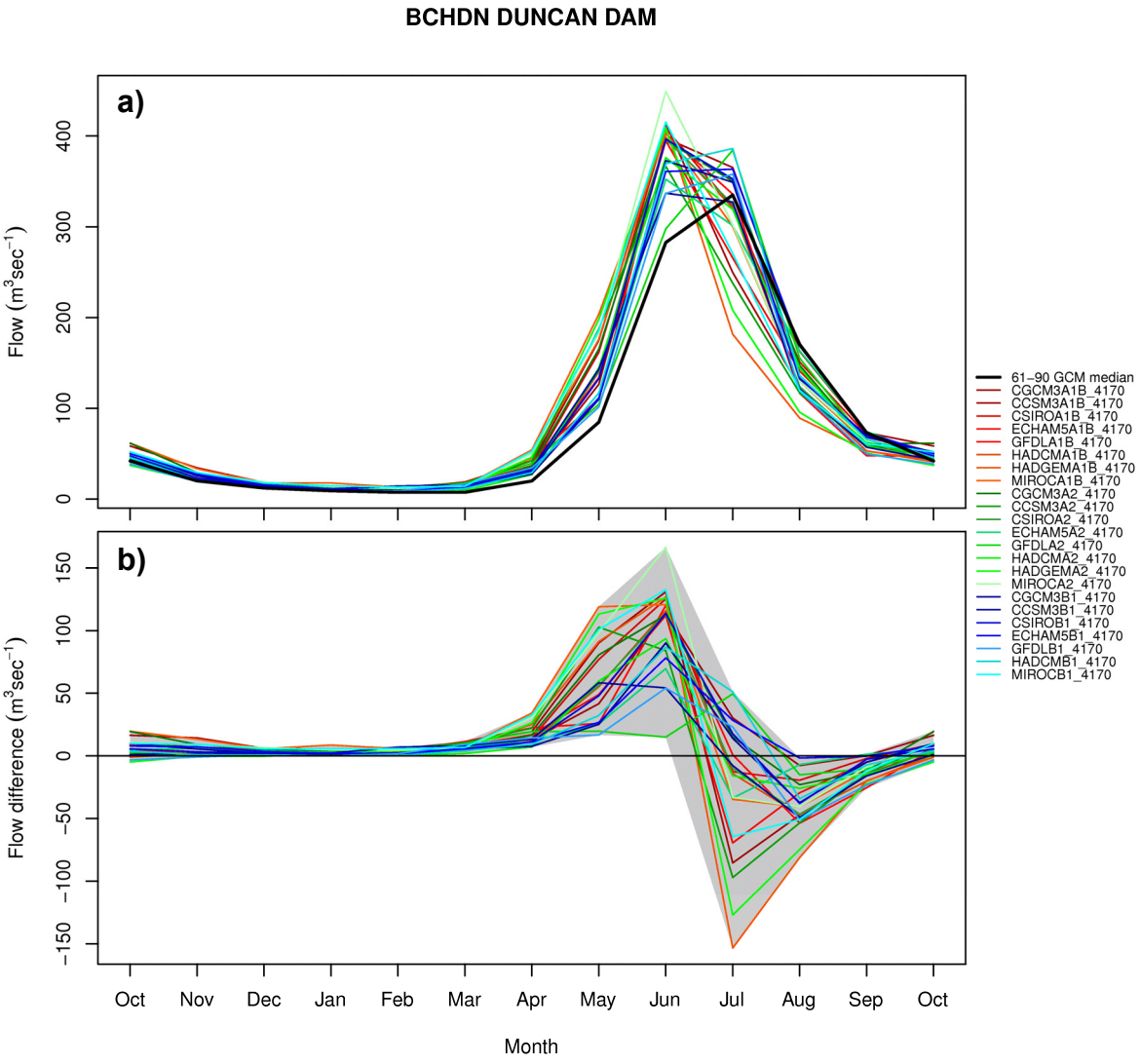

Figure 4-29. Median monthly discharge for the Duncan River at Duncan Dam (BCHDN) showing: a) historic (1961 - 1990) and future (2041 - 2070) discharge, and b) the 2050s anomaly. Historic discharge (black line) is presented as the full ensemble median (23 runs x 30 years) and each future discharge value is the median of each GCM run (1 run x 30 years). Anomalies represent the future monthly median minus the historic ensemble monthly median.

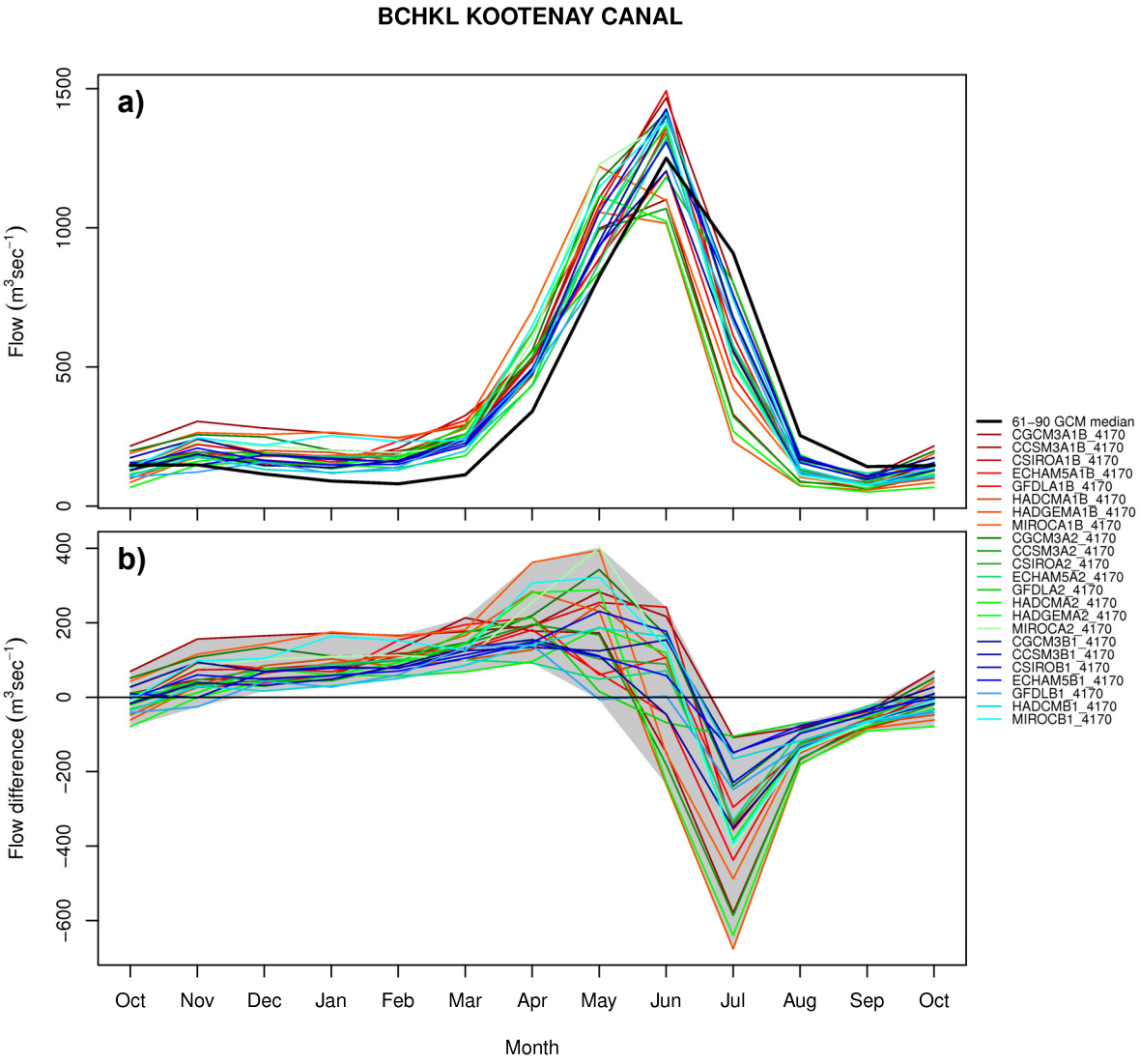

Figure 4-30. Median monthly discharge for the Kootenay River at Kootenay Canal (BCHKL) showing: a) historic (1961 - 1990) and future (2041 - 2070) discharge, and b) the 2050s anomaly. Historic discharge (black line) is presented as the full ensemble median (23 runs x 30 years) and each future discharge value is the median of each GCM run (1 run x 30 years). Anomalies represent the future monthly median minus the historic ensemble monthly median.

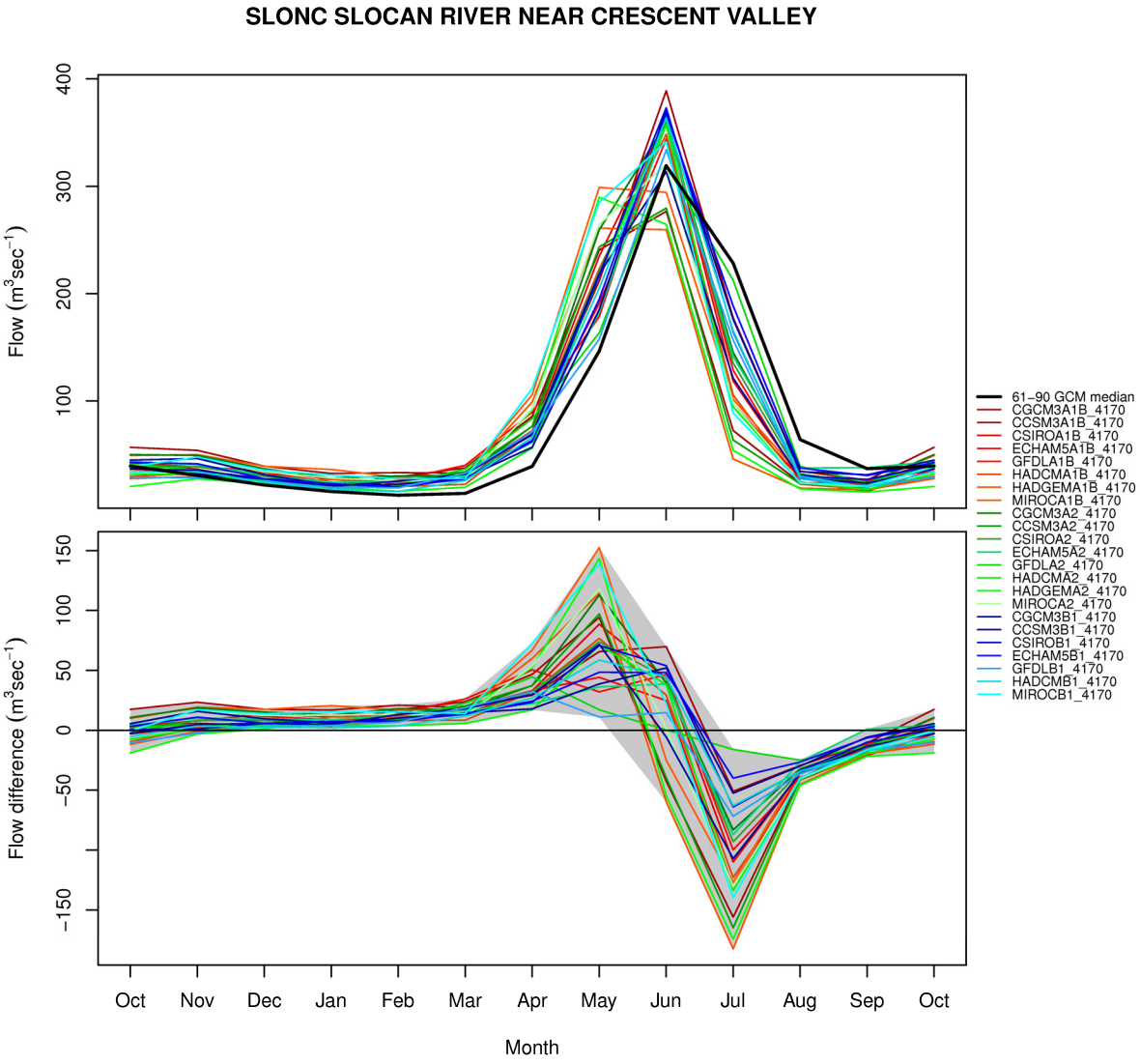

Figure 4-31. Median monthly discharge for the Slocan River near Crescent Valley (SLONC) showing: a) historic (1961 - 1990) and future (2041 - 2070) discharge, and b) the 2050s anomaly. Historic discharge (black line) is presented as the full ensemble median (23 runs x 30 years) and each future discharge value is the median of each GCM run (1 run x 30 years). Anomalies represent the future monthly median minus the historic ensemble monthly median.

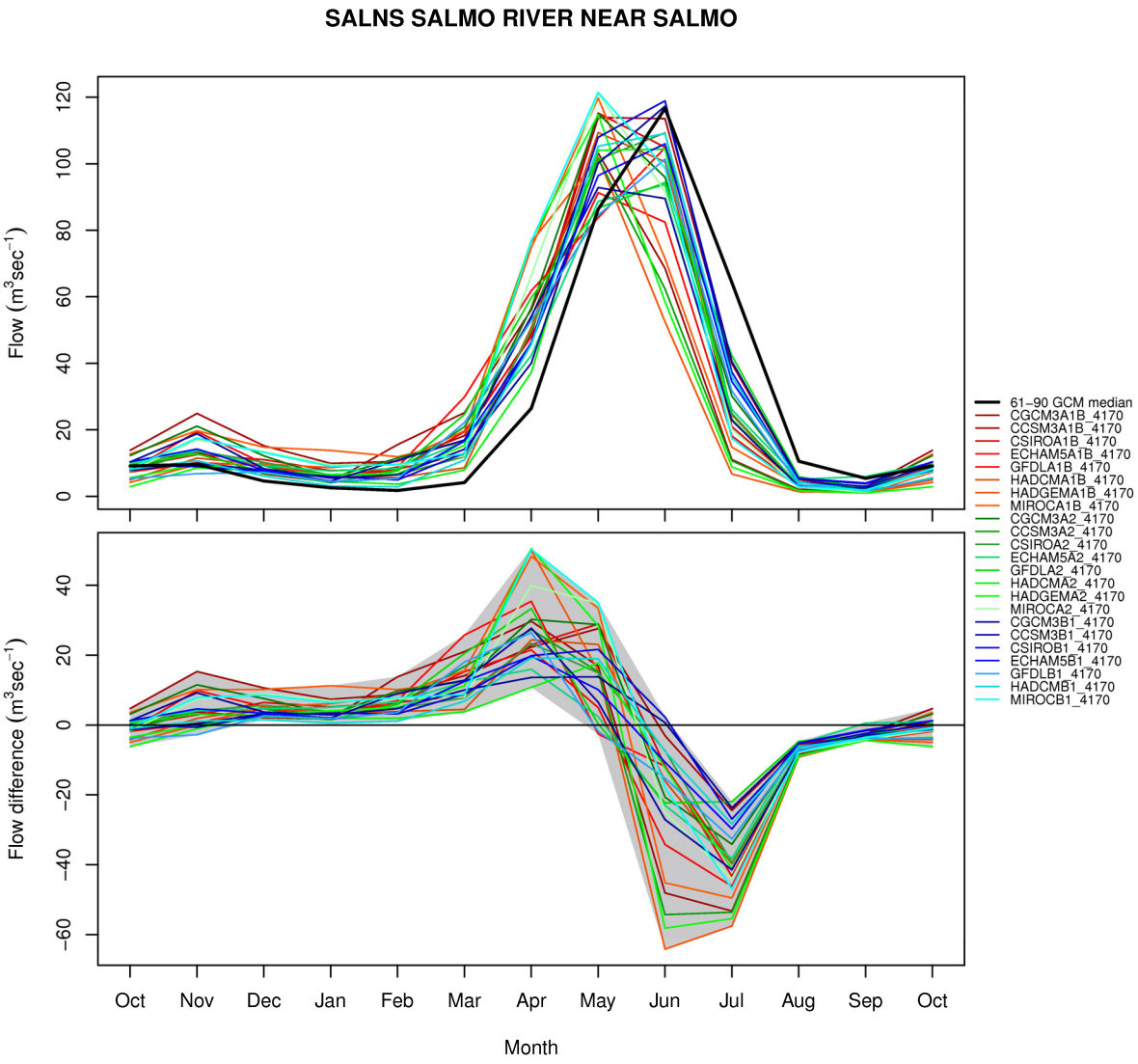

Figure 4-32. Median monthly discharge for the Salmo River near Salmo (SALNS) showing: a) historic (1961 - 1990) and future (2041 - 2070) discharge, and b) the 2050s anomaly. Historic discharge (black line) is presented as the full ensemble median (23 runs x 30 years) and each future discharge value is the median of each GCM run (1 run x 30 years). Anomalies represent the future monthly median minus the historic ensemble monthly median.

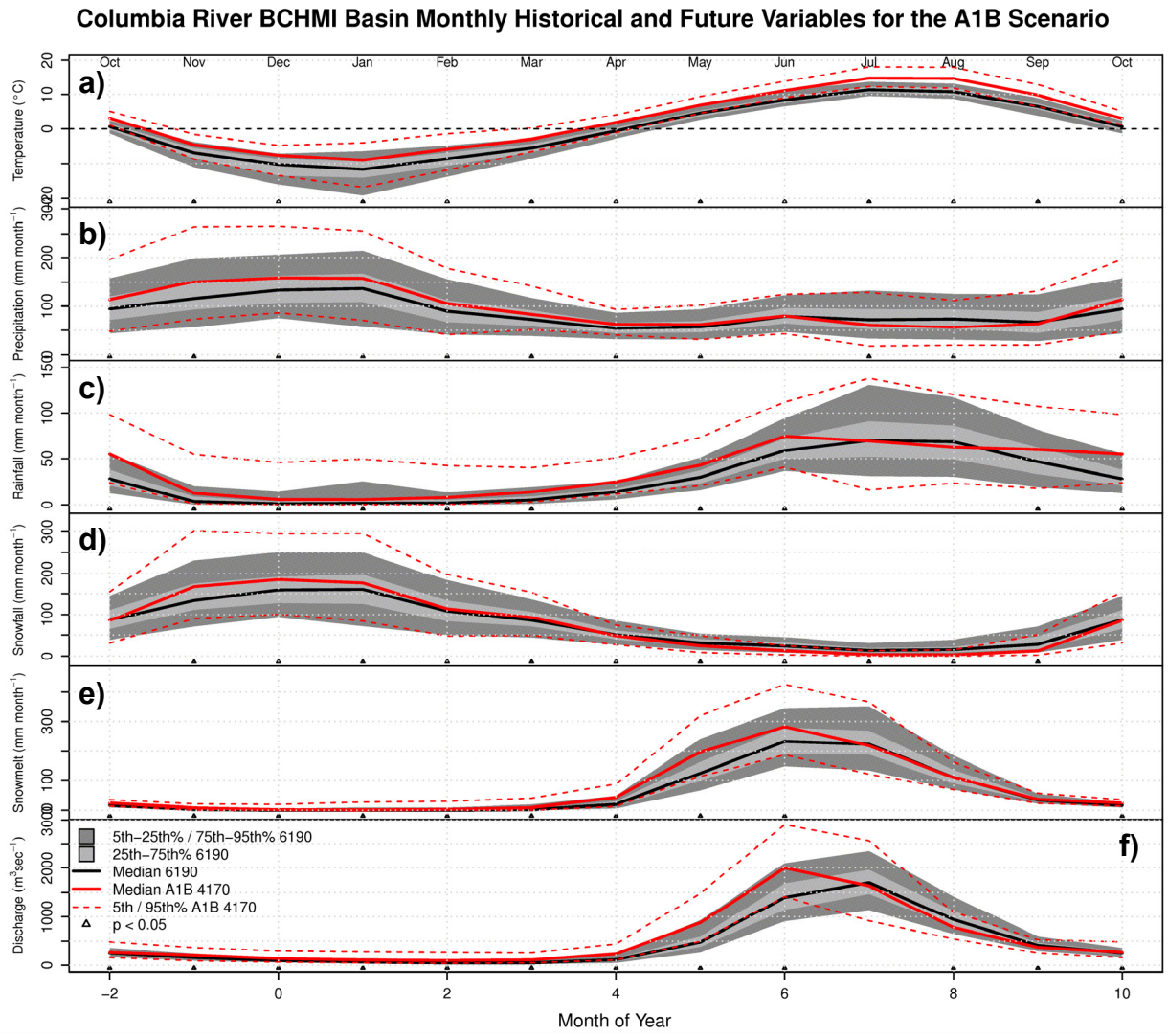

Figure 4-33. Comparison of historic (1961 - 1990) and future (2041 - 2070) monthly a) temperature, b) precipitation, c) rainfall, d) snowfall, e) snowmelt, and f) discharge statistics for the A1B ensemble for the Columbia River at Mica Dam (BCHMI). Temperature, precipitation, rainfall, snowfall and snowmelt are spatial averages for the entire basin. Historic values are represented by the median, inter-quartile range, and the 5th and 95th percentiles. For clarity of presentation, future values are only represented by the median, 5th and 95th percentiles. Those months and variables where the future and historic monthly ensembles are significantly different are indicated by a triangle.

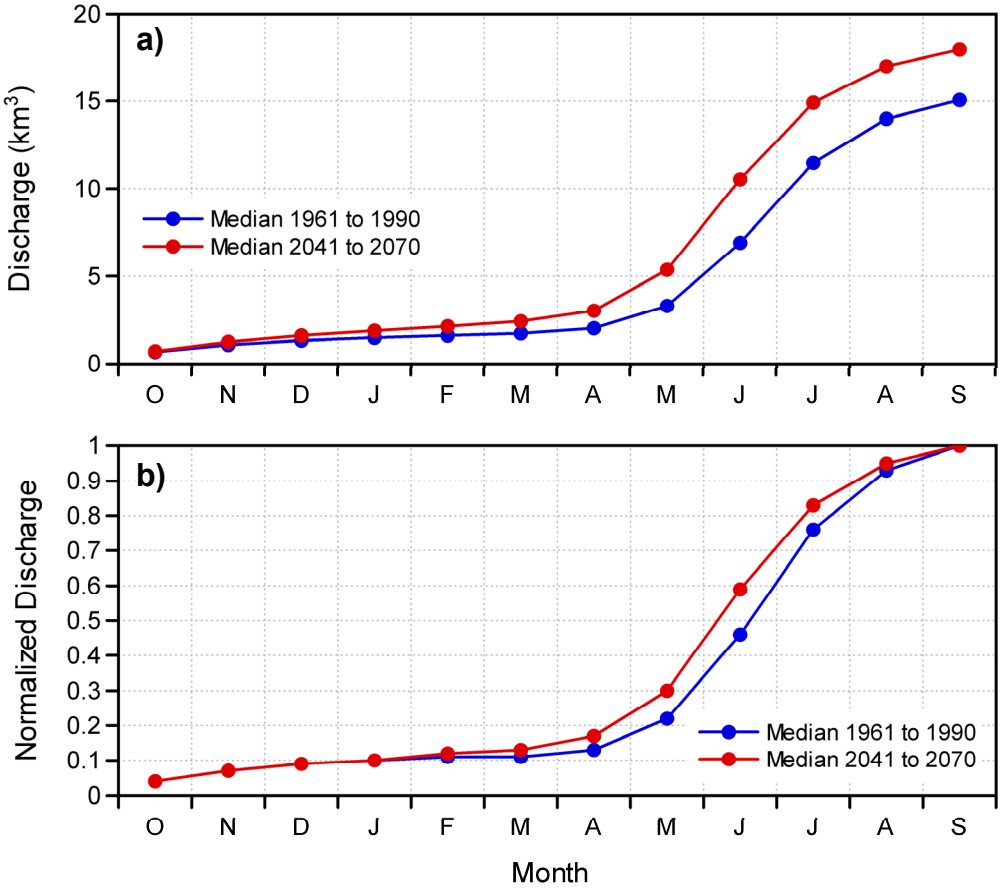

Figure 4-34. Cumulative median A1B historic and future monthly discharge over the water year (October through September) for the Columbia River at Mica Dam (BCHMI). Panels show a) absolute discharge and b) discharge normalized by the respective historic or future water year total.

4.3.4 Snowpack and Runoff

As was the case for both the Peace and Campbell study areas, changes in discharge in the Upper Columbia can be, in large part, diagnosed by changes in snow storage and precipitation phase. Climate change effects on snow storage in the Upper Columbia are shown in the three panels of Figure 4-35. In the historic period most of the Upper Columbia study area receives the majority of winter precipitation in the form of snow ($SWE_p/P_w \geq 0.5$; Figure 4-35a). A sizeable portion of the study area also has SWE_p/P_w ratios in excess of 1.0, indicating high-elevation areas of perennial snow and glaciers. Only the extreme southern end of the study area and the southern half of the Rocky Mountain trench region receive more winter precipitation in the form of rain than snow. In the 2050s, despite warmer temperatures (Table 4-5; Figure 4-19), most of the study area is still projected to receive proportionately more winter precipitation as snow than rain (Figure 4-35b). This reveals that although the future is projected to get warmer, much of the study area is at a high enough elevation that winter temperatures in the 2050s will remain sufficiently low as to continue generating most winter precipitation as snow. Nevertheless, there is a general decline in SWE_p/P_w over the study area in the 2050s, the area of $SWE_p/P_w > 1.0$ has shrunk, the region of predominantly winter rainfall is projected to expand in the south, and most valley-bottom areas will experience proportionately higher rainfall than snowfall. The 2050s median A1B relative anomaly of

April 1WE is given in Figure 4-35c. The sign of the anomaly shows a strong relationship with elevation; median SWE anomalies are negative at low elevation (i.e., valley-bottoms), increasing to positive anomalies with increasing elevation. At low elevation, higher temperatures result in more winter precipitation falling as rain, less as snow and, despite higher fall and winter precipitation, total snow accumulation is reduced (in some areas by as much as < -50%). At high elevation, increased precipitation still falls predominantly as snow despite higher temperatures, which results in increased snow accumulation in the 2050s. In fact, in the northern Selkirk Mountains between Golden and Revelstoke, median SWE anomaly indicates much higher (>20%) snow accumulation in the 2050s compared to the 1970s (Figure 4-35c). In absolute terms, the A1B median 2050s anomaly of April 1 SWE over the entire study area is only about -30 mm. This indicates that projections of decreased snow water at low elevation are largely offset by projections of increased snow water at high elevation.

The seasonal runoff anomalies generally reflect the changes in precipitation and snow storage already discussed. These anomalies are shown graphically in the four panels of Figure 4-36, which shows the median A1B 2050s composite map of runoff anomalies for the Upper Columbia for winter, spring, summer and fall. Runoff anomalies are positive throughout the study area during the winter (Figure 4-36a), which is a function of both increased precipitation and proportionately more precipitation falling as rain instead of snow. The anomalies tend to decrease with increasing elevation (i.e., proportionately less additional rainfall with increasing elevation and lower air temperatures). The winter runoff anomalies explain the increase in winter discharge experienced uniformly across all project sites. Nevertheless, although large in relative terms, the winter runoff changes (and streamflow changes; compare to Figure 4-33f) are small in absolute terms. In the spring the median runoff anomalies are positive throughout most of the study area (Figure 4-36b). However, there is a much stronger elevation gradient of increasing anomalies with increasing elevation, which is opposite to that of the winter anomalies. At some valley-bottom locations the anomalies are near zero or even negative, with a large region of negative runoff anomalies around the southern bend of the Kootenay River (in the BCHKL drainage). Although spring runoff anomalies reflect increased spring precipitation over the study area, they are primarily in response to increased snowmelt brought on by elevated temperatures (Table 4-5, Figure 4-19 and Figure 4-20). In fact, the runoff anomalies appear strongly positively correlated with the projected peak SWE anomalies (Figure 4-35c). In the summer, the median 2050s runoff anomalies are predominantly negative, although some high-elevation areas in the northern portion of the study area (which are mostly glaciated) exhibit positive runoff anomalies (Figure 4-36c), suggesting increased glacial runoff during the summer months. Fall runoff anomalies exhibit a more complex signal with no clear elevation relationship, where marginal increases in runoff are projected in most of the study area, but with a large region of reduced runoff in the Rocky Mountains. This complexity is generally reflected in the seasonal discharge changes, which show the least consistency between GCM runs during the fall months (Figure 4-22 through Figure 4-30).

4.3.5 Glacier Mass Balance

The impacts of climate change on glaciers in the Upper Columbia was assessed by examining mass balance changes in the 135 glacier cells identified in the glacier mask (Figure 3-5). Mass balance is calculated by comparing 1 October SWE for the years 2070 and 1995. The date 1 October is used under the assumption that seasonal snow cover is minimal at this time of year, such that any remaining SWE can be considered ‘glacier ice’. The year 1995 (as opposed to 1990) is chosen as the historical date as this represents the only time when the VIC simulations were constrained to observations. The difference between 2070 and 1995 SWE will give an estimate of the projected trend in glacier mass balance between the respective end years of the historical and future periods.

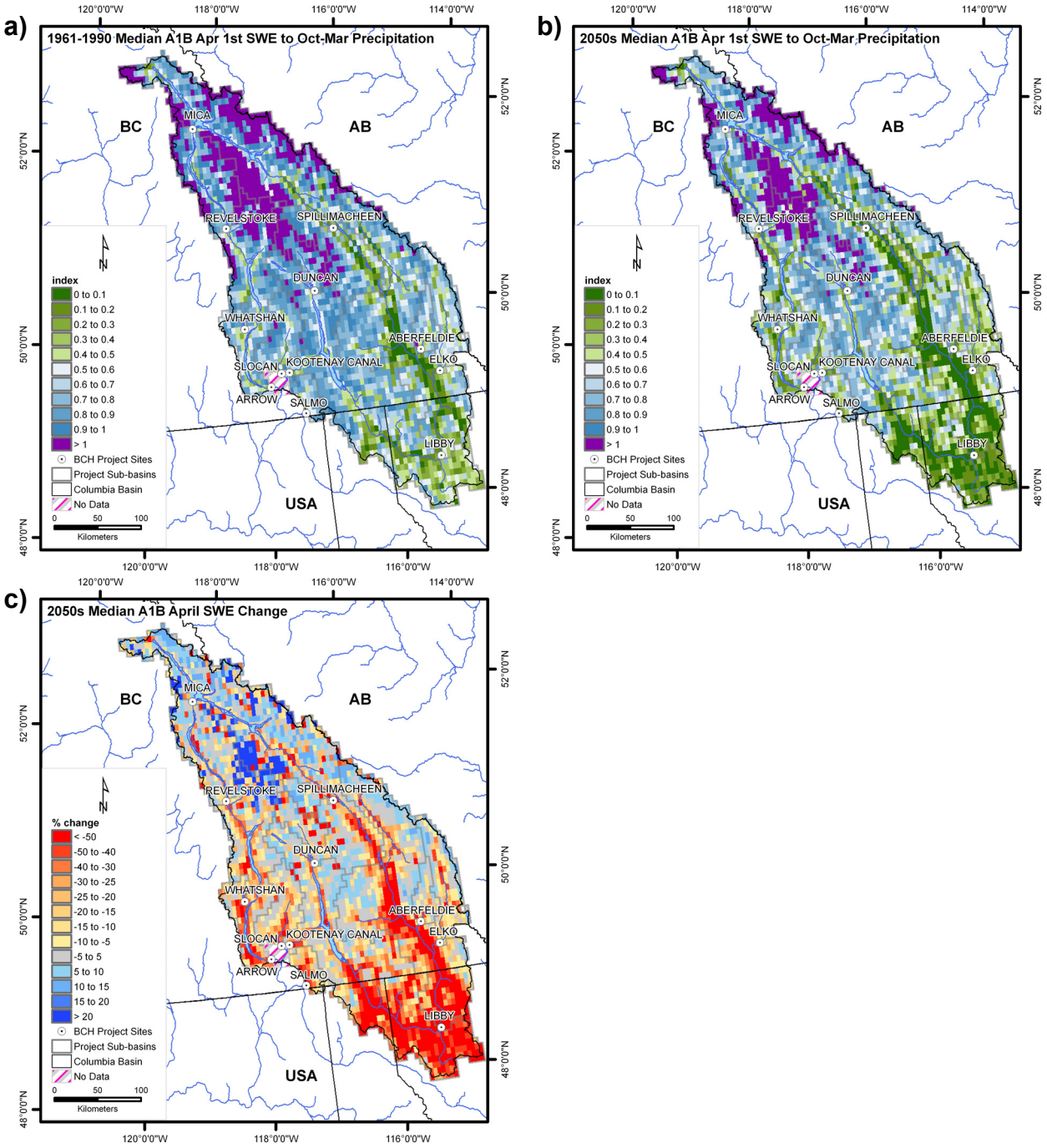

Figure 4-35. Snow storage in the Upper Columbia study area, given as the median of the A1B ensemble of the ratio of April 1 SWE to winter precipitation (October through March) for the a) 1970s, and b) the 2050s; and c) the median A1B April 1 SWE anomaly.

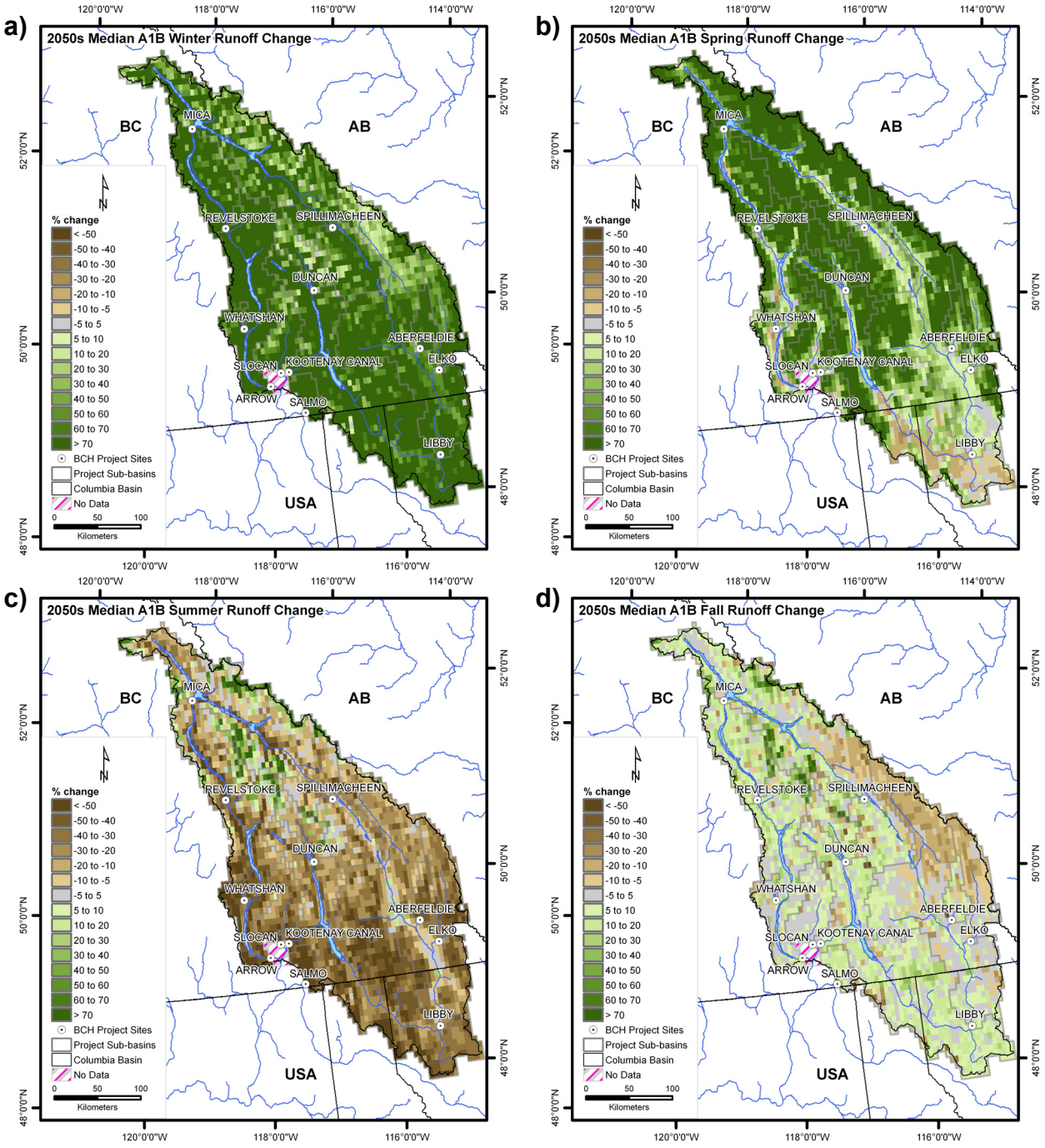

Figure 4-36. Median A1B 2050s seasonal runoff anomalies for the Upper Columbia study area for a) winter, b) spring, c) summer, and d) fall.

Glacier mass changes are projected to vary by elevation (e.g., *Schiefer et al*., 2007). Plotting cumulative ice volume by band elevation for 1995 and 2070 indicates that glacier mass loss will be greatest at low elevation (Figure 4-37a). Whereas the lowest glacier elevation in the VIC model was 1,200 m in 1995, projections suggest that glaciers in the 135 selected cells will not exist below 2,100 m by the year 2070. Cumulative mass balance varies with elevation (Figure 4-37b), increasing rapidly from -68 m to -15 m below 1,800 m elevation, then ranging between -15 to -12 m between elevations 1,600 and 2,400 m. Above 2,400 m, cumulative mass balance becomes increasingly less negative with elevation. Total cumulative mass balance is negative for the composite A1B median (-2.3 m), negligible for the composite A2 median (-0.4 m), and becomes positive for the composite B1 median (6.3 m) (Figure 4-37b). Projected volume losses over the 75-year period from 1995 to 2070 are -0.12, -0.02 and 0.34 km^3/year for the median of the A1B, A2 and B1 scenarios, respectively. These projected depletion rates are substantially slower (and opposite in the case of B1) than trends observed over recent decades. Over the period 1985 to 1999, Schiefer et al. (2007) reported mass balance trends of -0.54 and -1.23 km^3/year in the Southern Rocky and Columbia Mountains, respectively. The cumulative mass balance for North American cordillera glaciers from 1960 to 2004 is estimated at roughly -23 m water equivalent (Dyurgerov and Meier 2005; Kaser et al 2006), but considerable regional variability exists, ranging from approximately -42 m in the St. Elias Mountains to 15 m in the northern Coast Mountains (Dyurgerov and Meier 2005). The discrepancy between historical and projected glacier depletion rates in south-eastern BC may be attributed to projections of increased winter precipitation in the future (Table 4-5).

The variation of mass balance with elevation relates to the variation of temperature and precipitation with elevation. Below approximately 2,400 m it would seem that warmer temperatures are projected to dominate over increased winter precipitation, whereas above this elevation the converse is true, a response that is consistent between emissions scenarios. Cumulative mass balance becomes positive at approximately 2600 m for the B1 scenario. Given that the precipitation anomalies for the A1B, A2 and B1 scenarios are all roughly equal (particularly during the winter), it would appear that the differences in glacier mass balance are driven by differences in the magnitude of the temperature anomalies between A1B (warmest) to B1 (least warm) (Table 4-5), where A1B and A2 changes are roughly 0.5 °C to 1.0 °C warmer than B1. Unfortunately, the mass balance data does not reveal specific details on the relative importance of seasonal temperature and precipitation anomalies to changes to glacier mass balance (e.g., Oerlemans and Reichert 2000).

Projected changes in glacier area are estimated by comparing the fraction of each grid cell, based on elevation bands, that was covered by glacier ice in 1995 and 2007. An elevation band is assumed to be either entirely glacier-covered or completely glacier-free, and it was assumed that a band is glacier-free if it's 1 October SWE is < 1.0 m. In 1995 it was assumed that all 135 glacier cells were completely covered in ice, for a total glacier area of approximately 4,050 km^2 (based on a nominal grid cell area of 30 km^2). In 2070 this area is projected to shrink considerably, to 2,042, 2,155 and 2,435 km^2 for the median A1B, A2 and B1 scenario composites, respectively (Figure 4-37c). These absolute changes correspond to annual changes of -26.7, -25.2 and -21.5 km^2/year, respectively, which are a faster rate of area depletion than have been observed in the past twenty years (1985 to 2005) in the Upper Columbia region (Bolch et al. 2010 give trends of -16.3 and -10.7 km^2/year in the southern Rockies and southern interior, respectively). Therefore, despite positive total mass balance for the A2 and B1 scenarios, glacier ice is projected to occupy a considerably smaller footprint by 2070. A composite map of median A1B glacier mass balance by grid cell is shown in Figure 4-38. Glacier mass balance is negative below roughly 51^o north latitude, but above this latitude, mass balance generally correlates with elevation, increasing from negative to positive values with increasing grid-cell elevation.

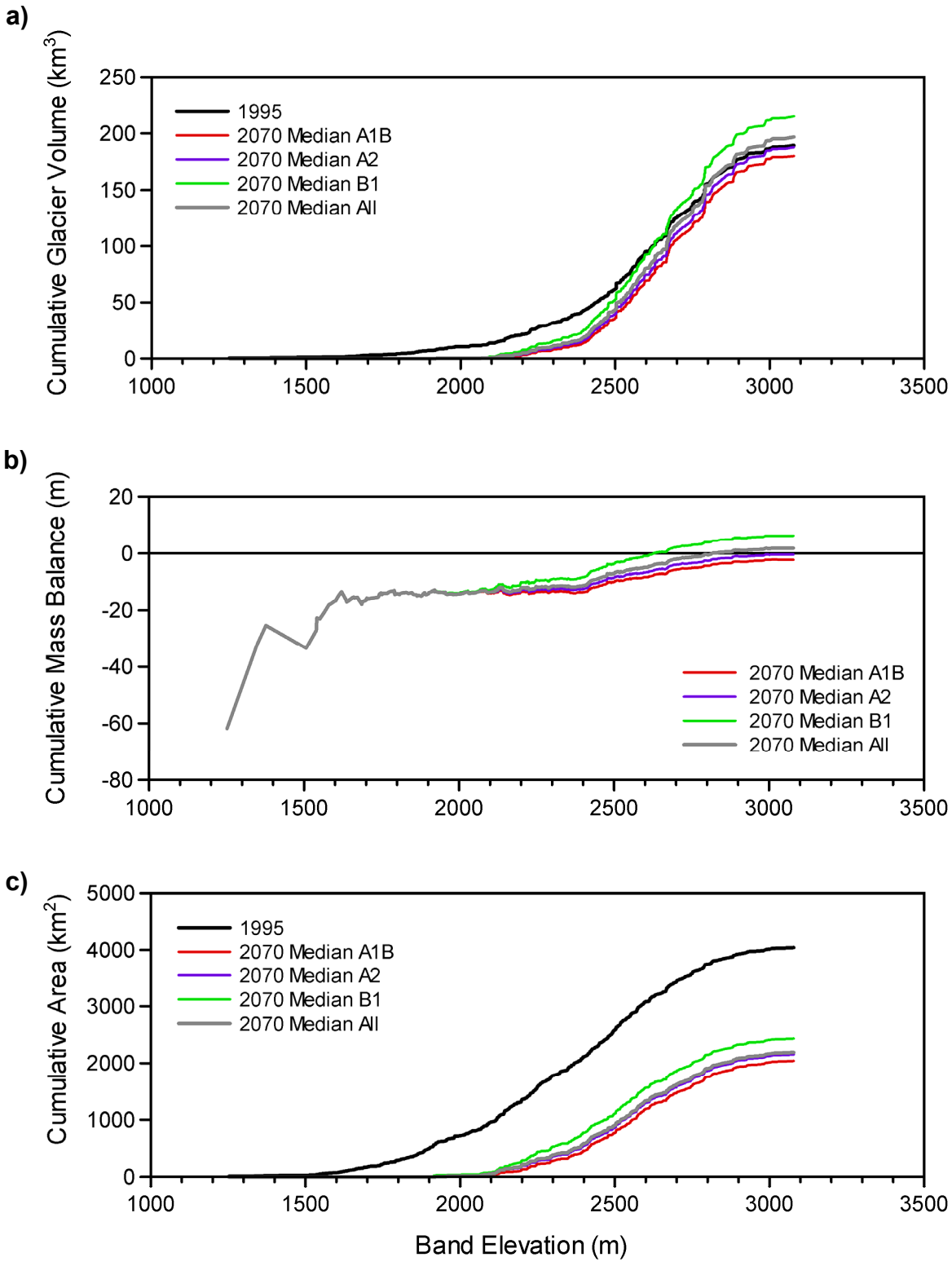

Figure 4-37. Glacier mass and area by band elevation for glacier cells in the Upper Columbia study area comparing year 1995 to median year 2070 projections, showing a) cumulative volume, b) cumulative mass balance (2070 minus 1995), and c) cumulative area.

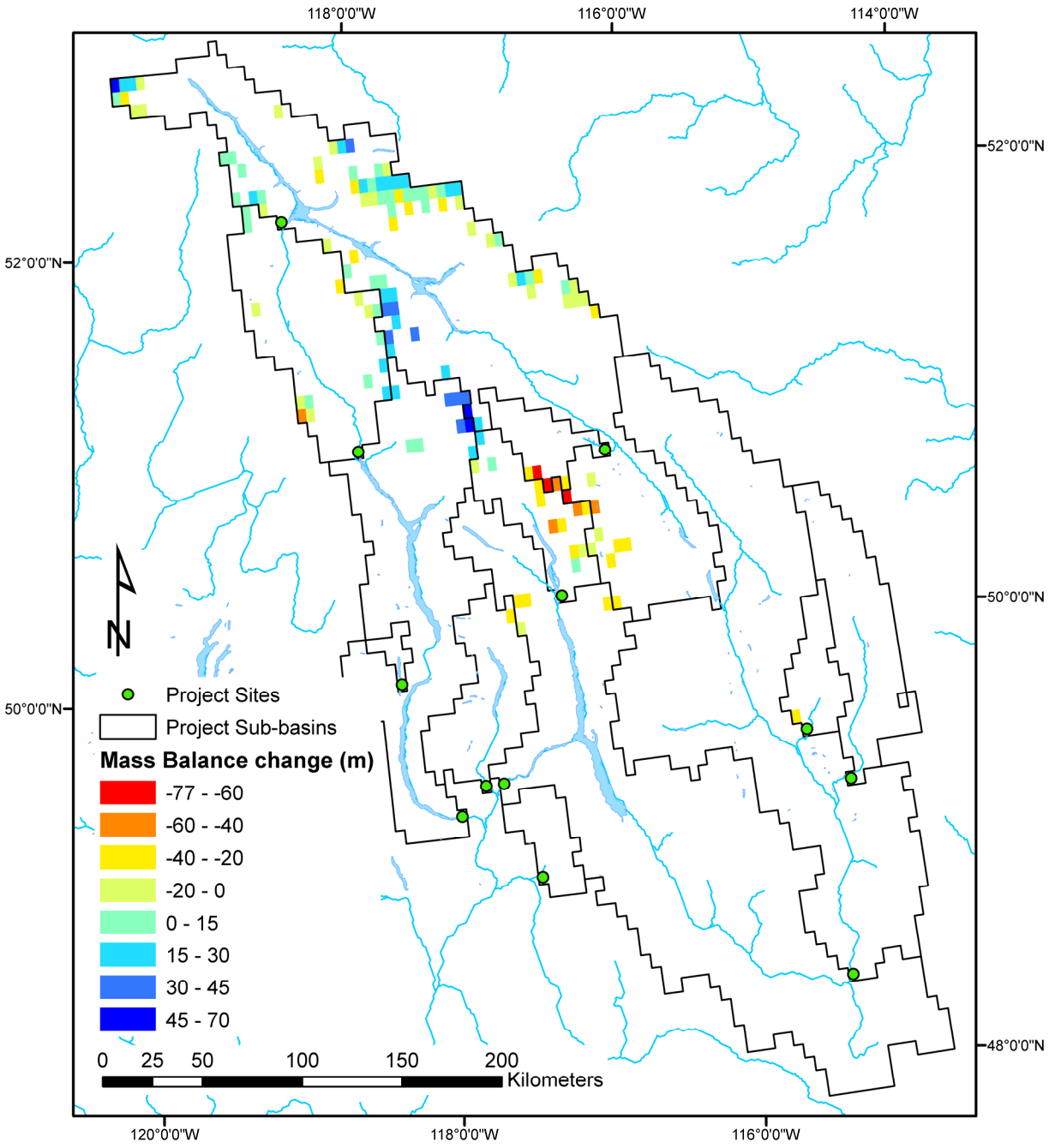

Figure 4-38. Year 1995 to 2070 median A1B glacier mass balance by grid cell in the Upper Columbia study area.

Given the important effect of temperature change on glacier mass balance, and the general decrease of temperature with elevation, it is suspected that the lack of glacier dynamics in the VIC model may serve to underestimate potential glacier mass loss, and possibly overestimate area loss (Stahl et al. 2008*)*. In reality, it would be expected that positive ice accumulation at high elevation would be dynamically redistributed to lower elevations (Ritter 2010), where it would be subjected to increased melt rates

brought on by warmer temperatures; an important feedback mechanism that is not modelled in the current work. In the VIC model 'glacier' melt is modelled using the standard albedo depletion curves for snow melt (see Schnorbus et al. 2010). Consequently, glacier albedo values may be overestimated and the important albedo feedback mechanism may be underestimated (Kaser et al. 2006). As such, the mass balance projections provided herein are likely overly optimistic, particularly the positive mass balance projected for the B1 scenario. Nevertheless, the results generated by the VIC model serve to illustrate the highly sensitive nature of glacier mass balance to rather subtle variations in temperature and precipitation change. Consequently, we do not preclude the possibility of (increasingly) positive glacier mass balance in the higher elevations of the Upper Columbia study area.

5. Conclusions and Future Work

This study utilized a suite of eight GCMs driven by three emissions scenarios, intended to capture a range of high, medium and low projected greenhouse gas emissions, to project a wide range of potential climate responses for the 2050s time period (2041-2070). The projections for the 2050s range from a future with relatively less warming and moistening ("cool/dry") to relatively more warming and moistening ("warm/wet"). The climate projections were statistically downscaled and used to drive the spatially-distributed VIC hydrologic model at high-resolution. The resultant hydrologic response was captured for three study areas in British Columbia (the Peace, Campbell and Upper Columbia), reflecting variation in local and regional hydrologic response across a range of climatic and physiographic regimes. Streamflow projections were made for specific project sites within the study areas, corresponding to current BC Hydro heritage asset sites, potential sites of future hydro-electric development (i.e., Site C), as well as several natural drainages. The general conclusion of this work can be summarized as follows:

- All projections indicate higher temperatures in all seasons in all study areas by 2050s, with strong agreement between GCMs and emissions scenarios. The highest temperature increase is projected for the winter season in the Peace and summer in the Upper Columbia, with essentially uniform temperature changes projected throughout the year for the Campbell.
- Precipitation projections are less robust for the 2050s (i.e., the range of individual GCM projections includes both positive and negative changes), but suggest increased precipitation in the winter, spring and fall for all study areas and all emissions scenarios. Regional differences for summer precipitation projections are apparent, with decreased precipitation projected for the Campbell and Upper Columbia study areas (southern BC) versus negligible changes in summer precipitation projected for the Peace study area (northern BC).
- Annual discharge is projected to increase in the Peace River study area, a response that is generally consistent between project sites, although local inflow to the Peace River above Pine River shows a weaker response. For the most part, changes are statistically significant (future values tend to be higher than historic values). Differences between GCM runs and inter-annual variability for any given GCM-driven ensemble are larger than streamflow differences between emissions scenarios. This indicates that in the 2050s projections of annual discharge are insensitive to the three emissions trajectories.
- Annual discharge changes for the Campbell River study area are projected to be negligible, with no statistically significant differences projected for either the A2 or B1 scenarios. Only the A1B ensemble indicates statistically significant increases in annual discharge (although only a 4% difference in median historic and future discharge is projected). For this small coastal watershed, the hydro-climatic response to mid-21st century A1B emissions may be sufficiently stronger than that from either A2 or B1 such that annual discharge displays a detectably different response. Nevertheless, as the climate response for this small study area is likely derived from a very limited number of GCM model grid cells, this result may also be easily attributed to model noise in the GCM response.
- Annual discharge in the Upper Columbia study area is projected to increase at the majority of project sites for all emissions scenarios. For the most part, a specific response to the three emissions scenarios is indistinguishable for the 2050s time period, with inter-annual and variability in GCM response being the dominant source of variability.
- Monthly streamflow projections for the Peace River project sites show a consistent response of higher future discharge during fall and winter, earlier onset of spring freshet, higher peak monthly discharge, and reduced discharge during late summer and early fall. Changes in the timing and duration of the spring freshet result in the largest absolute changes in monthly discharge. For the 2050s time period differences in the monthly discharge response between the three emissions scenarios are negligible.
- Monthly streamflow projections for the Campbell River study area show a strong shift in seasonality due to a transition from a hybrid nival-pluvial regime to an almost exclusively pluvial regime, although remnant freshet runoff is still projected to occur in the 2050s. This transition results in large

increases in fall and winter discharge, and decreases in spring, summer, and early fall discharge, resulting in a longer and more severe low flow period. As with annual discharge, the monthly streamflow response in the 2050s appears strongest for the A1B emissions scenario.

- Monthly streamflow projections for the Upper Columbia are generally consistent at all sites, manifesting as increased discharge during the late fall and winter, and earlier onset of the spring freshet, with higher discharge during the spring and early summer but reduced discharge during the late summer and early fall. Between sites, projections are less consistent regarding changes in the month of peak discharge as well as changes in the magnitude of peak monthly discharge. Variation in the monthly hydrologic response is primarily due to variation in the climate response between different GCMs. The effect of the three emissions scenarios is indistinguishable in the 2050s.
- At all three study areas, increases in annual discharge are attributed to projected changes in 2050s annual precipitation. Therefore, the variation in annual discharge response between study areas is due primarily to regional variation in projected precipitation trends. Increased annual precipitation is projected for the interior study areas (Peace and Upper Columbia) but negligible changes are projected for the coastal Campbell River study area.
- Changes in monthly streamflow timing, seasonality and magnitude are largely attributed to projected changes in the dynamics of natural snow storage, including 1) changes in the proportion of winter precipitation as rainfall versus snowfall, 2) changes in seasonal snow accumulation, and 3) changes in the timing and magnitude of snowmelt. The most prominent regional variation is apparent in the degree to which snow storage dynamics in the three study areas respond to projected climate response.
- The coastal Campbell River site is projected to undergo the most dramatic change, shifting from what is already a transitional hybrid regime to a predominantly pluvial regime. Although the Peace River in northeastern BC shows signs of shifting to a more hybrid regime in the 2050s, it will still retain sufficient snow that the monthly hydrograph will maintain the characteristic signal of a nival regime, albeit with a freshet that will be advanced in time. Although still responsive to changes in temperature and precipitation, overall the Upper Columbia arguably shows the least sensitivity to climate change. This is largely attributed to a hypsometry that places much of the study area at high enough elevation to avoid significant changes in snow storage dynamics, despite rising temperatures. In fact, in contrast to the Peace and Campbell, snow storage throughout much of the Upper Columbia reflects trends of increasing winter precipitation more so than rising temperatures.
- It bears repeating that, with the possible exception of the Campbell River study area, any difference in the climatic response of the three emissions trajectories, as specified by the A1B, A2 and B1 scenarios, is not large enough to generate any distinguishable difference in the annual or monthly streamflow response by the 2050s. For the most part, any possible hydro-climatic signal attributable to differential emissions is overshadowed by inter-annual variability and differences in the climatic sensitivity between individual global climate models.
- Glacier mass balance in the Upper Columbia study area is projected to vary with elevation, being predominantly negative at elevation below 2,400 m and increasingly more positive at elevation above 2,400 m. Cumulative mass balance between 1995 and 2070 for the entire study area, based on the ensemble medians for the A1B, A2, and B1 scenarios, is projected to be -2.3 m, -0.4 m, and +6.3 m, respectively. Differences in overall cumulative mass balance are mainly attributed to differences in projected temperature changes, which become progressively less pronounced for the A1B, A2 and B1 scenarios, respectively. Glacier area is projected to shrink by roughly 50% for all three emissions scenarios. Nevertheless, the projected trends in mass balance and glacier area may be under- and over-estimated, respectively, due to the absence of glacier dynamics in the hydrology model.

Our analysis was based on using updated data and the peer-reviewed methodology. Nevertheless, we recognize limitations in our approach, which serve to guide future efforts and inform potential future work. In addition, there will be opportunities to revisit and update past hydrologic projections with a new generation of climate projections based on updated climate models driven by new emissions scenarios. Some specific recommendations are summarized.

As indicated, it is essential that projections of glacier mass balance response to climate change be further refined by incorporating a dynamical glacier response within the hydrologic modelling process. This would allow for a more direct and realistic assessment of the potential hydrologic response of glacierized watersheds, particularly during late summer, as a consequence of a more realistic glacier mass, volume, area and hypsometry response to transient climate warming. This feedback can be introduced through an empirical volume-area scaling relationship for glaciers (Chen and Ohmura 1990; Bahr et al. 1997), as incorporated into a conceptual hydrologic model of climate change impacts on glacier runoff by Stahl et al. (2008). However, this method may not represent glacier dynamics properly, and the timescale for glacier adjustment to climate change is not explicitly accounted for. A more sophisticated approach is offered by Marshall and Clarke (1999), where snow accumulation and melt are simulated over subgrid elevation bands in the grid cells of a hydrological or climate model. Glaciers grow at high elevations where annual accumulation exceeds melt, and a simple representation of glacier dynamics is used to simulate the downslope transfer of mass in each grid cell. A higher-order representation of glacier mass balance and dynamics using a more physically-based approach at higher spatial resolution is also a possibility. Such an approach has been adopted for individual glaciers (e.g., Schneeberger et al. 2001).

Extension of the current work into the investigation of sub-monthly hydrologic and streamflow phenomenon, such as changes in the magnitude and frequency of extreme, or threshold design events, is clearly an issue of great relevance in water resources management. However, this will require explicit projections of transient hydrologic and streamflow change at a daily timescale, which will in turn require the direct downscaling of the daily transient climate response. Therefore, future effort should be devoted to further refinement of statistical downscaling approaches. This may include extension of the BCSD approach to a daily timeframe, or adoption of alternative statistical downscaling approaches designed for daily time steps, such as Constructed Analogues (Hidalgo et al. 2008). Regardless, the ability of statistical methods to downscale a daily transient signal will be affected by potential limitations of the GCMs in accurately representing daily statistics at high spatial and temporal resolution. Dynamical downscaling represents an attractive alternative approach, able to realistically simulate regional climate features such as orographic precipitation, extreme climate events and regional-scale climate anomalies (Fowler et al. 2007). However, limitations still exist in that 1) model skill depends strongly on biases inherited from the driving GCMs, such that RCM output must still be bias-corrected and statistically downscaled (Wood et al. 2004; Fowler et al. 2007), and 2) the approach is computationally expensive and cannot typically provide as large an ensemble of climate projections as statistical downscaling (Mote and Salathé 2010).

In the very near future, climate projections from the Coupled Model Intercomparison Project, Phase 5 (CMIP5) model suite (Taylor et al. 2009), run using the new Representative Concentration Pathway (RCP) scenario paradigm (Moss et al. 2008) will soon be available. These new climate projections will form the basis of the IPCC's upcoming fifth Assessment Report. These climate projections will be based on output from the latest generation of global climate models, many of them incorporating explicit accounting of physical, chemical and biological mechanisms governing the rates of change of the elements of the Earth System, including explicit carbon budgets and dynamic coupling with the terrestrial and marine biospheres (so-called Earth System Models; ESMs), giving a potentially more complete picture of the climate response to greenhouse gas emissions. Therefore, there is considerable incentive to revisit and update the current study by conducting hydrologic projections in the Peace, Campbell and Columbia study areas based on the latest CMIP5 results.

It will be informative to extend the current hydrologic projections out to the end of the 21st century. As reported, the hydrologic projections for the 2050s period (i.e., mid-21st century) suggest that the difference in climatic response due to different emission trajectories is indistinguishable. However, scenario differences are anticipated to become substantial by the end of the 21st century, at which time the A2 scenario will result in the largest impacts, the B1 scenario the smallest, and the A1B scenario intermediate impacts. Hydrologic impacts projected for the 2050s based on the chosen emissions scenarios are expected to become even more pronounced by the end of the 21st century.

(BLANK)

References

Adam J.C. and D.P. Lettenmaier, 2003: Adjustment of global gridded precipitation for systematic bias. *Journal of Geophysical Research*, 108(D9), 4257, doi: 10.1029/2002JD002499.

Adam, J.C., E.A. Clark, D.P. Lettenmaier and E.F. Wood, 2006: Correction of global precipitation products for orographic effects. *Journal of Climate*, 19: 15-38.

Adam, J.C., A.F. Hamlet and D.P. Lettenmaier, 2009: Implications of global climate change for snowmelt hydrology in the twenty-first century. *Hydrological Processes*, 23: 962-972.

Annan, J.D., and J.C. Hargreaves, 2010: Reliability of the CMIP3 ensemble. *Geophysical Research Letters*, 37, L02703, doi: 10.1029/2009GL041994

Auer Jr., H., 1974: The rain versus snow threshold temperatures. *Weatherwise*, 27: 67

Bahr, D.B., M.F. Meier and S.D. Peckham, 1997: The physical basis of glacier volume-areas scaling. *Journal of Geophysical Research*, 102: 20,355-20,362.

Barnett, T.P., J.C. Adam and D.P. Lettenamier, 2005: Potential impacts of a warming climate on water availability in snow-dominated regions. *Nature*, 438: 303-309.

Barnett, T.P., D.W. Pierce, H.G. Hidalgo, C. Bonfils, B.D. Santer, T. Das, G. Bala, A.W. Wood, T. Nozawa, A.A. Mirin, D.R. Cayan and M.D. Dettinger, 2008: Human-induced changes in the hydrology of the western United States. *Science*, 319: 1080-1083.

Barry, R.G., 1992: *Mountain weather and climate*, 2nd edition. London and New York, Routledge, 402 p.

Bartlett, P.A., M.D. Mackay, and D.L. and Verseghy, 2006: Modified snow algorithm in the Canadian Land Surface Scheme: Model runs and sensitivity analysis at three boreal forest stands. Atmosphere-Ocean, 43(3): 207-222.

Batjes, N.H. (ed.), 1995: A homogenized soil data file for global environmental research: A subset of FAO, ISRIC and NRCS profiles (Version 1.0). Working Paper and Preprint 95/10b, International Soil Reference and Information Centre, Wageningen.

BC Hydro, 2007: *Columbia River projects water use plan. Revised for acceptance by the Comptroller of Water Rights*, 11 January 2007. 41 pp. Last accessed 5 October 2010. http://www.bchydro.com/planning_regulatory/water_use_planning.html.

BC Hydro, 2009: Peace River Site C Hydro Project. *Stage 2 report: Consultation and Technical Review*. 102 pp. Last accessed 5 October 2010. http://www.bchydro.com/planning_regulatory/site_c.html.

BC Hydro, 2010: *Generation System*. Last accessed 14 December, 2010. http://www.bchydro.com/about/our_system/generation.html.

BC Ministry of Forests and Range, 2009: *Provincial-level projection of the current mountain pine beetle outbreak*. Research Branch, BC Ministry of Forests and Range. Last accessed 14 March 2011. http://www.for.gov.bc.ca/hre/bcmpb/cumulative/1999.htm.

British Columbia Integrated Land Management Bureau (BCILMB), 1995: Baseline thematic mapping: Present landuse mapping, Release 1.0.

Bennett, K.E., A.T. Werner, and M. Schnorbus, 2009: Uncertainties in hydrologic and climate change impact analyses in a headwater basin of the Peace River watershed. In: *Proceedings of the 17th International Northern Research Basins Symposium and Workshop*, Iqaluit-Pangnirtung-Kuujjuaq, Canada, August 12-18, 2009.

Blöschl, G. and A. Montanari, 2010: Climate change impacts – throwing the dice? *Hydrological Processes*, 24: 374-381.

Bolch, T., B. Menounos and R. Wheate, 2010: Landsat-based inventory of glaciers in western Canada, 1985-2005. *Remote Sensing of Environment*, 114: 127-137.

Bonfils, C., B.D. Santer, D.W. Pierce, H.H. Hidalgo, G. Bala, T. Das, T.P. Barnett, D.R. Cayan, C. Doutriaux, A.W. Wood, A. Mirin and T. Nozawa, 2008: Detection and attribution of temperature changes in the mountainous western United States. *Journal of Climate*, 21: 6404-6424.

Bras, R.L., 1990: *Hydrology: An introduction to hydrologic science*. Addison-Wesley Publishing Company, Reading, MA, 643 pp.

Campbell, G.S. and J.M. Norman, 1998: *An introduction to environmental biophysics, 2nd Ed*. Springer-Verlag, New York, 286 pp.

Carroll, A.L., J. Regniere, J.A. Logan, S.W. Taylor, B.J. Bentz and J.A. Powell, 2006: Impacts of climate change on range expansion by mountain pine beetle. Mountain Pine Beetle Initiative Working Paper 2006-14, Natural Resources Canada, Canadian Forest Service, Pacific Forestry Centre, Victoria, BC. 20 pp.

Chen, J. and A. Ohmura. 1990: Estimation of alpine glacier water resources and their change since the 1870s. Hydrology of Mountainous Regions. I-Hydrological Measurements of the Water Cycle. *IAHS Publication* 193: 127-135.

Christensen, N.S., A.W. Wood, N. Voisin, D.P. Lettenmaier and R.N. Palmer, 2004: The Effects of Climate Change on the Hydrology and Water Resources of the Colorado River Basin. *Climatic Change*, 62 (1-3): 337-363.

Climate Impacts Group, 2009: *The Washington Climate Change Impacts Assessment,* M.M. Elsner, J. Littell, and L.W. Binder (Eds). Center for Science in the Earth System, Joint Institute for the Study of the Atmosphere and Oceans, University of Washington, Seattle, Washington. Last accessed 23 April 2010. http://www.cses.washington.edu/db/pdf/wacciareport681.pdf.

Climate Prediction Centre (CPC), National Weather Service, National Oceanic and Atmospheric Administration, Accessed 2 December, 2010. http://www.cpc.ncep.noaa.gov/products/analysis_monitoring/ensostuff/ensoyears.shtml.

Cohen, S.J., K.A. Miller, A.F. Hamlet and W. Avis, 2000: Climate change and resource management in the Columbia River basin. *International Water Resources Association*, 25(2): 253-272.

Cosby, B.J., G.M. Hornberger, R.B. Clapp, and T.R. Ginn, 1984: A statistical exploration of the relationships of soil moisture characteristics to the physical properties of soils. *Water Resources Research*, 20: 682-690.

Dale, V.H., L.A. Joyce, S. McNulty, R.P. Neilson, M.P. Ayres, M.D. Flannigan, P.J. Hanson, L.C. Irland, A.E. Lugo, C.J. Peterson, D. Simberloff, F.J. Swanson, B.J. Stocks and B.M. Wotton, 2001: Climate change and forest disturbance, *Bioscience*, 51(9): 723-734.

Daly, C., 1994: A statistical-topographic model for mapping climatological precipitation over mountainous terrain. *Journal of Applied Meteorology*, 33: 140–158.

Demarchi, D.A., 1996: An introduction to the ecoregions of British Columbia. Wildlife Branch, Ministry of Environment, Lands and Parks, Victoria, BC. Last accessed 18 August 2010. http://www.env.gov.bc.ca/ecology/ecoregions/intro.html..

Demaria, E.M., B. Nijssen and T. Wagener, 2007: Monte Carlo sensitivity analysis of land surface parameters using the Variable Infiltration Capacity model. *Journal of Geophysical Research*, 112, D11113, doi: 10.1029/2006JD007534.

Déry, S.J., K. Stahl, R.D. Moore, P.H. Whitfield, B. Menounos and J.E. Burford, 2009: Detection of runoff timing changes in pluvial, nival, and glacial rivers of western Canada. *Water Resources Research*, 45, W04426, doi: 10.1029/2008WR006975.

Dickinson, R.E., A. Henderson-Sellars, C. Rosenzweig and P.J. Sellars, 1991: Evapotranspiration models with canopy resistance for use in climate models, a review. *Agricultural and Forest Meteorology*, 54: 373-388.

Ducoudré, N.I., K. Laval and A. Perrier, 1993: SECHIBA, a new set of parameterizations of the hydrologic exchanges at the land-atmosphere interface within the LMD atmosphere general circulation model. *Journal of Climate*, 6: 248-273.

Dyurgerov, M.B. and M.F. Meier, 2005: Glaciers and the changing earth system: A 2004 snapshot. Occasional Paper No. 58, Institute of Arctic and Alpine Research, University of Colorado at Boulder, Boulder, CO. 65 pp.

Easterling, D. R., T. R. Karl, J. H. Lawrimore, and S. A. Del Greco, 1999: United States Historical Climatology Network Daily Temperature, Precipitation, and Snow Data for 1871-1997. ORNL/CDIAC-118, NDP-070. Carbon Dioxide Information Analysis Center, Oak Ridge National Laboratory, U.S. Department of Energy, Oak Ridge, Tennessee.

Elsner, M.M., L. Cuo, N. Voisin, J.S. Deems, A.F. Hamlet, J.A. Vano, K.E.B. Mickelson, S.-Y. Lee and D.P. Lettenmaier, 2010: Implications of 21st century climate change for the hydrology of Washington State. *Climatic Change*, 102: 225-260, doi: 10.1007/s10584-010-9855-0

FAO, 1995: The digital soil map of the world, version 3.5. FAO, Rome.

Farr, T.G. et al., 2007: The shuttle radar topography mission. *Reviews of Geophysics*, 45, RG2004, doi: 10.1029/2005RG000183.

Fernandes, R., C. Butson, S. Leblanc and R. Latifovic, 2003: Landsat-5 TM and Landsat-7 ETM+ based accuracy assessment of leaf area index products for Canada derived from SPOT-4 VEGETATION data. *Canadian Journal of Remote Sensing*, 29(2): 241-258.

Fish and Wildlife Compensation Program, 2000: Campbell River Watershed, in *Watershed Plans,* Volume 2 of Bridge-Coastal Fish & Wildlife Restoration Program Strategic Plan, Chapter 2. http://www.bchydro.com/bcrp/about/strategic_plan.html.

Flannigan, M.D. and C.E. Van Wagner, 1991: Climate change and wildfire in Canada. *Canadian Journal of Forest Research*, 21: 66-72.

Fleming, S.W. and G.K.C. Clarke, 2003: Glacial control of water resource and related environmental responses to climatic warming: Empirical analysis using historical streamflow data from northwestern Canada. *Canadian Water Resources Journal*, 28: 69-86.

Fleming, S.W. and P.H. Whitfield, 2010: Spatiotemporal mapping on ENSO and PDO surface meteorological signals in British Columbia, Yukon, and southeast Alaska. *Atmosphere-Ocean*, 48(2): 122-131.

Fleming, S.W., P.H. Whitfield, R.D. Moore and E.J. Quilty, 2007: Regime-dependent streamflow sensitivities to Pacific climate modes cross the Georgia-Puget transboundary ecoregions. *Hydrological Processes*, 21: 3264-3287.

Fowler, H.J., S. Blenkinsop and C. Tebaldi, 2007: Linking climate change modelling to impacts studies: Recent advances in downscaling techniques for hydrological modelling. *International Journal of Climatology*, 27: 1547-1578.

Gavin, D.G., D.J. Hallett, F.S. hu, K.P. Lertzman, S.J. Prichard, K.J. Brown, J.A. Lynch, P. Bartlein and D.L. Peterson, 2007: Forest fire and climate change in western North America: insights from sediment charcoal records. *Paleoecology*, 5(9): 499-506.

Gedalof, Z. and A.A. Berg, 2010: Tree ring evidence for limited direct CO_2 fertilization of forests over the 20th century. *Global Biogeochemical Cycles*, 24, GB3027, doi: 10.1029/2009GB003699.

Global Soil Data Task. 2000: *Global Soil Data Products CD-ROM (IGBP-DIS)*. CD-ROM. International Geosphere-Biosphere Programme, Data and Information System, Potsdam, Germany. Available from Oak Ridge National Laboratory Distributed Active Archive Center, Oak Ridge, Tennessee, U.S.A.

Gonzalez, P., R.P. Neilson, J.M. Lenihan and R.J. Drapek, 2010: Global patterns in the vulnerability of ecosystems to vegetation shifts due to climate change. *Global Ecology and Biogeography*, 19(6): 755-768.

Gray, D.M. and T.D. Prowse, 1993: Snow and floating ice. Chapter 7 *in* D.R. Maidment (ed.), Handbook of Hydrology. McGraw-Hill, New York, NY. 1424 p.

Hamlet, A.F. and D.P. Lettenmaier, 1999: Effects of climate change on hydrology and water resources in the Columbia River Basin, *Journal of the American Water Resources Association*, 35 (6): 1597-1623

Hamlet, A.F. and D.P. Lettenmaier, 2005: Production of temporally consistent gridded precipitation and temperature fields for the continental United States. *Journal of Hydrometeorology*, 6: 330-336.

Hamlet, A.F., P.W. Mote, M. Clark and D.P. Lettenmaier, 2005: Effects of temperature and precipitation variability on snowpack trends in the western United States. Journal of Climate, 18(21):4545–4561

Hamlet, A.F. and D.P. Lettenmaier, 2007: Effects of 20th century warming and climate variability on flood risk in the western U.S. *Water Resources Research*, 43, W06427, doi: 10.1029/2006WR005099.

Hamlet, A.F., S.-Y. Lee, K.E.B. Mickelson and M.M. Elsner, 2010: Effects of projected climate change on energy supply and demand in the Pacific Northwest and Washington State. *Climatic Change*, doi. 10.1007/s10584-010-9857-7.

Hamann, A. and T. Wang, 2005: Models of climatic normals for genecology and climate change studies in British Columbia. *Agricultural and Forest Meteorology*, 128: 211-221.

Hayhoe, K., D. et al., 2004: Emission pathways, climate change, and impacts on California. *Proceedings of the National Academy of Science*, 101(34): 12422-12427.

Helsel, D.R. and R.M. Hirsch, 2002: Statistical methods in water resources. Book 4, chapter A3*in* Techniques of Water Resources Investigations. U.S. Geological Survey. 522 pp.

Hidalgo, H.G., M.D. Dettinger and D.R. Cayan, 2008: *Downscaling with constructed analogues: Daily precipitation and temperature fields over the United Sates*. Report No. CEC-500-2007-123, California Energy Commission, Sacramento, CA. 48 p.

Huang, J,-G., Y. Bergeron, B. Denneler, F. Berninger and J. Tardif, 2007: Response of forest trees to increased atmospheric CO_2. *Critical Reviews in Plant Sciences*, 26: 265-283.

Hughes, P. Y., E. H. Mason, T. R. Karl, and W. A. Brower, 1992: United States Historical Climatology Network Daily Temperature and Precipitation Data. ORNL/CDIAC-50, NDP-042. Carbon Dioxide Information Analysis Center, Oak Ridge National Laboratory, U.S. Department of Energy, Oak Ridge, Tennessee.

IPCC, 2007: Summary for Policymakers. In: *Climate Change 2007: The Physical Science Basis. Contribution of Working Group I to the Fourth Assessment Report of the Intergovernmental Panel on Climate Change* [Solomon, S., D. Qin, M. Manning, Z. Chen, M. Marquis, K.B. Averyt, M.Tignor and H.L. Miller (eds.)]. Cambridge University Press, Cambridge, United Kingdom and New York, NY, USA.

Joint Institute for the Study of Oceans and Atmospheres (JISAO), 2010: *Pacific decadal oscillation (PDO)*. Last accessed 2 December, 2010. http://jisao.washington.edu/pdo.

Jackson, R.B., J. Canadell, J.R. Ehleringer, H.A. Mooney, O.E. Sala and E.D. Schulze, 1996: A global analysis of root distributions for terrestrial biomes. *Oecologia*, 108(3): 389-411.

Kalnay, E. M. et al., 1996: The NCEP/NCAR 40-year reanalysis project. *Bulletin of the American Meteorological Society*, 77: 437-471.

Kaser, G., J.G. Cogley, M.B. Dyurgerov, M.F. Meier and A. Ohmura, 2006: Mass balance of glaciers and ice caps: Consensus estimates for 1961 – 2004. *Geophysical Research Letters*, 33, L19501, doi: 10.1029/2006GL027511.

Kern J.S., 1995: Evaluation of soil water retention models based on basic soil physical properties. Soil Sci. Soc. Am. J., 59, 1134-1141.

Kienzle, S.W., 2008: A new temperature based method to separate rain and snow. *Hydrological Processes*, 22: 5067-5085.

Kim, J., 2001: A nested modeling study of elevation-dependent climate change signals in California induced by increased atmospheric $C0_2$. *Geophysical Research Letters*, 28: 2951-2954.

Kimball, J.S., S.W. Running, and R. Nemani, 1997: An improved method for estimating surface humidity from daily minimum temperature. *Agriculture and Forestry Meteorology*, 85: 87–98.

Kimmins, J.P., 2005: Forest ecology, in *Forestry Handbook for British Columbia*, S.B. Watts and L. Tolland (Eds.), The Forestry Undergraduate Society, Faculty of Forestry, University of British Columbia, Vancouver, BC, pp 434-471.

Knowles, N. and D.R. Cayan, 2004: Elevational dependence of projected hydrologic changes in the San Francisco estuary and watershed. *Climatic Change*, 62: 319-336.

Knutti, R., G. Abramowitz, M. Collins, V. Eyring, P.J. Gleckler, B. Hewiston, and L. Mearns, 2010: Good practice guidance paper on assessing and combining multi model climate projections. In: *Meeting Report of the Intergovernmental Panel on Climate Change expert meeting on assessing and combining multi model climate projections*, Stocker, T.F., D. Qin, G, -K. Plattner, M. Tignor, and P.M. Midgley (eds.). IPCC Working Group I Technical Support Unit, University of Bern, Bern, Switzerland.

Leavesley, G.H., 1994: Modeling the effects of climate change on water resources – A review. *Climatic Change*, 28: 159-177.

Liang, X., D.P. Lettenmaier and E.F. Wood, 1994: A simple hydrologically based model of land surface water and energy fluxes for general circulation models. *Journal of Geophysical Research*, 99(D7): 14,415-14,428

Liang, X., E.F. Wood, and D.P. Lettenmaier, 1996: Surface soil moisture parameterization of the VIC-2L model: Evaluation and modifications. *Global and Planetary Change*, 13(1-4), 195-206.

Logan, J.A. and J.A. Powell, 2001: Ghost forest, global warming, and the mountain pine beetle (*Coleoptera: Scolytidae*). *American Entomologist*, 47(3): 160-173.

Lohmann, D., R. Nolte-Holube, and E. Raschke, 1996: A large-scale horizontal routing model to be coupled to land surface parameterization schemes. *Tellus*, 48A: 708-721.

Lohmann, D., E. Raschke, B. Nijssen, and D.P. Lettenmaier, 1998a: Regional scale hydrology: I. Formulation of the VIC-2L model coupled to a routing model. *Hydrological Sciences Journal*, 43(1): 131-141.

Lohmann, D., E. Raschke, B. Nijssen and D.P. Lettenmaier, 1998b: Regional scale hydrology: II. Application of the VIC-2L model to the Weser River, Germany. *Hydrological Sciences Journal*, 43(1): 143-151.

Loukas, A., L. Vasiliades and N.R. Dalezios, 2002a: Potential climate change impacts on flood producing mechanisms in southern British Columbia, Canada using the CGCMA1 simulation results. *Journal of Hydrology*, 259: 163-188.

Loukas, A., L. Vasiliades and N.R. Dalezios, 2002b: Climatic impacts of the runoff generation processes in British Columbia, Canada. *Hydrology and Earth System Sciences*, 6(2): 211-227.

Ludwig, R., I. May, R. Turcotte, L. Vexcovi, M. Braun, J.-F. Cyr, L.-G. Fortin, D. Chaumont, S. Biner, I. Chartier, D. Caya and W. Mauser, 2009: The role of hydrological model complexity and uncertainty in climate change impact assessment. *Advances in Geosciences*, 21: 63-71.

Malcolm, J.R., A. Markham, R.P. Neilson and M. Garaci, 2002: Estimated migration rates under scenarios of global climate change. *Journal of Biogeography*, 29: 835-849.

Mantua, N., I. Tohver and A. Hamlet, 2010: Climate change impacts on streamflow extremes and summertime stream temperature and their possible consequences for freshwater salmon habitat in Washington State. *Climatic Change*, doi: 10.1007/s10584-010-9845-2.

Marlon, J.R. et al., 2009: Wildfire response to abrupt climate change in North America. *Proceedings of the National Academy of Science of the USA*, 106(8): 2519-2524

Maurer, E.P. and H.G. Hidalgo, 2008: Utility of daily vs. monthly large-scale climate data: An intercomparison of two statistical downscaling methods. *Hydrology and Earth System Sciences*, 12: 551-563.

Maurer, E.P., A.W. Wood, J.C. Adam, D.P. Lettenmaier, and B. Nijssen, 2002: A long-term hydrologically based dataset of land surface fluxes and states for the conterminous United States. *Journal of Climate*, 15: 3237-3251.

Meehl, G.A., C. Covey, T. Delworth, M. Latif, B. McAvaney, J. F. B. Mitchell, R. J. Stouffer, and K. Taylor, 2007a: The WCRP CMIP3 multimodel dataset: A new era in climate change research. *Bulletin of the American Meteorological Society*, 88: 1383-1394.

Meehl, G.A., T.F. Stocker, W.D. Collins, P. Friedlingstein, A.T. Gaye, J.M. Gregory, A. Kitoh, R. Knutti, J.M. Murphy, A. Noda, S.C.B. Raper, I.G. Watterson, A.J. Weaver and Z.-C. Zhao, 2007b: Global Climate Projections. In: *Climate Change 2007: The Physical Science Basis. Contribution of Working Group I to the Fourth Assessment Report of the Intergovernmental Panel on Climate Change* [Solomon, S.,D. Qin, M. Manning, Z. Chen, M. Marquis, K.B. Averyt, M. Tignor and H.L. Miller (eds.)]. Cambridge University Press, Cambridge, United Kingdom and New York, NY, USA.

Mekis, É. and W.D. Hogg, 1999: Rehabilitation and analysis of Canadian daily precipitation time series. *Atmosphere-Ocean*, 37: 53-85.

Merritt, W.S., Y. Alila, M. Barton, B. Taylor, S. Cohen and D. Neilsen, 2006: Hydrologic response to scenarios of climate change in sub watersheds of the Okanagan basin, British Columbia. *Journal of Hydrology*, 326: 79-108.

Milly, P.C.D., J. Betancourt, M. Falkenmark, R.M. Hirsch, Z.W. Kunderzewicz, D.P. Lenttenmaier and R.J. Stouffer, 2008: Stationarity is Dead: Wither water management?, *Science*, 319: 573-574.

Ministry of Energy, 2010a: Electricity and Alternative Energy Division, Last accessed 14 December, 2010. http://www.empr.gov.bc.ca/EAED/Pages/default.aspx.

Ministry of Energy, 2010b: Electric Generation and Supply, Last accessed 22 December, 2010. http://www.empr.gov.bc.ca/EPD/Electricity/supply/Pages/default.aspx.

Moore, R.D. and I.G. McKendry, 1996: Spring snowpack anomaly patterns and winter climatic variability, British Columbia, Canada. Water Resources Research, 32(3): 623-632.

Moore, R.D., S.W. Fleming, B. Menounos, R. Wheate, A. Fountain, K. Stahl, K. Holm and M. Jakob, 2009: Glacier change in western North America: influence on hydrology, geomorphic hazards and water quality. *Hydrological Processes*, 23: 42-61.

Moss, R., et al., 2008: *Towards New Scenarios for Analysis of Emissions, Climate Change, Impacts, and Response Strategies*. Intergovernmental Panel on Climate Change, Geneva, 132 pp.

Mote, P.W. and E.P. Salathé Jr., 2010: Future climate in the Pacific Northwest. *Climatic Change*, 102: 29-50.

Mote, P.W., E.A. Parsons, A.F. Hamlet, W.S. Keeton, D. Lettenmaier, N. Mantua, E.L. Miles, D.W. Peterson, D.L. Peterson, R. Slaughter and A.K. Snover, 2003: Preparing for climatic change: The water, salmon, and forests of the Pacific Northwest. *Climatic Change*, 61: 45-88.

Mote, P.W., A.F. Hamlet, M.P. Clark and D.P. Lettenmaier, 2005: Declining mountain snowpack in western North America. *Bulletin of the American Meteorological Society*, 86: 39-49.

Nakićenović, N. and R. Swart (Eds.), 2000: *IPCC special report on emissions scenarios*. Cambridge University Press, Cambridge, UK. 612 pp.

Nash, J.E. and J.V. Sutcliffe, 1970: River flow forecasting through conceptual models: Part I – A discussion of principles. *Journal of Hydrology*, 10: 282-290.

Nijssen, B., G.M. O'Donnell, A.F. Hamlet and D.P. Lettenmaier, 2001: Hydrologic sensitivity of global rivers to climate change. Climatic Change, 50: 143-175.

Oerlemans, J. and B.K. Reichert, 2000: Relating glacier mass balance to meteorological data by using a seasonal sensitivity characteristic. *Journal of Glaciology*, 46(152): 1-6.

Payne, J.T., A.W. Wood, A.F. Hamlet, R.N. Palmer and D.P. Lettenmaier, 2004: Mitigating the effects of climate change on the water resources of the Columbia River basin, *Climatic Change*, 62 (1-3): 233-256.

Pierce, D.W., T.P. Barnett, H.H. Hidalgo, T. Das, C. Bonfils, B.D. Santer, G. Bala, M.D. Dettinger, D.R. Cayan, A. Mirin, A.W. Wood and T. Nozawa, 2008: Attribution of declining western U.S. snowpack to human effects. *Journal of Climate*, 21: 6425-6444.

Prudhomme, C. and H. Davies, 2009: Assessing uncertainties in climate change impact analyses on the river flow regimes in the UK. Part 2: future climate. *Climatic Change*, 93: 197-222.

Quick, M.C., 1995: The UBC Watershed Model, Chapter 8, In: V.P. Singh (ed.), *Computer Models of Watershed Hydrology*. Water Resources Publications, Highlands Ranch, CO. 1144 pp.

Raupach, M.R., G. Marland, P. Ciais, C. Le Quéré, J.G. Canadell, G. Klepper and C.B. Field, 2007: Global and regional drivers of accelerating CO_2 emissions. Proceedings of the National Academy of Science, 14(4), doi: 10.1073/pnas.0700609104.

Regonda, S.K., B. Rajagopalan, M. Clark and J. Pitlick, 2005: Seasonal cycle shifts in hydroclimatology over the western United States. *Journal of Climate*, 18: 372-384.

Ritter, M.E., 2010: *The Physical Environment: an Introduction to Physical Geography*. Last accessed 10 December, 2010. http://www.uwsp.edu/geo/faculty/ritter/geog101/textbook/title_page.html.

Roberts, J., 2000: The influence of physical and physiological characteristics of vegetation on their hydrologic response. *Hydrological Processes*, 14: 2885-2901.

Rodenhuis, D., A.T. Werner, K.E. Bennett, and T.Q. Murdock, 2007: Research plan for hydrologic impacts. Pacific Climate Impacts Consortium, University of Victoria, Victoria, BC, 34 pp.

Rodenhuis, D., K.E. Bennett, A.T. Werner, T.Q. Murdock and D. Bronaugh, 2009: Climate overview 2007: Hydro-climatology and future climate impacts in British Columbia. Pacific Climate Impacts Consortium, University of Victoria, Victoria, BC, 132 pp.

Rodenhuis, D., B. Music, M. Braun and D. Caya, 2010: Climate diagnostics of future water resources in BC watersheds. Pacific Climate Impacts Consortium, University of Victoria, Victoria, BC, 58 pp.

Romolo, L., T.D. Prowse, D. Blair, B.R. Bonsal and L.W. Martz, 2006: The synoptic climate controls on hydrology in the upper reaches of the Peace River Basin. Part I: snow accumulation. *Hydrological Processes*, 20: 4097-4111.

Ryan, M.G., D. Binkley, and J.H. Fownes, 1997: Age-related decline in forest productivity: Pattern and process. *Advances in Ecological Research*, 27: 213-262.

Salathé Jr., E.P., 2005: Downscaling simulations of future global climate with application to hydrologic modeling. International Journal of Climatology, 25: 419-436

Schaap, M.G., F.J. Leij, and M .Th. van Genuchten, 1998: Neural Network Analysis for Hierarchical prediction of Soil Hydraulic Properties. *Soil Science Society of America Journal*, 62:847-855.

Schiefer, E., B. Menounos and R. Wheate, 2007: Recent volume loss of British Columbia glaciers, Canada. Geophysical Research Letters, 34, L16503, doi: 10.1029/2007GL030780.

Schindler, D.W. and W.F. Donahue, 2006: An impending water crisis in Canada's western prairie provinces. *Proceedings of the National Academy of Science*, doi: 10.1073/pnas.0601568103.

Scholes, R.J., D. Skole, and J.S. Ingram, 1995: A global database of soil properties: Proposal for implementation. IGBP-DIS working paper # 10, University of Paris, France.

Schneeberger, C., Albrecht, O., Blatter, H., Wild, M. and Hock, R., 2001: Modelling the response of glaciers to a doubling in atmospheric CO_2: a case study of Störglaciaeren, northern Sweden. *Climate Dynamics* 17 (11): 825-834.

Schnorbus, M., K. Bennett and A. Werner, 2010: Quantifying the water resource impacts of mountain pine beetle and associated salvage harvest operations across a range of watershed scales: hydrologic modelling of the Fraser River basin. Information Report BC-X-423, Pacific Forestry Centre, Canadian Forest Service, Victoria, BC, 64 pp.

Sheffield, J. and E.F. Wood, 2008: Projected changes in drought occurrence under future global warming from multi-model, multi-scenario, IPCC AR4 simulations. *Climate Dynamics*, 31: 79-105.

Shepard, D.S., 1984: Computer mapping: The SYMAP interpolation algorithm, in *Spatial Statistics and Models*, G.L. Gaille and C.J. Willmott (Eds.), Reidel, pp. 133-145.

Shuttleworth, W.J., 1993: Evaporation, in *Handbook of Hydrology*, D.R. Maidment (Ed.), McGraw-Hill, New York, NY, Chapter 4.

Stahl, K. and R.D. Moore, 2006: Influence of watershed glacier coverage on summer streamflow in British Columbia, Canada. *Water Resources Research*, W06201, doi: 10.1029/2006WR005022.

Stahl, K., R.D. Moore and I.G. McKendry, 2006: The role of synoptic-scale circulation in the linkage between large-scale ocean-atmosphere indices and winter surface climate in British Columbia, Canada. *International Journal of Climatology*, 26: 541-560.

Stahl, K., R.D. Moore, J.A. Floyer, M.G. Asplin and I.G. McKendry, 2006: Comparison of approaches for spatial interpolation of daily air temperature in a large region with complex topography and highly variable station density. *Agricultural and Forest Meteorology*, 139: 224-236.

Stahl, K., R.D. Moore, J.M. Shea, D.G. Hutchinson and A. Cannon, 2008: Coupled modelling of glacier and streamflow response to future climate scenarios. *Water Resources Research,* 44, W02422, doi: 10.1029/2007WR005956.

Storck, P., and D.P. Lettenmaier, 1999: Predicting the effect of forest canopy on ground snow accumulation and ablation in maritime climates, in *Proceedings of the 67th Western Snow Conference*, C. Troendle (Ed.), Colorado State University, Fort Collins.

Taylor, K.E., R.J. Stouffer and G.A. Meehl, 2009: *A Summary of the CMIP5 Experiment Design*. Available from http://cmip-pcmdi.llnl.gov/cmip5/.

Tebaldi, C., and R. Knutti, 2007: The use of the multi-model ensemble in probabilistic climate projections. *Philosophical Transactions of the Royal Society: Series A*, 365: 2053-2075.

Thornton, P.E. and S.W. Running, 1999: An improved algorithm for estimating incident sola radiation from measurements of temperature, humidity, and precipitation. *Agricultural and Forest Meteorology*, 93: 211-228.

Toth, B., A. Pietroniro, F.M. Conly and N. Kouwen, 2006: Modelling climate change impacts in the Peace and Athabasca catchment and delta: I – hydrological model application. *Hydrological Processes*, 20: 4197-4214.

van Genuchten, M. Th., 1980: A closed form equation for predicting the hydraulic conductivity of unsaturated soils. *Soil Science Society of America Journal*, 44:892-898.

Vano, J.A., N. Voisin, L. Cuo, A.F. Hamlet, M.M. Elsner, R.N. Palmer, A. Polebitski and D.P. Lettenmaier, 2010a: Climate change impacts on water management in the Puget Sound region, Washington State, USA. *Climatic Change*, doi: 10.1007/s10584-010-9846-1.

Vano, J.A., N. Voisin, M.J. Scott, N. Voisin, C.O. Stöckle, A.F. Hamlet, K.E.B. Mickelson, M.M. Elsner and D.P. Lettenmaier, 2010b: Climate change impacts on water management and irrigated agriculture in the Yakima River Basin, Washington, USA. *Climatic Change*, doi: 10.1007/s10584-010-9856-z.

VanRheenen, N. T., Wood, A. W., Palmer, R. N., and Lettenmaier, D. P., 2004: Potential Implications of PCM Climate Change Scenarios for California Hydrology and Water Resources, *Climatic Change,* 62: 257–281.

Vincent, L.A., and D.W. Gullett, 1999: Canadian historical and homogeneous temperature datasets for climate change analyses. *International Journal of Climatology*, 19: 1375-1388.

Walther, G.-R., E. Post, P. Convey, A. Menzel, C. Parmesan, T.J.C. Beebee, J.-M. Fromentin, O.Hoegh-Guldberg and F. Bairlein, 2002: Ecological responses to recent climate change. *Nature*, 416: 389-395.

Wang, T., Hamann, A., Spittlehouse, D., and Aitken, S. N., 2006: Development of scale-free climate data for western Canada for use in resource management. *International Journal of Climatology*, 26(3):383-397.

Werner, A.T., 2011: *BCSD downscaled transient climate projections for eight select GCMs over British Columbia, Canada*. Pacific Climate Impacts Consortium, University of Victoria, Victoria, BC, 63 pp.

Westfall, J. and T. Ebata, 2007: *2007 Summary of forest health conditions in British Columbia*. Forest Practices Branch, BC Ministry of Forests and Range. Pest Management Report No. 15, 81 pp.

Whitfield, P.H. and A.J. Cannon, 2000: Recent variations in climate and hydrology in Canada. *Canadian Water Resources Journal*, 25: 19-65.

Whitfield, P.H., C.J. Reynolds and A.J. Cannon, 2002: Modelling streamflow in present and future climates: Examples from the Georgia Basin, British Columbia. *Canadian Water Resources Journal*, 27: 427-456.

Wigmosta, M.S., L.W. Vail, and D.P. Lettenmaier, 1994: A distributed hydrology-soil-vegetation model for complex terrain. *Water Resources Research*, 30(6): 1665-1679.

Wilby, R.L., 2005: Uncertainty in water resource model parameters used for climate change impact assessment. *Hydrological Processes*, 19: 3201-3219.

Wilby, R.L and T.M.L. Wigley, 1997: Downscaling general circulation model output: A review of methods and limitations. Progress in Physical Geography, 21(4): 530-548.

Wood, A.W., E.P. Maurer, A. Kumar, and D.P. Lettenmaier, 2002: Long-range experimental hydrologic forecasting for the eastern United States. *Journal of Geophysical Research*, 107(D20), 4429, doi: 10.1029/2001JD000659.

Wood, A.W., L.R. Leung, V. Sridhar and D.P. Lettenmaier, 2004: Hydrologic implications of dynamical and statistical approaches to downscaling climate model outputs. *Climatic Change*, 62: 189-216.

Wulder, M.A., J.A. Dechka, M.A. Gillis, J.E. Luther, R.J. Hall, A. Beaudoin and S.E. Frankon, 2003: Operational mapping of the land cover of the forested area of Canada with Landsat data: EOSD land cover program. *The Forestry Chronicle*, 79(6): 1075-1083.

Wulder, M.A., M. Cranny, R.J. Hall, J. Luther, A. Beaudoin, J.C. White, D.G. Goodenough and J. Dechka, 2008: Satellite land cover mapping of Canada's forests: The EOSD land cover project, in *North American Land Cover Summit*, J.C. Campbell, K.B. Jones, J.H. Smith and M.T. Koeppe (Eds.), Association of American Geographers, Washington, DC.

Yapo, P.O., H.V. Gupta and S. Sorooshian, 1998: Multi-objective global optimization for hydrologic models. *Journal of Hydrology*, 204: 83-97.

List of Figures

(BLANK)

List of Tables

(BLANK)

List of Appendices

(BLANK)

Appendix A: Overview and Inventory of VIC Modelling Data

The Variable Infiltration Capacity (VIC) hydrology model was used to quantify the hydrologic impacts of climate change within the Peace, Campbell and Upper Columbia basins. The VIC model is a spatially-distributed macro-scale hydrology that was applied at a spatial resolution of 1/16° (approximately 27-31 km^2, depending upon latitude). Using the specified boundary conditions (temperature, precipitation and wind speed) and initial states, the VIC model solves the 1-dimensional water and energy balance for each grid cell. The VIC model was run at a daily timestep (one-hour timestep for the snow model), generating daily data describing hydrologic storage changes and resultant fluxes for each grid cell. The runoff fluxes ("surface runoff" and "baseflow") are then collected and routed downstream using an offline routing model.

The hydrologic modelling data being inventoried and described in this appendix can be classified into three broad categories:

- External forcings (i.e., meteorological data)
- VIC model grid cell output (of two types, cell-average values as "flux" output, and elevation band-average values as "band" output)
- Routing model output (i.e., streamflow)

The full suite of data consists of 24 separate data sets generated from 24 simulation runs of the hydrologic and routing models. Each run corresponds to a unique climate forcing, specified as being either observed or derived from a global climate model (GCM), with corresponding grid-cell and routing output. A general description of the three data categories is provided in the following sections.

External Forcings

Forcings data sets are composed of individual files (one per 1/16° grid cell) in a domain covering all of British Columbia and a portion of the northwestern United States. The forcing data is composed of a suite of such data sets composed of a single observed (or base) data set, interpolated from station observations, and 23 data sets derived by statistically downscaling output from select global climate models (GCMs) and emissions scenarios. Specific details are as follows:

- Spatial Resolution: 1/16°, one file for every grid cell (per data set)
- Spatial domain: see Figure A1.
- Time Step: Daily
- File Format: Binary
- Variables (units) (per file):
    - Precipitation (mm)
    - Minimum temperature (°C)
    - Maximum temperature (°C)
    - Wind (m/s)
- Data sets available: Specified by data source (observed or GCM), emissions scenario (A1B, A2 or B1) and time period in Table A1.

VIC Model Cell Output

During each simulation run the VIC model generates output for each model grid cell. This output quantifies the various components of the water and energy balance at each model time step, describing the

hydrologic state within (e.g., snow water equivalent, soil moisture, etc.) and the fluxes entering, moving within or exiting the grid cell (e.g., rainfall, runoff, snowmelt, evaporation, etc.). Output is available for every grid cell for all 24 model runs (based on observed forcings plus forcings from 23 different climate projections). Output is captured in the form of two output files per run per grid cell, for every gird cell in the model domain covering the Peace, Campbell and Upper Columbia study areas. One file capture grid-cell average (weighted by vegetation class and elevation band areas) states and fluxes (so-called "flux" files); the second file captures select states and fluxes for individual elevation bands per grid cell (so-called "band" files).

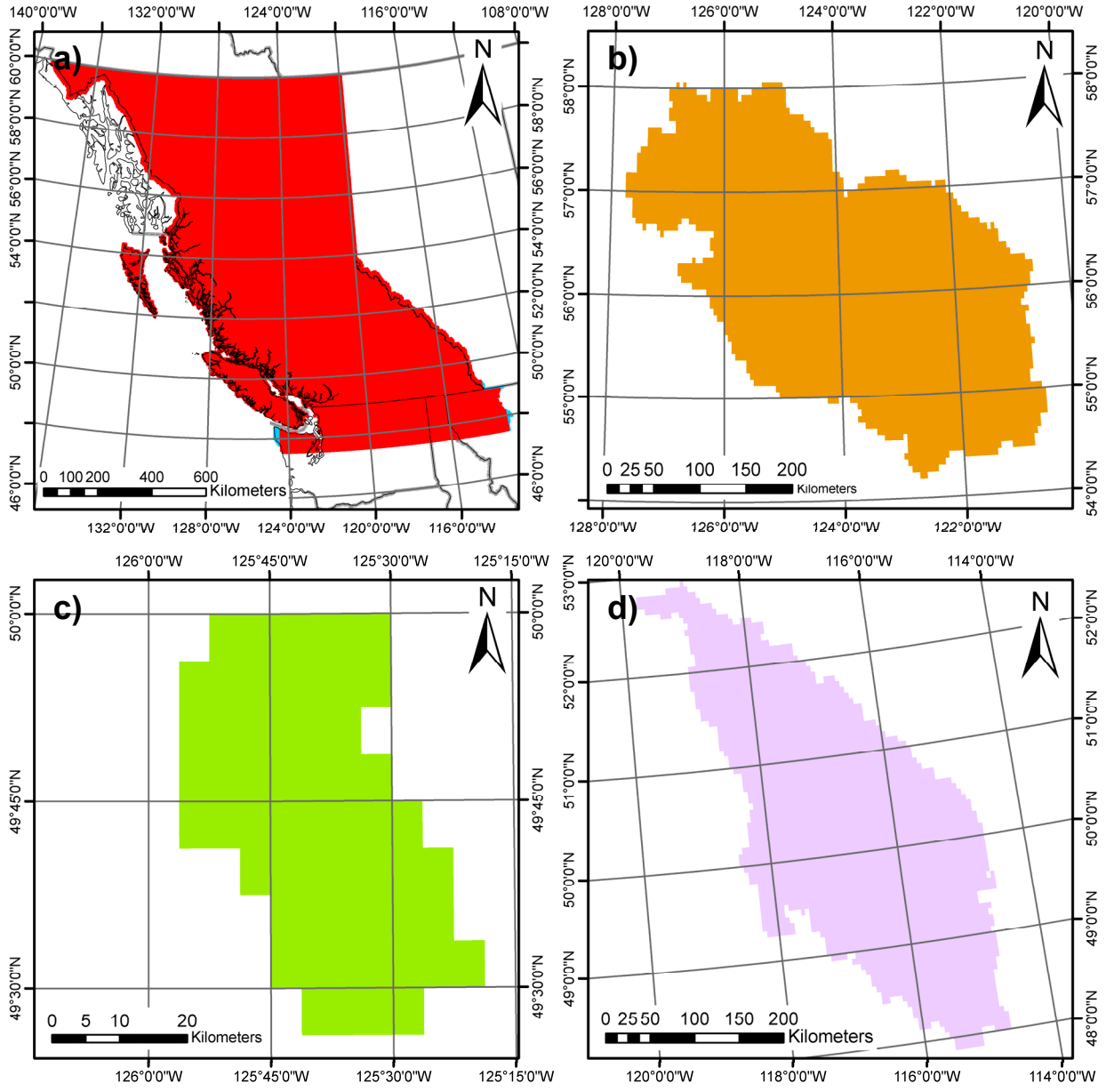

Figure A1. Colored shading showing the spatial domain of a) the external forcing data used to drive the VIC hydrologic model (note that the spatial domain of the observed data (blue shading) differs slightly from that for the downscaled climate projections (red shading)); and spatial domain of the VIC model output data (flux and band files) for the b) Peace, c) Campbell, and d) Upper Columbia River study areas. Note that scale varies in each frame.

Table A1. External Forcings Data Set Description

Model & Scenario	Time Period
Observed/BASE	1950-2006
CCSM3 A1B	1950-2099
CCSM3 A2	1950-2099
CCSM3 B1	1950-2099
CGCM3.1 A1B	1950-2100
CGCM3.1 A2	1950-2100
CGCM3.1 B1	1950-2100
CSIRO35 A1B	1950-2100
CSIRO35 A2	1950-2100
CSIRO35 B1	1950-2100
ECHAM5 A1B	1950-2100
ECHAM5 A2	1950-2100
ECHAM5 B1	1950-2100
GFDL CM2 A1B	1950-2100
GFDL CM2 A2	1950-2100
GFDL CM2 B1	1950-2100
HADCM A1B	1950-2100
HADCM A2	1950-2099
HADCM B1	1950-2100
HADGEM1 A1B	1950-2098
HADGEM1 A2	1950-2098
MIROC 3.2 A1B	1950-2100
MIROC 3.2 A2	1950-2100
MIROC 3.2 B1	1950-2100

Flux Output

Flux output files capture values for select flux and state variables as an area-average for each grid cell. Specific details of the *flux* output are as follows:

- Spatial Resolution: 1/16°, one file for every grid cell (per data set)
- Spatial Domain: see Table A2 and Figure A1
- Time Step: Daily
- Format: ASCII
- Variables (units):
    - Precipitation (mm)
    - Total net evaporation (mm)
    - Surface runoff (mm)
    - Baseflow from the bottom soil layer (mm)
    - Total moisture interception storage in canopy (mm)

- Rainfall (mm)
- Air Temperature (°C)
- Soil liquid content for each soil layer (mm)
- Net evaporation from canopy interception (mm)
- Net transpiration from vegetation (mm)
- Net evaporation from bare soil (mm)
- Net sublimation from snow stored in vegetation canopy (mm)
- Total net sublimation from snow pack (surface and blowing) (mm)
- Root zone soil moisture (mm)
- Snow water equivalent in snow pack (including vegetation intercepted snow) (mm)
- Depth of snow pack (cm)
- Fractional area of snow cover (fraction)
- Snow interception storage in canopy (mm)
- Snow Melt (mm)
- Snowfall (mm)
- Average surface albedo (fraction)
- Snow pack albedo (fraction)
- Net downward shortwave flux (W/m^2)
- Net downward radiation flux (W/m^2)

- Data sets available: Specified by data source (observed or GCM), emissions scenario (A1B, A2 or B1) and time period for each study area in Table A3. Note that for the Columbia projection runs, output data is divided into two time periods as a result of the re-setting of the glacier state on 1 October, 1995.

Table A2. Number of VIC Model Output Files and Routing Model Sites Per Model Run

Basin	Flux Files	Band Files	Routing Sites
Campbell	58	58	1
Peace	3975	3975	24
Columbia	3001	3001	38

Band Output

Band output files capture select fluxes and states, mainly with respect to snow, for each elevation band within a single grid cell. Each band file contains five values per band-specific output variable, where five is the maximum number of elevation bands per grid cell. As the actual number of elevation bands per grid cell varies with local relief, varying from one to five, some band values are null for cells with less than five bands. The band file also captures some cell-average variables. Specific details of the *band* output are as follows:

- Spatial Resolution: 1/16°, one file for every grid cell (per data set)
- Spatial Domain: see Table A2 and Figure A1
- Time Step: Daily
- Format: ASCII

- Band-specific Variables (units): values for the following variables are provided for each of five elevation bands
    - Snow water equivalent in snow pack (mm)
    - Depth of snow pack (cm)
    - Snow interception storage in canopy (mm)
    - Fractional area of snow cover (fraction)
- Cell-average Variables:
    - Potential evaporation (transpiration only) from current vegetation and current canopy resistance (mm)
    - Potential evaporation (transpiration only) from current vegetation without canopy resistance (mm)
- Data sets available: Specified by data source (observed or GCM), emissions scenario (A1B, A2 or B1) and time period for each study area in Table A3. Note that for the Columbia projection runs, output data is divided into two time periods as a result of the re-setting of the glacier state on 1 October, 1995.

Table A3. Data Set Description of VIC Model Output

Forcings	Time Period		
	Campbell	Peace	Upper Columbia
Observed/BASE	1950-2006	1950-2006	1950-2006
CCSM3 A1B	1950-2099	1950-2099	1950-2006, 1995-2098
CCSM3 A2	1950-2099	1950-2099	1950-2006, 1995-2098
CCSM3 B1	1950-2099	1950-2099	1950-2006, 1995-2098
CGCM3.1 A1B	1950-2099	1950-2099	1950-2006, 1995-2098
CGCM3.1 A2	1950-2099	1950-2099	1950-2006, 1995-2098
CGCM3.1 B1	1950-2099	1950-2099	1950-2006, 1995-2098
CSIRO35 A1B	1950-2098	1950-2098	1950-2006, 1995-2098
CSIRO35 A2	1950-2098	1950-2098	1950-2006, 1995-2098
CSIRO35 B1	1950-2098	1950-2098	1950-2006, 1995-2098
ECHAM5 A1B	1950-2099	1950-2099	1950-2006, 1995-2098
ECHAM5 A2	1950-2099	1950-2099	1950-2006, 1995-2098
ECHAM5 B1	1950-2098	1950-2098	1950-2006, 1995-2098
GFDL CM2 A1B	1950-2099	1950-2099	1950-2006, 1995-2098
GFDL CM2 A2	1950-2099	1950-2099	1950-2006, 1995-2098
GFDL CM2 B1	1950-2099	1950-2099	1950-2006, 1995-2098
HADCM A1B	1950-2099	1950-2099	1950-2006, 1995-2098
HADCM A2	1950-2099	1950-2099	1950-2006, 1995-2098
HADCM B1	1950-2098	1950-2098	1950-2006, 1995-2098
HADGEM1 A1B	1950-2098	1950-2098	1950-2006, 1995-2098
HADGEM1 A2	1950-2098	1950-2098	1950-2006, 1995-2098
MIROC 3.2 A1B	1950-2099	1950-2099	1950-2006, 1995-2098
MIROC 3.2 A2	1950-2098	1950-2098	1950-2006, 1995-2098
MIROC 3.2 B1	1950-2099	1950-2099	1950-2006, 1995-2098

Routing Model Output

The routing model is run as a post-processing step, wherein the VIC-generated fluxes of fast runoff and baseflow are aggregated and routed through the model drainage network. In this fashion the routing model is used to estimate streamflow or, discharge, at a specified point (or points) along the channel network. Consequently, unlike the VIC output data, streamflow output is not captured for each cell, but only for certain pre-specified cells, generally corresponding to Water Survey of Canada (WSC) gauge locations or BC Hydro project sites. Raw routing model output is the estimate of streamflow based on fast runoff and baseflow integrated from all cells upstream of that point. Streamflow based on local drainage only (i.e., exclusive of upstream project sites) has also been estimated for certain sites. Specific details of the *routing* output are as follows:

- Spatial Resolution: n/a
- Spatial Domain: individual project or calibration sites (see Table 2-2 and Table 3-1 in main report for description of sites); see Table A2
- Time Step: Daily, Monthly, and Annually per site
- Format: ASCII
- Variables (units): Streamflow (m^3/s)
- Data sets available: Specified by data source (observed or GCM), emissions scenario (A1B, A2 or B1) and time period for each study area in Table A4. Note that for the Columbia projection runs, output data is divided into two time periods as a result of the re-setting of the glacier state on 1 October, 1995.

Table A4. Data Set Description of Routing Model Output

Forcings	Time Period by Study Area		
	Campbell	Peace	Upper Columbia
Observed/BASE	1950-2006	1950-2006	1950-2006
CCSM3 A1B	1950-2099	1950-2098	1950-2006, 1995-2098
CCSM3 A2	1950-2099	1950-2098	1950-2006, 1995-2098
CCSM3 B1	1950-2099	1950-2098	1950-2006, 1995-2098
CGCM3.1 A1B	1950-2099	1950-2098	1950-2006, 1995-2098
CGCM3.1 A2	1950-2099	1950-2098	1950-2006, 1995-2098
CGCM3.1 B1	1950-2099	1950-2098	1950-2006, 1995-2098
CSIRO35 A1B	1950-2098	1950-2098	1950-2006, 1995-2098
CSIRO35 A2	1950-2098	1950-2098	1950-2006, 1995-2098
CSIRO35 B1	1950-2098	1950-2098	1950-2006, 1995-2098
ECHAM5 A1B	1950-2099	1950-2098	1950-2006, 1995-2098
ECHAM5 A2	1950-2099	1950-2098	1950-2006, 1995-2098
ECHAM5 B1	1950-2098	1950-2098	1950-2006, 1995-2098
GFDL CM2 A1B	1950-2099	1950-2098	1950-2006, 1995-2098
GFDL CM2 A2	1950-2099	1950-2098	1950-2006, 1995-2098
GFDL CM2 B1	1950-2099	1950-2098	1950-2006, 1995-2098
HADCM A1B	1950-2099	1950-2098	1950-2006, 1995-2098
HADCM A2	1950-2099	1950-2098	1950-2006, 1995-2098
HADCM B1	1950-2098	1950-2098	1950-2006, 1995-2098
HADGEM1 A1B	1950-2098	1950-2098	1950-2006, 1995-2098
HADGEM1 A2	1950-2098	1950-2098	1950-2006, 1995-2098
MIROC 3.2 A1B	1950-2099	1950-2098	1950-2006, 1995-2098
MIROC 3.2 A2	1950-2098	1950-2098	1950-2006, 1995-2098
MIROC 3.2 B1	1950-2099	1950-2098	1950-2006, 1995-2098

(BLANK)

Appendix B: Historic and Future Monthly Discharge Percentiles for the A1B Projections Ensemble for all Project Sites

Table B1. Historic and future monthly discharge percentiles for the A1B ensemble for all project sites.

Month	Historic (1961 to 1990) Discharge (m^3/s)					Future (2041 to 2070) Discharge (m^3/s)					Discharge Anomaly (m^3/s)				
	5P	25P	50P	75P	95P	5P	25P	50P	75P	95P	5P	25P	50P	75P	95P
						Peace: Peace River at Williston Dam (BCGMS)									
Oct	501	668	821	956	1277	433	621	839	1064	1427	-68	-47	18	108	150
Nov	397	581	690	846	1122	474	668	897	1181	1591	77	86	207	334	470
Dec	249	345	428	584	886	293	469	735	966	1507	44	124	307	382	621
Jan	158	218	302	469	1002	212	380	643	1019	1624	54	163	341	550	622
Feb	116	161	244	401	944	180	290	604	960	1658	64	129	360	559	714
Mar	93	136	213	374	831	163	355	623	961	1618	69	219	410	587	787
Apr	131	267	466	638	1057	384	720	978	1241	1800	253	453	512	603	743
May	952	1250	1489	1871	2397	1279	1766	2131	2466	3204	327	516	643	595	807
Jun	2003	2582	2951	3508	4117	1542	2350	2947	3605	4574	-462	-232	-5	97	457
Jul	1280	1812	2243	2825	3704	632	1084	1411	1826	2736	-648	-728	-832	-999	-968
Aug	605	804	966	1214	1644	357	527	661	817	1053	-248	-277	-305	-397	-591
Sep	494	644	763	961	1270	325	464	618	798	1129	-168	-180	-146	-163	-141
						Peace: Peace River above Pine River, near Site C (PEAPN)									
Oct	529	713	893	1040	1389	451	654	892	1108	1564	-79	-59	-1	68	175
Nov	445	629	742	912	1204	505	712	969	1287	1669	60	83	227	375	465
Dec	275	383	470	640	948	319	514	800	1025	1573	44	131	329	385	624
Jan	182	249	340	502	1063	239	418	689	1082	1720	58	169	349	580	656
Feb	142	187	284	442	1019	207	334	652	1017	1793	64	147	368	576	774
Mar	118	167	256	420	917	190	400	664	1024	1750	72	232	408	604	832
Apr	168	313	505	694	1122	436	783	1039	1331	2004	268	470	535	637	883
May	1025	1310	1584	1943	2550	1361	1886	2267	2616	3352	336	576	683	674	802
Jun	2116	2715	3137	3709	4348	1645	2497	3177	3812	4828	-472	-218	41	103	480
Jul	1420	2028	2449	3057	4010	706	1179	1551	2013	2988	-714	-848	-898	-1045	-1023
Aug	664	885	1059	1359	1827	387	576	722	905	1187	-276	-309	-337	-453	-641
Sep	534	701	836	1066	1444	352	505	668	884	1282	-182	-196	-168	-182	-162

Table B1. Continued.

Month	Historic (1961 to 1990) Discharge (m^3/s)					Future (2041 to 2070) Discharge (m^3/s)					Discharge Anomaly (m^3/s)				
	5P	25P	50P	75P	95P	5P	25P	50P	75P	95P	5P	25P	50P	75P	95P
						Peace: Peace River at Taylor (PEACT)									
Oct	57	85	112	148	220	44	76	107	147	262	-14	-9	-5	-2	42
Nov	60	85	106	139	211	56	85	136	189	280	-4	0	31	50	70
Dec	44	63	82	125	218	45	85	134	216	320	0	21	52	91	102
Jan	34	51	79	120	234	44	89	162	232	414	10	38	83	112	180
Feb	30	49	74	125	209	49	92	145	232	477	19	43	71	107	268
Mar	32	52	85	142	243	62	121	193	275	442	30	68	108	133	198
Apr	75	111	179	240	357	151	240	315	396	558	76	129	135	157	201
May	245	338	412	520	696	192	365	478	625	835	-53	26	66	105	139
Jun	240	363	479	602	824	106	209	323	447	750	-134	-154	-156	-156	-75
Jul	106	163	211	285	462	55	94	124	174	282	-52	-69	-87	-111	-180
Aug	52	76	98	130	185	35	52	67	85	122	-17	-24	-31	-44	-63
Sep	43	70	91	122	171	28	48	69	98	164	-15	-22	-21	-24	-6
						Campbell: Campbell River at Strathcona Dam (BCSCA)									
Oct	17	47	76	108	158	15	48	80	116	187	-3	1	4	8	29
Nov	48	75	105	143	199	59	99	132	177	240	10	24	27	34	41
Dec	40	62	92	125	162	57	96	136	168	215	17	34	44	42	53
Jan	30	54	75	112	171	46	84	134	174	248	15	29	59	62	77
Feb	28	46	65	86	141	47	79	109	148	229	18	32	43	62	88
Mar	38	54	70	90	109	60	91	108	129	154	21	36	38	39	45
Apr	60	81	92	106	125	78	92	105	123	143	18	11	13	17	18
May	96	113	128	143	166	51	71	93	119	157	-46	-42	-35	-24	-9
Jun	76	112	135	158	189	19	29	46	76	132	-56	-83	-90	-82	-57
Jul	27	50	69	97	135	8	11	16	25	47	-19	-38	-54	-72	-88
Aug	10	17	24	34	50	4	6	8	11	19	-6	-11	-16	-24	-31
Sep	7	12	18	25	43	3	6	10	16	28	-4	-6	-8	-9	-15

Table B1. Continued.

Month	Historic (1961 to 1990) Discharge (m^3/s)					Future (2041 to 2070) Discharge (m^3/s)					Discharge Anomaly (m^3/s)				
	5P	25P	50P	75P	95P	5P	25P	50P	75P	95P	5P	25P	50P	75P	95P
						Upper Columbia: Spillimacheen River near Spillimacheen (SPINS)									
Oct	8.1	10.6	13.4	16.1	21.5	7.5	11.5	15.1	20.5	33.3	-0.6	0.9	1.7	4.4	11.8
Nov	4.7	6.5	8.3	10.2	13.4	4.7	8.1	11.9	16.2	23.9	0.1	1.6	3.6	5.9	10.5
Dec	3.0	4.0	5.0	6.0	7.9	3.2	5.4	7.7	10.3	17.5	0.2	1.5	2.7	4.3	9.6
Jan	1.9	2.5	3.2	4.1	8.1	2.4	3.9	5.9	9.0	18.6	0.5	1.4	2.7	4.9	10.6
Feb	1.3	1.8	2.3	3.2	6.8	1.9	3.2	4.9	8.4	16.3	0.6	1.4	2.7	5.2	9.4
Mar	1.1	1.5	2.2	3.4	7.4	1.9	3.5	5.8	9.5	16.6	0.9	2.1	3.7	6.1	9.2
Apr	2.6	5.0	7.2	9.2	12.4	7.3	10.9	13.8	18.1	25.6	4.7	5.9	6.6	8.9	13.2
May	14.6	19.8	28.1	36.0	55.4	24.9	37.7	50.9	65.8	96.2	10.2	17.9	22.8	29.8	40.8
Jun	59.4	79.8	99.5	121.9	158.1	93.7	125.9	144.3	166.2	214.6	34.3	46.1	44.8	44.3	56.5
Jul	65.4	94.9	115.3	132.0	164.4	40.0	61.6	89.7	121.8	173.1	-25.4	-33.3	-25.6	-10.2	8.7
Aug	31.8	40.1	49.2	62.1	89.3	23.7	30.4	35.8	43.2	53.9	-8.1	-9.7	-13.4	-18.9	-35.4
Sep	14.5	17.6	21.1	24.5	32.1	11.5	14.9	18.2	21.5	26.7	-2.9	-2.6	-2.9	-3.0	-5.4
						Upper Columbia: Columbia River at Mica Dam (BCHMI)									
Oct	168	215	250	290	354	153	213	266	348	485	-15	-1	16	58	131
Nov	91	128	154	186	237	88	148	205	267	364	-4	20	51	81	127
Dec	57	75	93	113	147	61	99	133	179	295	4	24	39	66	148
Jan	36	49	62	78	136	47	73	102	159	277	11	24	41	81	141
Feb	26	35	45	63	116	36	64	93	153	266	10	28	49	91	149
Mar	21	30	45	67	109	46	71	106	165	256	24	41	61	98	147
Apr	47	75	110	146	201	104	174	234	308	440	57	100	124	162	239
May	268	382	480	599	927	495	670	880	1097	1483	228	288	400	498	555
Jun	910	1144	1400	1686	2100	1417	1763	1995	2284	2895	508	619	595	598	795
Jul	1136	1472	1698	1961	2351	916	1275	1631	2032	2562	-220	-196	-67	72	211
Aug	650	808	944	1129	1417	545	683	781	918	1098	-105	-125	-163	-211	-319
Sep	295	355	410	467	595	251	313	368	427	529	-44	-42	-42	-40	-66

Table B1. Continued.

Month	Historic (1961 to 1990) Discharge (m^3/s)					Future (2041 to 2070) Discharge (m^3/s)					Discharge Anomaly (m^3/s)				
	5P	25P	50P	75P	95P	5P	25P	50P	75P	95P	5P	25P	50P	75P	95P
						Upper Columbia: Columbia River at Revelstoke Dam (BCHRE)									
Oct	56	77	92	117	148	47	77	103	146	223	-9	0	11	29	75
Nov	25	37	51	65	88	26	51	76	107	161	1	13	25	41	73
Dec	13	20	26	34	52	14	29	45	72	130	2	9	19	38	78
Jan	7	11	15	23	61	10	20	34	63	130	4	9	20	40	68
Feb	5	7	12	20	52	8	20	35	71	141	4	13	23	52	89
Mar	4	7	15	27	50	13	29	51	85	141	10	22	37	57	91
Apr	19	36	52	73	96	51	94	128	168	238	31	58	76	95	141
May	126	182	229	292	429	241	319	392	470	593	115	138	163	177	164
Jun	377	481	555	653	808	487	616	689	794	998	110	136	134	141	190
Jul	379	521	608	706	830	258	390	534	662	865	-121	-132	-74	-44	35
Aug	192	260	310	383	519	125	164	205	260	366	-67	-96	-105	-123	-153
Sep	93	118	142	167	232	62	84	107	134	193	-31	-34	-35	-33	-39
						Upper Columbia: Whatshan River at Whatshan Dam (BCWAT)									
Oct	1.0	2.4	3.8	5.1	7.8	0.5	1.8	3.3	5.5	9.8	-0.5	-0.6	-0.5	0.5	2.0
Nov	1.1	2.5	3.4	4.5	6.8	0.9	2.7	4.7	6.9	9.7	-0.3	0.3	1.3	2.4	3.0
Dec	0.7	1.3	1.7	2.3	3.5	0.8	2.0	3.0	4.4	7.0	0.1	0.6	1.3	2.1	3.5
Jan	0.4	0.7	0.9	1.2	2.3	0.7	1.2	2.0	3.3	6.2	0.3	0.5	1.1	2.0	3.9
Feb	0.3	0.4	0.6	0.9	2.0	0.6	1.0	2.0	3.6	6.4	0.3	0.5	1.4	2.7	4.4
Mar	0.3	0.4	1.0	1.7	3.5	0.9	2.2	3.7	6.0	9.6	0.6	1.8	2.7	4.3	6.1
Apr	3.1	4.9	6.6	8.8	11.1	6.9	10.7	14.2	17.5	22.3	3.9	5.8	7.6	8.7	11.2
May	15.6	20.8	23.5	26.4	32.3	15.3	22.3	26.2	30.5	37.3	-0.4	1.6	2.7	4.1	4.9
Jun	12.6	19.6	24.2	29.2	35.7	4.2	8.7	13.9	20.4	31.5	-8.4	-11.0	-10.3	-8.8	-4.2
Jul	3.2	5.0	7.6	11.6	17.6	1.1	1.9	2.8	4.8	7.4	-2.1	-3.1	-4.9	-6.8	-10.2
Aug	1.2	1.8	2.8	4.0	6.6	0.4	0.7	1.1	1.8	4.1	-0.7	-1.1	-1.6	-2.1	-2.5
Sep	0.7	1.4	2.3	4.2	6.9	0.3	0.5	1.0	2.2	5.4	-0.4	-0.9	-1.3	-2.0	-1.5

Table B1. Continued.

Month	Historic (1961 to 1990) Discharge (m^3/s)					Future (2041 to 2070) Discharge (m^3/s)					Discharge Anomaly (m^3/s)				
	5P	25P	50P	75P	95P	5P	25P	50P	75P	95P	5P	25P	50P	75P	95P
						Upper Columbia: Columbia River at Keenlyside Dam (BCHAR)									
Oct	92	130	170	208	292	69	126	174	245	400	-23	-5	4	37	108
Nov	54	90	117	155	220	65	114	184	245	344	11	24	67	90	124
Dec	22	41	55	76	108	39	69	103	154	254	16	28	49	78	146
Jan	14	23	33	50	111	25	47	89	140	267	11	23	56	90	156
Feb	9	17	28	47	104	20	52	83	148	256	11	34	55	102	152
Mar	12	22	42	66	113	39	73	121	187	284	27	51	79	121	171
Apr	80	112	155	201	251	145	239	307	379	518	66	127	151	179	266
May	307	410	479	564	691	433	550	654	761	906	126	141	175	196	215
Jun	637	764	860	992	1181	668	834	955	1090	1343	31	70	95	98	162
Jul	602	759	874	1015	1190	421	576	768	914	1146	-181	-183	-106	-101	-44
Aug	326	414	520	599	744	203	274	335	434	609	-123	-140	-185	-165	-135
Sep	159	199	249	298	388	114	141	174	218	341	-45	-58	-75	-79	-48
						Upper Columbia: Elk River at Elko Dam (BCHEL)									
Oct	8	13	19	26	42	6	9	15	25	46	-3	-4	-4	-1	5
Nov	8	15	21	27	42	7	14	25	35	50	-1	0	4	7	8
Dec	7	13	18	23	33	8	17	25	33	50	1	4	7	10	17
Jan	6	10	13	18	32	9	16	23	35	61	3	6	10	17	28
Feb	5	8	11	16	34	9	15	24	38	62	4	7	13	21	29
Mar	4	7	10	16	28	9	16	26	43	68	5	9	16	27	40
Apr	8	16	23	34	47	23	37	50	67	100	15	21	26	33	54
May	51	72	95	121	176	76	117	150	185	243	26	45	55	64	66
Jun	108	157	189	237	289	61	110	158	221	332	-48	-47	-31	-16	43
Jul	31	50	72	102	182	19	24	34	54	95	-13	-26	-38	-48	-87
Aug	15	18	23	30	44	10	12	15	19	26	-5	-6	-8	-11	-18
Sep	9	13	16	23	31	7	8	10	14	21	-3	-4	-6	-9	-10

Table B1. Continued.

Month	Historic (1961 to 1990) Discharge (m^3/s)					Future (2041 to 2070) Discharge (m^3/s)					Discharge Anomaly (m^3/s)				
	5P	25P	50P	75P	95P	5P	25P	50P	75P	95P	5P	25P	50P	75P	95P
						Upper Columbia: Bull River near Wardner (BULNW)									
Oct	3.1	6.2	10.4	14.8	26.5	1.7	4.2	8.5	16.5	30.7	-1.4	-1.9	-2.0	1.7	4.2
Nov	3.5	7.3	11.0	14.3	24.3	2.8	8.8	15.3	20.7	33.3	-0.7	1.5	4.3	6.4	9.0
Dec	2.9	4.8	6.4	9.1	13.3	3.7	7.5	11.2	15.8	26.2	0.8	2.7	4.8	6.7	13.0
Jan	1.7	2.8	3.7	5.8	13.0	2.7	5.0	8.6	14.3	29.4	0.9	2.3	4.9	8.6	16.5
Feb	1.4	1.8	2.7	4.6	12.7	1.9	3.9	7.9	17.4	29.3	0.5	2.1	5.2	12.8	16.6
Mar	1.1	1.6	2.8	5.0	11.2	2.1	4.9	10.2	17.4	31.0	1.0	3.3	7.4	12.4	19.8
Apr	3.0	6.9	10.7	17.1	26.0	9.5	18.4	27.0	35.6	60.7	6.5	11.6	16.2	18.5	34.8
May	35.3	47.4	60.8	75.1	102.3	45.1	70.4	84.9	102.3	128.6	9.8	23.0	24.1	27.2	26.3
Jun	62.2	86.1	101.8	121.7	142.7	34.9	62.6	91.8	123.4	163.8	-27.2	-23.4	-10.1	1.7	21.1
Jul	18.7	30.7	47.4	63.5	102.5	7.3	12.3	21.1	33.6	58.3	-11.4	-18.4	-26.3	-29.9	-44.1
Aug	4.7	9.4	13.8	18.2	29.8	2.0	3.1	4.6	7.2	11.7	-2.7	-6.3	-9.2	-11.0	-18.1
Sep	2.4	5.7	8.0	11.5	17.3	1.1	1.8	2.9	4.5	11.3	-1.3	-3.8	-5.1	-7.0	-6.1
						Upper Columbia: Duncan River at Duncan Dam (BCHDN)									
Oct	27	34	41	47	62	25	38	48	66	95	-2	4	7	19	33
Nov	13	17	20	24	29	12	19	27	36	51	0	2	7	12	21
Dec	8	11	12	14	16	8	12	16	21	36	0	1	4	7	20
Jan	6	8	9	10	16	7	9	12	17	31	1	1	3	7	15
Feb	5	7	7	9	14	6	8	11	18	33	1	2	4	9	19
Mar	5	6	7	10	16	7	10	15	21	39	2	4	8	12	23
Apr	11	15	19	25	34	20	30	40	54	80	9	15	20	28	46
May	44	65	85	109	159	81	119	158	198	265	37	54	73	88	106
Jun	180	233	284	339	426	293	358	403	458	562	114	126	119	119	136
Jul	217	287	335	384	462	155	218	294	374	497	-62	-69	-41	-10	35
Aug	114	144	171	203	254	85	108	126	153	199	-29	-36	-45	-50	-55
Sep	51	61	73	85	102	40	50	61	74	98	-12	-12	-12	-11	-4

Table B1. Continued.

Month	Historic (1961 to 1990) Discharge (m^3/s)					Future (2041 to 2070) Discharge (m^3/s)					Discharge Anomaly (m^3/s)				
	5P	25P	50P	75P	95P	5P	25P	50P	75P	95P	5P	25P	50P	75P	95P
						Upper Columbia: Kootenay River at Kootenay Canal (BCHKL)									
Oct	62	102	142	195	299	41	81	133	217	349	-21	-21	-9	22	50
Nov	56	107	150	202	307	61	130	225	303	451	5	23	75	101	144
Dec	38	79	114	144	211	62	144	193	272	407	24	64	80	128	196
Jan	33	63	88	121	199	62	134	183	269	426	29	71	95	148	227
Feb	32	60	81	116	183	69	132	203	277	415	37	71	122	162	232
Mar	50	82	114	155	216	127	189	265	348	509	77	107	151	193	293
Apr	202	280	339	402	497	335	459	554	651	861	133	179	215	249	364
May	562	720	823	964	1156	666	890	1026	1216	1442	104	169	203	252	285
Jun	880	1090	1246	1424	1675	703	1020	1265	1541	1913	-177	-70	19	117	238
Jul	429	701	910	1154	1541	166	293	479	760	1141	-264	-408	-432	-394	-400
Aug	139	190	265	369	618	61	83	111	160	256	-78	-106	-154	-209	-362
Sep	77	108	142	187	256	38	56	71	98	166	-39	-52	-71	-89	-90
						Upper Columbia: Slocan River near Crescent Valley (SLONC)									
Oct	17	27	39	50	70	13	24	37	58	93	-5	-3	-2	8	24
Nov	13	24	31	39	56	12	26	41	57	81	-1	2	10	18	25
Dec	9	17	22	26	35	11	23	31	41	61	2	6	9	15	27
Jan	8	13	16	20	30	12	18	26	35	61	4	5	11	15	31
Feb	7	10	12	16	24	10	17	25	38	59	4	7	13	22	35
Mar	7	10	14	19	30	13	21	31	45	73	6	11	17	26	44
Apr	21	30	39	50	68	40	63	82	104	145	19	33	43	55	78
May	84	122	145	185	254	141	193	234	291	362	57	72	89	106	108
Jun	224	283	320	375	437	172	257	341	407	498	-53	-26	22	33	61
Jul	96	159	229	300	406	33	56	103	166	278	-63	-103	-126	-134	-129
Aug	32	47	62	87	147	15	20	25	35	63	-17	-27	-37	-52	-84
Sep	20	27	37	50	71	11	15	21	30	53	-9	-12	-16	-20	-18

Table B1. Continued.

Month	Historic (1961 to 1990) Discharge (m^3/s)					Future (2041 to 2070) Discharge (m^3/s)					Discharge Anomaly (m^3/s)				
	5P	25P	50P	75P	95P	5P	25P	50P	75P	95P	5P	25P	50P	75P	95P
	Upper Columbia: Salmo River near Salmo (SALNS)														
Oct	2.0	4.8	9.1	15.5	26.1	1.0	3.6	7.8	14.5	29.5	-1.0	-1.2	-1.3	-1.0	3.4
Nov	1.3	5.4	9.3	14.0	24.9	1.8	8.1	16.0	25.6	41.2	0.5	2.8	6.7	11.5	16.3
Dec	0.8	3.1	4.7	6.9	11.5	1.3	5.9	10.5	17.7	34.5	0.6	2.8	5.8	10.9	23.0
Jan	0.5	1.6	2.4	3.7	9.3	1.7	3.6	7.5	14.4	37.2	1.2	1.9	5.1	10.8	27.9
Feb	0.5	1.1	1.7	3.5	10.4	1.5	3.8	9.3	20.3	40.1	0.9	2.7	7.6	16.9	29.7
Mar	0.7	1.5	3.7	7.4	17.1	3.5	8.5	18.2	29.8	54.6	2.7	7.0	14.5	22.4	37.5
Apr	9.9	17.9	25.6	34.9	49.5	26.1	44.9	60.2	74.0	98.2	16.1	27.0	34.6	39.2	48.7
May	54.5	74.4	85.7	101.4	128.2	63.2	87.8	103.4	121.6	148.3	8.7	13.4	17.7	20.2	20.1
Jun	73.5	100.9	118.2	134.1	156.7	27.0	57.3	88.6	118.1	164.5	-46.6	-43.6	-29.6	-16.0	7.8
Jul	18.1	41.0	61.4	83.8	121.6	3.7	9.3	17.5	35.8	68.5	-14.4	-31.7	-43.9	-48.0	-53.1
Aug	3.6	6.4	10.7	17.6	36.7	0.9	1.6	2.8	5.0	9.9	-2.8	-4.8	-7.9	-12.7	-26.8
Sep	1.4	3.2	5.4	9.8	18.4	0.4	0.9	1.8	3.5	9.6	-1.0	-2.3	-3.6	-6.3	-8.8

(BLANK)

Appendix C: Historic and Future Monthly Discharge Percentiles for the A2 Projections Ensemble for all Project Sites

Table C1. Historic and future monthly discharge percentiles for the A2 ensemble for all project sites.

Month	Historic (1961 to 1990) Discharge (m^3/s)					Future (2041 to 2070) Discharge (m^3/s)					Discharge Anomaly (m^3/s)				
	5P	25P	50P	75P	95P	5P	25P	50P	75P	95P	5P	25P	50P	75P	95P
						Peace: Peace River at Williston Dam (BCGMS)									
Oct	501	680	827	960	1277	455	659	827	1032	1363	-46	-22	0	71	86
Nov	399	585	695	846	1096	491	711	886	1105	1455	93	126	191	259	359
Dec	249	345	428	582	886	324	464	656	937	1432	75	119	227	355	546
Jan	158	218	300	469	974	201	321	562	987	1843	42	103	262	518	870
Feb	121	161	244	398	926	146	272	479	884	1764	25	111	234	486	839
Mar	93	136	212	373	796	131	280	519	869	1426	38	144	306	496	630
Apr	130	265	452	625	1050	318	638	888	1135	1712	188	373	435	510	661
May	963	1251	1496	1879	2397	1262	1695	2012	2495	3300	299	444	516	617	903
Jun	2059	2582	3015	3533	4141	1646	2387	2912	3558	4650	-413	-195	-103	25	510
Jul	1294	1822	2259	2845	3726	730	1111	1528	1968	2777	-564	-711	-731	-877	-950
Aug	605	811	972	1250	1648	367	571	699	842	1156	-238	-240	-273	-408	-492
Sep	512	652	772	976	1271	384	500	656	845	1221	-128	-152	-116	-131	-50
						Peace: Peace River above Pine River, near Site C (PEAPN)									
Oct	529	736	904	1052	1389	486	695	908	1132	1499	-43	-42	4	80	110
Nov	458	640	757	912	1203	537	758	941	1182	1534	78	118	184	270	331
Dec	279	387	470	635	948	357	511	711	998	1564	78	124	241	364	616
Jan	182	251	338	502	1049	227	351	611	1010	1893	45	100	274	508	844
Feb	142	187	284	442	995	167	306	512	915	1942	24	119	227	474	947
Mar	118	167	254	408	906	157	319	570	948	1589	39	151	316	540	684
Apr	167	307	496	674	1114	362	692	966	1225	1834	195	385	470	551	719
May	1027	1325	1590	1980	2550	1304	1787	2123	2608	3530	277	461	533	628	981
Jun	2120	2720	3174	3727	4455	1717	2504	3112	3789	5011	-403	-216	-61	62	556
Jul	1440	2036	2482	3088	4084	810	1238	1714	2154	3014	-630	-798	-769	-934	-1069
Aug	664	890	1083	1386	1883	392	629	768	943	1302	-272	-262	-315	-443	-580
Sep	546	710	850	1082	1446	418	549	724	933	1375	-128	-161	-127	-149	-71

Table C1. Continued.

Month	Historic (1961 to 1990) Discharge (m^3/s)					Future (2041 to 2070) Discharge (m^3/s)					Discharge Anomaly (m^3/s)				
	5P	25P	50P	75P	95P	5P	25P	50P	75P	95P	5P	25P	50P	75P	95P
						Peace: Peace River at Taylor (PEACT)									
Oct	58	87	115	150	220	44	78	111	163	246	-14	-8	-4	12	26
Nov	60	87	108	139	220	53	91	134	180	281	-7	5	27	40	61
Dec	45	63	82	122	218	47	79	124	185	343	2	15	41	63	125
Jan	35	51	79	120	225	40	77	131	224	433	5	26	52	103	207
Feb	31	49	74	123	204	40	74	134	225	381	9	26	61	102	177
Mar	32	52	82	140	238	47	106	164	262	417	16	54	82	122	179
Apr	73	111	177	240	355	123	202	291	382	516	49	92	114	142	162
May	245	351	426	523	696	212	337	483	646	857	-34	-15	56	123	161
Jun	243	375	493	614	825	129	210	329	490	775	-115	-165	-164	-125	-50
Jul	106	165	218	296	504	64	98	136	194	298	-43	-68	-82	-102	-206
Aug	55	77	101	133	191	33	55	72	94	150	-22	-22	-29	-38	-41
Sep	44	71	92	125	187	35	50	73	107	179	-9	-21	-19	-18	-8
						Campbell: Campbell River at Strathcona Dam (BCSCA)									
Oct	17	47	76	108	159	15	57	86	112	170	-3	9	9	3	11
Nov	48	75	105	143	199	56	91	126	164	228	7	16	21	21	29
Dec	40	62	92	125	161	57	92	130	164	219	16	30	38	39	58
Jan	30	54	75	112	171	41	68	112	164	254	11	14	38	52	83
Feb	28	46	65	86	141	43	76	100	129	206	15	29	35	43	65
Mar	38	54	70	89	109	56	81	100	122	156	18	27	30	32	46
Apr	60	81	92	106	125	68	90	104	119	142	8	9	12	14	17
May	96	113	128	142	163	42	77	98	124	164	-54	-36	-30	-18	1
Jun	77	113	136	158	189	19	34	53	87	137	-58	-79	-83	-71	-52
Jul	27	50	69	97	138	8	12	17	28	58	-19	-38	-52	-69	-80
Aug	10	17	25	35	52	5	6	9	13	20	-6	-11	-16	-22	-31
Sep	7	13	18	25	44	3	6	10	16	30	-4	-6	-8	-9	-14

Table C1. Continued.

Month	Historic (1961 to 1990) Discharge (m^3/s)					Future (2041 to 2070) Discharge (m^3/s)					Discharge Anomaly (m^3/s)				
	5P	25P	50P	75P	95P	5P	25P	50P	75P	95P	5P	25P	50P	75P	95P
						Upper Columbia: Spillimacheen River near Spillimacheen (SPINS)									
Oct	8.1	10.6	13.4	16.1	21.5	7.1	10.9	14.7	19.2	29.5	-1.0	0.2	1.3	3.1	8.0
Nov	4.7	6.5	8.3	10.2	13.4	4.3	7.7	10.7	15.0	22.7	-0.4	1.2	2.3	4.7	9.3
Dec	3.0	4.0	5.0	6.0	7.9	2.8	5.1	7.0	9.9	17.3	-0.2	1.1	2.0	3.9	9.4
Jan	1.9	2.5	3.2	4.1	8.1	1.9	3.2	4.9	8.7	18.7	0.0	0.7	1.7	4.7	10.7
Feb	1.3	1.8	2.3	3.2	6.8	1.4	2.6	4.3	7.5	15.2	0.1	0.8	2.0	4.3	8.4
Mar	1.1	1.5	2.2	3.4	7.4	1.4	2.8	5.2	8.7	17.7	0.3	1.3	3.0	5.3	10.3
Apr	2.6	5.0	7.2	9.2	12.4	5.7	9.1	12.8	16.5	25.0	3.1	4.1	5.6	7.3	12.6
May	14.6	19.8	28.1	36.0	55.4	22.3	33.9	47.8	66.7	103.8	7.7	14.0	19.8	30.7	48.4
Jun	59.4	79.8	99.5	121.9	158.1	84.5	117.3	134.8	161.8	207.1	25.1	37.4	35.3	39.9	49.0
Jul	65.4	94.9	115.3	132.0	164.4	39.4	64.6	97.7	122.6	165.6	-26.0	-30.3	-17.6	-9.4	1.2
Aug	31.8	40.1	49.2	62.1	89.3	23.7	30.2	36.6	42.8	56.5	-8.1	-9.9	-12.6	-19.3	-32.8
Sep	14.5	17.6	21.1	24.5	32.1	11.7	15.2	17.9	21.5	27.0	-2.8	-2.3	-3.2	-3.0	-5.1
						Upper Columbia: Columbia River at Mica Dam (BCHMI)									
Oct	168	215	250	290	354	152	205	264	325	448	-16	-10	14	35	94
Nov	91	128	154	186	237	86	144	188	245	368	-5	16	34	59	131
Dec	57	75	93	113	147	54	96	127	172	271	-3	21	34	58	124
Jan	36	49	62	78	136	34	64	91	151	317	-2	15	29	73	181
Feb	26	35	45	63	116	30	53	86	143	237	4	17	42	81	121
Mar	21	30	45	67	109	29	60	98	152	282	7	30	53	85	173
Apr	47	75	110	146	201	87	148	209	283	401	40	73	99	137	199
May	268	382	480	599	927	469	630	829	1070	1496	201	248	349	471	569
Jun	910	1144	1400	1686	2100	1306	1644	1876	2216	2850	396	500	476	530	751
Jul	1136	1472	1698	1961	2351	929	1355	1674	1956	2474	-208	-117	-24	-5	124
Aug	650	808	944	1129	1417	564	680	773	898	1180	-86	-128	-171	-231	-237
Sep	295	355	410	467	595	257	313	362	421	544	-38	-42	-48	-46	-50

Table C1. Continued.

Month	Historic (1961 to 1990) Discharge (m^3/s)					Future (2041 to 2070) Discharge (m^3/s)					Discharge Anomaly (m^3/s)				
	5P	25P	50P	75P	95P	5P	25P	50P	75P	95P	5P	25P	50P	75P	95P
Upper Columbia: Columbia River at Revelstoke Dam (BCHRE)															
Oct	56	77	92	117	148	42	73	100	137	201	-15	-4	7	21	53
Nov	25	37	51	65	88	22	49	67	93	163	-3	12	16	28	74
Dec	13	20	26	34	52	11	28	42	67	123	-2	8	16	33	71
Jan	7	11	15	23	61	6	16	28	57	151	-1	5	13	34	90
Feb	5	7	12	20	52	7	16	31	63	132	2	8	20	43	81
Mar	4	7	15	27	50	8	23	47	79	150	4	17	32	52	100
Apr	19	36	52	73	96	47	79	117	152	220	28	43	64	79	124
May	126	182	229	292	429	227	296	374	451	611	101	115	145	159	182
Jun	377	481	555	653	808	460	575	660	775	999	83	94	105	122	191
Jul	379	521	608	706	830	262	415	547	655	857	-117	-106	-60	-50	27
Aug	192	260	310	383	519	134	169	202	258	376	-58	-91	-108	-125	-142
Sep	93	118	142	167	232	64	84	102	131	189	-28	-34	-40	-36	-43
Upper Columbia: Whatshan River at Whatshan Dam (BCWAT)															
Oct	1.0	2.4	3.8	5.1	7.8	0.5	1.5	3.2	5.1	9.1	-0.5	-0.9	-0.6	0.0	1.4
Nov	1.1	2.5	3.4	4.5	6.8	0.8	2.6	4.1	5.7	8.6	-0.3	0.2	0.7	1.2	1.8
Dec	0.7	1.3	1.7	2.3	3.5	0.6	1.7	2.7	4.2	6.8	-0.1	0.4	1.0	1.9	3.3
Jan	0.4	0.7	0.9	1.2	2.3	0.4	1.1	1.7	3.0	7.0	0.0	0.3	0.8	1.8	4.7
Feb	0.3	0.4	0.6	0.9	2.0	0.4	0.9	1.6	3.1	6.3	0.2	0.4	1.1	2.2	4.3
Mar	0.3	0.4	1.0	1.7	3.5	0.5	1.8	3.2	5.4	9.7	0.3	1.4	2.2	3.7	6.2
Apr	3.1	4.9	6.6	8.8	11.1	6.5	9.7	13.1	16.1	20.9	3.5	4.8	6.4	7.3	9.8
May	15.6	20.8	23.5	26.4	32.3	15.4	22.0	26.8	30.1	36.1	-0.2	1.2	3.3	3.7	3.8
Jun	12.6	19.6	24.2	29.2	35.7	5.2	9.7	15.6	20.0	29.2	-7.5	-9.9	-8.7	-9.2	-6.5
Jul	3.2	5.0	7.6	11.6	17.6	1.2	2.2	3.2	4.5	8.3	-1.9	-2.9	-4.4	-7.1	-9.4
Aug	1.2	1.8	2.8	4.0	6.6	0.5	0.8	1.3	2.0	4.3	-0.7	-1.1	-1.5	-2.0	-2.3
Sep	0.7	1.4	2.3	4.2	6.9	0.3	0.6	1.0	2.4	4.9	-0.4	-0.8	-1.3	-1.9	-2.0

Table C1. Continued.

Month	Historic (1961 to 1990) Discharge (m^3/s)					Future (2041 to 2070) Discharge (m^3/s)					Discharge Anomaly (m^3/s)				
	5P	25P	50P	75P	95P	5P	25P	50P	75P	95P	5P	25P	50P	75P	95P
						Upper Columbia: Columbia River at Keenlyside Dam (BCHAR)									
Oct	92	130	170	208	292	71	113	164	236	363	-21	-17	-6	27	70
Nov	54	90	117	155	220	51	105	158	221	313	-3	14	41	66	92
Dec	22	41	55	76	108	26	62	98	150	243	3	21	43	74	135
Jan	14	23	33	50	111	16	39	69	127	291	2	16	36	77	180
Feb	9	17	28	47	104	17	41	72	125	217	8	24	44	79	113
Mar	12	22	42	66	113	27	69	108	164	285	15	47	66	98	172
Apr	80	112	155	201	251	156	210	284	353	459	76	98	128	153	207
May	307	410	479	564	691	452	548	646	764	919	145	139	168	199	228
Jun	637	764	860	992	1181	658	795	943	1056	1299	21	31	83	64	117
Jul	602	759	874	1015	1190	425	629	772	901	1119	-177	-131	-102	-113	-72
Aug	326	414	520	599	744	220	285	350	442	639	-106	-129	-170	-157	-105
Sep	159	199	249	298	388	113	145	172	225	332	-46	-54	-77	-73	-56
						Upper Columbia: Elk River at Elko Dam (BCHEL)									
Oct	8	13	19	26	42	6	9	16	22	41	-2	-4	-3	-5	-1
Nov	8	15	21	27	42	6	14	23	32	47	-2	-1	1	5	5
Dec	7	13	18	23	33	6	16	22	32	52	-1	3	5	10	19
Jan	6	10	13	18	32	6	14	21	33	60	0	3	7	14	27
Feb	5	8	11	16	34	6	12	21	33	61	1	4	10	17	27
Mar	4	7	10	16	28	7	14	23	38	62	3	7	12	22	34
Apr	8	16	23	34	47	17	33	48	60	91	9	17	25	27	44
May	51	72	95	121	176	72	111	140	188	265	22	39	46	66	88
Jun	108	157	189	237	289	60	116	170	212	302	-48	-40	-19	-25	13
Jul	31	50	72	102	182	19	27	37	53	94	-12	-23	-35	-50	-88
Aug	15	18	23	30	44	11	13	15	19	30	-4	-5	-8	-11	-13
Sep	9	13	16	23	31	7	9	11	14	23	-3	-4	-5	-8	-8

Table C1. Continued.

Month	Historic (1961 to 1990) Discharge (m^3/s)					Future (2041 to 2070) Discharge (m^3/s)					Discharge Anomaly (m^3/s)				
	5P	25P	50P	75P	95P	5P	25P	50P	75P	95P	5P	25P	50P	75P	95P
						Upper Columbia: Bull River near Wardner (BULNW)									
Oct	3.1	6.2	10.4	14.8	26.5	1.6	4.2	8.5	13.9	28.3	-1.5	-2.0	-1.9	-0.9	1.8
Nov	3.5	7.3	11.0	14.3	24.3	2.6	7.4	13.4	19.8	30.1	-0.8	0.1	2.3	5.5	5.8
Dec	2.9	4.8	6.4	9.1	13.3	2.5	6.8	10.4	15.0	28.7	-0.3	2.0	4.0	5.8	15.4
Jan	1.7	2.8	3.7	5.8	13.0	2.2	4.2	7.1	13.5	30.3	0.4	1.4	3.5	7.7	17.3
Feb	1.4	1.8	2.7	4.6	12.7	1.8	3.4	6.6	13.6	26.9	0.4	1.5	3.9	9.0	14.2
Mar	1.1	1.6	2.8	5.0	11.2	1.5	3.8	8.1	14.2	30.6	0.4	2.2	5.3	9.2	19.4
Apr	3.0	6.9	10.7	17.1	26.0	7.8	15.9	24.1	35.0	51.1	4.7	9.0	13.4	17.8	25.1
May	35.3	47.4	60.8	75.1	102.3	48.7	67.0	83.9	100.9	134.3	13.4	19.6	23.1	25.8	32.0
Jun	62.2	86.1	101.8	121.7	142.7	36.7	64.1	91.6	116.8	157.1	-25.4	-22.0	-10.2	-4.9	14.4
Jul	18.7	30.7	47.4	63.5	102.5	7.8	13.6	21.5	33.5	55.8	-10.9	-17.2	-25.9	-30.0	-46.7
Aug	4.7	9.4	13.8	18.2	29.8	2.2	3.3	4.8	7.3	14.9	-2.5	-6.1	-9.1	-11.0	-14.9
Sep	2.4	5.7	8.0	11.5	17.3	1.2	1.7	3.1	5.4	11.3	-1.2	-3.9	-4.9	-6.0	-6.0
						Upper Columbia: Duncan River at Duncan Dam (BCHDN)									
Oct	27	34	41	47	62	24	36	47	61	88	-3	2	6	14	26
Nov	13	17	20	24	29	12	19	24	32	48	-1	2	5	8	19
Dec	8	11	12	14	16	8	12	15	20	30	-1	1	3	6	14
Jan	6	8	9	10	16	5	9	11	16	36	-1	1	2	6	20
Feb	5	7	7	9	14	5	8	10	15	29	0	1	3	7	15
Mar	5	6	7	10	16	5	9	14	20	39	0	3	6	10	23
Apr	11	15	19	25	34	17	27	35	49	70	6	12	16	23	36
May	44	65	85	109	159	76	109	148	198	284	31	44	63	88	125
Jun	180	233	284	339	426	263	333	379	452	555	84	100	94	114	129
Jul	217	287	335	384	462	150	231	306	364	478	-67	-56	-29	-19	16
Aug	114	144	171	203	254	86	109	128	147	202	-28	-36	-43	-56	-52
Sep	51	61	73	85	102	40	50	60	73	91	-11	-11	-13	-12	-11

Table C1. Continued.

Month	Historic (1961 to 1990) Discharge (m^3/s)					Future (2041 to 2070) Discharge (m^3/s)					Discharge Anomaly (m^3/s)				
	5P	25P	50P	75P	95P	5P	25P	50P	75P	95P	5P	25P	50P	75P	95P
Upper Columbia: Kootenay River at Kootenay Canal (BCHKL)															
Oct	62	102	142	195	299	37	79	126	185	347	-25	-23	-16	-10	48
Nov	56	107	150	202	307	50	126	188	274	380	-6	19	38	71	73
Dec	38	79	113	144	212	55	118	183	262	391	18	39	70	118	179
Jan	32	63	88	121	199	50	105	168	258	396	18	42	80	137	197
Feb	32	61	81	116	183	58	125	170	235	418	26	64	89	119	234
Mar	49	81	114	155	216	109	174	222	302	504	60	93	108	147	289
Apr	202	280	338	402	497	329	418	513	623	824	127	138	175	221	327
May	561	720	823	964	1152	665	853	1002	1208	1541	104	132	179	243	389
Jun	880	1090	1249	1424	1675	701	1018	1271	1503	1839	-179	-72	22	79	164
Jul	429	701	910	1154	1541	181	332	521	737	1155	-248	-369	-389	-418	-386
Aug	139	190	265	369	618	63	89	120	156	253	-76	-101	-144	-213	-365
Sep	77	108	142	187	256	38	55	74	108	181	-39	-53	-68	-79	-76
Upper Columbia: Slocan River near Crescent Valley (SLONC)															
Oct	17	27	39	50	70	12	24	37	51	86	-5	-3	-3	1	17
Nov	13	24	31	39	56	10	25	38	51	72	-3	1	7	12	15
Dec	9	17	22	26	35	9	20	30	39	64	-1	3	8	13	30
Jan	8	13	16	20	30	7	17	22	32	59	-1	4	7	13	29
Feb	7	10	12	16	24	9	15	22	31	53	2	5	9	15	29
Mar	7	10	14	19	30	11	19	28	40	73	4	9	14	21	44
Apr	21	30	39	50	68	35	54	74	95	132	13	24	35	46	64
May	84	122	145	185	254	132	179	227	276	379	49	58	82	91	124
Jun	224	283	320	375	437	165	268	331	394	473	-60	-15	11	19	36
Jul	96	159	229	300	406	35	64	111	170	263	-61	-96	-118	-129	-143
Aug	32	47	62	87	147	16	21	26	36	61	-16	-26	-36	-52	-86
Sep	20	27	37	50	71	11	15	21	32	56	-8	-12	-16	-18	-14

Table C1. Continued.

Month	Historic (1961 to 1990) Discharge (m^3/s)					Future (2041 to 2070) Discharge (m^3/s)					Discharge Anomaly (m^3/s)				
	5P	25P	50P	75P	95P	5P	25P	50P	75P	95P	5P	25P	50P	75P	95P
	Upper Columbia: Salmo River near Salmo (SALNS)														
Oct	2.0	4.8	9.1	15.5	26.1	0.9	3.5	7.2	13.6	29.4	-1.1	-1.3	-1.9	-1.9	3.3
Nov	1.3	5.4	9.3	14.0	24.9	1.2	6.6	13.4	22.2	37.2	-0.1	1.3	4.0	8.1	12.3
Dec	0.8	3.1	4.7	6.9	11.5	0.7	5.1	9.4	16.7	34.3	0.0	2.0	4.7	9.8	22.8
Jan	0.5	1.6	2.4	3.7	9.3	0.6	3.0	6.2	12.8	35.3	0.1	1.4	3.8	9.1	26.0
Feb	0.5	1.1	1.7	3.5	10.4	1.1	3.4	6.9	15.2	33.8	0.6	2.3	5.3	11.7	23.4
Mar	0.7	1.5	3.7	7.4	17.1	2.0	7.2	15.0	27.6	55.3	1.2	5.6	11.2	20.2	38.2
Apr	9.9	17.9	25.6	34.9	49.5	23.7	38.2	53.9	68.2	91.5	13.8	20.3	28.3	33.3	42.0
May	54.5	74.4	85.7	101.4	128.2	62.2	84.6	102.0	123.4	155.5	7.7	10.2	16.3	22.0	27.4
Jun	73.5	100.9	118.2	134.1	156.7	31.9	61.2	92.6	118.6	152.6	-41.6	-39.7	-25.5	-15.5	-4.1
Jul	18.1	41.0	61.4	83.8	121.6	4.6	10.5	21.2	34.6	67.3	-13.5	-30.5	-40.3	-49.2	-54.3
Aug	3.6	6.4	10.7	17.6	36.7	1.0	1.9	3.2	4.9	9.3	-2.6	-4.6	-7.5	-12.8	-27.3
Sep	1.4	3.2	5.4	9.8	18.4	0.4	0.9	1.9	3.9	10.7	-1.1	-2.3	-3.5	-5.9	-7.7

(BLANK)

Appendix D: Historic and Future Monthly Discharge Percentiles for the B1 Projections Ensemble for all Project Sites

Table D1. Historic and future monthly discharge percentile for the B1 ensemble for all project sites.

Month	Historic (1961 to 1990) Discharge (m^3/s)					Future (2041 to 2070) Discharge (m^3/s)					Discharge Anomaly (m^3/s)				
	5P	25P	50P	75P	95P	5P	25P	50P	75P	95P	5P	25P	50P	75P	95P
						Peace: Peace River at Williston Dam (BCGMS)									
Oct	521	678	831	979	1234	501	700	903	1111	1453	-20	22	73	133	219
Nov	395	579	689	836	1123	506	649	843	1095	1419	110	70	154	259	297
Dec	245	343	428	578	863	293	429	615	828	1274	47	86	187	251	412
Jan	163	218	298	441	986	182	293	493	850	1542	19	75	195	409	556
Feb	118	161	244	415	925	146	241	433	764	1579	28	80	189	349	654
Mar	94	134	212	359	722	132	237	463	757	1402	38	103	252	398	680
Apr	133	266	454	616	957	306	593	846	1071	1712	172	327	393	455	755
May	981	1298	1515	1897	2430	1244	1667	2038	2483	3292	263	369	524	586	862
Jun	2104	2665	3056	3552	4202	1941	2692	3215	3758	4884	-163	27	159	206	682
Jul	1309	1882	2377	2996	3822	878	1424	1868	2405	3377	-431	-458	-509	-591	-445
Aug	606	843	1004	1301	1688	509	645	811	977	1278	-97	-198	-192	-324	-410
Sep	495	668	794	979	1311	420	563	727	915	1267	-75	-105	-67	-63	-44
						Peace: Peace River above Pine River, near Site C (PEAPN)									
Oct	569	733	907	1076	1382	529	750	973	1201	1632	-39	17	66	125	250
Nov	437	638	742	910	1213	542	710	920	1192	1533	105	72	178	283	320
Dec	276	385	469	631	932	326	476	670	883	1403	49	92	200	252	471
Jan	188	250	340	494	1058	210	325	544	934	1646	22	74	205	440	588
Feb	146	189	278	436	992	178	279	474	808	1734	32	90	196	372	742
Mar	118	168	254	403	844	159	274	510	832	1559	41	106	256	429	715
Apr	168	303	497	673	1045	351	663	915	1190	1850	184	359	418	516	805
May	1041	1385	1620	1987	2544	1338	1805	2159	2678	3513	297	421	539	691	969
Jun	2218	2819	3280	3762	4462	2077	2858	3418	4061	5198	-142	39	138	299	736
Jul	1460	2077	2574	3325	4164	951	1569	2063	2600	3678	-509	-507	-511	-725	-486
Aug	667	915	1109	1439	1881	555	711	914	1080	1417	-111	-205	-195	-358	-464
Sep	535	726	879	1101	1462	454	618	808	992	1413	-81	-108	-71	-109	-49

Table D1. Continued.

Month	Historic (1961 to 1990) Discharge (m^3/s)					Future (2041 to 2070) Discharge (m^3/s)					Discharge Anomaly (m^3/s)				
	5P	25P	50P	75P	95P	5P	25P	50P	75P	95P	5P	25P	50P	75P	95P
						Peace: Peace River at Taylor (PEACT)									
Oct	58	89	117	153	245	51	85	125	166	280	-6	-4	8	14	35
Nov	61	87	107	142	225	62	95	126	171	262	0	8	19	29	36
Dec	44	63	83	125	219	50	82	122	187	299	6	19	40	61	80
Jan	36	52	79	116	244	40	72	120	223	406	5	19	41	108	162
Feb	32	48	75	123	199	43	76	130	213	382	12	28	54	90	183
Mar	32	51	84	134	231	50	99	154	243	365	18	47	71	109	134
Apr	75	111	175	234	359	131	214	287	392	513	55	103	112	158	155
May	276	357	442	544	730	260	369	501	670	901	-17	12	59	126	171
Jun	257	395	513	615	878	172	304	425	565	871	-85	-91	-89	-50	-8
Jul	121	166	233	328	502	83	135	178	241	377	-38	-32	-56	-87	-125
Aug	59	81	104	134	201	46	68	86	111	162	-13	-13	-18	-23	-39
Sep	46	73	95	131	190	38	63	87	118	201	-9	-10	-8	-13	11
						Campbell: Campbell River at Strathcona Dam (BCSCA)									
Oct	18	49	78	108	156	18	53	80	119	190	0	4	2	11	33
Nov	45	75	106	143	202	63	96	123	160	219	18	20	18	17	18
Dec	40	62	92	125	162	58	91	122	154	210	17	28	30	29	47
Jan	29	54	73	109	169	40	69	114	157	232	10	15	41	48	63
Feb	28	43	65	86	139	43	68	96	133	207	15	24	31	47	69
Mar	36	53	69	89	108	43	83	102	122	153	8	29	33	33	45
Apr	60	81	92	104	126	73	91	104	121	141	14	10	13	17	16
May	98	113	127	143	162	57	88	107	131	154	-41	-26	-20	-12	-8
Jun	76	116	136	160	189	28	47	72	96	143	-48	-69	-64	-64	-46
Jul	27	51	72	98	139	10	15	23	36	67	-16	-35	-49	-62	-73
Aug	10	17	25	35	52	5	8	10	14	23	-5	-9	-15	-22	-29
Sep	7	13	19	26	44	4	8	13	21	36	-3	-4	-6	-5	-8

Table D1. Continued.

Month	Historic (1961 to 1990) Discharge (m^3/s)					Future (2041 to 2070) Discharge (m^3/s)					Discharge Anomaly (m^3/s)				
	5P	25P	50P	75P	95P	5P	25P	50P	75P	95P	5P	25P	50P	75P	95P
	Upper Columbia: Spillimacheen River near Spillimacheen (SPINS)														
Oct	8.1	10.6	13.5	16.3	21.6	8.4	12.1	14.8	19.5	29.4	0.3	1.5	1.3	3.2	7.7
Nov	4.6	6.5	8.3	10.1	13.4	5.0	7.8	10.4	14.1	20.0	0.4	1.3	2.1	4.0	6.7
Dec	2.9	4.0	4.9	5.9	8.1	3.3	5.1	6.4	8.7	14.6	0.4	1.1	1.5	2.8	6.5
Jan	1.8	2.5	3.2	4.0	8.7	2.3	3.3	4.8	7.6	18.1	0.5	0.7	1.6	3.5	9.5
Feb	1.3	1.8	2.2	3.2	7.4	1.7	2.5	3.8	7.6	16.3	0.3	0.7	1.6	4.4	8.9
Mar	1.1	1.5	2.1	3.5	7.4	1.3	2.7	5.0	8.0	14.6	0.2	1.2	2.9	4.5	7.2
Apr	2.7	5.0	7.1	9.1	12.5	6.1	9.2	12.0	15.9	25.1	3.4	4.2	4.8	6.8	12.6
May	14.7	20.1	28.2	35.7	55.3	20.2	30.1	40.6	56.1	87.1	5.5	10.0	12.4	20.4	31.8
Jun	63.4	79.3	98.2	120.6	159.2	86.3	110.5	130.2	152.7	193.9	22.9	31.2	31.9	32.1	34.7
Jul	64.6	96.0	116.4	134.1	164.5	53.9	84.5	115.2	142.3	176.6	-10.7	-11.5	-1.2	8.2	12.1
Aug	32.0	40.1	48.7	62.4	92.4	28.0	34.4	38.9	45.7	62.3	-3.9	-5.7	-9.8	-16.7	-30.1
Sep	14.7	17.6	21.2	24.4	32.2	13.4	16.2	19.4	22.5	28.7	-1.3	-1.4	-1.8	-1.9	-3.5
	Upper Columbia: Columbia River at Mica Dam (BCHMI)														
Oct	168	213	249	290	355	162	221	269	334	456	-6	8	20	44	101
Nov	91	126	154	183	237	103	144	183	240	343	12	19	29	57	105
Dec	52	75	92	111	146	66	92	118	159	251	14	17	25	49	105
Jan	36	49	61	76	142	42	62	89	138	303	6	13	28	62	161
Feb	27	36	44	62	118	33	50	76	136	251	7	15	32	75	133
Mar	22	30	44	70	112	28	63	98	143	246	6	33	54	73	133
Apr	47	75	111	147	203	96	148	195	272	405	49	73	84	126	203
May	270	389	484	604	924	417	583	733	911	1346	147	194	249	307	421
Jun	917	1141	1374	1663	2093	1232	1580	1815	2116	2614	316	439	441	453	520
Jul	1126	1472	1718	1981	2359	1062	1566	1832	2136	2653	-64	93	114	156	294
Aug	655	808	929	1128	1488	595	728	829	960	1318	-60	-79	-100	-168	-170
Sep	299	354	410	462	611	265	326	384	442	560	-34	-28	-27	-20	-51

Table D1. Continued.

Month	Historic (1961 to 1990) Discharge (m^3/s)					Future (2041 to 2070) Discharge (m^3/s)					Discharge Anomaly (m^3/s)				
	5P	25P	50P	75P	95P	5P	25P	50P	75P	95P	5P	25P	50P	75P	95P
						Upper Columbia: Columbia River at Revelstoke Dam (BCHRE)									
Oct	57	76	92	117	149	51	82	106	138	208	-5	5	14	20	59
Nov	25	37	51	63	88	29	47	67	89	137	4	10	16	26	49
Dec	12	20	25	33	51	15	25	35	61	106	4	6	10	28	55
Jan	7	11	14	22	63	10	16	25	53	147	3	5	10	31	85
Feb	5	7	11	19	52	7	12	25	59	114	2	5	14	40	63
Mar	4	6	15	27	52	7	26	48	73	129	3	20	33	46	77
Apr	19	36	54	75	99	46	78	108	149	224	27	42	55	74	125
May	136	186	234	295	426	198	281	340	419	554	62	94	106	124	128
Jun	385	480	551	648	797	447	571	653	746	930	62	91	101	97	133
Jul	375	525	615	717	830	320	499	619	715	913	-56	-27	4	-1	83
Aug	189	257	309	386	522	151	202	242	284	407	-38	-55	-67	-102	-115
Sep	93	119	142	167	229	73	94	118	144	202	-20	-25	-24	-23	-26
						Upper Columbia: Whatshan River at Whatshan Dam (BCWAT)									
Oct	1.1	2.4	3.8	5.1	7.8	1.2	2.4	3.6	5.5	9.2	0.1	-0.1	-0.2	0.5	1.4
Nov	1.1	2.4	3.4	4.5	6.4	1.3	3.0	4.3	5.9	8.8	0.2	0.5	0.9	1.4	2.3
Dec	0.6	1.3	1.7	2.3	3.4	0.9	1.7	2.7	3.6	5.9	0.3	0.3	0.9	1.3	2.5
Jan	0.4	0.7	0.9	1.2	2.5	0.6	1.1	1.5	2.7	5.8	0.2	0.3	0.6	1.5	3.3
Feb	0.3	0.4	0.6	0.9	2.0	0.4	0.8	1.3	2.9	5.7	0.1	0.3	0.8	2.0	3.7
Mar	0.3	0.4	1.0	1.7	3.9	0.5	1.8	3.4	5.0	8.9	0.3	1.3	2.5	3.2	5.1
Apr	3.0	4.9	6.8	8.8	11.2	6.0	9.4	12.7	15.6	21.0	3.0	4.5	5.9	6.8	9.8
May	15.9	21.0	23.6	26.7	32.2	17.8	22.2	26.0	30.2	36.7	1.9	1.2	2.4	3.5	4.5
Jun	12.2	19.5	24.2	29.3	35.3	6.9	13.7	18.4	23.1	33.2	-5.3	-5.8	-5.8	-6.2	-2.1
Jul	3.1	5.0	7.5	11.6	17.8	1.7	2.9	4.2	5.7	9.9	-1.5	-2.1	-3.4	-5.9	-7.9
Aug	1.2	1.8	2.8	4.0	6.6	0.6	1.0	1.5	2.1	4.9	-0.5	-0.8	-1.3	-1.8	-1.6
Sep	0.7	1.4	2.4	4.2	7.3	0.4	0.7	1.6	3.0	6.5	-0.3	-0.7	-0.8	-1.3	-0.8

Table D1. Continued.

Month	Historic (1961 to 1990) Discharge (m^3/s)					Future (2041 to 2070) Discharge (m^3/s)					Discharge Anomaly (m^3/s)				
	5P	25P	50P	75P	95P	5P	25P	50P	75P	95P	5P	25P	50P	75P	95P
						Upper Columbia: Columbia River at Keenlyside Dam (BCHAR)									
Oct	91	130	170	210	299	95	134	178	241	378	4	4	8	31	79
Nov	53	88	117	155	216	71	113	166	207	301	18	25	49	52	85
Dec	21	40	54	74	109	35	59	88	139	209	14	19	34	65	100
Jan	13	23	32	49	134	22	36	59	125	237	9	13	27	76	103
Feb	9	17	26	46	96	16	34	69	117	201	7	16	42	71	105
Mar	12	22	41	66	115	22	64	110	156	236	10	43	69	90	121
Apr	79	113	159	202	251	146	211	282	345	462	67	98	123	143	211
May	308	411	481	565	688	429	521	594	703	912	121	110	113	138	224
Jun	648	760	857	980	1165	682	811	927	1038	1281	34	50	70	58	116
Jul	594	762	876	1016	1196	522	741	853	993	1192	-71	-21	-23	-23	-4
Aug	322	413	523	599	746	269	335	408	486	640	-53	-78	-115	-113	-106
Sep	161	201	249	297	389	122	153	197	249	365	-39	-48	-53	-48	-24
						Upper Columbia: Elk River at Elko Dam (BCHEL)									
Oct	8	13	19	27	41	8	12	18	29	44	-1	-1	-1	3	3
Nov	8	15	22	27	42	7	16	25	34	53	-1	1	3	7	10
Dec	8	13	18	22	32	9	16	23	32	44	1	3	6	9	12
Jan	7	11	13	18	33	8	14	21	33	59	2	3	8	15	26
Feb	5	8	11	16	33	7	12	20	32	56	2	4	10	16	23
Mar	4	7	10	16	29	6	14	24	35	55	2	7	13	19	26
Apr	8	16	24	34	46	18	33	46	59	86	10	17	22	25	40
May	53	72	95	121	173	75	103	133	168	248	23	31	38	46	74
Jun	107	157	190	235	297	79	139	191	248	324	-28	-18	1	12	27
Jul	32	51	70	103	187	23	36	50	70	119	-9	-15	-20	-33	-69
Aug	15	18	23	30	44	12	15	18	22	30	-3	-3	-5	-8	-13
Sep	10	13	16	23	31	8	10	13	17	28	-2	-3	-3	-6	-3

Table D1. Continued.

Month	Historic (1961 to 1990) Discharge (m^3/s)					Future (2041 to 2070) Discharge (m^3/s)					Discharge Anomaly (m^3/s)				
	5P	25P	50P	75P	95P	5P	25P	50P	75P	95P	5P	25P	50P	75P	95P
						Upper Columbia: Bull River near Wardner (BULNW)									
Oct	3.1	6.2	10.6	15.0	26.4	2.6	5.9	9.9	17.9	30.6	-0.4	-0.3	-0.7	2.9	4.2
Nov	3.5	7.4	11.1	14.4	23.1	3.3	9.5	14.3	20.4	32.6	-0.2	2.1	3.2	6.1	9.5
Dec	3.0	4.8	6.4	9.0	13.2	4.0	6.7	9.5	13.6	23.3	1.1	1.9	3.2	4.7	10.1
Jan	1.7	2.8	3.6	5.7	13.0	2.4	4.0	7.0	12.7	27.9	0.7	1.3	3.4	7.0	14.9
Feb	1.4	1.8	2.6	4.6	12.7	1.7	2.9	6.1	14.1	26.9	0.3	1.1	3.5	9.5	14.2
Mar	1.1	1.6	2.6	5.0	11.2	1.4	3.5	7.9	12.5	25.1	0.4	2.0	5.3	7.5	13.9
Apr	3.0	6.9	11.3	17.4	26.1	8.5	15.6	23.1	32.8	48.9	5.5	8.7	11.8	15.4	22.8
May	35.1	48.3	61.1	75.0	101.9	47.1	62.7	79.2	93.6	124.6	12.0	14.5	18.0	18.7	22.7
Jun	62.0	85.7	101.1	120.5	143.8	48.7	78.7	104.0	129.3	166.5	-13.4	-7.0	2.9	8.8	22.7
Jul	18.1	31.5	46.8	62.8	103.4	11.5	22.1	32.0	42.8	71.0	-6.7	-9.4	-14.8	-20.0	-32.5
Aug	4.7	9.4	13.8	18.4	29.3	2.8	4.6	6.3	9.7	15.5	-1.9	-4.8	-7.5	-8.7	-13.9
Sep	2.3	5.6	7.9	11.5	17.3	1.4	2.5	4.0	6.5	14.7	-0.9	-3.1	-3.9	-5.0	-2.6
						Upper Columbia: Duncan River at Duncan Dam (BCHDN)									
Oct	27	34	41	47	62	29	39	48	60	89	2	5	7	13	26
Nov	13	17	20	24	29	13	18	24	32	43	1	2	4	8	13
Dec	8	10	12	14	16	9	12	14	18	28	0	1	2	4	11
Jan	6	8	9	10	17	7	9	11	15	32	0	1	2	4	16
Feb	5	7	7	8	14	6	8	9	15	30	1	1	2	7	16
Mar	5	6	7	10	17	6	10	13	19	34	1	4	6	9	17
Apr	11	15	19	25	34	18	25	35	47	69	7	10	15	22	35
May	45	66	85	109	157	71	99	128	167	245	26	33	42	58	88
Jun	181	232	279	337	430	255	318	367	425	530	74	86	89	88	100
Jul	214	287	337	388	464	188	281	350	407	506	-26	-7	14	19	42
Aug	114	144	170	202	264	93	120	136	167	226	-21	-24	-34	-35	-39
Sep	52	61	74	85	103	42	54	66	76	97	-9	-7	-8	-9	-6

Table D1. Continued.

Month	Historic (1961 to 1990) Discharge (m^3/s)					Future (2041 to 2070) Discharge (m^3/s)					Discharge Anomaly (m^3/s)				
	5P	25P	50P	75P	95P	5P	25P	50P	75P	95P	5P	25P	50P	75P	95P
Upper Columbia: Kootenay River at Kootenay Canal (BCHKL)															
Oct	62	102	142	195	302	57	98	144	200	388	-5	-4	2	5	86
Nov	64	107	151	203	306	65	142	197	277	444	1	35	46	74	138
Dec	40	79	112	144	213	59	114	167	241	382	19	35	54	97	169
Jan	32	63	89	121	200	56	96	156	236	393	24	33	67	115	193
Feb	31	61	81	117	179	61	117	163	230	365	30	56	82	113	186
Mar	49	81	114	158	215	86	169	235	313	405	37	88	121	156	190
Apr	201	279	344	405	494	312	430	507	617	792	110	151	163	211	298
May	560	718	828	965	1150	704	828	984	1127	1442	143	110	155	162	292
Jun	867	1084	1227	1411	1701	789	1116	1325	1517	1920	-77	32	98	106	219
Jul	426	692	905	1153	1552	244	504	703	919	1276	-182	-188	-202	-233	-275
Aug	138	189	261	370	621	80	116	146	197	329	-58	-73	-115	-172	-293
Sep	77	109	143	185	249	49	70	89	127	220	-28	-39	-53	-57	-30
Upper Columbia: Slocan River near Crescent Valley (SLONC)															
Oct	18	27	39	50	70	18	28	40	53	89	0	1	1	3	19
Nov	13	23	31	39	55	15	27	38	51	75	1	4	7	12	20
Dec	9	17	21	26	35	13	22	28	38	54	4	5	7	12	19
Jan	8	12	16	20	31	10	16	22	31	56	2	4	6	12	25
Feb	7	10	12	16	25	10	15	21	31	52	3	5	9	15	27
Mar	7	10	14	19	31	10	20	28	40	61	4	10	14	21	31
Apr	21	30	39	50	68	37	52	72	90	139	15	22	33	40	70
May	87	122	146	187	255	132	168	209	249	342	44	46	63	62	88
Jun	227	282	319	371	437	186	295	352	400	497	-41	13	33	29	60
Jul	91	159	229	300	411	46	102	158	218	319	-45	-57	-70	-82	-92
Aug	32	46	62	88	148	18	25	32	44	73	-14	-22	-30	-44	-75
Sep	20	27	37	50	70	13	18	25	38	65	-7	-10	-12	-12	-5

Table D1. Continued.

Month	Historic (1961 to 1990) Discharge (m^3/s)					Future (2041 to 2070) Discharge (m^3/s)					Discharge Anomaly (m^3/s)				
	5P	25P	50P	75P	95P	5P	25P	50P	75P	95P	5P	25P	50P	75P	95P
	Upper Columbia: Salmo River near Salmo (SALNS)														
Oct	2.2	4.8	9.3	15.4	26.3	1.8	5.0	9.0	15.1	34.3	-0.5	0.2	-0.3	-0.4	8.0
Nov	1.4	5.3	9.4	14.1	24.9	2.1	7.8	13.1	22.0	38.4	0.7	2.5	3.7	7.9	13.5
Dec	0.8	3.1	4.7	6.6	11.8	1.6	4.9	8.2	14.1	25.1	0.8	1.8	3.6	7.4	13.4
Jan	0.5	1.7	2.4	3.6	9.6	1.0	2.8	5.1	9.7	27.8	0.5	1.1	2.7	6.0	18.3
Feb	0.6	1.2	1.7	3.6	10.3	1.0	2.6	5.8	14.0	34.0	0.4	1.4	4.1	10.4	23.7
Mar	0.7	1.6	3.8	7.5	17.7	1.3	6.7	15.7	25.2	45.2	0.6	5.1	11.9	17.7	27.5
Apr	9.9	18.1	26.3	36.0	49.8	23.5	37.0	51.3	65.6	89.1	13.6	19.0	25.0	29.6	39.3
May	55.2	74.7	86.4	101.6	128.6	70.1	84.7	99.4	118.6	150.3	14.9	10.0	13.0	17.0	21.7
Jun	72.2	100.1	117.2	132.6	155.4	40.6	81.3	102.7	124.1	164.2	-31.6	-18.8	-14.5	-8.5	8.8
Jul	16.9	40.3	60.3	83.6	126.0	6.7	18.1	31.2	49.2	82.3	-10.2	-22.2	-29.1	-34.4	-43.7
Aug	3.5	6.2	10.5	17.9	36.5	1.6	2.9	4.2	6.6	12.3	-1.9	-3.3	-6.3	-11.3	-24.2
Sep	1.5	3.2	5.6	9.7	18.3	0.6	1.4	2.8	5.1	12.6	-0.9	-1.8	-2.8	-4.6	-5.7